

e-ISSN : 2320-0847

p-ISSN : 2320-0936



AJER

American Journal of Engineering Research

Volume-2 Issue-5



AJER

American Journal of Engineering Research

**American Journal of
Engineering Research**

Editorial Board

American Journal of Engineering Research (AJER)

**Dr. Jonathan Okeke
Chimakonam**

Qualification: PHD
Affiliation: University of Calabar
Specialization: Logic, Philosophy of
Maths and African Science,
Country: Nigeria

Dr. ABDUL KAREEM

Qualification: MBBS, DMRD, FCIP, FAGE
Affiliation: UNIVERSITI SAINS Malaysia
Country: Malaysia

Dr. sukhmander singh

Qualification: Phd
Affiliation: Indian Institute Of
Technology, Delhi
Specialization : PLASMA PHYSICS
Country: India

Dr. Nwachukwu Eugene Nnamdi

Qualification: Phd
Affiliation: Michael Okpara University of
Agriculture, Umudike, Nigeria
Specialization: Animal Genetics and
Breeding
Country: Nigeria

Dr. June II A. Kiblasan

Qualification : Phd
Specialization: Management, applied
sciences
Country: PHILIPPINES

Dr. Narendra Kumar Sharma

Qualification: PHD
Affiliation: Defence Institute of Physiology
and Allied Science, DRDO
Specialization: Proteomics, Molecular
biology, hypoxia
Country: India

Prof. Dr. Shafique Ahmed Arain

Qualification: Postdoc fellow, Phd
Affiliation: Shah Abdul Latif University
Khairpur (Mirs),
Specialization: Polymer science
Country: Pakistan

Dr. Alcides Chaux

Qualification: MD
Affiliation: Norte University, Paraguay,
South America
Specialization: Genitourinary Tumors
Country: Paraguay, South America

Dr. Md. Nazrul Islam Mondal

Qualification: Phd
Affiliation: Rajshahi University, Bangladesh
Specialization: Health and Epidemiology
Country: Bangladesh

CONTENTS

Volume-2 Issue-5

S.No.	Title Name	Page No.
01.	Construction of Canonical Polynomial Basis Functions for Solving Special Nth -Order Linear Integro-Differential Equations Taiwo O. A and Raji M. T	01-10
02.	Heat Exchanger Network Retrofit Design by Eliminating Cross Pinch Heat Exchangers Beabu K. Piagbo, Kenneth K. Dagde	11-18
03.	Production of Wine from Ginger and Indian Gooseberry and A Comparative Study of Them over Commercial Wine Giri Nandagopal.M.S, Praveen.S.Nair	19-38
04.	Study on an Eco-Friendly Corrosion and Scale Inhibitor in Simulated cooling water Defang Zeng, Huan Yan	39-43
05.	Ore-Forming Fluid Characteristics of the Naoyangping-Damogou zinc-fluorite ore deposit, Pingli County, Shaanxi Province, China Moussounda Kounga Claude, Zheng Youye, Yang Xingke	44-49
06.	Multiple Histogram Technique for Robust Skin Color Based Segmentation Noor A. Ibraheem ¹ , Rafiqul Z. Khan	50-54
07.	Strength of Blended Cement Sandcrete & Soilcrete Blocks Containing Cassava Waste Ash and Plantain Leaf Ash L. O. Ettu, M. S. W. Mbajiorgu, and J. I. Arimanwa	55-60
08.	Distribution of Arsenic and Heavy Metals from Mine Tailings dams at Obuasi Municipality of Ghana Crentsil Kofi Bempah, Anthony Ewusi, Solomon Obiri-Yeboah, Stephen Boahen Asabere, Francis Mensah, Juliana Boateng, Hans-Jürgen Voigt	61-70
09	Promoting best practice design intent in 3D CAD for engineers through a task analysis Keelin Leahy	71-77
10.	Implementing Short Term Scheduler and Preemptive Algorithm in Grid Computing Scheduling CH.V.T. E.V Laxmi, K.Somasundaram,	78-83
11.	Parameter Optimization In Image Enhancement Using PSO Nirmal Singh, Maninder kaur, K.V.P Singh	84-90
12.	Mechanism Study on Flocculating Organnic Pollutants By Chitosan with Different Molecular In Wastewater Zeng De-fang, Liu Jun, Yan Huan	91-95
13.	CDMA2000 Radio Measurements at 1.9GHz and Comparison of Propagation Models in Three Built-Up Cities of South-South, Nigeria. Isabona Joseph, Isaiah Gregory Peter	96-106
14.	Invention of the plane geometrical formulae - Part II Mr. Satish M. Kaple	107-113

15.	Adsorption of Copper by Ethylenediamine-modified cross-linked magnetic chitosan resin (EMCMCR) Miss Priwiya Peter, Prof .S. Gopalakrishnan, Dr.T.Kannadasan	114-121
16.	Some Fixed Point and Common Fixed Point Theorems in 2-Banach Spaces A.S.Saluja, Alkesh Kumar Dhakde	122-127
17.	Mathematical Modelling of Cassava Wastewater Treatment Using Anaerobic Baffled Reactor A.O. Ibeje, B.C.Okoro	128-134
18.	Geocasting and Multicasting Routing Operation in Mobile Ad Hoc Network R.Kruthika, Smitha Shekar.B, Harish.G	135-139
19.	Technical Review of peephole Technique in compiler to optimize intermediate code Vaishali Sanghvi, Meri Dedania, Kaushik Manavadariya, Ankit Faldu	140-144
20.	ICT Practice in Morocco's innovative teachers Ahmed Lablidi, Brahim Nachit, Abdelmjid Abourriche, Abdelwahed Namir, Mohammed Talbi	145-150
21.	Biodergradable Polymers in Food Packaging P.A.Pawar, Aachal.H.Purwar	151-164
22.	ELECTROHYDRAULIC SYSTEM FOR AUTOMATIC GAGE CONTROL (AGC) FOR TANDEM COLD MILL PLANT IN SARTID SMEDEREVO Slobodan Stefanovic, Radoje Cvejic, Zivoslav Adamovic, Dusko Kostic	165-172
23.	Input-Output Energy and Economic Analysis of Strawberry Production in Iran Rasol Loghmanpor, Reza Tabatabaekoloor, Asadollah Akram	173-177
24.	Optimization of weld bead geometry for stainless steel cladding deposited by GMAW. P, Sreeraj, T, Kannan, Subhasis Maji	178-187
25.	Facial Verification Technology for Use In Atm Transactions Aru, Okereke Eze, Ihekweaba Gozie	188-193
26.	Preventing ADDOS Attack by Using Secure TRNG Based Port Hopping T. Siva, E. S. Phalguna Krishna, K. Pavan Kumar	194-199
27.	A modified model for parabolic trough solar receiver M-C. EL JAI, F-Z. CHALQI	200-211

Construction of Canonical Polynomial Basis Functions for Solving Special N^{th} -Order Linear Integro-Differential Equations

¹Taiwo O. A and ²Raji M. T

¹Department of Mathematics, University of Ilorin

²Department of Mathematics and Statistics, The Poly., Ibadan

Abstract: The problem of solving special n^{th} -order linear integro-differential equations has special importance in engineering and sciences that constitutes a good model for many systems in various fields. In this paper, we construct canonical polynomial from the differential parts of special n^{th} -order integro-differential equations and use it as our basis function for the numerical solutions of special n^{th} -order integro-differential equations. The results obtained by this method are compared with those obtained by Adomian Decomposition method. It is also observed that the new method is an effective method with high accuracy. Some examples are given to illustrate the method.

Keyword: *Integro - differential equation, canonical polynomial, differential, collocation method*

I. INTRODUCTION

Integro - differential equation is an equation which involving both differential and integral equation. This type of problem arise in Science and Engineering because of complexity of this problem, we discover that in order to get an exact or analytical solution of the problems, numerical analyst are now to developed interest in this area and this motivated the researcher to study this class of problem. The Canonical Polynomial established by Liao [11-15] is thoroughly used by many researchers to handle a wide variety of scientific and engineering applications: linear and nonlinear, and homogeneous and inhomogeneous as well. It was shown by many authors [1, 5, 7, 8, 9, 21, 22] that this method provides improvements over existing numerical techniques. The method gives rapidly convergent series solution approximation of the exact solution if such a solution exists. Taiwo [23] motivated this researcher work due to some properties of Canonical polynomials reported in the work that:

- (i) Canonical Polynomial can be generated over any given interval of consideration;
- (ii) It can be easily programmed; and
- (iii) It can be generated recursively.

Without loss of generality, the researcher considers special n^{th} -order linear integro-differential equation (IDE) of the form:

$$y^n(x) + \sum_{j=0}^{n-1} P_j(x)y^{(j)}(x) = f(x) + \lambda_i \int_a^b K(x,t)y^{(p)}(t)dt \quad (1)$$

$$y(a) = a_0, \quad y'(a) = a_1, \quad y^{(n-1)}(a) = a_{n-1} \quad (2)$$

where a_i , are real constants, n, p are positive integers, $f(x), P_j(x)$ and $K(x,t)$ are given smooth functions, while $y(x)$ is to be determined.

Eq. (1)- (2) occur in various areas of engineering, mechanics, physics, chemistry, astronomy, economics, potential theory, electrostatics, etc. Many methods are usually used to handle the high-order IDE (1)-(2) such as the successive approximations, Adomian decomposition, Homotopy perturbation method, Taylor collocation, Haar Wavelet, Tau and Walsh series methods, Monte Carlo Method, Direct method based on Fourier and block-pulse functions, etc. [2-4, 6, 10, 16-17, 21-25], but due to the problems encountered by some of these authors in

integrating complex functions like e^{-x^2} , $e^{\cos\theta}$ etc, then the method serves as an advantage.

Significant of the study

The construction of a new basis called Canonical polynomials applied to the linear and non-linear problems That a good choice of basis plays an important role in both the accuracy and efficiency of a collocation method is well-known in the literature. The extension of Canonical polynomials as a new basis for collocation method is examined and the following observation were obtained. Canonical polynomials provide some computational advantage, among which are the following;

They are generated by a single recursive formula.

They are independent of the interval of consideration.

They are independent of the associated conditions.

They ensure highly stable method (A-stability) and optional order accuracy.

One major advantage of the approach is that it is easily friendly to error estimation.

We obtained that non linear problems are solved using the collocation method in terms of canonical polynomials for the sequence of linearized approximate problems. The Newton’s linearization process is used which guarantees a quadratic convergence rate of the iteration.

We also obtained that the method provides the solution in a rapidly convergent series with components that are elegantly computed.

With all these observation, the researcher conclude that canonical polynomial plays important role in term of accuracy and efficient.

II. CONSTRUCTION OF CANONICAL POLYNOMIAL

From the general equations, stated in (1)-(2), we define D as follows;

$$L \equiv \sum_{i=0}^n P_i \frac{d^i}{dx^i}$$

implies

$$L \equiv P_n \frac{d^n}{dx^n} + \dots + P_3 \frac{d^3}{dx^3} + P_2 \frac{d^2}{dx^2} + P_1 \frac{d}{dx} + P_0$$

and let

$$L\Phi_i(x) = x^i$$

$$Lx^i = P_n i(i-1)(i-2)\dots(i-n)x^{i-n} + \dots + P_3 i(i-1)(i-2)x^{i-3} + P_2 i(i-1)x^{i-2} + P_1 ix^{i-1} + P_0 x^i$$

$$L[L\Phi_i(x)] = P_n i(i-1)(i-2)\dots(i-n)L\Phi_{i-n}(x) + \dots + P_3 i(i-1)(i-2)L\Phi_{i-3}(x) + P_2 i(i-1)L\Phi_{i-2}(x) + P_1 L\Phi_{i-1}(x) + P_0 L\Phi_i(x)$$

$$x^i = P_n i(i-1)(i-2)\dots(i-n)\Phi_{i-n}(x) + \dots + P_3 i(i-1)(i-2)\Phi_{i-3}(x) + P_2 i(i-1)\Phi_{i-2}(x) + P_1 i\Phi_{i-1}(x) + P_0 \Phi_i(x)$$

$$\Phi_i(x) = \frac{1}{P_0} [x^i - P_1 i\Phi_{i-1}(x) - P_2 i(i-1)\Phi_{i-2}(x) - P_3 i(i-1)(i-2)\Phi_{i-3}(x) - \dots - P_n i(i-1)(i-2)\dots(i-n)\Phi_{i-n}(x)]$$

$$i \geq 0; P_0 \neq 0 \tag{3}$$

For the case $n = 3$, we define our operator as:

$$L \equiv P_3 \frac{d^3}{dx^3} + P_2 \frac{d^2}{dx^2} + P_1 \frac{d}{dx} + P_0$$

$$L\Phi_i(x) = x^i$$

$$Lx^i = P_3 i(i-1)(i-2)x^{i-3} + P_2 i(i-1)x^{i-2} + P_1 ix^{i-1} + P_0 x^i$$

$$L[L\Phi_i(x)] = P_3 i(i-1)(i-2)L\Phi_{i-3}(x) + P_2 i(i-1)L\Phi_{i-2}(x) + P_1 iL\Phi_{i-1}(x) + P_0 L\Phi_i(x)$$

$$x^i = P_3 i(i-1)(i-2)\Phi_{i-3}(x) + P_2 i(i-1)\Phi_{i-2}(x) + P_1 i\Phi_{i-1}(x) + P_0 \Phi_i(x)$$

$$\Phi_i(x) = \frac{1}{P_0} [x^i - P_1 i \Phi_{i-1}(x) - P_2 i(i-1) \Phi_{i-2}(x) - P_3 i(i-1)(i-2) \Phi_{i-3}(x)] \quad i \geq 0; P_0 \neq 0 \quad (4)$$

For $i = 0$:
$$\Phi_0(x) = \frac{1}{P_0}$$

For $i = 1$:
$$\Phi_1(x) = \frac{1}{P_0} (x - P_1 \Phi_0(x)) = \frac{x}{P_0} - \frac{P_1}{P_0^2}$$

For $i = 2$:
$$\Phi_2(x) = \frac{1}{P_0} [x^2 - 2P_1 \Phi_1(x) - 2P_2 \Phi_0(x)] = \frac{x^2}{P_0} - 2x \frac{P_1}{P_0^2} + 2 \frac{P_1^2}{P_0^3} - 2 \frac{P_2}{P_0^2}$$

For $i = 3$:
$$\Phi_3(x) = \frac{1}{P_0} [x^3 - 3P_1 \Phi_2(x) - 6P_2 \Phi_1(x) - 6P_3 \Phi_0(x)]$$

For $i = 3$:
$$\Phi_3(x) = \frac{x^3}{P_0} - \frac{3x^2 P_1}{P_0^2} + \frac{6x P_1^2}{P_0^3} - \frac{6P_1^3}{P_0^4} - \frac{6x P_2}{P_0^2} - \frac{6P_3}{P_0^2}$$

For $i = 4$:
$$\Phi_4(x) = \frac{1}{P_0} [x^4 - 4P_1 \Phi_3(x) - 12P_2 \Phi_2(x) - 24P_3 \Phi_1(x)]$$

$$= \left[\frac{x^4}{P_0} - \frac{4x^3 P_1}{P_0^2} + \frac{12x^2 P_1^2}{P_0^3} - \frac{24x P_1^3}{P_0^4} + \frac{24P_1^4}{P_0^5} - \frac{72P_1^2 P_2}{P_0^4} + \frac{48P_1 P_3}{P_0^3} - \frac{12x^2 P_2}{P_0^2} - \frac{24x P_3}{P_0^2} + \frac{24P_2^2}{P_0^3} \right]$$

Thus, from equation (4), we obtain the following

$$\Phi_0(x) = 1,$$

$$\Phi_1(x) = x - 1,$$

$$\Phi_2(x) = x^2 - 2x,$$

$$\Phi_3(x) = x^3 - 3x^2,$$

$$\Phi_4(x) = x^4 - 4x^3 + 24,$$

.
.
.
etc.

For the case $n = 4$, we define our operator as:

$$L \equiv P_4 \frac{d^4}{dx^4} + P_3 \frac{d^3}{dx^3} + P_2 \frac{d^2}{dx^2} + P_1 \frac{d}{dx} + P_0$$

$$L\Phi_i(x) = x^i$$

$$Lx^i = P_4 i(i-1)(i-2)(i-3)x^{i-4} + P_3 i(i-1)(i-2)x^{i-3} + P_2 i(i-1)x^{i-2} + P_1 ix^{i-1} + P_0 x^i$$

$$L[L\Phi_i(x)] = P_4 i(i-1)(i-2)(i-3)L\Phi_{i-4}(x) + P_3 i(i-1)(i-2)L\Phi_{i-3}(x) + P_2 i(i-1)L\Phi_{i-2}(x) + P_1 iL\Phi_{i-1}(x) + P_0 L\Phi_i(x)$$

$$x^i = P_4 i(i-1)(i-2)(i-3)\Phi_{i-4}(x) + P_3 i(i-1)(i-2)\Phi_{i-3}(x) + P_2 i(i-1)\Phi_{i-2}(x) + P_1 i\Phi_{i-1}(x) + P_0 \Phi_i(x)$$

$$\Phi_i(x) = \frac{1}{P_0} [x^i - P_1 i \Phi_{i-1}(x) - P_2 i(i-1) \Phi_{i-2}(x) - P_3 i(i-1)(i-2) \Phi_{i-3}(x) + P_4 i(i-1)(i-2)(i-3) \Phi_{i-4}(x)]$$

$$i \geq 0; P_0 \neq 0 \quad (5)$$

For i = 0:
$$\Phi_0(x) = \frac{1}{P_0}$$

For i = 1:
$$\Phi_1(x) = \frac{1}{P_0}(x - P_1\Phi_0(x)) = \frac{x}{P_0} - \frac{P_1}{P_0^2}$$

For i = 2:
$$\Phi_2(x) = \frac{1}{P_0}[x^2 - 2P_1\Phi_1(x) - 2P_2\Phi_0(x)] = \frac{x^2}{P_0} - 2x\frac{P_1}{P_0^2} + 2\frac{P_1^2}{P_0^3} - 2\frac{P_2}{P_0^2}$$

$$\Phi_3(x) = \frac{1}{P_0}[x^3 - 3P_1\Phi_2(x) - 6P_2\Phi_1(x) - 6P_3\Phi_0(x)]$$

For i = 3:
$$\Phi_3(x) = \frac{x^3}{P_0} - \frac{3x^2P_1}{P_0^2} + \frac{6xP_1^2}{P_0^3} - \frac{6P_1^3}{P_0^4} - \frac{6xP_2}{P_0^2} + \frac{6P_1P_2}{P_0^3} - \frac{6P_3}{P_0^2}$$

For i = 4:

$$\begin{aligned} \Phi_4(x) &= \frac{1}{P_0}[x^4 - 4P_1\Phi_3(x) - 12P_2\Phi_2(x) - 24P_3\Phi_1(x)] \\ &= [\frac{x^4}{P_0} - \frac{4x^3P_1}{P_0^2} + \frac{12x^2P_1^2}{P_0^3} - \frac{24xP_1^3}{P_0^4} + \frac{24P_1^4}{P_0^5} - \frac{48P_1P_2}{P_0^4} + \frac{24xP_2}{P_0^3} + \frac{24P_3}{P_0^3} - \frac{12x^2P_2}{P_0^2} + \frac{24xP_1}{P_0^3} - \frac{24P_1^2P_2}{P_0^4} \\ &\quad + \frac{24P_2^2}{P_0^3} - \frac{24xP_3}{P_0^2} + \frac{24P_1P_3}{P_0^3} - \frac{24P_4}{P_0^2}] \end{aligned}$$

Thus, from equation (5), we obtain the following

$$\Phi_n(x) = 1,$$

$$\Phi_1(x) = x - 1,$$

$$\Phi_2(x) = x^2 - 2x,$$

$$\Phi_3(x) = x^3 - 3x^2,$$

$$\Phi_4(x) = x^4 - 4x^3,$$

.

. etc

Let $y(x)$ be the exact solution of the integro-differential equation,

$$Dy(x) - \lambda \int_a^b m(x,t)y(t)dt = f(x), \quad x \in [a,b] \tag{6}$$

with

$$\sum_{m=1}^v [c_{jm}^{(1)}y^{(m-1)}(a) + c_{jm}^{(2)}y^{(m-1)}(b)] = d_j, \quad j = 1, \dots, v, \tag{7}$$

where $f(x)$ and $m(x,t)$ are given continuous functions $\lambda, a, b, c_{jm}^1, c_{jm}^2$ and d_j some given constants.

III. MATRIX REPRESENTATION FOR THE DIFFERENT PARTS

Let $\underline{V} := \{v_0(x), v_1(x), \dots\}$ be a polynomial basis by $\underline{V} := V\underline{X}$, where V is a non-singular lower triangular matrix and degree $(v_i(x)) \leq i$, for $i = 0, 1, 2, \dots$. Also for any matrix P , $P_v = VPV^{-1}$.

Now we convert the Eq. (6) and (7) to the corresponding linear algebraic equations in three parts; (a), (b) and (c).

(a). Matrix representation for $Dy(x)$:

Ortiz and Samara proposed in [18] an alternative for the Tau technique which they called the operational approach as it reduces differential problems to linear algebraic problems. The effect of differentiation, shifting and integration on the coefficients vector

$$\underline{\tilde{a}}_n := (\tilde{a}_0, \tilde{a}_1, \dots, \tilde{a}_n, 0, 0, \dots)$$

Of a polynomial $u_n(x) = \underline{\tilde{a}}_n X$ is the same as that of post-multiplication of $\underline{\tilde{a}}_n$ by the matrices η, μ and i respectively,

$$\frac{du_n(x)}{dx} = \underline{\tilde{a}}_n \eta X, \quad u_n(x) = \underline{\tilde{a}}_n \mu X \quad \text{and} \quad \int_0^x u_n(t) dt = \underline{\tilde{a}}_n i X$$

where

$$\eta = \begin{bmatrix} 0 & 0 & \dots & \dots \\ 1 & 0 & 0 & \dots \\ 0 & 2 & 0 & \dots \\ \dots & \dots & \dots & \dots \end{bmatrix}, \mu = \begin{bmatrix} 0 & 1 & \dots \\ 0 & 0 & 1 \dots \\ \dots & \dots & \dots \end{bmatrix}, i = \begin{bmatrix} 0 & 1 & \dots \\ 0 & 0 & 1/2 \dots \\ \dots & \dots & \dots \end{bmatrix}.$$

We recall now the following theorem given by Ortiz and Samara [18].

(b). Matrix representation for the integral term:

Let us assume that

$$m(x, t) = \sum_{i=0}^n \sum_{j=0}^n m_{ij} v_i(x) v_j(t), \quad \text{and} \quad y(x) = \sum_{i=0}^{\infty} a_i v_i(x) = \underline{aV}. \tag{8}$$

Then, we can write

$$\int_a^b m(x, t) y(t) dt = \sum_{i=0}^{\infty} \sum_{j=0}^n \sum_{k=0}^n m_{ij} a_i v_i(x) \int_a^b v_j(t) v_k(t) dt = \underline{aMV}, \tag{9}$$

where,

$$\underline{M} = \begin{bmatrix} \sum_{j=0}^n m_{0j} \alpha_{j0} & \dots & \sum_{j=0}^n m_{nj} \alpha_{j0} & 0 & 0 \\ \cdot & \cdot & \cdot & \cdot & \cdot \\ \sum_{j=0}^n m_{0j} \alpha_{jn} & \dots & \sum_{j=0}^n m_{nj} \alpha_{jn} & 0 & 0 \\ \cdot & \cdot & \cdot & \cdot & \cdot \end{bmatrix}$$

With,

$$\alpha_{jl} = \int_a^b v_j(t) v_l(t) dt, \quad \text{for} \quad j, l = 0, \dots, n.$$

(c). Matrix representation for the supplementary conditions:

Replacing $y(x) = \sum_{i=0}^{\infty} a_i v_i(x)$ in the left hand side of (7), it can be written as

$$\sum_{m=1}^v [c_{jm}^{(1)} y^{(m-1)}(a) + c_{jm}^{(2)} y^{(m-1)}(b)] = \sum_{i=0}^{\infty} \sum_{m=1}^v [c_{jm}^{(1)} v_i^{(m-1)}(a) + c_{jm}^{(2)} v_i^{(m-1)}(b)] = \underline{aB}_j, \tag{10}$$

where for $j = 1, \dots, v$,

$$\underline{B}_j = \begin{bmatrix} c_{jm}^{(1)} v_0(a) + c_{jm}^{(2)} v_0(b) \\ \sum_{m=1}^2 [c_{jm}^{(1)} v_1^{(m-1)}(a) + c_{jm}^{(2)} v_1^{(m-1)}(b)] \\ \vdots \\ \sum_{m=1}^v [c_{jm}^{(1)} v_{v-1}^{(m-1)}(a) + c_{jm}^{(2)} v_{v-1}^{(m-1)}(b)] \\ \vdots \end{bmatrix} \tag{11}$$

We refer to B as the matrix representation of the supplementary conditions and B_j as its j th column. The following relations for computing the elements of the matrix B can be deduced from (10):

$$b_{ij} = \sum_{m=1}^v [c_{jm}^{(1)} v_{v-1}^{(m-1)}(a) + c_{jm}^{(2)} v_{v-1}^{(m-1)}(b)] \quad \text{for } i, j = 1, 2, \dots, v, \tag{12}$$

and,

$$b_{ij} = \sum_{m=1}^v [c_{jkm}^{(1)} v_{v-1}^{(m-1)}(a) + c_{jkm}^{(2)} v_{v-1}^{(m-1)}(b)] \quad \text{for } i = v + 1, v + 2, \dots, j = 1, 2, \dots, v. \tag{13}$$

We introduce $\underline{d} = (d_1, d_2, \dots, d_v)$, the vector that contains right hand sides of conditions. Then the supplementary conditions take the form

$$\underline{a}B = \underline{d}. \tag{14}$$

It follows from (8) and (9) that

$$Dy(x) - \lambda \int_a^b m(x,t)y(t)dt = \underline{a}(\prod_v -\lambda M)\underline{V}. \tag{15}$$

Let $M_v := \prod_v -\lambda M$ and M_{vi} stands for its i th column and let $f(x) = \sum_{i=0}^n f_i v_i(x) = f\underline{V}$ with $f = (f_0, \dots, f_n, 0, 0, \dots)$. Then the coefficient of exact solution $y = \underline{a}\underline{V}$ of problem (6) and (7) satisfies the following infinite algebraic system:

$$\begin{cases} \underline{a}M_{vi} = f_i; & i = 0, \dots, n, \\ \underline{a}M_{vi} = 0; & i \geq n + 1, \\ \underline{a}B_j = d_j; & j = 1, 2, \dots, v. \end{cases} \tag{16}$$

setting,

$$G = (B_1, \dots, B_v, M_{v0}, M_{v1}, \dots),$$

and,

$$g = (d_1, \dots, d_v, f_0, f_1, \dots),$$

We can write instead of (16)

$$\underline{a}G = g. \tag{17}$$

Remark:

For $v = 0$ and $G_0(x) = 1$, Eq. (6) is transformed into a Fredholm integral equation of second kind and for $\lambda = 0$, it is transformed into a differential equation.

IV. DESCRIPTION OF THE METHOD

For the purpose of our discussion, we assume an approximate solution of the form

$$y_N(x) = \sum_{i=0}^N a_i \Phi_i(x) \tag{18}$$

Where a_i are constants to be determined and Φ_i are the canonical polynomials constructed above

We write equation (1) in the form:

$$y^n(x) + D(x) = f(x) + \lambda_i V(x) \quad \text{or } D(x) = I(x); i = 1, 2, \dots \tag{19}$$

So that

$$D(x) = \sum_{j=0}^n P_j(x)y^{(j)}(x), \tag{20}$$

$$V(x) = \int_a^b K(x,t)y(t)dt, \tag{21}$$

and

$$I(x) = f(x) + \lambda V(x) \quad (22)$$

Then, putting equation (18) into equation (1), we obtain

$$\sum_{i=0}^N a_i \mathcal{Q}_i^n(x) + \sum_{j=0}^{n-1} \sum_{i=0}^N a_j(x) a_i \mathcal{Q}_i^n(x) = f(x) + \lambda \int_a^b k(x,t) \sum_{i=0}^N a_i \mathcal{Q}_i(t) dt \quad (23)$$

$a_j(x)$ are known functions to be supplied,

a_i are unknown constants to be determined;

$\Phi_i(x)$ are canonical polynomial generated in section 2,

together with the following conditions:

$$\sum_{i=0}^N a_i \Phi_i(a) = a_0$$

$$\sum_{i=0}^N a_i \Phi_i'(a) = a_1$$

$$\sum_{i=0}^N a_i \Phi_i^{(n-1)}(a) = a_{n-1}$$

In equation (23) the integral part has to be evaluated after which the left over are then collocated at point $x = x_k$, to obtain

$$\sum_{i=0}^N a_i \Phi_i^n(x_k) + \sum_{j=0}^{n-1} \sum_{i=0}^N a_j(x_k) a_i \Phi_i^n(x_k) = f(x_k) + \lambda \int_a^b k(x_k,t) \sum_{i=0}^N a_i \Phi_i(t) dt \quad (24)$$

where,

$$x_k = a + \frac{(b-a)k}{N-2}; \quad k = 1, \dots, N-3$$

Thus, equation (24) give rise to (N-3) algebraic linear system of equations in (N+1) unknown constants. The remaining equations are obtained using the boundary conditions stated in equation (2).

These equations are then solved to obtain the unknown constants $a_i (i \geq 0)$ which are then substituted into equation (18) to obtain our approximate solution.

Remark: all these procedure discussed above have been translated and the entire process is automated by the use of symbolic algebraic program MATLAB 7.9 and no manual computation is required.

V. ERROR

In this section, we have defined our error as

$$e_N(x) = y(x) - y_N(x),$$

where $y(x)$ is the exact solution and $y_N(x)$ is the approximate solution computed for various values of N.

VI. NUMERICAL EXAMPLES

In this section, we consider some examples of third and fourth order linear integro-differential equations.

Reason:

Because of frequent occurrence of problem in fluid dynamics and biological model in science and engineering we decided to pick some problem which are commonly used and compared the result obtained by analytic solution result available.

- * Mathematical modelling of real life, physics and engineering problems usually results in these classes.
- * Many mathematical formulations of physical phenomena contains integro-differential equation, these equations arise in fluid dynamics, biological models and chemical kinetics.
- * Integro-differential equations are usually difficult to solve analytically so it is required to obtain an efficient approximate solution.
- * Therefore the need of this study, and also to discuss the existence and uniqueness of the solutions for these classes of problems.
- * The present work is motivated by the desire to obtain analytical and numerical solutions to boundary value problems for high-order integro-differential equations.

Example 1: Consider the third order linear integro differential equation

$$y'''(x) - xy''(x - \pi/2) - y'(x - \pi) = x \sin(x) + \int_{-\pi/2}^{\pi} [xy'(t) - ty(t) + ty''(t - \pi)]dt$$

with the conditions

$$y(0) = 1, y'(0) = 0, y''(0) = -1$$

and exact solution is $y(x) = \cos(x)$. We use the absolute error to measure the difference between the numerical and exact solutions. In table 1 result obtained for N=6, 7, 8 are given with the exact solution.

Table 1a: Table of result of Example 1

X	Exact solution	N=6	N=7	N=8
		New method	New method	New method
$-\pi/2$	0	0	0	0
$-2\pi/5$	0.30902	0.308796	0.3089668	0.309015916
$-3\pi/10$	0.58779	0.583085	0.5877655	0.587784962
$-\pi/5$	0.80902	0.807776	0.80901055	0.809015988
$-\pi/10$	0.95106	0.950922	0.95104963	0.951055998
0	1	1	1	1
$\pi/10$	0.95106	0.950922	0.95105059	0.951055998
$\pi/5$	0.80902	0.807776	0.80901055	0.809015988
$3\pi/10$	0.58779	0.583085	0.5877655	0.587784962
$2\pi/5$	0.30902	0.308796	0.3089668	0.309015916
$\pi/2$	0	0	0	0

Table 1b: Table of errors for example 1

X	Exact solution	N=6	N=7	N=8
		Error of New method	Error of New method	Error of New method
$-\pi/2$	0	0.0000E+00	0.0000E+00	0.0000E+00
$-2\pi/5$	0.30902	2.2400E-04	5.3200E-05	4.0840E-06
$-3\pi/10$	0.58779	4.7050E-03	2.4500E-05	5.0380E-06
$-\pi/5$	0.80902	1.2440E-03	9.4500E-06	4.0120E-06
$-\pi/10$	0.95106	1.3800E-04	1.0370E-05	4.0020E-06
0	1	0.0000E+00	0.0000E+00	0.0000E+00
$\pi/10$	0.95106	1.3800E-04	9.4100E-06	4.0020E-06
$\pi/5$	0.80902	1.2440E-03	9.4500E-06	4.0120E-06
$3\pi/10$	0.58779	4.7050E-03	2.4500E-05	5.0380E-06
$2\pi/5$	0.30902	2.2400E-04	5.3200E-05	4.0840E-06
$\pi/2$	0	0.0000E+00	0.0000E+00	0.0000E+00

Example 2: Consider the third order linear integro differential equation

$$y'''(x) - xy''(x - \pi/2) - y(x - \pi/2) = 2 - x \cos(x) + \int_{\pi/2}^{\pi} [xy'(t) - ty(t) + ty''(t - \pi/2) + xy(t - \pi/2)]dt$$

with the conditions

$$y(0) = 1, y'(0) = 0, y''(0) = 0$$

and exact solution is $y(x) = \sin(x)$

Table 2a: Table of result of Example 2 for the value of N

X	Exact solution	N=5	N=7
		New method	New method
$-\pi/2$	-1	-1.00E+00	-1.00E+00
$-2\pi/5$	-0.9511	-9.63E-01	-9.67E-01
$-3\pi/10$	-0.8090	-9.16E-01	-9.04E-01
$-\pi/5$	-0.5878	-6.78E-01	-7.85E-01
$-\pi/10$	-0.3090	-4.26E-01	-4.58E-01
0	0	0.00E+00	0.00E+00
$\pi/10$	0.3090	4.26E-01	4.58E-01
$\pi/5$	0.5878	6.78E-01	7.85E-01
$3\pi/10$	0.8090	9.16E-01	9.04E-01
$2\pi/5$	0.9511	9.63E-01	9.67E-01
$\pi/2$	1	1	1

Table 2b: Table of errors of Example 2 for the value of N

X	Exact solution	N=5	N=7
		Error of New method	Error of New method
$-\pi/2$	-1	0.0000E+00	0.0000E+00
$-2\pi/5$	-0.9511	1.1900E-02	1.5900E-02
$-3\pi/10$	-0.809	1.0700E-01	9.5000E-02
$-\pi/5$	-0.5878	9.0200E-02	1.9700E-01
$-\pi/10$	-0.309	1.1700E-01	1.4900E-01
0	0	0.0000E+00	0.0000E+00
$\pi/10$	0.309	1.1700E-01	1.4900E-01
$\pi/5$	0.5878	9.0200E-02	1.9700E-01
$3\pi/10$	0.809	1.0700E-01	9.5000E-02
$2\pi/5$	0.9511	1.1900E-02	1.5900E-02
$\pi/2$	1	0.0000E+00	0.0000E+00

Example 3: Consider the linear boundary value problem for the fourth-order integro differential equation.

$$y^{(iv)}(x) = x(1 + e^x) + 3e^x + y(x) - \int_0^1 y(t)dt \quad a < x < b$$

with the conditions

$$y(0) = 1, y'(0) = 1, y(1) = 1 + e, y'(1) = 2e$$

The exact solution of the above boundary value problem is $y(x) = 1 + xe^x$

Table 3a: Table of results of Example 3 for various value of N

X	Exact solution	N=6	N=8
		New method	New method
1	1	1	1
0.1	1.111	1.10856	1.11062115
0.2	1.244	1.23912	1.24375129
0.3	1.405	1.40154	1.40295678
0.4	1.597	1.58745	1.58921410
0.5	1.824	1.81309	1.82056380
0.6	2.093	2.06289	2.09263967
0.7	2.410	2.25290	2.36349645
0.8	2.780	2.66534	2.76798420
0.9	3.214	3.20256	3.21389340
1	3.718	3.71528	3.71681830

Table 3b: Table of errors of example 3 for various value of N

X	Exact solution	N=6	N=8
		Error of new method	Error of new method
1	1	0.00000E+00	0.00000E+00
0.1	1.111	2.44000E-3	3.788500E-4
0.2	1.244	4.88000E-3	2.487100E-4
0.3	1.405	3.46000E-3	2.043220E-3
0.4	1.597	9.55000E-3	7.785900E-3
0.5	1.824	1.09100E-2	3.436200E-3
0.6	2.093	3.01100E-2	3.603300E-4
0.7	2.41	1.57100E-1	4.650355E-2
0.8	2.78	1.14660E-1	1.201580E-2
0.9	3.214	1.14400E-2	1.066000E-4
1	3.718	2.72200E-3	1.181700E-3

VII. DISCUSSION AND CONCLUSION

In this paper, Canonical polynomial has been successfully used as a basis function for the numerical solution of special n^{th} -order integro-differential equations. The solution obtained by means of the canonical polynomial is an infinite power series for appropriate conditions, which can be in turn, expressed in a closed form. The results obtained here are compared with result of Sezer and Gulsu [21] and revealed that Canonical polynomial is a powerful mathematical tool for the numerical solutions of special n^{th} -order linear integro-differential equations in terms of accuracy achieved.

REFERENCES

- [1]. Abbasbandy, S. (2008) Soliton solution for the Fitzhugh-Nagumo equation with the homotopy analysis method, applied mathematical modelling 32, 27006-2714 doi: 10.1016/j.chaos.2006.10.037.
- [2]. Asady, B. And Kajani M. T. (2005) Direct method for solving integro differential equations using hybrid fourier and block-pulse functions, Intern. J. Computer Math., 82, No. 7, 889-895.
- [3]. Danfu, H. And Xufeng, S. (2007). Numerical solution of integro-differential equations by using CaS wavelet operational matrix of integration, Appl. Math. Comput., 194 460-466.
- [4]. Golbadai, A. And Javidi, M. (2007) Application of He's homotopy perturbation method for the n^{th} -order integro-differential equations, Appl. Math. Comput., 190 1409-1415.
- [5]. Hayat, T. And Sajid, M. (2007) On analytic solution for thin film flow of a fourth grade fluid down a vertical cylinder, Physical Letters A 361, 316-322.
- [6]. Hosseini, S. And Shahmorad, S. (2002) A matrix formulation of the tau method and Volterra linear integrodifferential equations, Korean J. Comput., Appl. Math., 9 (2) 497-507.
- [7]. Inc, M. (2008) Application of homotopy analysis method for fin efficiency of convective straight fins with temperature-dependent thermal conductivity, Math. Comput. Simul. Doi:10.1016/j.matcom.2007.11.009.
- [8]. Inc, M. (2007) On exact solution of Laplace equation with Dirichlet and Neumann boundary conditions by the homotopy analysis method, Physics Letters A 365, 412-415.
- [9]. Inc, M. (2008) On numerical solution of Burgers' equation by homotopy analysis method, Physics Letters A 356-360.
- [10]. Karamete, A and Sezer, M (2002), A Taylor collocation method for the solution of linear integro-differential equations, Intern. J. Computer Math., 79(9), 987-1000.
- [11]. Liao, S. J. (2003), Beyond Perturbation: Introduction to the Homotopy Analysis Method, Chapman and Hall/CRC Press, Boca Raton.
- [12]. Liao, S. J. (2004), On the homotopy analysis method for nonlinear problems, Appl. Math. Comput. 147, 499-513.
- [13]. Liao, S. J. (2008), Notes on the homotopy analysis method: some definitions and theorems, communications in Nonlinear Science and Numerical simulation, Doi:10.1016/j.cnsns.2008.04.013.
- [14]. Liao, S. J. And Tan, Y. (2007) A general approach to obtain series solutions to nonlinear differential equations. Studies in Applied Mathematics, 119, 297-355.
- [15]. Liao, S. J. (2003), An explicit analytic solution to the Thomas-Fermi equation, Appl. Math. Comput. 144, 495-506.
- [16]. Maleknejad, K. And Mirzaee, F. (2006), Numerical solution of integro-differential equations by using rationalized Haar functions method, Ky-bernetes, Int. J. Syst. Math. 35, 1735-1744.
- [17]. Nas, S. Yalcinbas, S. And Sezer, M. (2000), A Taylor polynomial approach for solving high-order linear Fredholm integro-differential equations Int. J. Math. Educ. Sci. Technol., 31 92, 213-225.
- [18]. Ortiz, E.L., Samara H. (1981) An operational approach to the Tau method for the numerical solution of non-linear differential equations, Computing 27, 15-25.
- [19]. Rahimi-Ardabili, M. Y and Shahmorad, S. (2007), Iterative numerical solution of non-linear integro-differential equations by the Tau method, Appl. Math. Comput. 193, 514-522.
- [20]. Rashidinia, J. And Zarebnia, M. (2007), The numerical solution of integro-differential equation by means of the Sinc method, Appl. Math. Comput. 188, 1124-1130.
- [21]. Sezer, M. And Gulsu, M (2005) Polynomial solution of the most general linear Fredholm Integrodifferential difference equations by means of Taylor matrix method, Complex Variables, 50 (50), 367-382.
- [22]. Tan, y. And Abbasbandy, S. (2008) Homotopy analysis method for quadratic Riccati differential equation, Communications in Nonlinear Science and Numerical Simulation 13, 539-546.
- [23]. Taiwo O. A. (1991), Collocation approximation for simple perturbed boundary problem. Ph.D Thesis, Unpublished, University of Ilorin, Ilorin.
- [24]. Tavassoli Kajani, M., Ghasemi, M. And Babolian, E. (2006), Numerical solution of linear integro-differential equation by using sine-cosine wavelets, Appl. Math. Comput. 180, 569-574.
- [25]. Wang, W. (2006), An algorithm for solving the higher-order nonlinear Volterra-Fredholm integro-differential equation with mechanization, Appl. Math. Comput. 172, 1-23.
- [26]. Wang s. And He, J. (2007) Variational iteration method for solving integro-differential equations, Physics Letter A, 327, 188-191.
- [27]. Yalcinbas, S. And Sezer, M. (2000) The approximate solution of high-order linear Volterra-Fredholm integrodifferential equations in terms of Taylor polynomials, Appl. Math. Comput., 112, 291-308.
- [28]. Zhao, J. And Corless, R. M. (2006) Compact finite difference method for integro-differential equations, Appl. Math. Comput., 177, 271-288.

Heat Exchanger Network Retrofit Design by Eliminating Cross Pinch Heat Exchangers

Beabu K. Piagbo¹, Kenneth K. Dagde²

¹ School of Science and Engineering, Teesside University Middlesbrough, TS1, 3BA, United Kingdom

² Department of Chemical/Petrochemical Engineering, Rivers State University of Science and Technology, Port Harcourt, PMB 5080, Port Harcourt, Rivers State, Nigeria

Abstracts: The rising cost of energy and environmental concerns are leading the petrochemical industry to search for methods of reducing energy consumption in refinery operations. To address this issue the research presented in this paper explores retrofit design for increasing the energy efficiency of Crude Distillation Units (CDUs). The case study presented uses monitored plant data from the preheat section of the CDU in a Refinery in the Niger Delta region of Nigeria, West Africa. Aspen Energy Analyser® software developed by Aspen Technologies is used in the analysis of this data. The research findings suggest that a retrofit design eliminating all cross pinch heat exchangers is the best retrofit design in terms of improving the energy performance of CDUs. There was an 84.62% and 92.31% reduction in the number of the heat exchangers used and the number of shells respectively. There were 16.57%, 2.74%, and 13.98% reductions in the operating cost, capital cost, and total cost respectively. 3.68% of the area became available for heat transfer. These gains were achieved despite a 12.27% increase in the heating demand. This design is therefore recommended to be applied after additional cost consideration.

Keywords: Aspen Energy Analyser®, Cross Pinch Heat Exchangers, Heat Exchanger Network, Retrofitting.

I. INTRODUCTION

Retrofitting heat exchanger networks falls under the broad category of research known as process integration. Process integration started as heat integration. Interest in which initially arose due to energy crisis in the 1970's. Process integration now includes several methods of combining processes to reduce the consumption of energy or other resources or harmful emissions to the environment [1]. The beginning of research in process integration is traced to Hohmann [2]. However, Hohmann's research was not pursued until Linnhoff and Flower developed Hohmann's work and in 1977 developed Pinch technology – the technique on which most heat integration applications are performed today [1, 3]. In a comprehensive review of the subject matter from 1975 – 2008, Morar & Agachi [3] identified Linnhoff, Floudas, Grossmann, Morari, Yee, Ciric, Saboo, Mathisen, Asante, Smith, Aguilera, and Marcheti as the most significant contributors to heat integration research. This is because their works signifies a turning point in the heat integration research field – with them came the introduction of pinch technology, mathematical programming techniques, and insights into the dynamic behaviour of heat exchanger networks. Also, their works are mostly cited by other researchers in the field as they extend, improve and make practical application of their research. A review of the literature shows that the heat exchanger retrofitting problem could be solved using either of or a combination of the following techniques: Pinch analysis technique [4, 5, 6, 7, 8]; Mathematical Programming Technique [9, 10, 11, 12]; Combination of Pinch analysis & Mathematical programming technique [13, 14]; Simulated Annealing and Genetic Algorithm technique [15, 16, 17, 18, 19, 20, 21]; and Path analysis technique [22]. The reader may consult the cited authors for a full discussion of these techniques. This research uses monitored plant data from the preheat section of the Crude Distillation Unit (CDU) of a Refinery to demonstrate that a retrofit design eliminating all cross pinch heat exchangers is the best retrofit design for a heat exchanger network with gross pinch rule violation. The case study was taken from a refinery in the Niger Delta region of Nigeria, West Africa, and as pointed out by Ajao and Akande [23], almost all industrial equipment stock in Nigeria were imported

during the era of cheap energy, hence they are energy inefficient. True to this statement, serious pinch rule violations were noticed during the analysis. Aspen Energy Analyser® of Aspen Technologies Limited was used for the analysis. The software combines pinch technology and mathematical programming to provide an automatic retrofit design for heat exchanger networks. Retrofitting was recommended after the analysis of the heat exchanger network. The retrofit design eliminates cross pinch heat exchangers.

II. MATERIALS AND METHODS

A. Process mapping

The study is mainly concerned with the preheat section of the Crude Distillation Unit (CDU) of a refinery in Port Harcourt Nigeria. The heat exchangers and process streams involved in crude preheating as the crude flows from storage to the distillation column are shown in Fig. 1. The process consists of 11 streams – 3 cold streams and 8 hot process streams. The cold streams are heated by 24 heat exchangers from a temperature of about 29.9°C to 344°C before it enters the distillation column where the components are separated. The cold streams include the crude from storage stream, the desalted crude stream, and the pre-flashed crude stream. 8 hot process streams are used to preheat the cold streams, these includes atmospheric residue, stripped kerosene, stripped Light Diesel Oil (LDO), stripped Heavy Diesel Oil (HDO), Heavy Vacuum Gas Oil (HVGO), and the 3 Pump Around streams – Top Pump Around, Kerosene Pump Around, and LDO Pump Around [24].

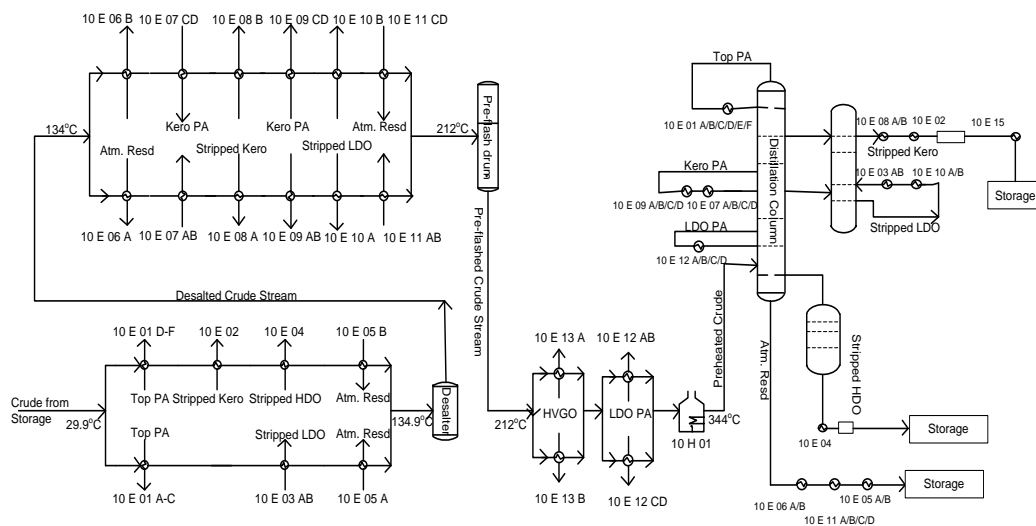


Fig. 1: rocess Map [24]

Table 1 and 2 show the process stream and utility stream data obtained from the process flow diagram and operating data of the Crude Distillation Unit obtained from the refinery.

Table 1 Extracted Process Streams Data [24]

Process Stream Data						
Name	Inlet Temp (°C)	Outlet Temp (°C)	Density (Kg/m ³)	Flow rate M ³ /hr	Flow Rate Kg/H	Specific Heat Capacity (Kcal/Kg°C)
Top Pump Around	152.4	96.7	788	747	588636	0.5919
Kerosene Pump Around	226.3	184	833	451	375683	0.6413
	184	154.9	833	451	375683	0.6038
LDO Pump Around	278.7	233.6	858	152	130416	0.6777
Stripped Kerosene	227.9	168	828	96	79488	0.6447
Stripped LDO	168	35.6	828	96	79488	0.5913
	280	207	863	158	136354	0.6769
	207	38.9	863	158	136354	0.6132
Stripped HDO	316	65.6	898	18	16164	0.6943
Atmospheric Residue	328	204	944	150	141600	0.6872
	204	164	944	150	141600	0.5838
	164	95.4	944	150	141600	0.5505
HVGO	241	222	927	10	9270	0.6203
Crude from Storage	29.9	134.9	841	310	260710	0.4648
Desalted Crude	134	212	841	306	257346	0.5567
Pre-flashed Crude	212	344	841	529	444889	0.6256

Table 2 Utility Streams Data [24]

Utility Stream Data					
Name	Inlet Temp (°C)	Outlet Temp (°C)	Heat Transfer Coeff (Kj hm ⁻² °C)	Flow Rate Kg/H	Specific Heat Capacity (Kcal Kg ⁻¹ °C)
Air	25	30	399.60	43074232.05	0.5919
Cooling Water	20	25	13500.00	84786.75	0.6777
Fuel Oil	400	350	720.00	479529.21	0.6256

The basic information needed for the simulation includes the inlet and outlet temperature of the process and utility streams, and the enthalpy or heat capacity value of the streams. The data was extracted correctly taking into consideration basic data extraction principles such as – avoiding mixing of the streams at different temperatures; extracting streams on the safe side; segmenting streams with varying enthalpies; and not extracting true utility streams that can be replaced by other streams [25]. The specific heat capacity of petroleum products were calculated using the empirical formula:

$$C_p = \frac{1}{\sqrt{d}} [0.402 + 0.00081t] \tag{1}$$

where *d* is the specific gravity of the petroleum product at 15°C, *t* is the temperature in °C, and *C_p* is the specific heat (Kcal/Kg°C).

The extracted data was later imputed into Aspen Energy Analyser® for the analysis of the design and retrofitting of the existing design.

B. Heat Exchanger Network Analysis

The heat exchanger network is represented using a grid diagram as shown in Fig. 2. In order to avoid the error of solving the wrong problem, care was taken to represent the heat exchanger network as it appears on the case studies’ process flow diagram as shown in Fig. 1. The heat exchangers network was fully solved with all process streams satisfied. This is necessary to enter the retrofit design mode of the simulation software.

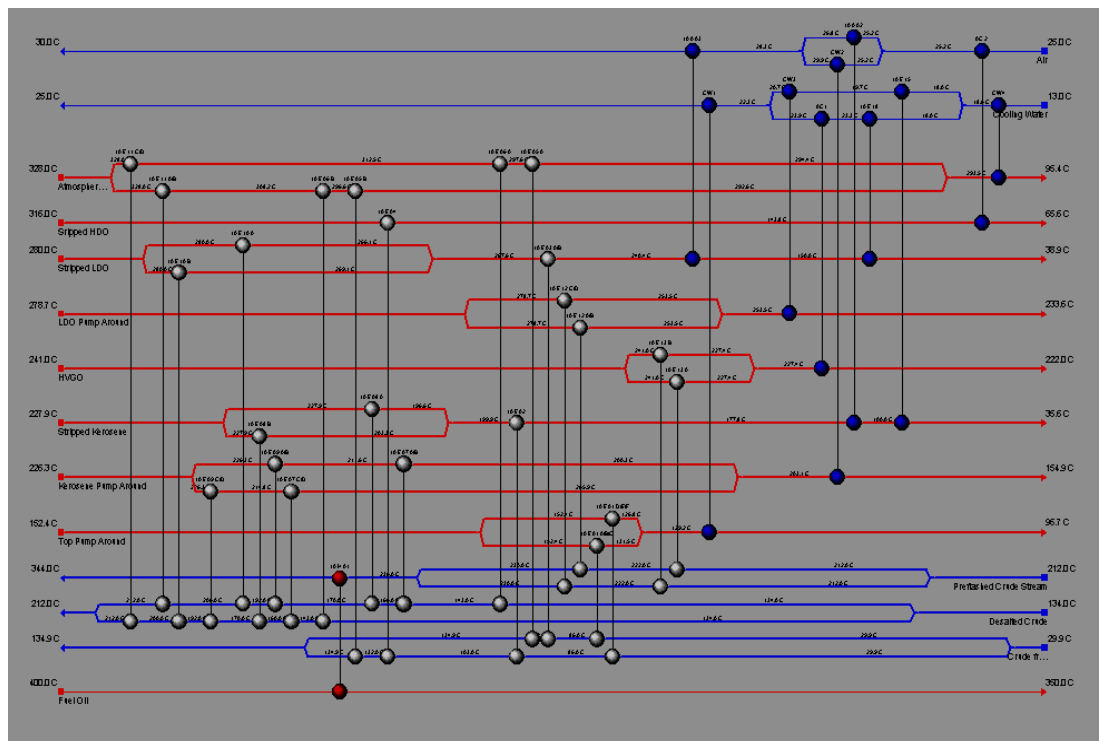


Fig. 2 Grid Diagram Representations of the Heat Exchangers

The analysis of the heat exchanger network determines the targets - energy requirement, area requirement, Pinch temperature, number of design units, and the cost index targets - based on the imputed process and utility stream data. The targets were generated based on the composite curves and minimum

approach temperature, ΔT_{min} . Targeting provides the optimal operating condition for an ideal heat exchanger network based on the imputed process and utility streams. The range targeting feature of the software was used to determine the optimal minimum approach temperature ΔT_{min} for the design. The minimum approach temperature provided a balance between the capital and operating costs. Figs. 3 and 4 show the composite and grand composite curves used for energy and utility targeting, while Table 3 shows the generated targets.

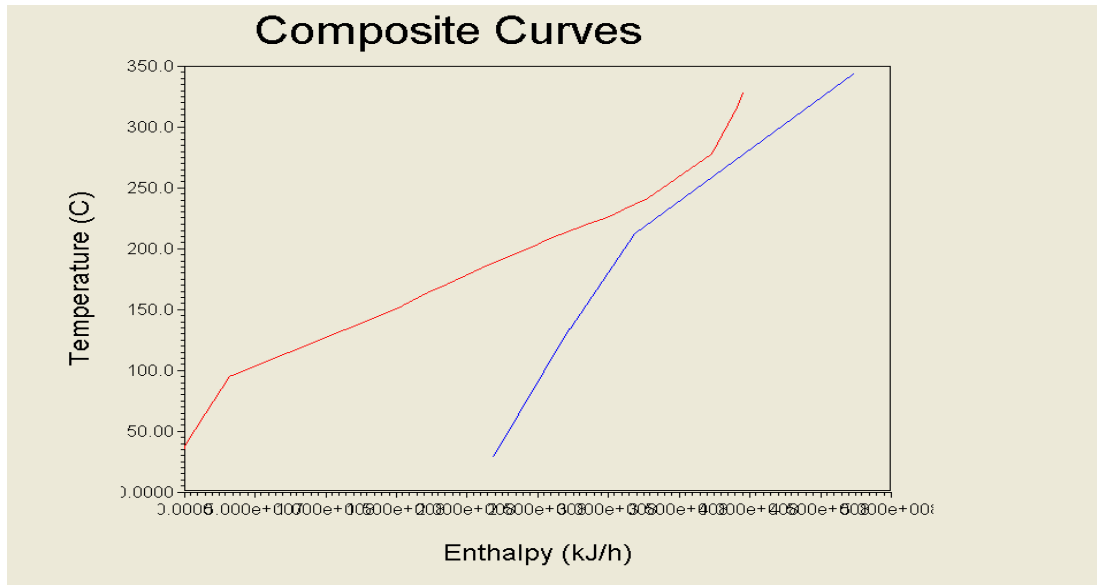


Fig. 3 Composite Curve showing Temperature – Enthalpy Relationship

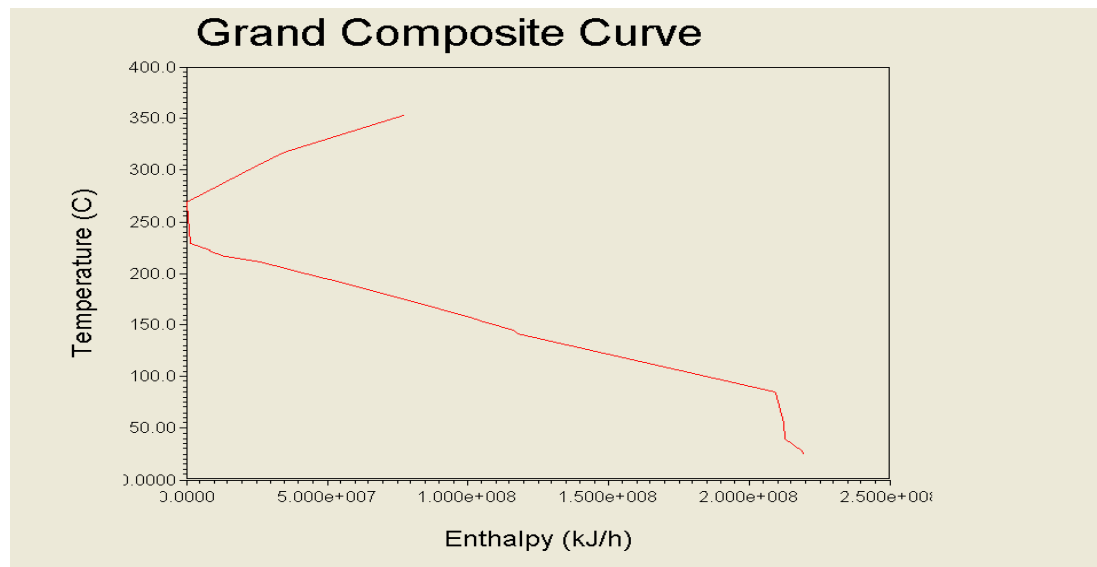


Fig. 4 Grand Composite Curve used for Utility Targeting

Table 3 Targets based on the Case Study Data

Target Summary		
Energy Target (Kj/h)	Area Target (m²)	Pinch Temp
Heating 7.759*10 ⁷	Counter Current 2.601*10 ⁴	Hot Cold
Cooling 2.196*10 ⁸	1-2 Shell & Tube 3.223*10 ⁴	278.7 258.2
		45.5 25.0
Number of Units	Cost Index Targets	
Total Minimum 13	Capital (Cost) 7.759*10 ⁷	
Minimum MER 4	Operating (cost/s) 0.2581	
Shells 26	Total Annual (cost/s) 0.3187	

The energy targets are calculated using composite curves. The composite curve provides a counter current picture of heat transfer, and can be used to determine the minimum energy target for the process. From Table 3 the energy target for the process is 7.759×10^7 KJ/h and 2.196×10^7 KJ/h for the heating and cooling respectively, while the area target is 3.223×10^4 m² for the shell and tube heat exchanger.

The calculation also show that a minimum of 13 units is required to build the heat exchanger network, but from the process flow diagram about 24 process to process heat exchangers are used in the network showing that the network is above the unit targets. The cost index targets are based on Aspen Energy Analyser® default cost and economic parameters, since cost and operations information could not be obtained for the case study.

III. RESULTS AND DISCUSSION

A Heat Exchanger Network Performance

The heat exchanger network performance was evaluated based on the targets in Table 3. The comparison of the targets and the performance of the heat exchanger network are depicted in Table 5. It can be seen that the heat exchanger performance differs greatly from the target values.

Table 5 Heat Exchanger Network Performance Data

Network Performance				
Parameter	Network Value	Target Value	Deviation	% Deviation
Heating Value (KJ/h)	1.328×10^8	7.759×10^7	5.521×10^7	71.15
Cooling Value (KJ/h)	2.748×10^8	2.196×10^8	5.52×10^7	25.14
Number of Units	24	13	11	84.62
Number of Shells	50	26	24	92.31
Total Area (m ²)	1.735×10^4	3.223×10^4	-1.488×10^4	-46.17

The heating and cooling value are above the target by 71.15% and 25.14% respectively. This is due to gross pinch rule violation as shown in the cross-pinch heat exchangers of Table 4. The consequence of a cross-pinch heat transfer is that both the cold and hot utility will increase by the cross-pinch duty. This results in an increase in the heat exchanger network size beyond the target [4, 24]. For the 278.70°C/258.20°C pinch temperature, there is cross pinch load of 5.517×10^7 KJ/h, while for the 45.5°C/25°C pinch temperature, the cross pinch load is 1.717×10^8 KJ/h.

Table 4 Cross Pinch Table

HEN Design Cross Pinch		
Heat Exchanger	278.70/258.20	45.50/25.00
E-249 (KJ/h)	3.284×10^7	
10 E 11 A-D (KJ/h)	7.193×10^6	
10 E 18 A/B	6.013×10^6	7.263×10^7
10 E 06 A/B (KJ/h)	5.395×10^6	
10 E 04 (KJ/h)	1.752×10^6	
E-248 (KJ/h)	1.470×10^6	
10 E 10 A-B (KJ/h)	5.020×10^6	
10 E 16 (KJ/h)		3.656×10^7
CW 2 (KJ/h)		4.675×10^6
CW 1 (KJ/h)		3.972×10^7
CW 3 (KJ/h)		7.361×10^6
10 E 15 (KJ/h)		1.072×10^7
Total (KJ/h)	5.517×10^7	1.717×10^8

The number of heat exchanger units and number of shells is above the target value by 84.62% and 92.31% respectively. While the target value generated by the software suggest that at least 13 heat exchangers having 26 shells can be used to accomplish the crude heating demand, the network actually uses 24 heat exchangers having 50 shells. The network design however uses less area than the target area. While this is good, area optimisation is not enough. The equipment cost also needs to be optimised.

From the network performance it can be seen that the operational network design is far above target. The cross load is quite high supporting the fact that the heat exchanger network was designed during the cheap energy era. It also shows that pinch technology was not applied during the design of the heat exchanger network. Thus a retrofit is needed. This will help to eliminate the cross loads and optimise energy utilisation during crude preheating.

B Retrofit Design

To ensure that the software performs the retrofit efficiently, the following approach was used. The scope of the problem was reduced by minimising stream segmentation, and reducing the number of heat exchangers in the network. This simplifies the network and increases the efficiency of the model. The process to process heat exchangers were in pairs, in the retrofit design one of the two heat exchangers is used. This does not alter the design since one is always in use while the other is on standby. The simplified network design for retrofit purpose is shown in Fig. 5.

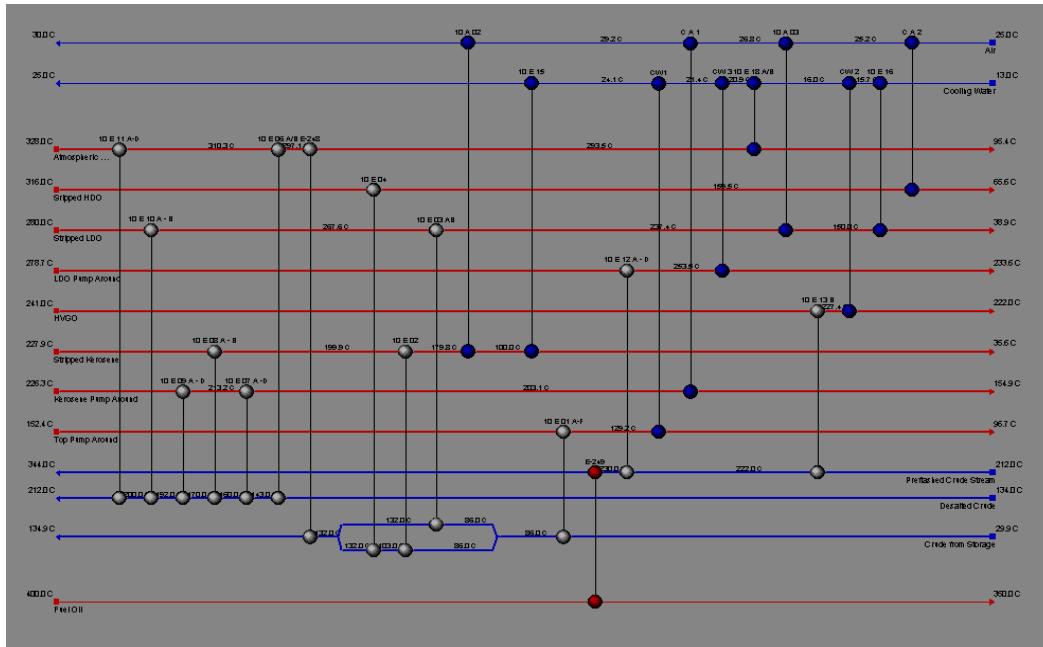


Fig. 5: Retrofit Design Grid Diagram

The retrofit design with no cross pinch violation is shown in Fig. 6. The same number of heat exchangers is used to accomplish the heating of the crude but some of the process stream temperatures are altered to avoid transferring heat across the pinch. The modifications made to the process streams to achieve this are shown in Piagbo [26]. Other retrofit designs such as modifying utility heat exchangers; re-sequencing heat exchangers; re-piping heat exchangers; addition of new heat exchangers; and addition of new area, did not provide an economically viable option as the design eliminating cross pinch heat exchangers [27]

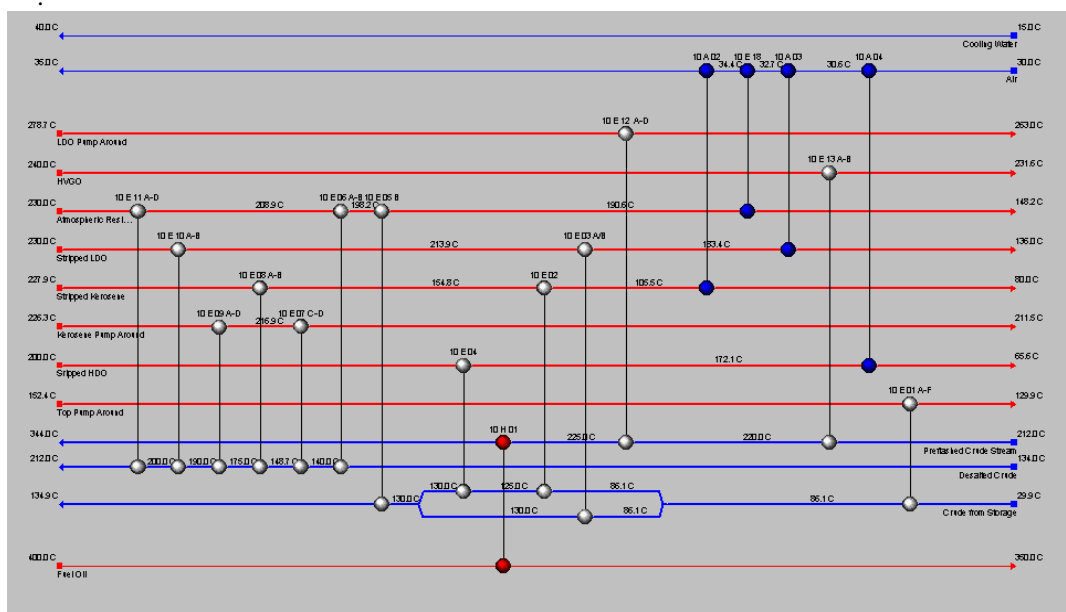


Fig. 6 Retrofit Designs Eliminating Cross Pinch Heat Exchangers

Table 6 Comparison of Retrofit Design Eliminating Cross Pinch Heat Exchangers with Base Case

Eliminating Cross Pinch Exchangers				
Network Cost Indexes				
Parameter	Retrofit Design	Base Case	Deviation	% Deviation
Heating (Cost/sec)	0.1313	0.1169	0.0144	12.32
Cooling (Cost/sec)	3.887*10 ²	8.709*10 ²	-482.2	-55.37
Operating (Cost/sec)	0.1702	0.2040	-0.0338	-16.57
Capital (Cost)	4.554*10 ⁶	4.682*10 ⁶	-128000	-2.74
Total Cost (Cost/sec)	0.2166	0.2518	-0.0352	-13.98
Network Performance				
Parameter	Retrofit Design	Base Case	Deviation	% Deviation
Heating Value (KJ/h)	1.491*10 ⁸	1.328*10 ⁸	1.63*10 ⁷	12.27
Cooling Value (KJ/h)	2.413*10 ⁷	2.748*10 ⁸	2.5067*10 ⁸	-91.22
Number of Units	18	24	-6	-25
Number of Shells	47	50	-3	-6
Total Area (m ²)	1.805*10 ⁴	1.735*10 ⁴	700	4.04

Table 6 compares the network cost indices and the network performance of the retrofit design eliminating all cross pinch exchangers and the original case study design. From the table, the value of the retrofit design eliminating all cross pinch exchangers is clearly seen. Despite the 12.3% increase in heating cost and heating value respectively, the retrofit design operates at about 14% reduced total cost compared with the case study design. There is significant reduction in the cooling cost and cooling duty by 55.37% and 91.22% respectively. The 18.97% reduction in the number of shells and 47.1% reduction in the number of exchanger units translate into a 16.57% and 2.74% reduction in operating cost and capital cost respectively. The 4.04% increase in total area of the retrofit design over the original design is understandable because pinch principle violation and misapplication of the driving force principle leads to reduced area in the network design [14].

The retrofit design 'eliminating cross pinch exchangers' provides huge energy and cost savings as can be seen in the reduction in cooling value, operating cost, capital cost and total cost. There is a 16.57% reduction in the operating cost. This confirms the fact that for HEN with gross cross pinch violation or misapplication of the ΔT_{min} driving force principle, providing a retrofit design that eliminates the cross pinch and proper application of the minimum driving force provides viable retrofitting option [4, 14, 25]. This design is promising, however, the cost implication involved in the modification of the process temperatures and areas of the heat exchanger network have to be considered in implementing this design.

IV. CONCLUSION

Process integration has assumed an unusual dimension in process industries due to globalisation and the need for business concerns to remain economically viable in a stiff competitive economic environment. Process integration ensures that energy is conserved and properly utilised in the industry. Aspen Energy Analyser® software of Aspen Technologies was used for the retrofit operation. The software combines pinch technology and mathematical programming in providing automatic retrofit designs to existing heat exchanger networks. Besides retrofitting, the software also has capabilities for automatic heat exchanger network designs and simulation of individual heat exchangers. The analytical capability of the software was also useful in determining targets and minimum approach temperature requirement for a given set of process and utility data. The manually generated retrofit design which eliminates all cross pinch exchangers required some modification to the temperatures of the process streams to avoid violation of pinch principle and exchanging heat beyond the allowed minimum temperature requirement. The costs of these modifications need to be evaluated and compared with the operational cost savings to ascertain the economic viability of the design.

REFERENCES

- [1]. F. Friedler, Process integration, modelling and optimisation for energy saving and pollution reduction, *Applied Thermal Engineering* 30, 2010, 2270-80
- [2]. E.C Hohmann, Optimum Networks for Heat Exchange, PhD Dissertation University of southern California, Los Angeles CA 1971
- [3]. M. Morar, and P.S Agachi, Review: Important contributions in development and improvement of the heat integration techniques, *Computers & Chemical Engineering*, 34, 2010, 1171-79
- [4]. T.N Tjoe, Retrofit of Heat Exchanger Networks. Ph.D Thesis UMIST England. 1986.
- [5]. B. Linnhoff, T.N Tjoe, Using pinch technology for process retrofit, *Chemical Engineering*, 93, 1986, 47-60.

- [6]. B. Linnhoff, and E. Hindmarch, The Pinch Design Method for Heat Exchanger Networks. *Chemical Engineering Science* 38 (5), 1983, 745-763
- [7]. K.K Trivedi, B. K. O'Neill, and R.M. Roach, A new dual-temperature design method for the synthesis of heat exchanger networks, *Computers & Chemical Engineering*, 13, 1989, 667-85
- [8]. A. Carlsson, P.A. Franck, and T. Berntsson, Design better heat exchanger network retrofits, *Chemical Engineering Progress*, March; 1993, 87-96
- [9]. A.R. Ciric and C.A. Floudas, A retrofit approach for heat exchanger networks, *Computers & Chemical Engineering*, 13: 1989, 703-15
- [10]. A. R. Ciric and C.A. Floudas, A comprehensive optimization model of the heat exchanger network retrofit problem, *Heat Recovery Systems and CHP*, 10: 1990, 407-22
- [11]. T.F Yee and I.E Grossmann, A screening and optimization approach for the retrofit of heat-exchanger networks, *Industrial & Engineering Chemistry Research*, 30, 1991, 146-62
- [12]. K. Ma, C. Hui, and T.F. Yee, Constant approach temperature model for HEN retrofit. *Applied Thermal Engineering*, 20, 2000, 1505-33.
- [13]. V. Briones, and A. Kokossis, A new approach for the optimal retrofit of heat exchanger networks, *Computers & Chemical Engineering*, 20, 1996, S43-S48
- [14]. N.D.K. Asante, and X.X. Zhu, An automated and interactive approach for heat exchanger network retrofit, *Chemical Engineering Research and Design*,; 75, 1997, 349-360
- [15]. G. Athier, P. Floquet, L. Pibouleau, and S. Domenech, Synthesis of heat - exchanger network by simulated annealing and NLP procedures, *AIChE Journal*, 43: 1997, 3007-3020
- [16]. D. Bertsimas, and J. Tsitsiklis, Simulated annealing, *Statistical Science*, 8, 1993 10-15
- [17]. M. Ravagnani, A.P. Silva, P.A. Arroyo, and A.A Constantino, Heat exchanger network synthesis and optimisation using genetic algorithm, *Applied Thermal Engineering* 25: 2005, 1003-17.
- [18]. J. Jezowski, R. Bochenek, and G. Poplewski, On application of stochastic optimization techniques to designing heat exchanger and water networks, *Chemical Engineering and Processing: Process Intensification*, 46, 2007, 1160-74.
- [19]. B. Allen, M. Savard-Goguen, and L. Gosselin, Optimizing heat exchanger networks with genetic algorithms for designing each heat exchanger including condensers, *Applied Thermal Engineering*, 29, 2009, 3437-3444.
- [20]. E. Rezaei, and S. Shafiei, Heat exchanger networks retrofit by coupling genetic algorithm with NLP and ILP methods, *Computers & Chemical Engineering*, 33, 2009, 1451-59
- [21]. H. Soltani, and S. Shafiei, Heat exchanger networks retrofit with considering pressure drop by coupling genetic algorithm with LP (linear programming) and ILP (integer linear programming) methods, *Energy*, 36, 2011, 2381-91
- [22]. A. Osman, M.I. Abdul Mutalib, M. Shuhaimi, and K.A. Amminudin, Paths combination for HENs retrofit, *Applied Thermal Engineering*, 29: 2009, 3103-09.
- [23]. K.R. AJao, and H.F. Akande, Energy integration of crude distillation unit using pinch analysis. *The Researcher*, 1(2), 2009, 54-66
- [24]. New Port Harcourt Refinery Company Limited Brochure (NPHRC), Nigeria National Petroleum Corporation (NNPC), Bureau of Public Enterprises 2005: 1-15.
- [25]. LinnhoffMarch. Introduction to Pinch Technology [Pdf] Available: <http://www.ou.edu/class/che-design/a-design/Introduction%20to%20Pinch%20Technology-LinhoffMarch.pdf> [Accessed 25th March, 2011]. 1998.
- [26]. B. K. Piagbo, Using Simulation Modelling to Improve the Performance of Chemical Engineering Processes: Retrofitting of the Port Harcourt Refinery Heat Exchanger Network (HEN) as Case Study, Master Thesis Teesside University Middlesbrough England, 2011
- [27]. K. K. Dagde, B. K. Piagbo, Using Simulation Modelling to Improve the Performance of Chemical Engineering Processes: Part 2 – Retrofitting Heat Exchanger Network, *International Journal of Pure Applied Science and Technology*, 12 (2), 2012, 8-19, 2012

Production of Wine from Ginger and Indian Gooseberry and A Comparative Study of Them over Commercial Wine

Giri Nandagopal.M.S^a, Praveen.S.Nair^b

a,b- Post Graduate Scholars, Department of Chemical Engineering,
Kongu Engineering College, Perundurai, Erode, India- 638052.

Abstract: Wine is one of the functional fermented foods that have many health benefits. Commercially, wine is produced by the fermentation of yeast which involves the conversion of sugar to alcohol. Wine can act as a nutrient supplement for seasonal fruits and vegetables throughout the year. Using fruits and vegetables having medicinal and nutritional value as a substrate for wine production, the health benefits of them can be improved widely. Ginger and Indian gooseberry, which are known for its high medicinal and nutritional value are used as the substrate here. Fermentation is carried out with *Saccharomyces cerevisiae* commonly known as bakers yeast. Daily monitoring was done to study the composition and characteristics of the wine. The wine produced resembled the commercial wine in terms of its composition, taste and aroma. During the fermentation period the wines were analyzed for pH, titratable acidity, specific gravity, biomass content, alcohol and reducing sugar on a daily basis. pH show a decreased trend then attains minima and then increased. As the fermentation days proceed, the specific gravity increased and the alcohol percentage increased gradually. Batch 1 Amla (A1) showed a pH range of 3.79-3.56, specific gravity ranges from 1.09 -1.17 and alcohol content was 10.5%. Batch 2 Amla (A2) showed a pH range of 3.81-3.30, specific gravity ranges from 1.09 -1.167 and alcohol content was 10.35%. Batch 3 Amla (A3) showed a pH range of 3.83-3.34, specific gravity ranges from 1.032 -1.0967 and alcohol content was 8.64%. Batch 1 ginger (G1) showed a pH range of 3.77 -3.59, specific gravity ranges from 1.11 -1.178 and alcohol content was 7.94%. Batch 2 ginger (G2) showed a pH range of 3.89 -3.94, specific gravity ranges from 1.116 -1.162 and alcohol content was 6.81 %. Batch 3 ginger (G3) showed a pH range of 4.42 -4.01, specific gravity ranges from 1.144 -1.188 and alcohol content was 5.81%.

After the fermentation period parameters such as Tannin content, Phenol content, Free and Total SO₂, Alcohol content, Total Suspended Solids (°Brix), pH, Titratable Acidity and Specific Gravity were analyzed. These parameters were compared with that of commercial wine. The tannin content of the 3 batches of amla and ginger wine ranges between 3.1 to 0.4mg/100ml but the commercial wine contain only 0.28mg/ml. When comparing phenol content, the commercial wine showed a value of 0.20mg/ml but the 3 batches of wine had a higher range of 0.7 to 0.9mg/ml. The total suspended solids of the amla and ginger wines were between 43 to 45°brix. But for commercial wine the TSS was 32.23°brix. The pH showed a different trend. pH of amla is between 3.3 and 3.5 but for ginger it ranges from 3.7 and for commercial its 3.56 which is relatively higher than amla. The specific gravity is lower for the 3 batches of amla and ginger wine which ranges from 1.2 to 1.21 but 1.24 is the specific gravity of commercial wine. The titratable acidity showed for ginger wine is 2 to 3.5mg/ml but for amla it is 8.9 to 5.5mg/ml. the commercial wine had a value higher than ginger i.e., 4.2mg/ml. Thus the studies showed that the pH (except ginger), specific gravity and alcohol content were higher for commercial wine. But the phenol, tannin content and total suspended solids is higher for homemade wine. By comparing the titratable acidity with commercial wine, ginger wine showed lower value.

Keywords: ginger, amla, wine, product, substrate, biomass

I. INTRODUCTION

Home winemaking is an enjoyable, educational and satisfying hobby. Winemaking recipes make the process easy and simple instructions ensure success. The basic steps are easy to learn and practice. The traditional homemade wine base ingredient is the grape because it naturally contains the correct mix of sugar, moisture, tannin, and nutrients required for fermentation and preservation, and it even carries its own yeast. But

in truth, wine can be made from almost any non-toxic plant or plant part if additional ingredients are supplied in the correct amount. So the process of making wines from various types of fruits, vegetables and spices is no more complicated than making wine from grapes and it is a good preservation method. It needs extra preparation steps and some adjustments in sugar content, acid levels etc. Fermentation can extract valuable components from the raw materials used for production. Yeast is the magical ingredient that turns fruit juices into wine. In spontaneous fermentations, the 1st stages invariably being dominated by the alcohol-tolerant strains of *Saccharomyces cerevisiae*. This species is universally known as the 'wine yeast' and is widely preferred for initiating wine fermentations. The alcohol content of home-made wines is only about 7-8% which makes it consumable for persons of any age group. Though ginger wine contains small amounts of alcohol, it is not harmful, but health-giving, digestible, and stimulates the release of the hormone gastrin, which in turns stimulates the release of enzymes in the stomach. Thus, wine stimulates the release of digestive enzymes, which digest not only the alcohol but the many other nutrients found in wine. The proper dosage, or a moderate intake of wine, in addition to affecting cholesterol levels favourably, decreases the tendency of blood to clot and assists in dissolving clots, all important factors in protecting against heart disease. Research also indicates that moderate wine drinking may reduce the tendency of arteries to constrict during stress, lower blood pressure, and increase coronary artery diameter and blood flow. More recently, wine has been identified as a dependable source of quercetin, a potent anti-carcinogen, and of many flavonoids and other polyphenolic antioxidants. Considering the importance and medicinal value of wine from some special raw materials, it was very interesting to conduct the production of wine in a batch reactor setup in the laboratory. We selected Indian Gooseberry and Ginger for our study. Indian gooseberry (*Emblica officinalis* Gaertn.), is one of the useful fruit. It is consumed as a fresh fruit or in the form of food products like preserve. The fruit also forms an important constituent of many Ayurvedic preparations such as *aschyvanprashand triphala* and is regarded as "one of the best rejuvenating" herbs preparation of wine using the fruits of amla would be useful for imparting healthful properties to the wine. Ginger which act as a useful food preservative is a tuber that is consumed whole as a delicacy, medicine, or spice. It is the rhizome of the plant *Zingiber officinale*.

II. MATERIALS AND METHODS

Winemaking, or vinification, is the production of wine, starting with selection of different fruits and ending with bottling the finished wine. We had developed a batch reactor in our lab for wine production as shown in the fig 2 and 3.



Fig.2: Ginger Wine



Fig.3: Amla Wine

The picking of the fruits and spices is the first step in wine production. Crushing is the process of gently squeezing the fruits and spices and breaking the skins to start to liberate the contents. In our project, ginger is grinded and amla is used as it is. To start primary fermentation yeast is added. During this fermentation, which often takes between one and two weeks, the yeast converts most of the sugars in the fruits into ethanol (alcohol) and carbon dioxide. In our case, ginger takes about 14 days and amla about 21 days. Filtration in winemaking is used to accomplish the objective of clarification. In clarification, large particles that affect the visual appearance of the wine are removed.

4.2 Daily Monitoring

pH was measured using digital pH meter. The total sugars were estimated in terms of glucose by Nelson Somogyi method. Estimation of titratable acids was done by titrimetric method using 0.1N NaOH in terms of tartaric acid. Biomass was determined by dry weight method in g/ml. Alcohol percentage was calculated using specific gravity method. Specific gravity was also determined.

4.3 Final Analysis of Wine

Tannin content was estimated by Folin – Denis method in mg/100ml. Phenol content was determined by Folin Lowry method in mg/100ml. Free and total SO₂ was done by Ripper method in g/L. Total suspended solids was calculated in Degree Brix. Final analysis of all parameters such as pH, alcohol content specific gravity, sugar content, titratable acidity, and biomass were conducted using the methods described in daily analysis.

4.4 Analysis of Commercial Wine and Its Comparison

Estimate parameters such as pH, alcohol content specific gravity, sugar content, titratable acidity, biomass, tannin content, phenol content, free and total SO₂ and total suspended solids of the commercially available wine were conducted. The parameters of the homemade wine were compared with that of the commercially available wine.

III. RESULTS AND DISCUSSIONS

Production of wine from ginger and Gooseberry conducted in the lab in batch reactor set up. Process monitoring and final analysis of homemade wine has been conducted. Various parameters such as pH, Titratable acidity, biomass concentration, etc of homemade wine was determined. Experiments were conducted and results are given in tables 1 to 6 and figures 4 to 33. Final analysis of prepared wine and commercial wine was also conducted. Results are shown in Tables. The 1st batch ginger and amla wine samples were denoted as G1 and A1 respectively, similarly for 2nd batch G2 and A2 and for 3rd batch G3 and A3.

5.1 Process Monitoring (Daily)

Daily analysis of homemade wine (fermented medium) has been conducted. Various parameters such as pH, Titratable acidity, specific gravity, alcohol content, sugar concentration, biomass concentration, etc of each batch were determined day by day during the course of fermentation. Results are shown in tables 1-6 and shown in figures 4-33.

Parameters monitored during fermentation period:

- Variation in pH
- Sugar concentration
- Specific gravity
- Alcohol percentage
- Biomass
- Titratable acidity

Daily monitoring of G1, G2 and G3 were shown in tables – 4, 5, 6. And that of A1, A2 and A3 are shown in tables – 1, 2 and 3.

5.1.1 pH

Variation in pH in the fermentation medium during the course of process was as shown in the figure. pH showed a decrease trend then attains minima then increases. The initial pH of G1 was 3.77 which decrease to 3.41 on the 8th day and increased to 3.59 on 14th day. For G2, the pH started from 3.89 and decreased to 3.63 on 5th day and attains a steady value 3.94 on 18th day. On the 1st day the pH was 4.4 for G3 and then it decreased to 3.79 on 7th day and increased to 4.01 on 13th day (fig: 19, 24 and 29).

In case of A1, pH was 3.79 on 1st day which decreased to 3.25 on 12th day and showed an increment to 3.56 on 24th day. pH for A2 on 2nd day was 3.81 and showed a trend to decrease to 3.16 then increased to 3.33 on 22nd day. 3.83 was the starting pH of A3 which decreased to 3.16 on 12th day and then increased to 3.34 on 21st day (fig: 4, 9 and 14).

5.1.2 Substrate (Sugar) concentration

The sugar concentration of different wine samples – G1, G2, G3, A1, A2 and A3 has been obtained. As the figure shows, the sugar concentration of wine decreases as the fermentation days passed because of the utilization of substrate. The sugar concentration lies between 25 mg/100ml to 10mg/100ml.

In case of G1, the initial sugar concentration was 23.01mg/100ml which decreased to 11.63mg/100ml on 14th day. Sugar concentration for G2 on 2nd day was 24.81mg/100ml and shows a trend to decrease to 10mg/100ml on 18nd day. 24.44mg/100ml was the starting sugar concentration of G3 which decreased to 12.4mg/100ml on 13th day (fig: 23, 28 and 33). Initial sugar concentration of A1 was 21.78mg/100ml which decreased to 9.29 on the 24th day. For A2, the sugar concentration started from 26.00mg/100ml and decreased to 12.82mg/100ml on 22nd day. On the 1st day the sugar concentration was 22.30mg/100ml for A3 and then it decreased to 11.4mg/100ml on 21st day (fig: 5, 13 and 18).

5.1.3 Specific gravity

Estimation of specific gravity of G1, G2, G3, A1, A2 and A3 has been conducted. It has been studied that as the number of day's increases, the specific gravity also increases gradually. Specific gravity ranges from 1.10 to 1.18. Specific gravity for G1 on 1st day was 1.119 and shows a trend to increase to 1.178 on 14th day. 1.116 was the starting specific gravity of G2 which increased to 1.162 on 18th day. The initial specific gravity of G3 was 1.144 which increased to 1.188 on the 13th day (fig: 21, 26 and 31).

For A1, the specific gravity starts from 1.092 and increased to 1.17 on 24th day. On the 1st day the specific gravity was 1.09 for A2 and then it increased to 1.167 on 22nd day. In case of A3, specific gravity was 1.032 on 1st day which increased to 1.092 on 21st day (fig: 6, 12 and 17)

5.1.4 Alcohol percentage

By studying the alcohol content in volume percentage of G1, G2, G3, A1, A2 and A3 it can be concluded that the alcohol volume percentage increased as the number of day's increases. The figure indicates that the % alcohol was between zeros to 8 during the fermentation period of each batch. The initial alcohol percentage was zero for all wine samples – G1, G2, G3, A1, A2 and A3.

Final alcohol content for G1 was 11.63% on 14th day

G2 was 6.81% on 18th day.

G3 was 5.81% on 13th day (fig: 23, 28 and 33)

A1 was 10.5% on 24th day.

A2 was 10.35% on 22nd day.

A3 was 11.4% on 21st day (fig: 5, 13 and 18)

5.1.5 Biomass

Biomass estimation was conducted. The figure shows a rapid increase of biomass initially and reaches a maximum then tends to be steady. The initial biomass of G1 was 0.0056g/ml which increased to 0.019g/ml on the 11th day and decreased to 0.0119 on 14th day. For G2, the biomass started from 0.0021g/ml and increased to 0.033 on 11th day and decreased to 0.0162 on 18th day. On the 1st day the biomass was 0.0045g/ml for G3 and then it increased to 0.0160g/ml on 12th day and decreased to 0.0158g/ml on 13th day (fig: 22, 27 and 32).

In case of A1, biomass was 0.0063g/ml on 1st day which increased to 0.0167g/ml on 12th day and decreased to 0.0076g/ml on 24th day. Biomass for A2 on 2nd day was 0.0025g/ml and showed a trend to increase to 0.00184g/ml then decrease to 0.0112 on 22nd day. 0.0047g/ml was the starting biomass of A3 which increased to 0.0177g/ml on 16th day and then decreased to 0.011g/ml on 21st day (fig: 7, 11 and 16).

5.1.6 Titratable acidity

Titratable acidity of G1, G2, G3, A1, A2 and A3 was determined. The titratable acidity of wine shows a fluctuating trend as the number of days increase. The titratable acidity ranges from 3.5g/L tartaric acid to 7g/L tartaric acid. Titratable acidity of G1 ranges between 4.3 to 7.81 g/L tartaric acid. For G2, the range was 6.0 to 6.98 g/L tartaric acid. Initial titratable acidity of G3 was 4.12g/L tartaric acid and on 13th days it becomes 5.43g/L tartaric acid (fig: 20, 25 and 30).

In case of A1, 1st day titratable acidity was 4.12g/L tartaric acid and 5.43 g/L tartaric acid on final day. Titratable acidity for A2 on 2nd day was 3.33g/L tartaric acid and 10.5 g/L tartaric acid on final day. 2.50 was the starting titratable of A3 which increased to 12.45g/L tartaric acid on 21th day (fig: 5, 10 and 15).

5.2 Analyses of wine

Alcohol percentage, tannin content, phenol content, free and total SO₂, pH, specific gravity, titratable acidity and total suspended solid were estimated. Final analysis of wine was conducted after the fermentation period (i.e. after 15 days).

5.2.1 Alcohol Content

The Alcohol content of different wines during the aging period was 13.86% for A1, 12.10% for A2 and 10.62% for A3. Similarly for G1, G2 and G3 alcohol content was 10.62%, 9.25% and 8.64%. (table – 12).

5.2.2 Tannin content

Tannin content for A1, A2, and A3 were 3.06mg/ml, 3.14mg/ml and 2.19 mg/ml. Similarly for G1, G2, and G3 were 0.74mg/ml, 0.52mg/ml and 0.32mg/ml respectively (Table 7).

5.2.3 Phenol content

Phenol content for A1-0.69mg/ml, A2-0.58mg/ml, A3-0.30mg/ml, G1-2.96mg/ml, G2-2.59mg/ml and for G3 was 0.89 mg/ml (Table 8).

5.2.4 pH of wine

pH of A1 was 3.29 and that for A2 and A3 were 3.33 and 3.48 respectively. Similarly for G1, G2 and G3 were 3.68, 3.96 and 4.09 respectively (Table 10).

5.2.5 Free and Total SO₂

Free SO₂ for A1, A2, and A3 were 1.2g/L, 2.7g/L and 4.6 g/L respectively and this for G1, G2, and G3 were 6g/L, 31g/L and 48g/L.

2.5 g/L, 5.28 g/L, 15.6 g/L, 16.6 g/L, 39g/L and 78 g/L were the total SO₂ for A1, A2, A3, G1, G2 and G3 respectively (Table 9).

5.2.6 Titratable Acidity

Titratable acidity of different wine were 8.85, 8.4, 5.5, 3.45, 2.8 and 2.0 g/L tartaric acid for A1, A2, A3, G1, G2 and G3 respectively (Table 11).

5.2.7 Specific Gravity

Specific Gravity of different wine samples were 1.195 for A1 and 1.180 for A2, 1.114 for A3. Similarly specific gravity was 1.198 for G1, 1.180 for G2 and 1.204 for G3 (Table 13).

5.2.8 Total Suspended Solids

Total Suspended Solids in °Brix for A1, A2 and A3 was 42.7, 39.85 and 26.73. Similarly for G1, G2 and G3 were 43.18, 39.85 and 44.27 (Table 14).

5.3 Comparison

The comparison of final analysis of homemade wine with commercial wine was conducted and can be concluded that the pH (except ginger), specific gravity and alcohol content of commercial wine is higher than homemade wine. The pH of commercial wine (table- 15) was 3.56 but for A1, A2 and A3 (table- 10) were 3.29, 3.33, 3.48 whereas, for G1, G2 and G3 (table – 10) were 3.68, 3.96, 4.06 which is higher than commercial wine. 1.2407 is the specific gravity of commercial wine (table – 15) whereas for A1, A2, A3, G1, G2 and G3 (table – 13) were 1.195, 1.18, 1.14, 1.198, 1.1801 and 1.204. For commercial wine the percentage of alcohol is 80% (table – 15) but for homemade wines A1, A2, A3, G1, G2 and G3 (table – 12) is stated as 13.86%, 12.10%, 10.98%, 10.62%, 9.25% and 8.64%.

IV. CONCLUSION

Study mainly focused on the process monitoring of homemade wine during its fermentation period. The experimental investigation was aimed to study the variation in each parameter during the fermentation period. The final analysis of wine of various parameters – tannin content, alcohol content, pH, specific gravity were conducted. These studies were compared with that of commercially available wine. The study concludes that pH showed a decreasing trend and then attains minima then increases. The sugar concentration of wine decreases with increase in the number of days. It has been studied that as the number of day's passes, the specific gravity and volume percentage of alcohol also increases gradually. There was a rapid increase of biomass initially and reached a maxima then tend to decrease. The titratable acidity of wine showed a fluctuating trend as the number of days passes. Batch 1 Amla showed a pH range of 3.79-3.56, specific gravity ranges from 1.09 -1.17 and alcohol content was 10.5%. Batch 2 Amla showed a pH range of 3.81-3.30, specific gravity ranges from 1.09 -1.167 and alcohol content was 10.35%. Batch 3 Amla showed a pH range of 3.83-3.34, specific gravity ranges from 1.032 -1.0967 and alcohol content was 8.64%. Batch 1 ginger showed a pH range of 3.77 -3.59, specific gravity ranges from 1.11 -1.178 and alcohol content was 7.94%. Batch 2 ginger showed a pH range of 3.89 -3.94, specific gravity ranges from 1.116 -1.162 and alcohol content was 6.81 %. Batch 3 ginger showed a pH range of 4.42 -4.01, specific gravity ranges from 1.144 -1.188 and alcohol content was 5.81%. The final analysis of wine was conducted. The pH of commercial wine was 3.56 but for A1, A2 and A3 were 3.29, 3.33, 3.48 whereas, for G1, G2 and G3 were 3.68, 3.96, 4.06 which is higher than commercial wine. 1.2407 is the specific gravity of commercial wine whereas for A1, A2, A3, G1, G2 and G3 were 1.195, 1.18, 1.14, 1.198, 1.1801 and 1.204. For commercial wine the percentage of alcohol is 80% but for homemade wines A1, A2, A3, G1, G2 and G3 is stated as 13.86%, 12.10%, 10.98%, 10.62%, 9.25% and 8.64%. Homemade wines have relatively low alcohol content than the commercially available wine and there is no usage of either any preservative or any additives, so homemade wines are not harmful for health and are acceptable for daily usage. The results of process monitoring and final analysis will help a small scale wine industry or can refer the results to develop a small scale wine industry.

REFERENCES

- [1]. S K Soni, Namita Bansal and Raman Soni. 2009. "Standardization of conditions for fermentation and maturation of wine from Amla (*Emblica officinalis* Gaertn.)". *Natural Product Radiance*, Vol. 8(4) :436-444
- [2]. Rong-Rong Tian, Qiu-Hong Pan, Ji-Cheng Zhan., et al.2009. "Comparison of Phenolic Acids and Flavan-3-ols During Wine Fermentation of Grapes with Different Harvest Time". *Molecules*. 14, 827-838
- [3]. L. Wang Y. Xu G. Zhao and J. Li. 2004. "Rapid Analysis of Flavor Volatiles in Apple Wine Using Headspace Solid-Phase Microextraction". *Brewing Science and Technology*. VOL. 110.
- [4]. R. P. Bates and M. Sinisterra. 1977. "A Comparison of home, laboratory and quasi-industrial wine making procedures with stover grapes". *Florida Agricultural Experiment Stations Journal Series No. 836*.
- [5]. M.A.K.Ogunjobi and S.O Ogunwolu .2010. "Development ant Physicochemical evaluation of Wine from Cashew Apple Powder". *Journal of Food Technology* 8(1) 18-23.
- [6]. Nikhil Gupta, Soham Trivedi et al. ,2009, "Orange: Research analysis for wine study" ,*International Journal of Biotechnology Applications*, ISSN: 0975-2943, Volume 1, Issue 2, 2009, pp-10-15
- [7]. L Veeranjanya Reddy and O Vijaya Sarathi, 2009, "Production, optimization and characterization of wine from Mango (*Mangifera indica* Linn.)". *Natural Product Radiance*, Vol. 8(4), 426-435.
- [8]. Yannis Paraskevopoulos, 2009, "Optimization of the management conditions of malolactic fermentation in red wines of the nemea region".
- [9]. Daniel Weingart Barreto and Bernardo Dias Ribeiro. 2004, "Evaluation of oxidation processes of guarana tannins". *Escola de Química, UFRJ - Centro de Tecnologia, Bl.E*.
- [10]. Isak S. Pretorius, 2000. "Tailoring wine yeast for the new millennium: novel approaches to the ancient art of winemaking". *Yeast* 16: 675-729.
- [11]. D. Wang, Y. Xu. et al., 2004, "Fermentation Kinetics of Different Sugars by Apple Wine Yeast *Saccharomyces cerevisiae*". *Journal of the Institute of Brewing*, VOL. 110, NO. 4, 340-346.
- [12]. Ruiz-Larrea .F, B. Rojo-Bezares, et al.,2008 "Bacteriocins for wine microbiological control and reduction of SO₂ levels". *Instituto de Ciencias de la Vid y del Vino. Universidad de La Rioja. Complejo Científico Tecnológico*.

Table 1: Daily Monitoring Of Amla-1 (A1)

Days	pH	Titrateable Acidity (g/L tartaric acid)	Specific Gravity	% Alcohol	Sugar concentration (mg/ml)	Biomass (g/ml)
1	3.79	3.80	1.092	0	21.78	0.0063
4	3.65	3.33	1.103	1.013	19.92	0.0091
6	3.57	4.10	1.119	3.54	18.14	0.0116
8	3.47	4.56	1.123	3.71	17.26	0.0135
11	3.35	3.90	1.131	5.25	16.64	0.0154
12	3.25	5.33	1.136	5.94	15.55	0.0167
13	3.28	5.62	1.143	6.87	14.85	0.0168
14	3.33	6.23	1.149	7.6	14.12	0.0170
24	3.56	9.26	1.170	10.5	9.290	0.0172

TABLES AND GRAPHS

Table 2: Daily Monitoring Of Amla-2 (A2)

Days	pH	Titratable Acidity (g/Ltartaric acid)	Specific Gravity	% Alcohol	Biomass (g/ml)	Sugar concentration (mg/100ml)
2	3.81	3.3	1.09	0	0.0025	26.00
3	3.71	3	1.112	2.88	0.0040	25.91
4	3.70	2.4	1.119	3.95	0.0046	25.02
5	3.40	3.45	1.123	4.4	0.0057	24.37
8	3.2	6.45	1.136	6.16	0.0067	22.58
9	3.18	4	1.139	6.65	0.0082	20.67
10	3.16	3.75	1.143	7.1	0.0100	19.80
11	3.23	5.25	1.147	7.64	0.0146	19.11
15	3.25	5.4	1.155	8.72	0.0176	17.09
16	3.30	5.25	1.159	9.27	0.0184	16.48
17	3.31	7.05	1.16	9.4	0.0186	15.86
18	3.32	6	1.162	9.67	0.0188	15.20
22	3.3	10.5	1.167	10.35	0.0188	12.82

Table 3: Daily Monitoring Of Amla-3 (A3)

Days	pH	Titratable Acidity (g/Ltartaric acid)	Specific Gravity	% Alcohol	Biomass (g/ml)	Sugar concentration (mg/100ml)
1	3.83	2.50	1.032	0	0.0047	22.8
2	3.68	4.00	1.038	0.81	0.0067	22.0
5	3.27	7.80	1.040	1.35	0.0079	18.2
12	3.16	5.25	1.044	1.62	0.0122	16.8
13	3.25	9.30	1.00	2.62	0.0162	16.2
15	3.27	9.45	1.050	2.43	0.0195	16.0
16	3.30	10.05	1.055	3.10	0.0196	15.2
17	3.31	10.20	1.061	3.90	0.0198	14.8
19	3.32	11.11	1.069	5.00	0.0200	13.6
20	3.33	12.30	1.081	6.22	0.0210	12.2
21	3.34	12.45	1.096	8.64	0.022	11.4

Table 4: Daily Monitoring Of Ginger-1 (G1)

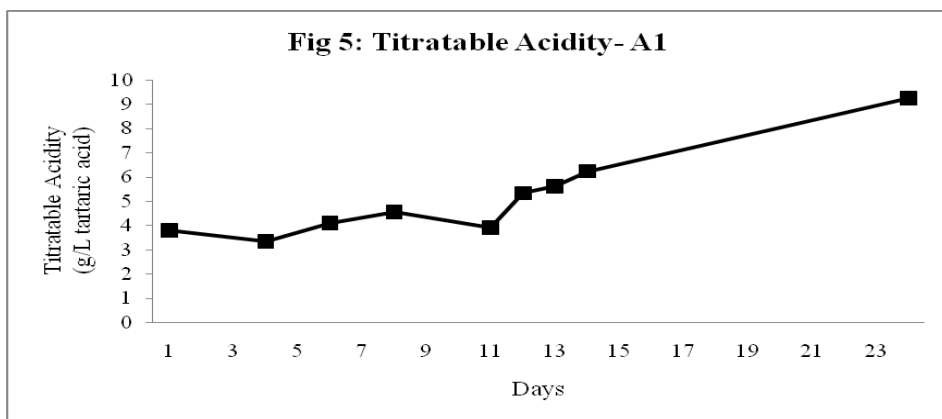
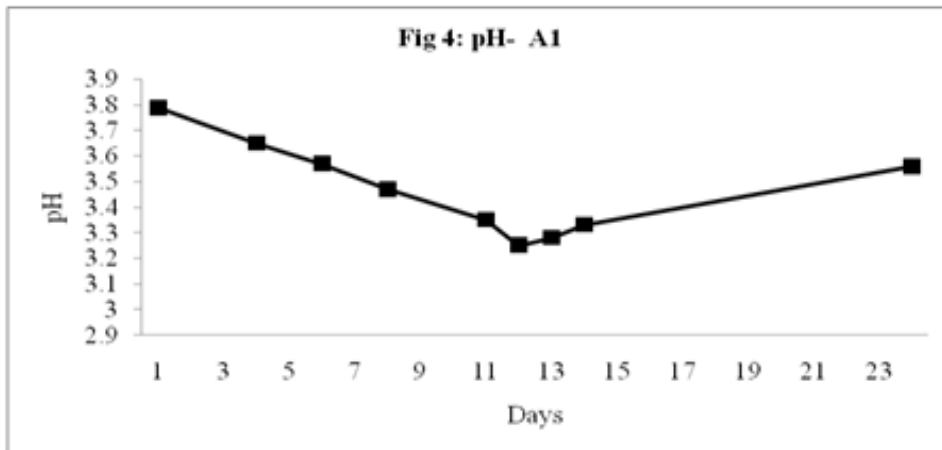
Days	pH	Titratable Acidity (g/L tartaric acid)	Specific gravity	% Alcohol	Sugar concentration (mg/100ml)	Biomass (g/ml)
1	3.77	4.30	1.119	0	23.01	0.0056
4	3.62	6.41	1.131	1.56	20.50	0.0109
6	3.57	5.87	1.147	3.72	18.67	0.0126
8	3.41	6.12	1.154	4.67	17.01	0.0139
11	3.52	5.89	1.164	6.02	15.39	0.0159
12	3.54	7.26	1.169	6.68	14.91	0.0160
13	3.55	7.56	1.172	7.14	13.13	0.0161
14	3.59	7.81	1.178	7.94	11.630	0.0163

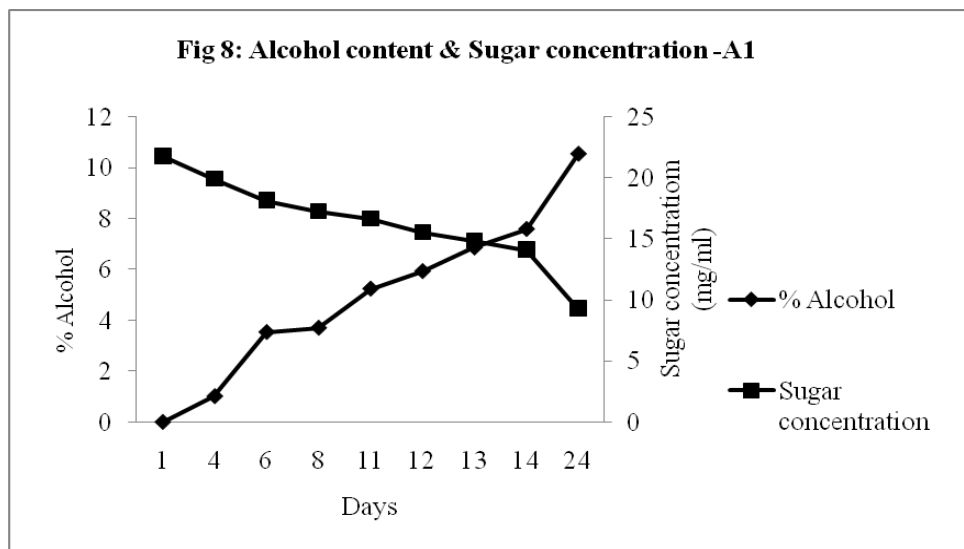
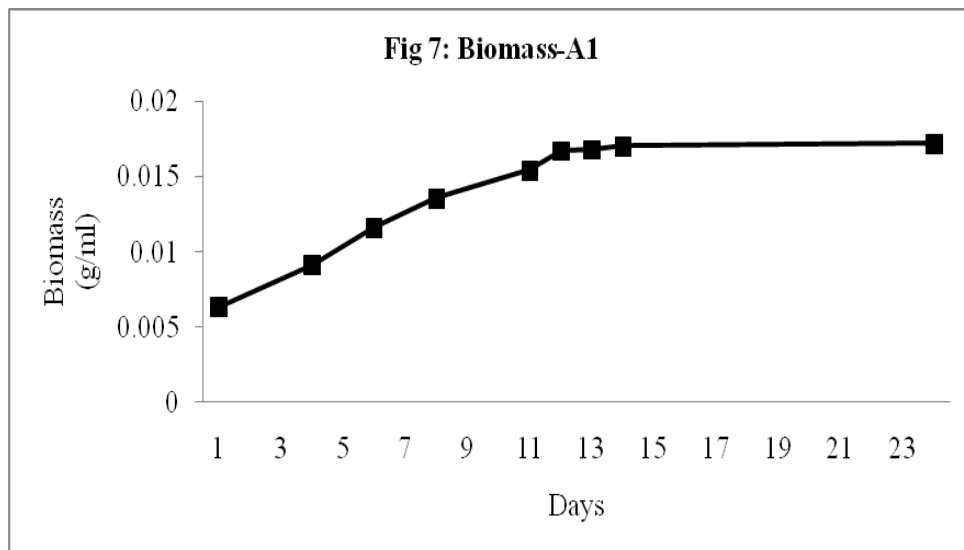
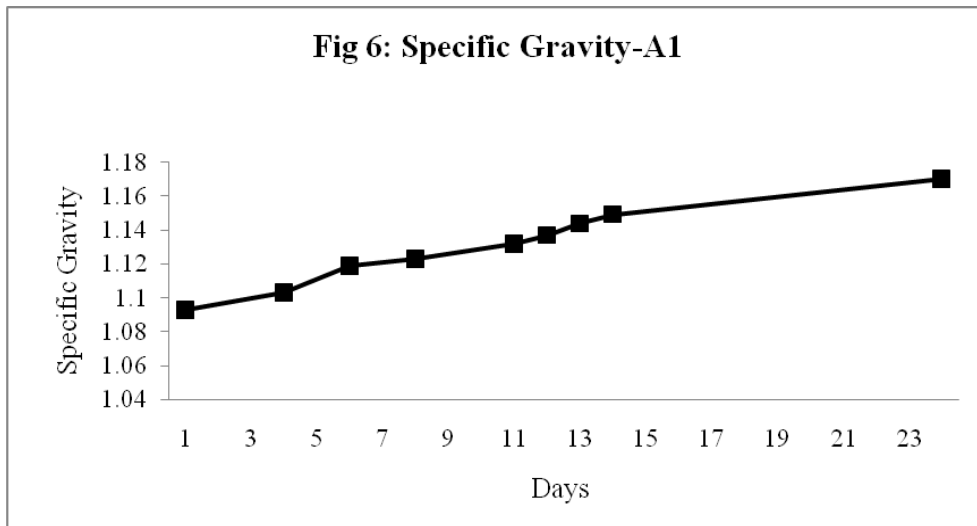
Table 5: Daily Monitoring Of Ginger-2 (G2)

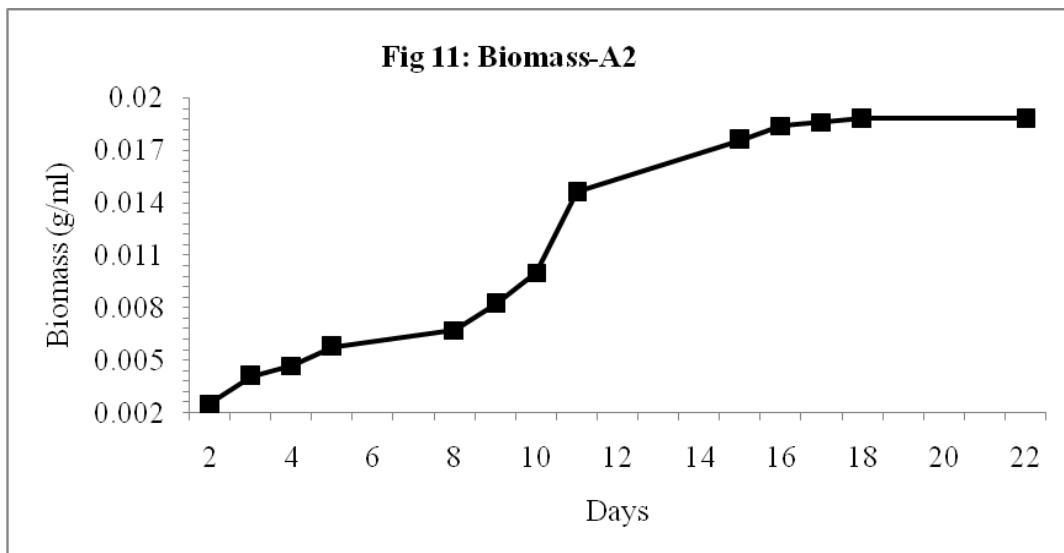
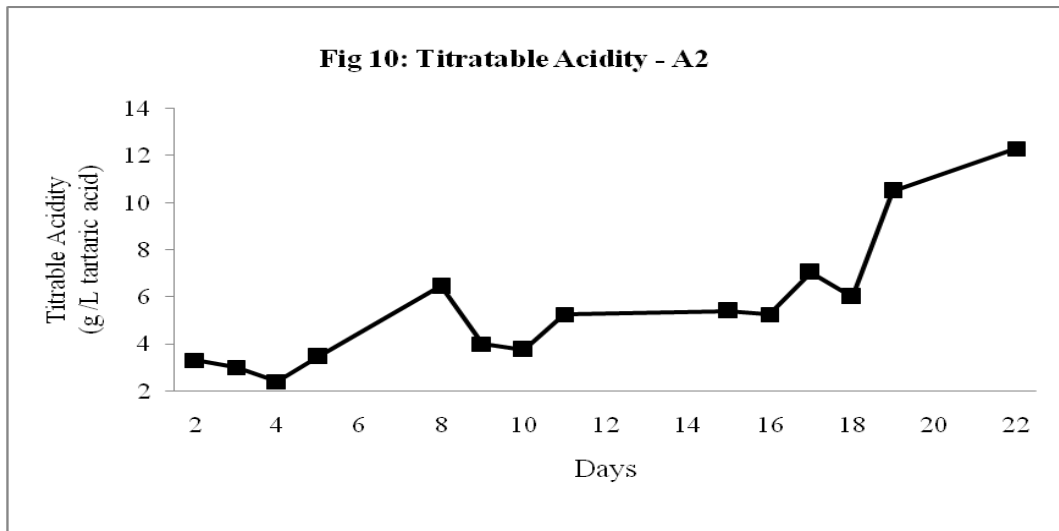
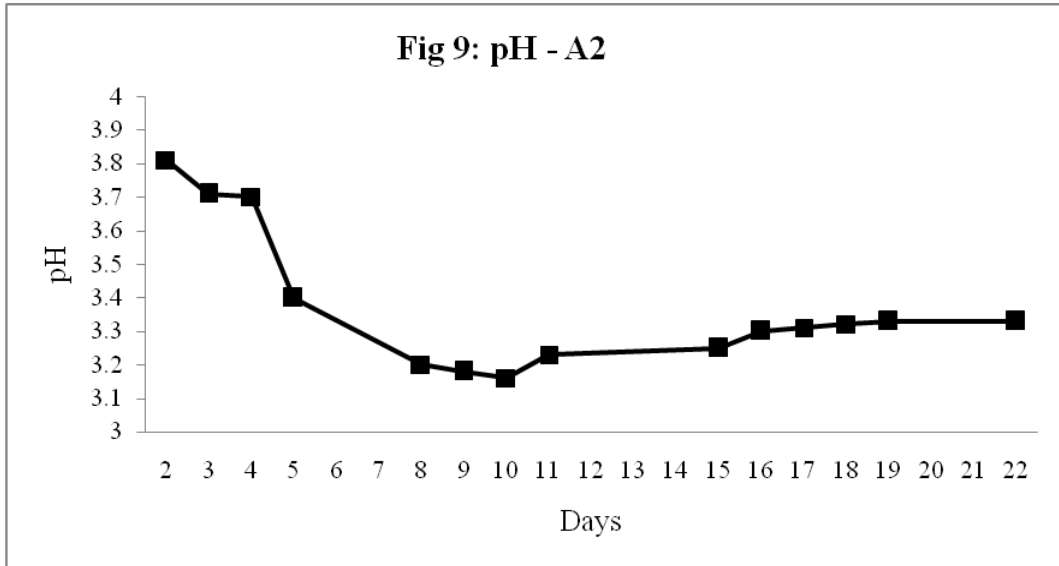
Days	pH	Titratable Acidity (g/L tartaric acid)	Specific Gravity	% Alcohol	Biomass (g/ml)	Sugar concentration (mg/100ml)
2	3.89	6.0	1.1160	0	0.0021	24.81
3	3.76	5.5	1.1186	0.945	0.0023	22.58
4	3.70	4.23	1.1237	1.54	0.0083	21.01
5	3.63	4.68	1.1240	1.67	0.0132	19.36
8	3.71	4.80	1.1267	2.04	0.0306	16.89
9	3.78	5.25	1.129	2.47	0.0310	16.13
10	3.80	5.55	1.133	2.93	0.032	15.62
11	3.83	5.78	1.142	4.14	0.033	14.89
15	3.89	6.3	1.149	5.05	0.038	12.00
16	3.91	6.52	1.153	5.59	0.039	12.52
17	3.92	6.70	1.157	6.13	0.040	11.88
18	3.94	6.98	1.162	6.81	0.04	10.01

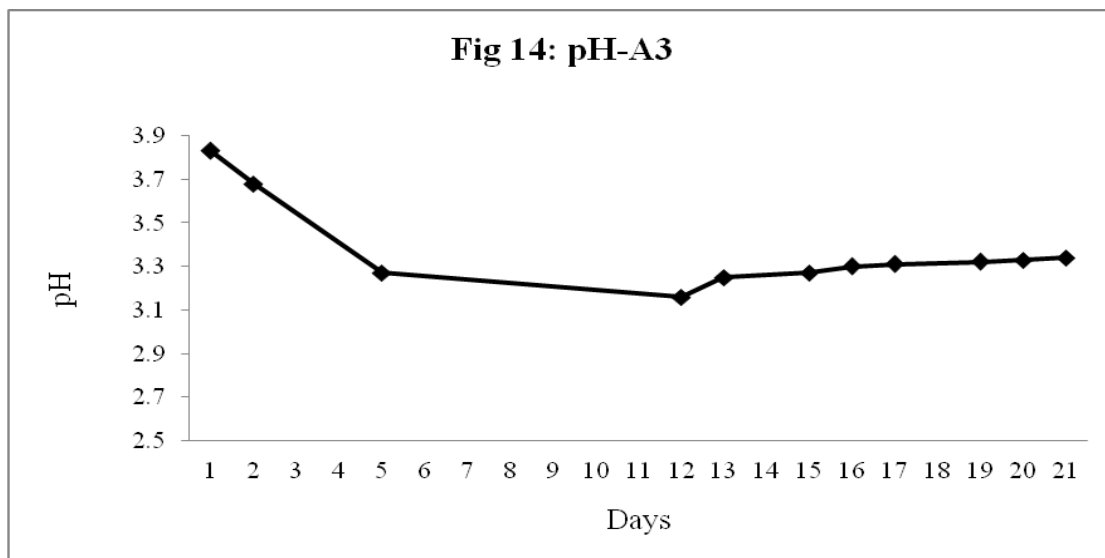
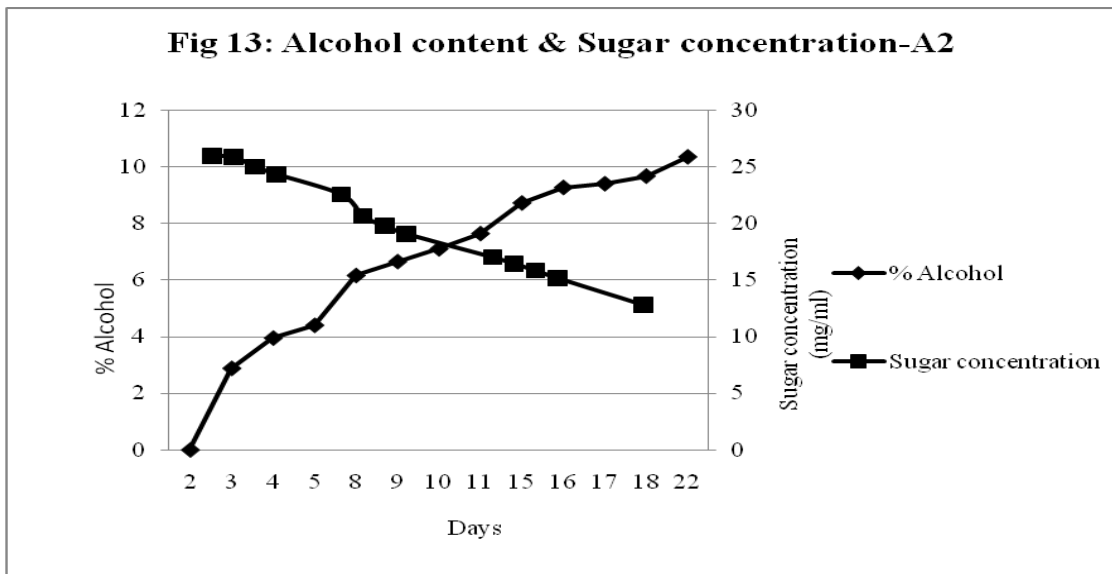
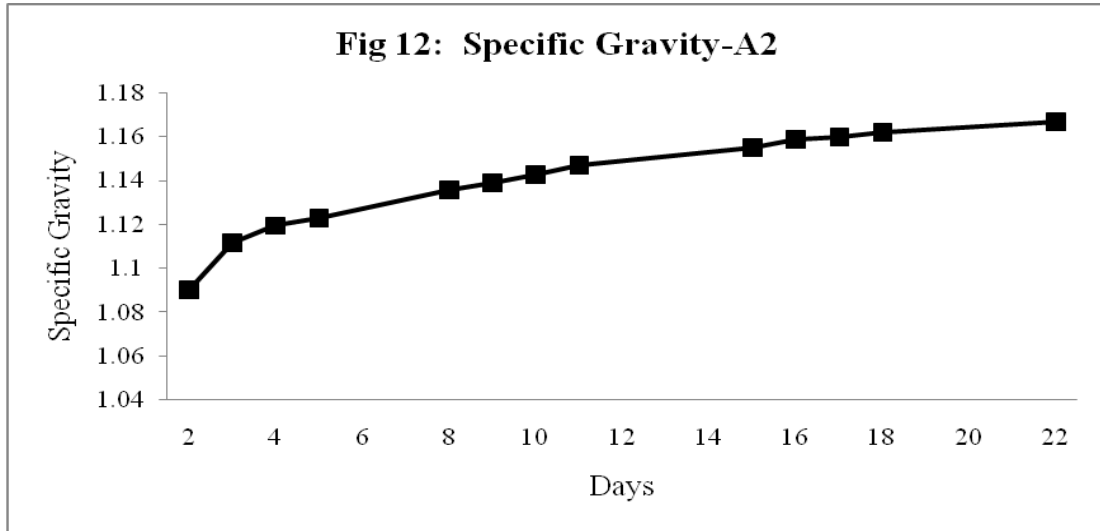
Table 6: Daily Monitoring Of Ginger-3 (G3)

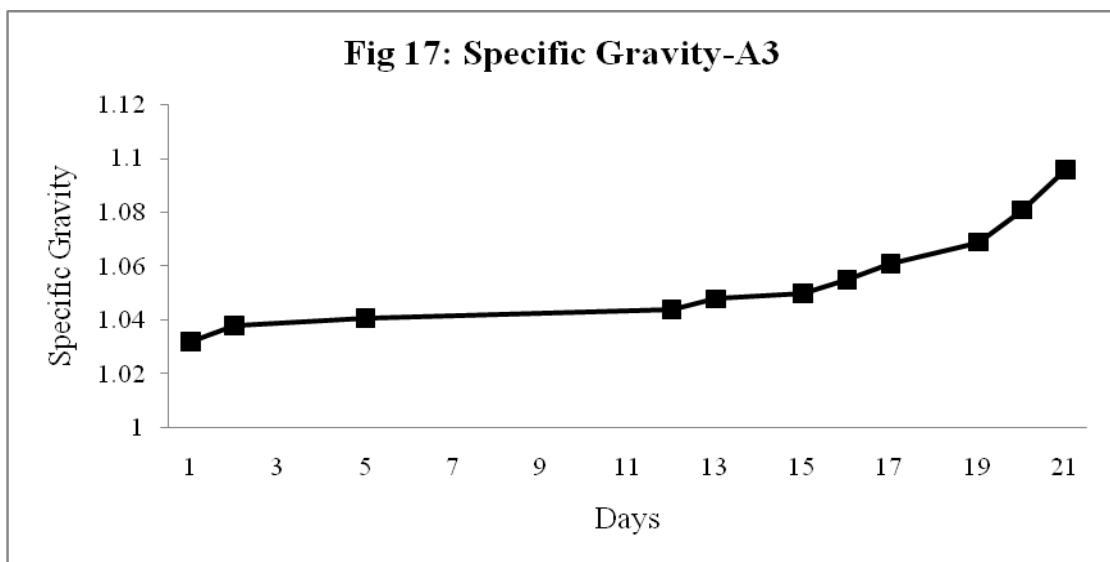
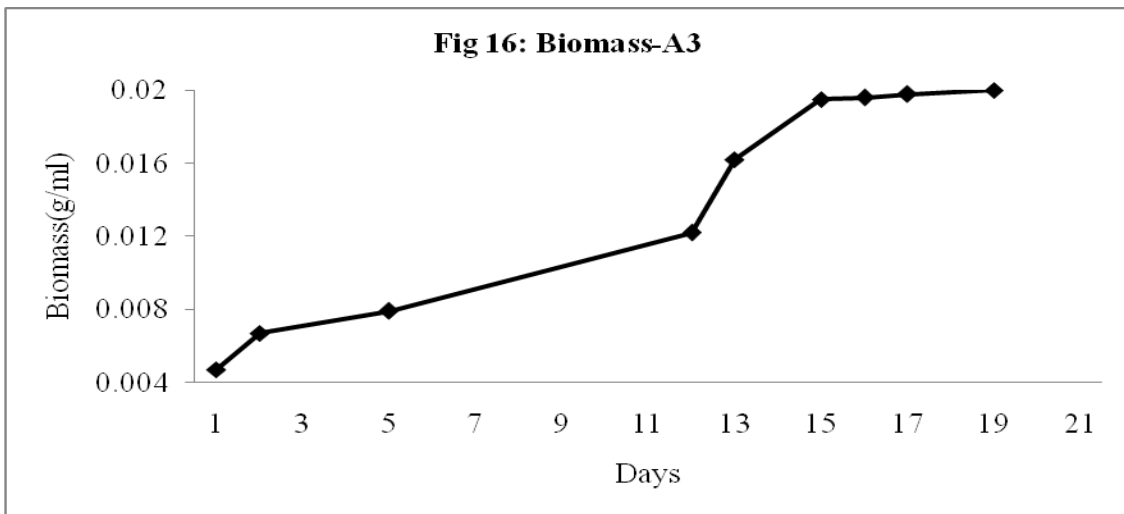
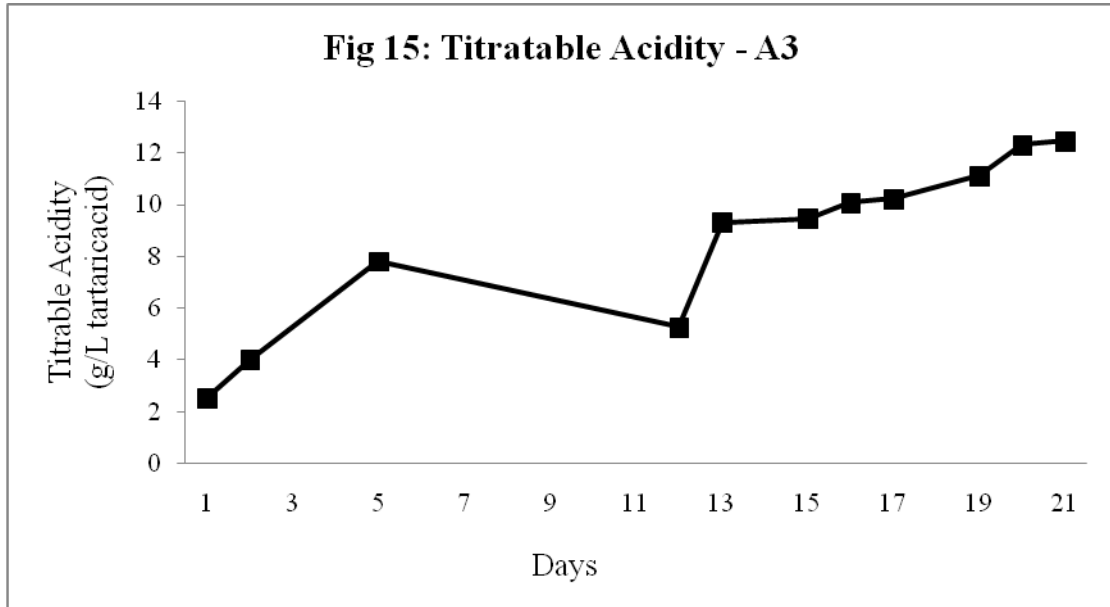
Days	pH	Titratable Acidity (g/L tartaric acid)	Specific Gravity	% Alcohol	Biomass (g/ml)	Sugar concentration (mg/100ml)
1	4.4	4.12	1.144	0	0.0045	24.44
2	3.96	4.39	1.150	0.356	0.0069	22.00
3	3.81	4.56	1.158	1.256	0.0082	20.20
5	3.72	4.78	1.162	1.890	0.0090	18.4
6	3.75	5.39	1.168	2.36	0.0116	18.0
7	3.79	5.22	1.174	2.51	0.0128	16.2
8	3.81	5.00	1.174	3.98	0.0137	15.7
9	3.82	5.04	1.176	4.25	0.0145	14.6
12	3.90	5.32	1.184	5.33	0.0160	12.8
13	4.01	5.43	1.188	5.81	0.0160	12.4

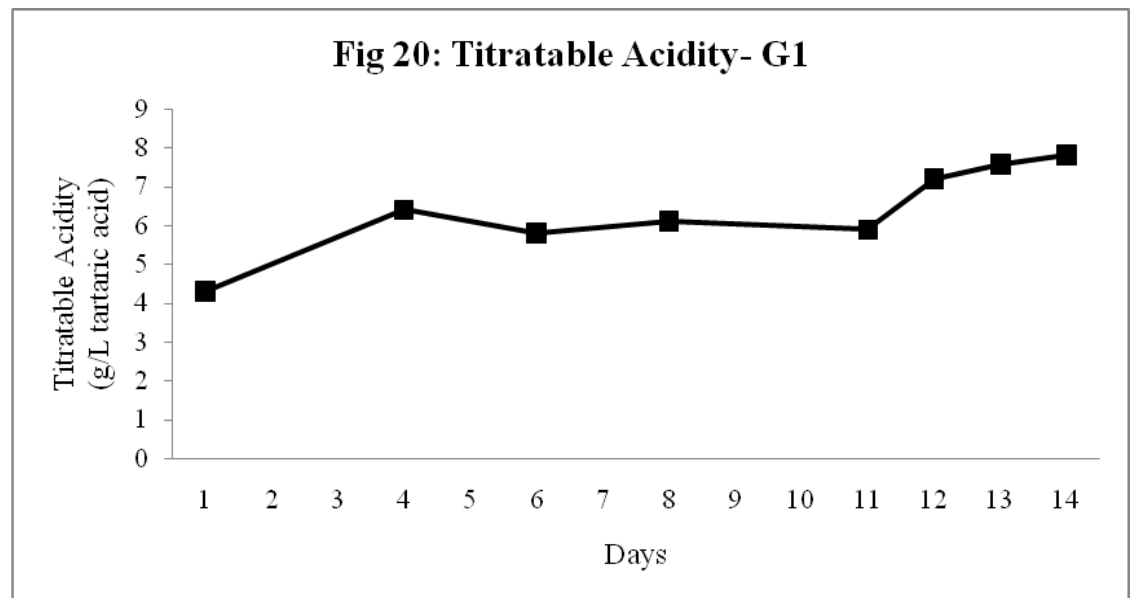
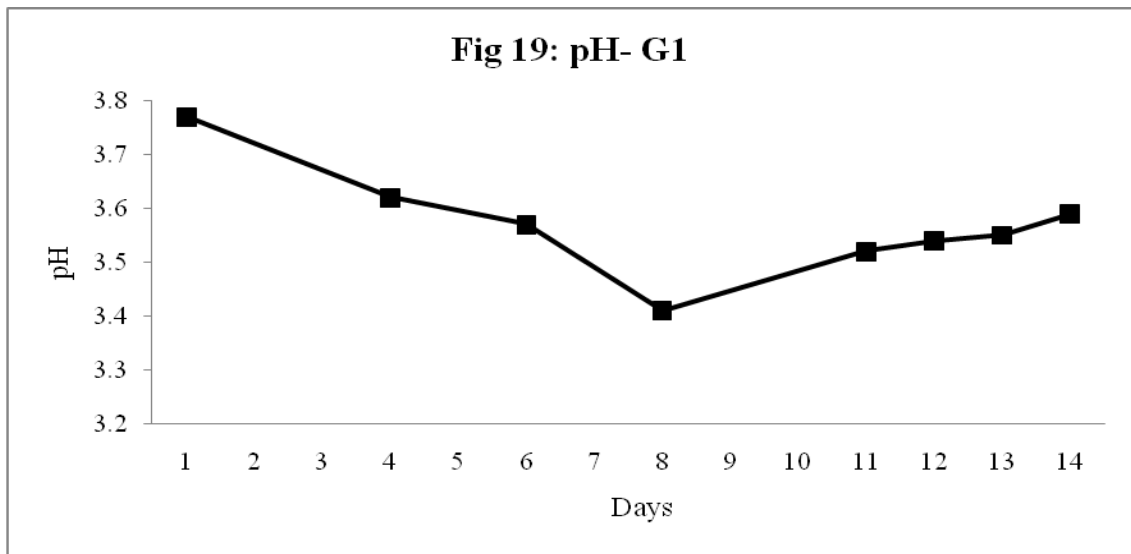
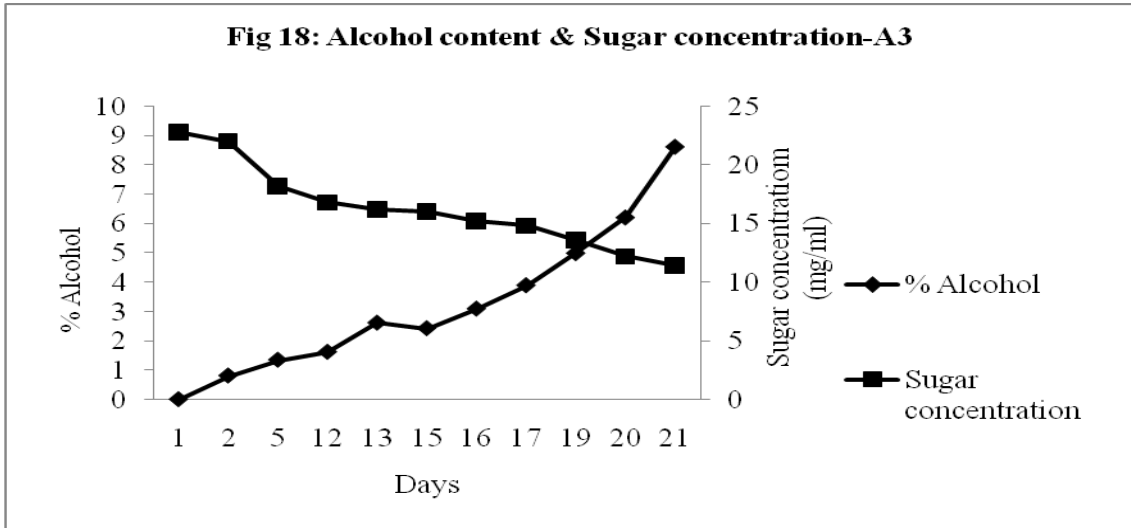


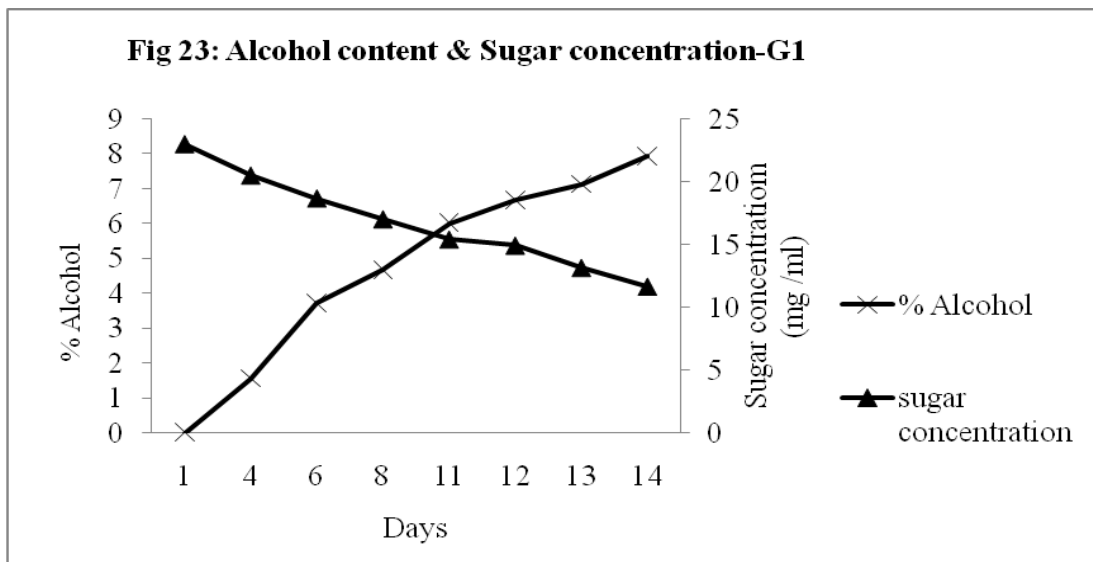
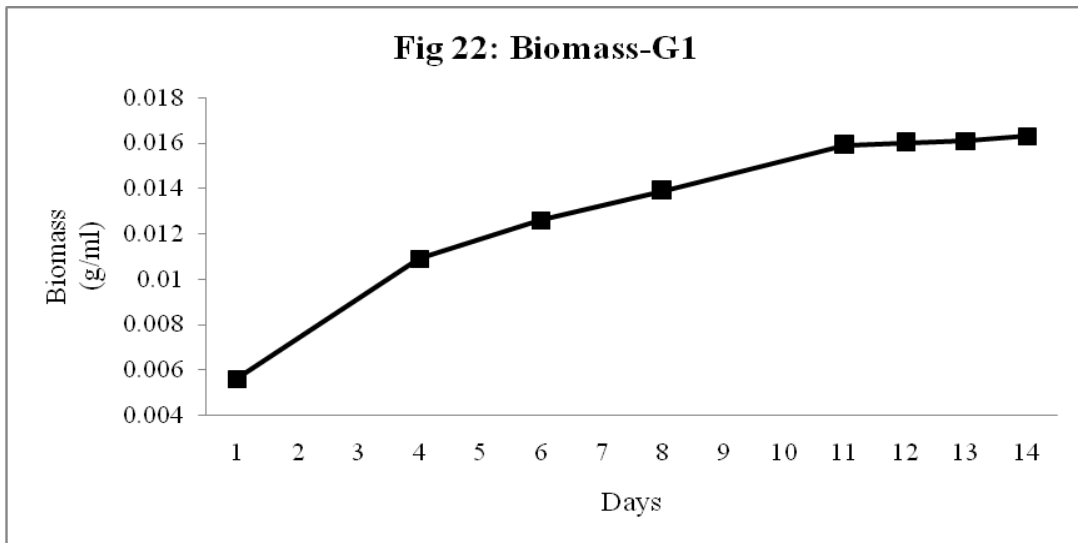
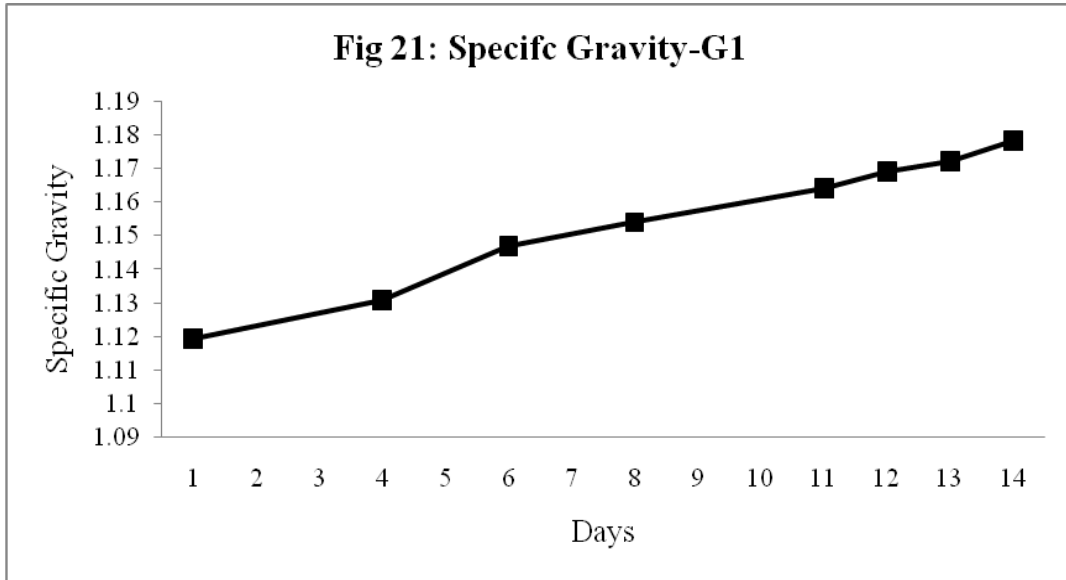


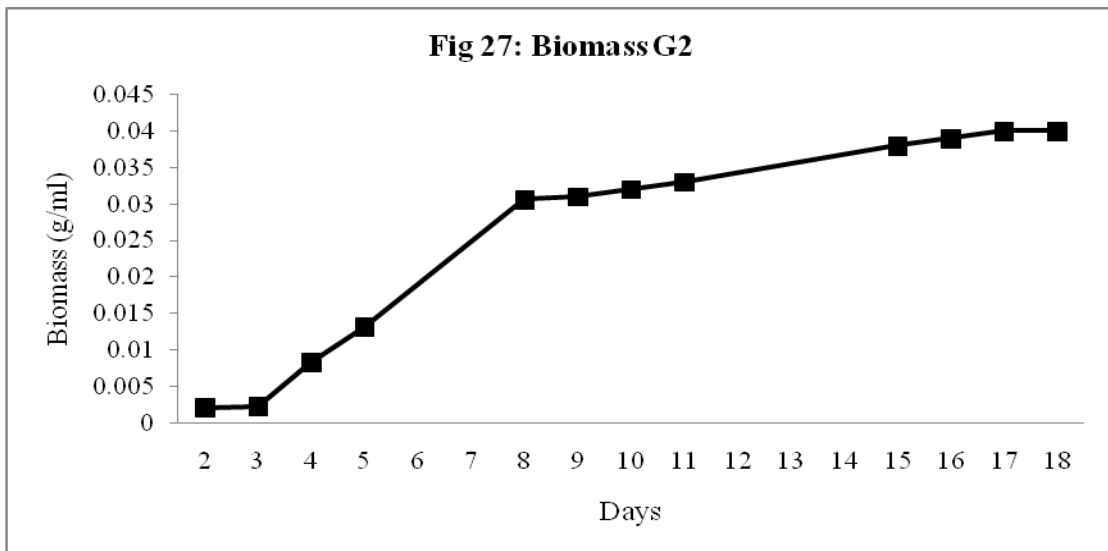
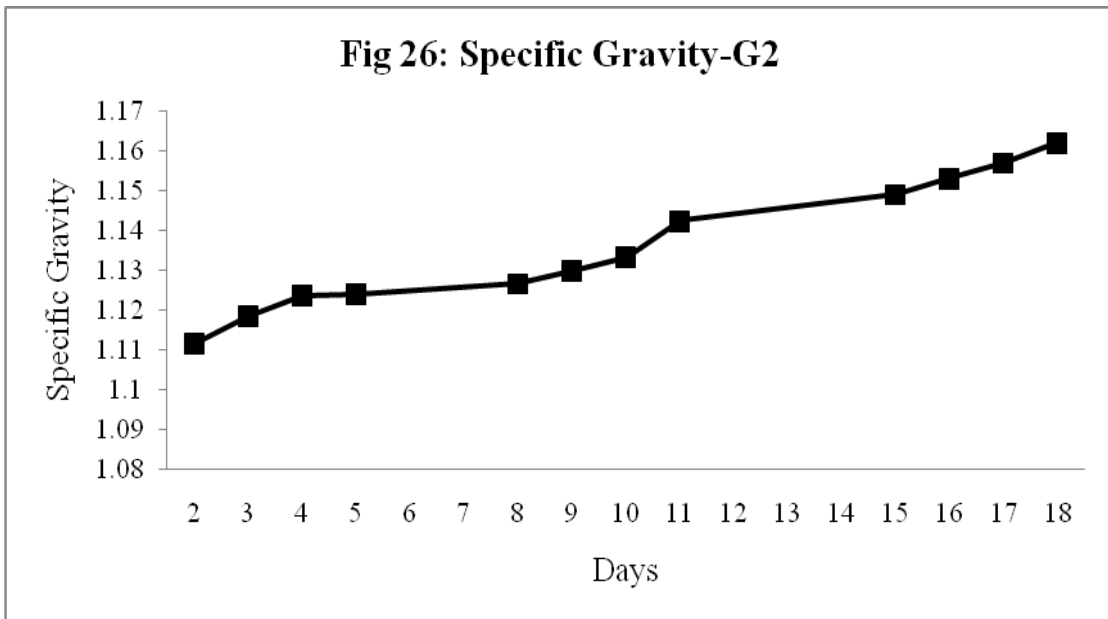
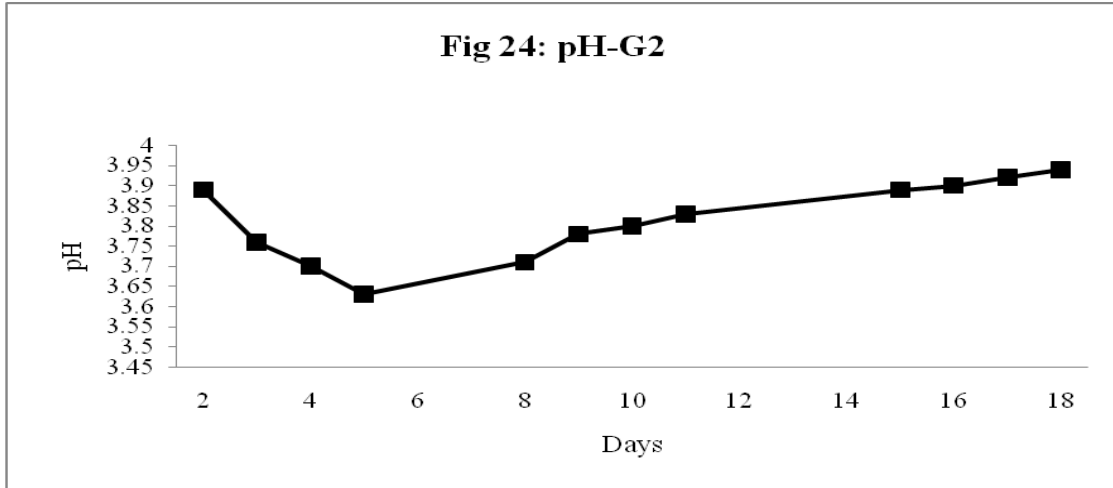


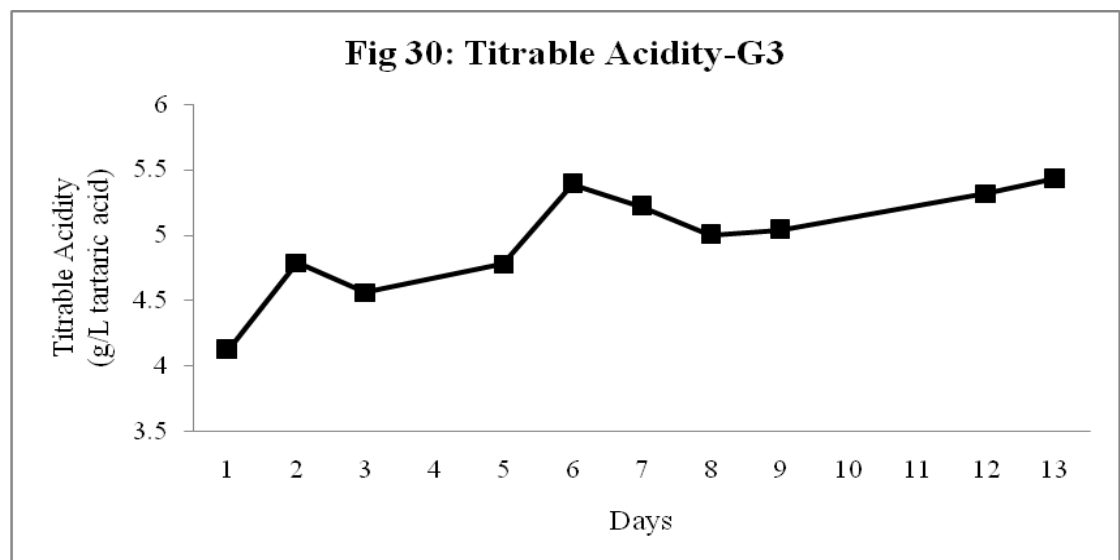
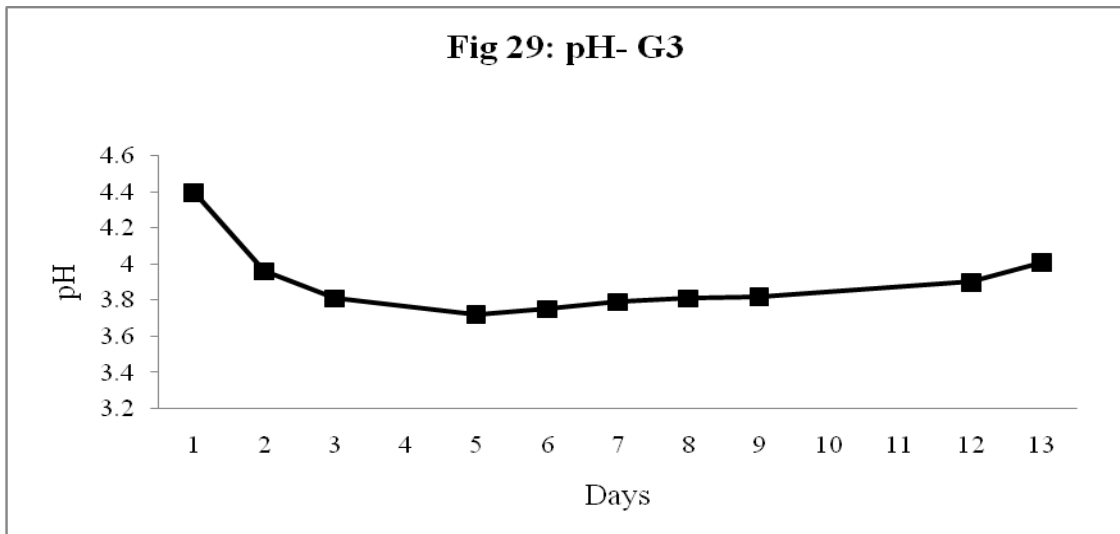
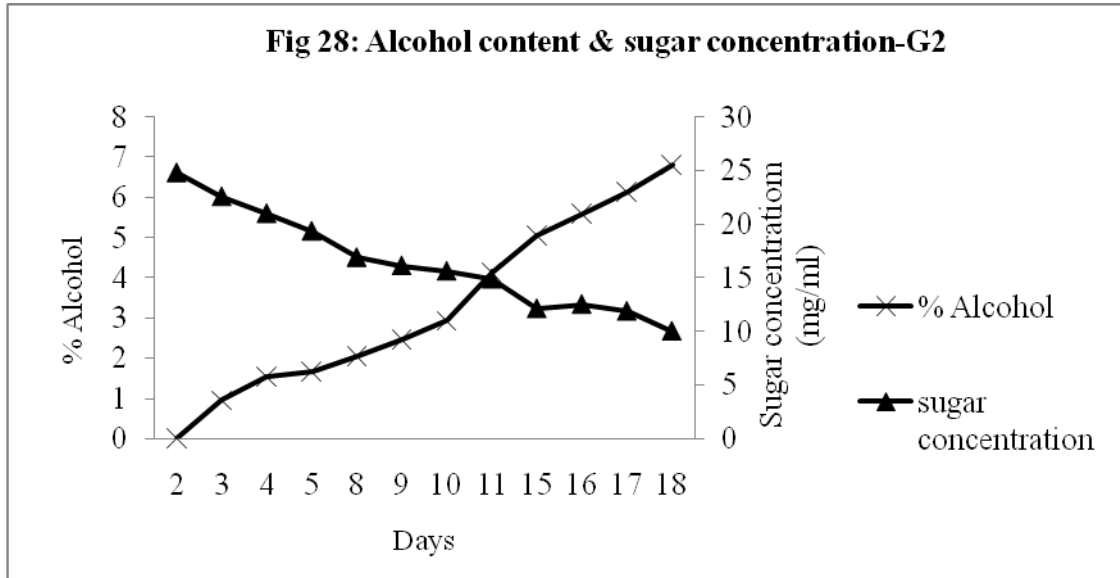












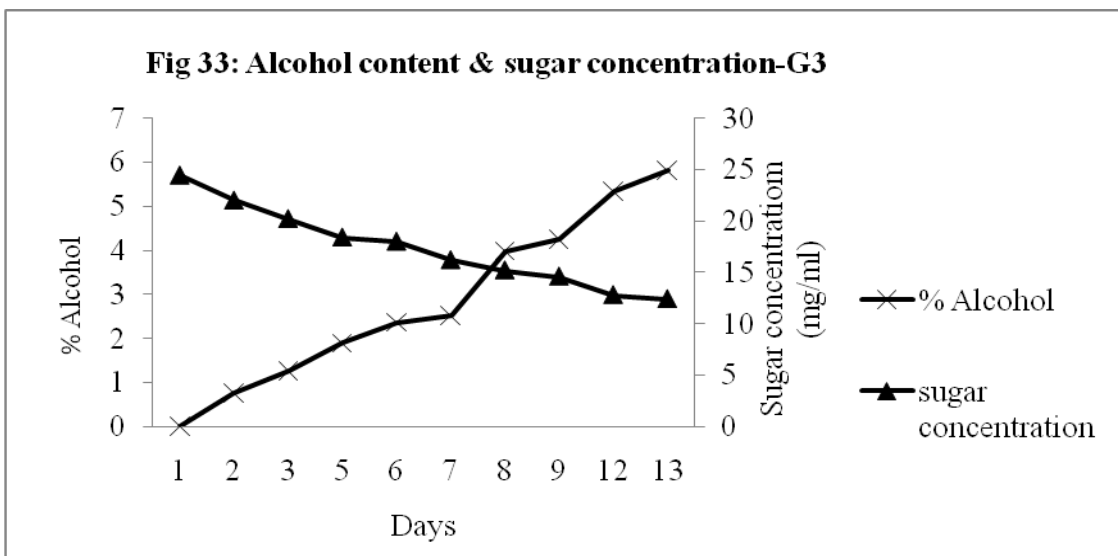
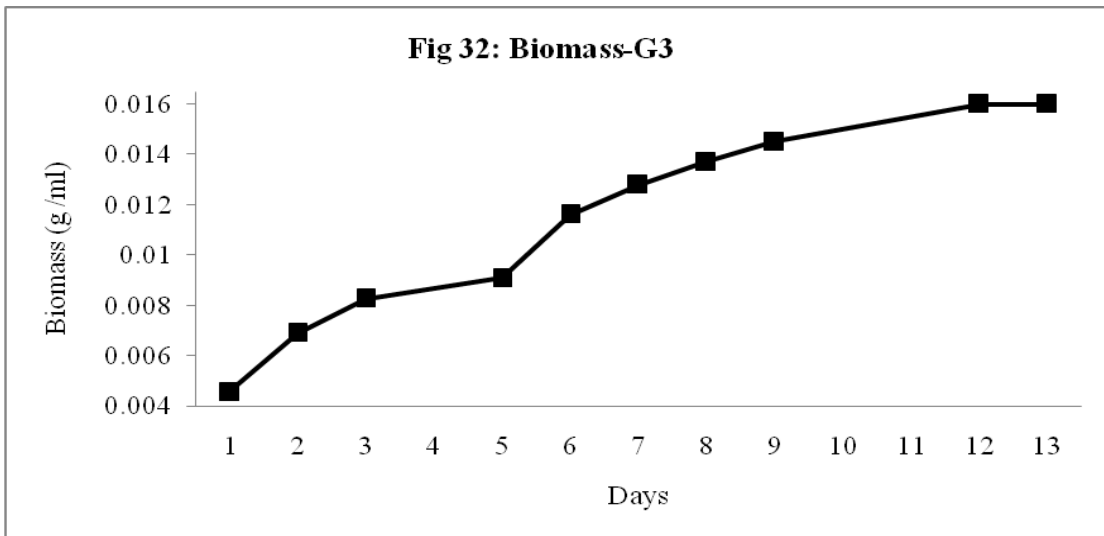
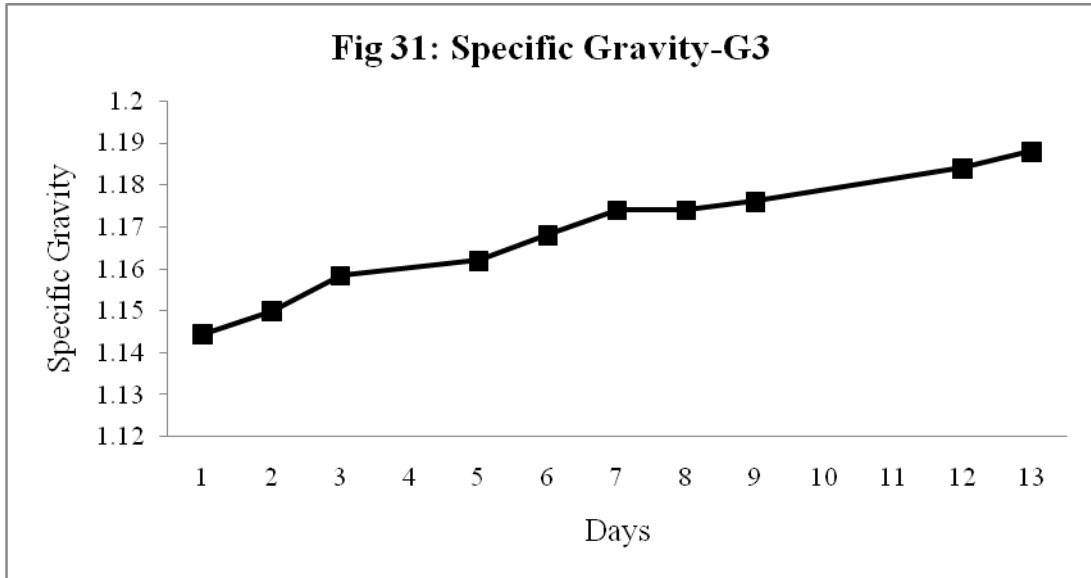


Table 7: Tannin content in wine

SL.No	Wine Sample	Tannin Content (mg/ml)
1	Amla-1	3.06
2	Amla-2	3.14
3	Amla-3	2.91
4	Ginger-1	0.74
5	Ginger-2	0.52
6	Ginger-3	0.32

Table 8: Phenol content in wine

SL.No	Wine Sample	Phenol Content (mg/ml)
1	Amla-1	0.69
2	Amla-2	0.58
3	Amla-3	0.30
4	Ginger-1	2.96
5	Ginger-2	2.59
6	Ginger-3	2.89

Table 9: Free and Total SO₂ content in wine

SL.No	Wine Sample	Free SO ₂ (g/L)	Total SO ₂ (g/L)
1	Amla-1	1.2	2.5
2	Amla-2	2.7	5.28
3	Amla-3	4.6	15.6
4	Ginger-1	6	16.6
5	Ginger-2	31	39
6	Ginger-3	48	78

Table 10: pH of wine

SL.No	Wine Sample	pH
1	Amla-1	3.29
2	Amla-2	3.33
3	Amla-3	3.48
4	Ginger-1	3.68
5	Ginger-2	3.96
6	Ginger-3	4.09

Table 11: Titratable Acidity of wine

SL.No	Wine Sample	Titrateable Acidity (g/L tartaric acid)
1	Amla-1	8.85
2	Amla-2	8.4
3	Amla-3	5.5
4	Ginger-1	3.45
5	Ginger-2	2.8
6	Ginger-3	2.0

Table 12: Alcohol content in wine

SL.No	Wine Sample	% Alcohol
1	Amla-1	13.86
2	Amla-2	12.10
3	Amla-3	10.98
4	Ginger-1	10.62
5	Ginger-2	9.25
6	Ginger-3	8.64

Table 13: Specific Gravity of wine

SL.No	Wine Sample	Specific Gravity
1	Amla-1	1.195
2	Amla-2	1.180
3	Amla-3	1.114
4	Ginger-1	1.198
5	Ginger-2	1.1801
6	Ginger-3	1.204

Table 14: Total Suspended Solids in wine

SL.No	Wine Sample	Total Suspended Solids °Brix
1	Amla-1	42.7
2	Amla-2	39.83
3	Amla-3	26.73
4	Ginger-1	43.18
5	Ginger-2	39.83
6	Ginger-3	44.27

Table 15: Analysis of Commercial Wine

Commercial Wine		
1	pH	3.56
2	Specific Gravity	1.2407
3	Titrateable Acidity (g/L tartaric acid)	4.2
4	% Alcohol	18
5	Tannin Content (mg/ml)	0.28
6	Phenol content (mg/ml)	0.20
7	Total Suspended Solids (°Brix)	32.23

Study on an Eco-Friendly Corrosion and Scale Inhibitor in Simulated cooling water

Defang Zeng¹, Huan Yan²

School of Resource and Environmental Engineering, Wuhan University of Technology,
Wuhan, Hubei 430070, P.R.China

Abstract: In this study, a composite eco-friendly phosphate-free corrosion and scale inhibitor used in simulated cooling water has been developed by sodium polyacrylate, zinc sulfate, sodium tungstate, sodium gluconate and triethanolamine. The corrosion and scale inhibition rate were respectively evaluated by weight loss experiment, the static scale inhibition test and electrochemical test. The results indicated that the corrosion and scale inhibitor was consisted of polyacrylate 14ppm, zinc sulfate 3ppm, sodium tungstate 7ppm, sodium gluconate 2ppm and triethanolamine 12ppm. The corrosion inhibition rate could reached 92.79%, and anti-scaling inhibition rate could reached 96.01%. The formula was efficient, phosphate-free and environmental, it would be widely used.

Keywords: Phosphate-free; scale inhibition; research; corrosion inhibition

I. INTRODUCTION

The use of water as thermal fluid in cooling water system usually leads to three problems namely: corrosion, scale and biological fouling processes. These phenomena are caused of the concentration of salts and suspended matters. [1-6] If these problems can not be solved timely, it will cause the production equipments of long period, full load and influence the safety and stable of equipments [4-7]. In order to limit the damage, many formulations have been developed to protect circuits, piping and materials structures against this scourge. Currently, agent used for simulated cooling water treatment are mainly phosphorus-containing formulas and they are easily to produce eutrophication and red tide phenomenon, so promoting a green chemistry and developing a phosphate-free water treatment agent have become the urgent matter. [8-12] In recent years, phosphate-free corrosion and scale inhibitors are mainly molybdate salts, chromic acid salts, natural polymer and synthetic polymer, when they are used alone, the dosage is large and the cost is high, so they are not widely used. In this paper, a multi-component phosphate-free corrosion and scale inhibitor has been prepared by sodium polyacrylate, zinc sulfate, sodium tungstate, sodium gluconate and triethanolamine. The corrosion and scale inhibition rate were evaluated by rotary hanging sheet corrosion test and static scale inhibition test. The mechanism of corrosion and scale inhibition was preliminarily investigated by corrosion electrochemistry test.

II. EXPERIMENTAL DETAILS

The scale inhibition rate was tested by calcium carbonate deposition. The corrosion and scale inhibitor was infused into 500mL volumetric flask which containing 240 mg/L Ca^{2+} , 366mg/L HCO_3^- and 4 mg/L sodium borate. The mixture was incubated for 10h at 80°C. After the bath, taking 25mL filter liquor, adding 5 ml NaOH and a small amount of calcium indicator, then titrated the filter liquor by ethylene diamine tetraacetic acid (EDTA) until the solution turned blue. The Ca^{2+} concentration after experiment was tested by

$$\rho = \frac{V \times 40.08 \times c}{25} \quad . \text{ In this formula, } v_0 \text{ is the amount of consumed EDTA, } C \text{ is the concentration}$$

of EDTA. The static scale inhibition rate η was calculated by the Formula (1).

$$\eta = \frac{v_2 - v_1}{v_0 - v_1} \times 100 \% \quad (1)$$

In this formula, v_0 is the amount of consumed EDTA without the addition of corrosion and scale inhibitors before incubation, v_2 is the amount of consumed EDTA with the addition of corrosion and scale inhibitors after incubation, and v_1 is the amount of consumed EDTA without the addition of corrosion and scale inhibitors after incubation.

The dynamic corrosion inhibition rate was tested by weight loss experiment, which was conducted in the simulated cooling water at $45^\circ\text{C} \pm 1^\circ\text{C}$ using a thermostat. Dried and accurately weighed the polished carbon steel sheets, then put the carbon steel sheets into beakers with 1 L simulated cooling water with and without corrosion and scale inhibitors. Distilled water was supplied for evaporating every 4 hours. After a period of 72 h, the carbon steel sheets were taken out, washed by ethanol, dried for 30 minutes, and then accurately weighed. The corrosion inhibition rate η was calculated by the Formula (2).

$$\eta(\%) = \frac{X_0 - X_1}{X_0} \times 100\% \quad (2)$$

In this formula, X_0 and X_1 are the weight loss values of carbon steel after 72 hours being immersed in the simulated cooling water without and with corrosion and scale inhibitors. The electrochemical measurements were carried out in a cell with three-electrode mode; platinum sheet and saturated calomel electrode (SCE) were used as counter and reference electrodes. The 1 cm^2 steel sample was abraded, washed and finally immersed in the simulated cooling water. Polarization curves measurements were performed using k4291602 Electrochemical System. When polarization curve test was carried out, the potential scan rate was adjusted to 0.5mv/s . Polarization curves could be achieved after data process.

Double distilled water and analytical reagent-grade CaCl_2 , NaHCO_3 were used for preparing the simulated cooling water and the characteristics of the simulated cooling water were given in Table 1.

Table 1. The characterization data of simulated cooling water

Parameter	pH	Ca^{2+} (mg/L)	Mg^{2+} (mg/L)	Cl^- (mg/L)	Total alkalinity (mmol/L)	Total hardness (mmol/L)
Value	7.3	105.36	65.45	254.35	4.36	4.90

III. RESULTS AND DISCUSSION

3.1. Confirming the best formula

Based on the principle of environment and economy, each component of the formula should be harmless or nontoxic, its concentration should be lower than the national standard requirements. From the aspect of economic benefits, its cost of the formula is lower than domestic phosphate corrosion and scale inhibitor, it will have market competitiveness and can be widely used.

Based on adequate experimental studies, the scale inhibitor formula was preliminary determined and it was consisted of sodium polyacrylate, zinc sulfate, sodium tungstate and sodium gluconate. The best proportion of them was determined by orthogonal test, table 2 showed the four factors and their levels .

Table 2 Factors and levels of orthogonal experiment

Level	Factor polyacrylic acid (A/mg/L)	zinc salt (B/mg/L)	sodium tungstate (C/mg/L)	sodium gluconate (D/mg/L)
1	10	1	2	5
2	12	2	4	6
3	14	3	6	7

The data in table 3 indicated that the best scale inhibitor formula was A3D3B3C1 . it was consisted of sodium polyacrylate 14mg/L, Sodium gluconate 7 mg/L, zinc sulfate 3 mg/L and Sodium tungstate 2 mg/L.

Table.3 Design of orthogonal experiment $L_9(3^4)$ and experiment results
 Table.3 Design of orthogonal experiment $L_9(3^4)$ and experiment results

sample	factor				Scale inhibition rate(%)
	A	B	C	D	
1	1	1	1	1	81.30
2	1	2	2	2	84.89
3	1	3	3	3	85.23
4	2	1	2	3	90.76
5	2	2	3	1	86.56
6	2	3	1	2	92.34
7	3	1	3	2	89.54
8	3	2	1	3	93.34
9	3	3	2	1	90.08
k1	83.81%	87.20%	88.99%	85.98%	
k2	89.89%	88.26%	88.58%	88.92%	
k3	90.99%	89.22%	87.11%	89.78%	
R	7.18%	2.02%	1.88%	3.8%	
influence factor	1	3	4	2	

Scale inhibition rate of the corrosion and scale inhibitor was shown in table 4 , scale inhibition rate reached 95.39% and it basically met the design requirements. Further measurement would be made to test corrosion inhibition rate.

Table 4 Results of scale inhibition rate

sample	the concentration of Ca^{2+} before experiment (mg/L)	the concentration of Ca^{2+} after experiment (mg/L)	Scale inhibition rate (%)
blank	240.00	66.53	—
1	240.00	232.01	95.39

Table 5 showed the corrosion inhibition rate only reached 89.62%, it couldn't meet the design requirements and further studies were needed.

Table 5 Results of corrosion inhibition rate

sample	corrosion rate (mm/a)	corrosion Inhibition rate (%)
blank	0.5879	—
1	0.0610	89.62

Through abundant tests before, triethanolamine was chosen to compound with the corrosion and scale inhibitor. The new formulas were given in table 6:

Table 6 Composition of new formula

sample	polyacrylic acid mg/L	sodium gluconate mg/L	zinc salt mg/L	sodium tungstate mg/L	Triethanolamine mg/L
2	14	7	3	2	8
3	14	7	3	2	10
4	14	7	3	2	12
5	14	7	3	2	14

Results in table 7 indicated that corrosion rate of formula 4 could reach 92.79% and it had good corrosion inhibition performance.

sample	corrosion rate (mm/a)	corrosion inhibition rate (%)
blank	0.5879	—
2	0.0610	89.62
3	0.0598	89.83
4	0.0424	92.79
5	0.0793	86.51

In table 8, the scale inhibition rate of formula 4 could reach 96.01%, it had excellent scale and corrosion inhibition performances, so formula 4 was designed as the best formula.

sample	the concentration of Ca^{2+} before experiment (mgL)	the concentration of Ca^{2+} after experiment (mgL)	Scale inhibition rate (%)
blank	240.00	66.53	—
4	240.00	233.08	96.01

3.2. Electrochemical analyses

The polarization curves of A3 carbon steel with and without formula 4 in the simulated cooling water were given in figure 1. The corrosion potential was shift to the positive after formula 4 was added and current density decreased, it indicated that the anode corrosion process was inhibited. sodium polyacrylate and sodium gluconate contains amount of hydroxy and carboxyl and they were hydrophilic groups. These molecules adsorbed on the active point or the entire metal surface, increasing the corrosion reaction activation energy, On the other hand, nonpolar groups of the corrosion inhibitor would form a layer of hydrophobic covered on the metal surface, it could obstructed charge or material transferred. So the efficient scale inhibitor was a anode type corrosion inhibitor^[13,14].

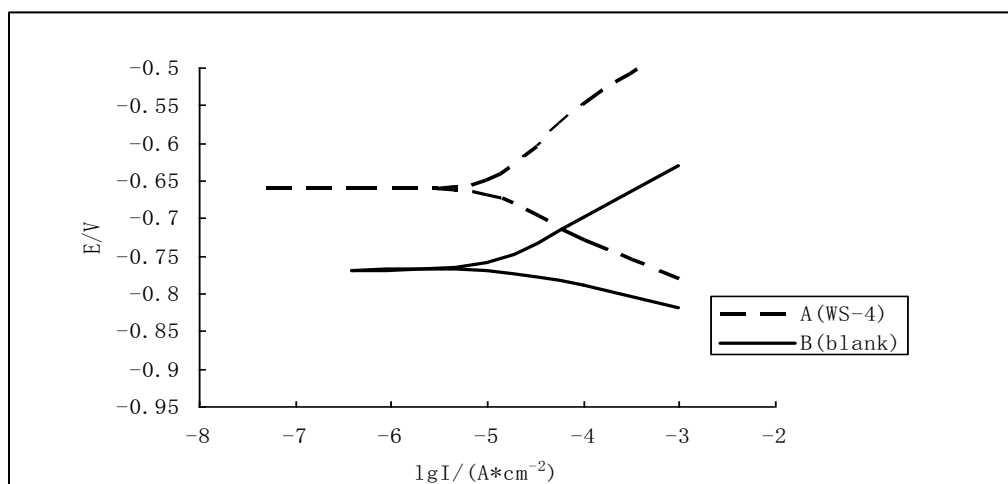


Figure 1 The polarization curve of the complex phosphate-free corrosion and scale inhibitors

3.3 Analysis of economic and environmental benefits

The phosphate-free corrosion and scale inhibitor was consist of sodium polyacrylate, zinc sulfate, sodium tungstate, sodium gluconate and triethanolamine . Each component of the formula was harmless or nontoxic, its concentration was lower than national minimum standards, it conformed to the requirements of environmental protection, at the same time, as the corrosion and scale inhibitor was phosphate-free, it would not cause eutrophication. Compared with other phosphate-free corrosion and scale inhibitors, this formula was of small toxicity, rich material sources, less dosage, lower cost and better performance. From the aspects of economic benefits, the cost of the phosphate-free corrosion and scale inhibitor was lower than the cost of domestic phosphate corrosion and scale inhibitor, it will have market competitiveness and can be widely used

IV. CONCLUSIONS

A composite eco-friendly phosphate-free corrosion and scale inhibitor used in simulated cooling water has been developed by sodium polyacrylate 14ppm, zinc sulfate 3ppm, sodium tungstate 7ppm, sodium gluconate 2ppm and triethanolamine 12ppm. The experimental results showed it was a kind of good corrosion and scale inhibitor whose corrosion inhibition rate and scale inhibition rate could reach 92.79% and 96.01%, respectively. Polarization curve test showed that the best formula was a kind of corrosion and scale inhibitor by mainly controlling anodic reaction and it was an anode type corrosion inhibitor.

V. ACKNOWLEDGEMENTS

This project was supported by Ministry of Science and Technology in China of SME Technology Innovation Foundation and Department of Science and Technology in Hubei Province, China of Science and Technology Research Foundation, express our thanks to those provided guidance and assistance

REFERENCES

- [1]. Patchaiah Kalaiselvi, Subbiah Chellammal, et al. 2010 *Artemisia pallens* as corrosion inhibitor for mild steel in HCl medium. *Materials Chemistry and Physics*, **120**(2), 643-648.
- [2]. L. G. Qing, H. J. Yi, Z. Y. Ming, et al. 2012 Acrylic Acid- Allylpolyethoxy Carboxylate Copolymer Dispersant for Calcium Carbonate and Iron(III) Hydroxide Scales in Cooling Water Systems. *Tenside Surfactants Detergents*, **49**(3), 216-224.
- [3]. R. Tourir, N. Dkhireche, M. Ebn Touhami, M. Lakhrissi, B. Lakhrissi and M. Sfaira. 2009 Corrosion and Scale Processes and Their Inhibition in Simulated Cooling Water Systems by Monosaccharides Derivatives: Part I: EIS Study. *Desalination*, **249**(3), 922-928.
- [4]. M.A. Quraishi, Ambrish Singh and Viond Kumar Singh. 2010 Green approach to corrosion inhibition of mild steel in hydrochloric acid and sulphuric acid solutions by the extract of *Murraya koenigii* leaves. *Materials Chemistry and Physics*, **122**(1), 114-122.
- [5]. Tourir, R, Dkhireche, N, Ebn Touhami, M, Sfaira, M.; Senhaji, O, Robin, J.J, Boutevin, B. and Cherkaoui. 2010 Study of phosphonate addition and hydrodynamic conditions on ordinary steel corrosion inhibition in simulated cooling water. *Materials Chemistry Physics*, **122** (1), 1-9.
- [6]. B. Labriti, N. Dkhireche, R. Tourir, M. Ebn Touhami, M. Sfaira, A. El Hallaoui, B. Hammouti and A. Alami. 2012 Synergism in Mild Steel Corrosion and Scale Inhibition by a New Oxazoline in Synthetic Cooling Water. *Arabian Journal for Science and Engineering*, **37**(5), 1293-1303.
- [7]. D. Lzydor and F. Piotr. 2011 Industrial Cooling Water Systems. Exploitation and environmentally Benign Total Inhibitive Protection. *Przemysl Chemiczny*, **90**(5), 737-741.
- [8]. Alfons Weisenburger, Georg Müller, Annette Heinzl, Adrian Jianu, Heinrich Muscher and Martin Kieser. 2011 Corrosion, Al containing corrosion barriers and mechanical properties of steels foreseen as structural materials in liquid lead alloy cooled nuclear systems. *Nuclear Engineering and Design*, **241**(5), 1329-1334.
- [9]. Aiyong HU. 2011 Analysis of water and energy saving measures in industrial circulating cooling water system. *Industry water and wastewater*, **42** (3), 1-4.
- [10]. Yavuz Sürme, A. Ali Gürten and Emel Bayol . 2011 Corrosion behavior of mild steel in the presence of scale inhibitor in sulfuric acid solution. *Protection of Metals and Physical Chemistry of Surfaces*, **47**(1), 117-120.
- [11]. David Hasson, Hilla Shemer and Alexander Sher. 2011 State of the Art of Friendly "Green" Scale Control Inhibitors. *Industrial & Engineering Chemistry Research*, **50**(12), 7601-7607.
- [12]. XY He, YH Cheng, LX Wang and P Huo. 2011 Study of Corrosion and Scale Inhibition Performances of PASP Complex Water Treatment Agents. *CAS*. **30**(8), 64-66
- [13]. R. Tourir, M. Cenoui, M. El Bakri and M. Ebn Touhami. 2008 Sodium Gluconate as Corrosion and Scale Inhibitor of Ordinary Steel in Simulated Cooling Water. *Corrosion Science*, **50**(6), 1530-1537.
- [14]. Li-Jun Gao, Jiu-Ying Feng, Bei Jin, Qiu-Na Zhang, Tian-Qin Liu, Yang-Qing Lun and Zhao-Jun Wu. 2011 Carbazole and Hydroxy Groups-tagged Poly(aspartic acid) Scale Inhibitor for Cooling Water System. *Chemistry Letters*, **40**(12), 1392-1394.

Ore-Forming Fluid Characteristics of the Naoyangping-Damogou zinc-fluorite ore deposit, Pingli County, Shaanxi Province, China

Moussounda Kounga Claude¹, Zheng Youye², Yang Xingke³

¹School of Earth Resources, China University of Geosciences, Wuhan 430074, PR China

²State Key laboratory of Geological Processes and Mineral Resources, China University of Geosciences, Wuhan 430074

³ Key Laboratory of Western China's Mineral Resources and Geological Engineering, Ministry of Education Chang'an University, 126 Yanta Road, Xi'an, 710054, PR China

Abstract: The Naoyangping-Damogou zinc-fluorite ore deposit is located in the North Dabashan Caledonian fold belt, in the east wing Pingli Anticlinorium, which is one of the most important zinc-fluorite-hosting faults in Shaanxi Province of China. Metallogenesis is controlled by F7 fault structure and other relevant fault structure systems and closely related to the trachyte side. Fluid inclusion (FI) petrography and microthermometry, and analysis of oxygen and hydrogen isotopes for fluid inclusions were conducted to determine the characteristics of the ore-forming fluids and the processes of zinc and fluorite mineralizations. Microthermometry data of FI indicated that ore-forming fluids are characterized by low salinity and low density. The data obtained from geothermometric studies of Sphalerite and fluorite associated with zinc-lead mineralization at the Naoyangping-Damogou mine are compatible with a structurally controlled, Sedimentary-hydrothermal origin. Homogenization and last ice melting temperature of primary fluid inclusion indicate that mineralization taken place over a temperature range 295-335°C and salinities of inclusion fluids range 0.53 to 1.33 wt.% TDS. Ore-forming fluids were dominated by magmatic components in the early mineralization period. In the present paper we report our preliminary research results of the data obtained from geothermometric studies of Sphalerite and fluorite at the Naoyangping-Damogou ore deposit. The present study builds on the existing geological, petrographic and geochemical information of Naoyangping-Damogou.

Keywords: Naoyangping-Damogou zinc-fluorite ore deposit, fluid inclusions, Pingli County, Shaanxi Province, China.

I. INTRODUCTION

The Naoyangping-Damogou zinc-fluorite ore deposit was discovered in the 2002s. It forms a well-known metallogenic belt in the North China craton. Previous studies focused on the geological characteristic and prospecting prospects of the Naoyangping-Damogou zinc-fluorite ore deposit (Wei D., et al. 2009 and Sun Jian et al., 2012), with the ore-forming fluids of zinc-fluorite ore deposit less studied. The Naoyangping-Damogou zinc-fluorite ore deposit is characterized by its broad veins, dense distribution of ore bodies, and continuous extension along strike. Geological surveys at shallow levels (< 190 m in depth) alone suggest that the resource is of an average size (2 millions tons of contained CaF₂). In the present paper we report our preliminary research results on the ore-forming fluids at the Naoyangping-Damogou zinc-fluorite ore deposit. The present study builds on the existing geological, petrographic and geochemical information of Naoyangping-Damogou.

II. GEOLOGICAL SETTINGS AND SAMPLES

The Naoyangping-Damogou zinc-fluorite deposit, located in the North Dabashan Caledonian fold belt at the east wing Pingli Anticlinorium (Geological Survey of Shaanxi Province, 1989, 2008). Geotectonically, the Naoyangping-Damogou Zn-CaF₂ ore deposit is located in the South Qinling orogen belt and North Dabashan belt contact zone. However, the metallogenesis of zinc-fluorite ore deposit is closely related to the

northern Dabashan Mountain side. Ore bodies are hosted to the North Dabashan Caledonian fold belt in the East wing of Pingli Anticlinorium (Zhang Guowei et al., 1997; TU Huaikui, 1997; 1999 and Wei D., et al. 2009).

The Naoyangping-Damogou Zn-(CaF₂) ore deposit is occurs in small scale and has varying mineral species. Its ore-forming and ore-controlling structures are also relatively complicated. The ore-forming and ore-controlling structures of the Naoyangping -Damogou mining area are located in the North Dabashan Caledonian tectonic belt (Fig.1).

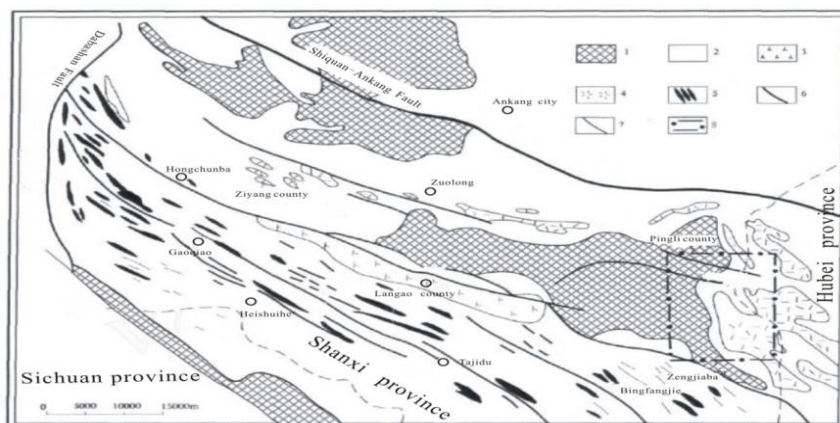


Fig.1 Regional geological tectonic sketch map of North Dabashan Mountain and study area location (Modified after Wei Dong et al., 2009)

- 1: Precambrian; 2: Early Paleozoic; 3: Basic overflow rocks; 4: intermediate-basic rocks; 5: Basic-ultrabasic rocks vein; 6: Main fault; 7: Secondary fault; 8: the range (scope) study area.

The region is situated within the eastern wing of Pingli Anticlinorium. This system is composed of numerous folds and faults, which generally have a north-west orientation. Two dominant faults sets are found in this region and are grouped according to their orientations, which include the nearly EW-, NW-SE, NWW-SEE and NE-SW-striking fault structures group, with the NWW-SEE fault structures being dominant. Most of the fault structures are characterized by multi-episodes activities. These fault sets appear closely associated with mineralization within the region, with several deposits commonly occurring along these faults (Fig.2). The strata in the region are dominated by the Middle Silurian Zhuxi Group (S₂zh) and Middle-Lower Silurian Meiziya Formation (S₁m), with the Lower Silurian Meiziya Formation strata is clay slate, sandy slate, carbonate-containing banded clay slate, sandy limestone and tuff sandstone. The Middle Silurian Zhuxi Group and Lower Silurian Meiziya Formation rocks are mostly distributed in the form of fault blocks because they were cut by faults and eroded and reworked by magmatic rocks. Regionally, a large area of alkali trachyte rocks is exposed in the east wing of Pingli Anticlinorium which always serves as the main ore-hosting country rocks for minerals and having an important significance in prospecting. There is generally no metallogenic control, but rocks in the Naoyangping-Damogou orefield. Magmatic activity in the Naoyangping-Damogou zinc-fluorite mining area is strong and is a part of multi-time activity of the Caledonian period into the strata. The main rock types in the orefield formed as a result of regional magmatic activities and can be divided into two main types: The first main type is basic-ultrabasic rock with low SiO₂ and the second consist of the neutral—intermediate-acidic—acidic rock with high SiO₂ (trachyte). Metallogenesis is closely related to the trachyte rock side and developed in the Naoyangping-Damogou-Jinshahe fault, and other small fault systems, which is regarded as the main ore-forming parent rock of the Naoyangping-Damogou orefield. The magmatic rocks are developed in the orefield; in space, microstructure (glass). There are two main types of magmatic rocks found in this orefield: that is: pyroxenite which is mainly located in the western part of the orefield, above the Dong-he Group, while the trachyte is to the east of microstructure (glass) pyroxenite; but to the west of Zhuxi Group. This type of distribution indicates that both microstructure (glass) pyroxenite and trachyte is stratiform feature in space. Chronologically speaking, microstructure (glass) pyroxenite is much older, while the trachyte is comparatively younger and both of them originated in early Silurian. Samples for fluid inclusion study were collected at different part of the study area and at both the top and bottom of the orebodies. Systematic fluid inclusion and isotopic geochemistry sampling was carried out based on ore and rock type, alteration, and location. A total of 11 fluid inclusions measured temperature and 14 isotopic geochemistry samples were collected (Table 1).

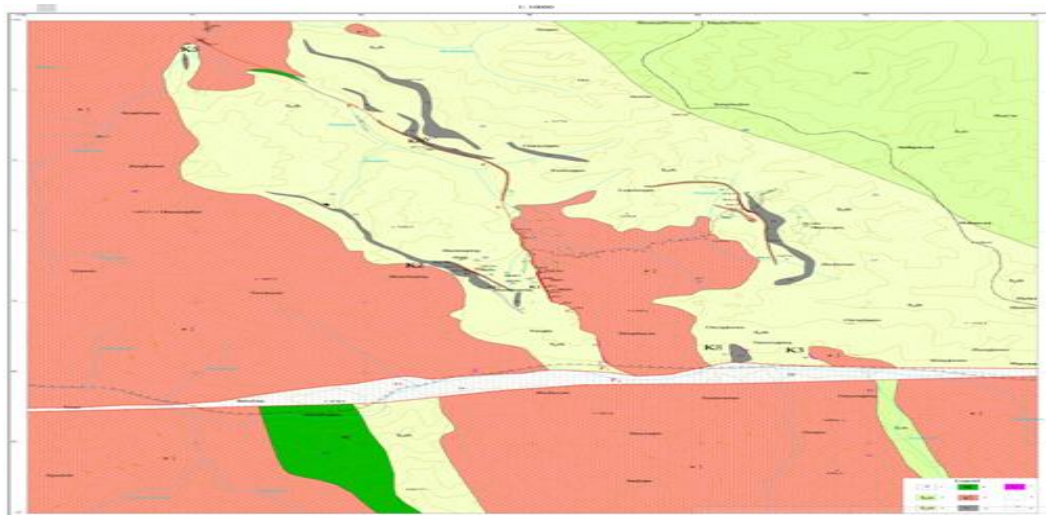


Fig.2 Geological sketch map of distribution schemes of the Naoyangping-Damogou zinc-fluorite ore deposit
 1: Quaternary system (Q_4), 2: Meiziya Group (S_{1m}), 3: Middle Silurian Zhuxi Group (S_{2zh}), 4: Basic sub-volcanic rock (M^3_3 = Diabase and Gabbro), 5: Intermediate sub-volcanic rock ($\chi\tau^3_3$), 6: Limestone (Ls), 7: Fluorite orebody (Fl), 8: Geological boundary, 9: F1: F1 fault

III. FLUID INCLUSION

3.1 Fluid inclusion petrography

Primary inclusion and secondary inclusion are easily found in the fluorite ore, and the primary inclusions are the dominant (fig.3), of which liquid-rich inclusions are the major and takes up 80 percent. Fluid inclusions with daughter mineral and fluid inclusions are rarely found, and gas inclusions are few. The shapes of inclusions are numerous, such as elliptical, nearly round, negative form, nearly triangle, and irregular form and so on, of which, the elliptical and the irregular are the dominant. The size of the inclusions fall between 5 and 25 μm , most of which between 10 and 15 μm . And most of the inclusions are distributed separately and randomly, and clustering inclusions are rarely found. Three types of fluid inclusions were identified based on their optical characteristics at room temperature, using the criteria of Roedder (1984) and phase transitions during microthermometry measurements (Fig. 3; Table 1).

Fluorite occurs as fine- to medium grained, euhedral crystals that postdate the trachyte. The fluorite crystals contain numerous two phase aqueous inclusions; rarely, gas-rich and single phase liquid-rich inclusions are present. The presence of coexisting gas- and liquid-rich inclusions is significant because this suggests that the homogenization temperatures closely approximate the true trapping temperatures (Goldstein and Reynolds, 1994). The fluorite-hosted inclusions provide the best direct measure of the temperatures reached.

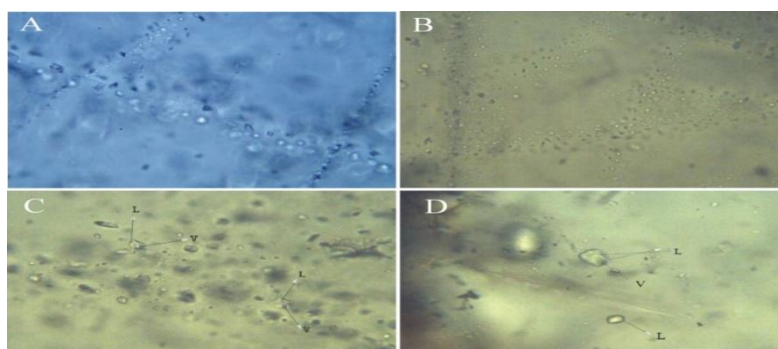


Fig.3. Different types of the Naoyangping-Damogou fluid inclusions: A & B are secondary inclusions; C & D are primary inclusions. A: Damogou K1 orebody 1085 middle section fluorite system of secondary inclusions; B: Naoyangping K3-PD10 fluorite system of secondary inclusions, C: Damogou K1 orebody 1136 middle section system of vapour- rich inclusions, and D: Damogou K1 orebody 1136 middle section system of pure liquid inclusions.

Table 1 Petrography and microthermometry for fluid inclusions in the Naoyangping-Damogou zinc-fluorite ore deposit

Sample No	Sampling location (Lithology)	Host minerals	Type of fluid inclusions	Range of Th (°C)		Phase type	Size (µm)	Gas-liquid ratios	Freezing point (°C)	Range of salinity	Density of fluid
LT01	K1-1085 middle-stage	Purple fluorite	Gas-liquid two-phase	295-335		Rich-liquid phase	10~15	1:4	-0.3~-0.8	0.53~1.33	0.658~0.663
						Pure gas phase	10				
LT03	K1-1136 middle-stage	White fluorite	Gas-liquid two-phase			Rich-liquid phase	5~15	1:8			
						Containing a daughter L+V+S	10~15	1:5			
						Pure liquid phase	10				
LT04	K1-1136 middle-stage	White fluorite	Gas-liquid two-phase			Rich-liquid phase	10~15	1:6			
LT05	K1-open pit	White fluorite	Gas-liquid two-phase			Rich-liquid phase	5~15	1:8			
LT06	K1-open pit	White fluorite	Gas-liquid two-phase	310-340		Rich-liquid phase	5~10	1:8			
LT09	K3-PD10	Purple fluorite	Gas-liquid two-phase			Rich-liquid phase	5~10	1:8			
						Containing a daughter L+V+S	10				
LT10	K3-PD10	Purple fluorite	Gas-liquid two-phase			Rich-liquid phase	5~10	1:6			
						Containing a daughter L+V+S	15				
						Containing a daughter L+S	10~25				
LT11	K3-PD10	Purple fluorite	Gas-liquid two-phase	289-329		Rich-liquid phase	5~15	1:6			
						Containing a daughter L+S	10				

L= liquid monophase, V= gas (vapour) monophase, L+V = rich liquid phase, L+V+S = liquid (L) + vapour (V) + solid (S) multiphase inclusions containing solids- contain solid crystalline phases known as daughter minerals, and L+S= rich liquid.

3.2 Microthermometry

Fluid-inclusion studies were performed on doubly polished fluorite samples taken from the mineralization area. Micro thermometric determinations were carried out using a Linkham TH600 heating and cooling stages of the State Key Laboratory of Continental Dynamics of Northwest University, Department of Geology, Xi'an (China). The heating rate during the phase transitions was controlled manually in the range of 5 to 15°C min⁻¹. Repeated measurements indicated that the reproducibility of the temperature determinations was better than ± 0.5 °C.

The majority of the fluid inclusions range in size from 5 to 15 µm. All of the investigated fluorite samples contain primary and secondary fluid inclusions using the definition of Roedder (1984). Primary fluid inclusions are observed as oval to triangle in regular, irregularly isolated or in groups along the fracture planes. Both primary and secondary fluid inclusion populations are dominated by four-phases comprising rich-liquid, pure liquid, pure gas and Containing a daughter liquid (L+V+S). Secondary fluid inclusions are characterized by spherical to square shapes that generally developed along two distinct fracture systems and have different morphological and micro thermometric properties. The homogenization temperatures (Th) of fluid inclusions were measured in 8 fluorite samples. The micro thermometric measurements on fluid inclusions in primary and secondary fluid inclusions showing that the Damogou fluorites were formed at temperatures range from 295°C to 335°C and 289°C to 329°C in Naoyangping area (Fig.4; table1). Fluid inclusions in fluorite contain major amounts of multi-phase inclusions containing solids-contain solid crystalline phases and sulfate-bearing daughter minerals. The Damogou inclusions, in general, are dominated by fluids that have low salinities and low densities. These inclusions, therefore, homogenize at moderate temperatures and their freezing point values indicate salinities ranging from -0.3°C to -3.3°C (Fig.5; table1). Homogenization temperatures of all these fluid inclusions in Naoyangping-Damogou are mostly in the range of 289°C to 340°C. The salinities of three types of inclusions varies remarkable and with low salinity from 0.53wt% -1.33wt% NaCl equivalent in NaCl daughter mineral bearing ones. This temperature range approximately corresponds to the main stage of hydrothermal mineralization.

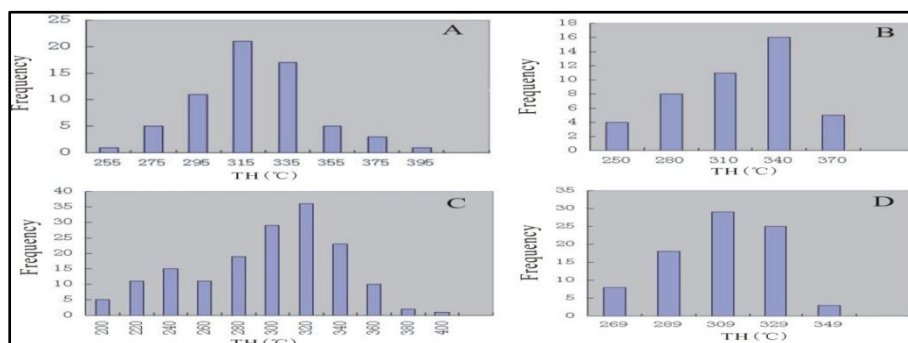


Fig.4 Histogram of fluid inclusion microthermometry of primary and secondary inclusions in the Naoyangping-Damogou ore deposit. A: TH of fluid inclusions in Damogou K1 orebody 1085; B: TH of fluid inclusions in Naoyangping K3 orebody, C: TH of fluid inclusions in Naoyangping K3 orebody, and D: TH of fluid inclusions in Naoyangping K3 orebody PD10. The data for the figures are from this study.

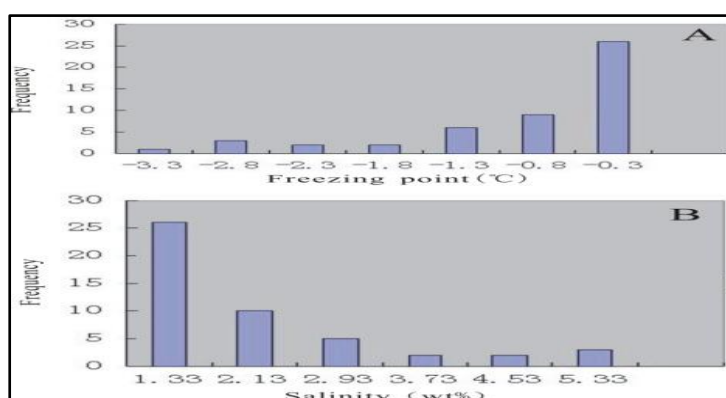


Fig. 5 Freezing point temperature and salinity of the Naoyangping-Damogou fluorite ore deposit. A. Freezing point temperature Damogou fluorite deposit and B: salinity of the Damogou fluorite deposit.

IV. OXYGEN AND HYDROGEN ISOTOPES

Oxygen and hydrogen isotopes analysis data were carried out by Geological survey of Shaanxi Province in the mining area, using MAT-252 mass spectrometer with standard mean ocean water (SMOW) is showed in the Fig.6. This figure illustrates the relative positions in Craig's diagram of H/O-isotopic of various fluid inclusions in fluorite from the Naoyangping-Damogou mining area. For comparison, there are also shown the analytical results for pyrite and sphalerite occurring in magmatic rocks from the same locality. From this figure we can see:

The fluids phase of inclusions in all fluorites and zinc occurring in magmatic rocks shows relatively large negative δD of the fluid inclusions hosted by pyrite in fluorite range between -115‰ and -95‰ and small positives $\delta^{18}O$ values (fluid inclusions hosted by fluorites range between 5‰ to 11‰). The relevant data points fall around the magmatic water line in Craig's diagram, suggesting that these fluorites, in spite of their occurrence in magmatic rocks, resulted from the magmatic water at the late stage.

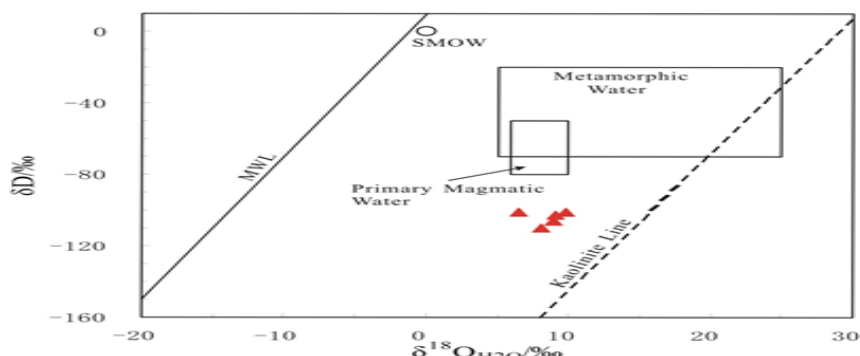


Fig.6 δD and $\delta^{18}O$ characteristics of the fluid inclusion water at Naoyangping-Damogou ore deposit (After: Geological Survey of Shaanxi Province, 2009).

From the Taylor (1974) δD - $\delta^{18}O$ isotopic diagram (Fig.5), fluids of the early period plot in and below the box for magmatic fluids. This suggests that early period fluids were derived only from primary magmatic water. The relevant points of ore-forming materials were derived mainly from deep-source magmas which had been brought about the alkali trachyte and Middle Silurian Zhuxi group from the deep interior. This indicates that for the hot-water sedimentary fluorite deposits of the ore-forming fluids were predominantly formation water or mixed water. It appears that while volcanism furnished abundant F for the formation of hot-water sedimentary fluorite deposits, volcanic hydrothermal solutions were also involved in the fluorite formation. As for the genetic type, the Naoyangping-Damogou is a strata-bound sedimentary-hydrothermal fluorite deposits associated with zinc-lead deposit.

V. ACKNOWLEDGMENTS

This study was supported by the Baosteel Resources Planning & Development Dept. of Baosteel Resources Co., Ltd (Shanghai) according to their research project license key (6100000820339) at Pingli County in the southeastern Shaanxi Province in the North Central China area.

REFERENCES

- [1]. Dong Wei, Ximin Chen, and Bangchao Wu (2009). Geological Characteristics and Ore Prospects of Zinc-Fluorite Deposit in Pingli Damogou, Shaanxi. *Northwestern Geology* 46(3), 77-85 (In Chinese with English abstract).
- [2]. Geological Survey of Shaanxi Province and Mineral Resources Bureau. (1989). *Regional Geology of Shaanxi*. Edit [M]. Geology Press, Beijing.
- [3]. Geological Survey of Shaanxi Province, (2008). 1:250,000 Geological map of Ankang sheet (I49C004001) (in Chinese).
- [4]. Geological Survey of Shaanxi Province, (2009). Damogou Zn-CaF₂ ore: structure-magmatic hydrothermal (in Chinese).
- [5]. Goldstein and Reynolds, (1994). Systematics of fluid inclusions in diagenetic minerals: Society for Sedimentary Geology Short Course 31, 199 pp.
- [6]. Roedder, E., (1984). Fluid inclusions. In: Ribbe, P.H., (Ed.), *Review in Mineralogy*, vol. 12, min.soci. of Am, Book Crafter, Inc. Michigan, 646 p.
- [7]. Sun Jian et al., (2012). Geological features and Potential analysis for fluorite prospecting in Naoyangping, Pingli County of Shaanxi Province. *Geology of Shaanxi*, V (02), 30-37 (in Chinese with English abstract).
- [8]. Taylor, H. P. (1974) The application of oxygen and hydrogen isotope studies to problems of hydrothermal alteration and ore deposition. *Econ. Geol.*, 69, 843-883.
- [9]. TU Huaikui, (1997). A preliminary discussion on geological setting and ore-forming characteristics of Ankang region, southern Shaanxi [J] *Geology of Shaanxi*, 11 (2): 9-11.
- [10]. TU Huaikui, (1999). Crustal evolution and characteristics of gold mineralization in north margin of Yangtze platform [J] *Geological Ore-Prospecting Symposium*, 14 (3) 172241.
- [11]. Zhang, G.W., Meng, Q.R., Yu, Z.P., Sun, Y., Zhou, D.W., Guo, A.L., (1997). Orogenesis and dynamics of the Qinling orogen. *Science in China, Series D* 39, 225-234.

Multiple Histogram Technique for Robust Skin Color Based Segmentation

Noor A. Ibraheem^{1,2}, Rafiqul Z. Khan²

¹Computer Science Department, Baghdad University, Iraq

²Computer Science Department, Aligarh Muslim University, India

Abstract: With the spreading of the ubiquitous computing; a growing demand for vision based recognition and communication. The first step in the latter demand is the segmentation process. Pixel based segmentation techniques have been widely used in the field of pattern recognition. The actual information that can be extracted from pixel based techniques is the color. In this work statistical technique based non-parametric skin distribution method has been proposed for modeling skin color pixel by modeling histogram based skin color approach on several color models and then unifies all the models into single model to produce a superior model. The idea of the proposed work is inspired from Hasan [1] but in their work they applied parametric technique for modeling skin color distribution using Gaussian Mixture model (GMM). Three metric are used to evaluate system performance. The proposed system achieved 99.08 classification rate, and the output results proved that the proposed system outperforms on other systems that applied single histogram base skin color segmentation on each color model separately.

Keywords: Skin Color, Segmentation, histogram, color space, normalized RGB, YCbCr, HSV.

I. INTRODUCTION

Segmentation is the process of locating specific regions of interest [1]. Different segmentation techniques have been applied for this purpose, one of these techniques is pixel based segmentation method. Pixel based methods principle rely on the idea that pixels are sharing some characteristics such as color in the same region [2]. Pixel based skin color segmentation methods witnessed widely diffusion in the fields of computer vision, pattern recognition [3], and image retrieval [4]. For gesture recognition systems, an accurate and robust segmentation are demanded [3] since it represent the first crucial step for recognition system. The pixel color considered as the most popular cue that provide an efficient classifying of the segmented region [5], where each pixel is classified into skin and non-skin pixel according to its intensity [3]. Although, the advantages of skin color segmentation methods, its invariance to size [6], and orientation [6], besides its assistance in face and hand video tracking [6] and can minimize the search space by seeking for the skin color only [1], it suffer from misclassification under variant illumination changes and occlusion with some other body parts such as face and arms [6][3]. However some restrictions on the user/ camera position [6][5] can reduce this problem. For building human skin color segmentation system, two consideration such be taken into account. Firstly, the selection of the color space, and secondly, reliable skin color modeling method [1][5]. Different statistical algorithms have been applied in pixel based skin color detection methods, varying from thresholding technique such as Explicitly defined skin region [1][5] to parametric model such as single Gaussian Model (GM) and Mixture of Gaussian Model or Mixture Gaussian Model (GMM), and non- parametric model such as histogram based lookup table (LUT) [5][1], and Bayes classifier. Each of the mentioned skin color modeling methods has different merits and the nature of the application determine the selection of the reliable modeling method and the perfect color space that fit with the selected skin color modeling method.

II. RELATED WORK

For the segmentation of skin color pixels, various techniques have been proposed. Some researches analyzed the skin color information for skin color detection by converting into different color space such as

normalized r-g, HSV and YCbCr. Techniques including parametric and non-parametric methods usually deal with the chrominance plane components of the color only and neglect the luminance component [6], to minimize the effecting of lighting ambient changes [6][5] and the overlapping with other background objects [6]. GM and GMM are parametric methods that model the distribution of skin color to classify the skin color, using some parameters mean, variance, and weights (in case of GMM method). These parameters initially extracted either from predefined training data set [1], or using some statistical method such as Expectation Maximization (EM) [7] or k-mean clustering [8]. However, the parameters should selected in prudence where bad initial estimation of GMM parameters can led to unpredictable classification results, as well as the increasing number if GMM mixtures considered computation / time [4] consuming and produce infeasible system [6]. On the other hand non-parametric methods provide general distribution of the color [6]. Lookup table (LUT) is a histogram based method [9] in which the probability of the skin color can be estimated using only the training data and no need for explicit model fitting [1][5][10]. Histogram one of the non-parametric methods that evaluate the probability density function of image intensities [6][11] by counting pixel frequencies of each color [11]. In this method, the color space components are partitioned or quantized into regular number of bins for simplicity and robust performance [10]. The non-parametric methods are fast [5] and efficient when adequate amount of training data are ready [6], however, insufficient amount of training data led up to inaccuracy of skin color distribution [6][11]. Hasan [1] proposed multiple of GMM system (MuGMM) on three different color models, i.e. normalized r-g, HSV, and YCbCr for modeling hand skin color. Hasan applied a separate GMM for each color model and obtained a probability for each color model and the maximum probability have been utilized as the final probability. Bayesian decision rule were used for classifying the skin pixels. [4] proposed segmentation method based on GMM by utilizing the property of converting gray-level image values into different modes of histogram [4], and built a normal distribution for each mode. The number of histogram modes as well as the GMM parameters has been estimated using EM algorithm [4]. [12] applied histogram back projection skin color model for face detection algorithm, HS color space are used to build the system and thresholding technique used to obtain the segmented binary image [12]. [13] suggested histogram-based self-constructing neural fuzzy inference network (SONFIN) system for Skin color segmentation, using HS color space [13]. The suggested system used HS Histogram information for training the SONFIN [13]. However, histogram-based approaches usually need great amount of training data [9][5], hence a large space for memory storage [9] which would already increase when the size of training data increase [6h]. [8] Gokalp applied GMM for modeling human skin color distribution. K-means algorithm is used for parameters initialization, EM algorithm for parameters estimation, and Minimum Description Length (MDL) algorithm for determining the number of GMM parameters. Using three different color models YES, chromatic space and log-opponent models [8]. [14] adopted YCbCr color space with GMM for skin color segmentation of hand gesture and test the efficiency of three different types of cameras (single color, stereo color and thermal camera) for better segmentation. [15] Studied different histogram bins and concluded that the best number of histogram bins for RGB color model is $32 \times 32 \times 32$ for a small amount of training data [15].

III. PROPOSED ALGORITHM

This work inspired from the method of [1] which build a skin color modeling system based on multiple Gaussian Mixture Model (MuGMM) from the most common three color spaces, as mentioned previously. In this work we adopted multiple histograms skin color modeling system to segment human skin color regions. The proposed system combine three color models, RGB, HSV, and YCbCr to produce a robust skin color model which can take advantages of the selected color spaces. In this system a histogram based approach has been applied on each color model, and then all the resulted histograms are integrated to form a new superior histogram technique called Multiple Histograms Technique (MHT). The proposed model has shown its efficiency when compared with histogram based approach applied on single color model. From the selected color models, only the chrominance components are utilized in the proposed system. The chrominance components are quantized into significant number of bins [5] that represent the range of color values [5] in an image region [16]. The 2D histogram are generated from these bins which are formed the lookup table LUT [5]. Each bin has the number of frequencies a specific color pixel appeared; this process is performed in the training stage of skin color to extract the probability distribution of skin color pixels [5]. The RGB histogram divides each of the RGB components into eight number of bins as in [10], this provide a $(8 \times 8 \times 8)$ histogram of 512 bins. Different study applied histogram on RGB color model and selected $32 \times 32 \times 32$ bin histograms [6]. In this work we applied the $(8 \times 8 \times 8)$ bins histogram.

The HSV histogram divides into eighteen regions for (H) component and three regions for the (S, V) components, this provide $18 \times 3 \times 3$ histograms of 162 bins. The YCbCr histogram divides the (Y) luminance component into eight regions, and (Cb, Cr) the chrominance components into four regions, which form $8 \times 4 \times 4$ histogram of 128 bins as in [16]. As mentioned previously

only the chrominance components are used (RG, HS, and CbCr) components to reduce the illumination change by removing the luminance component.

For a single color model histogram, the probability distribution p can be defined by equation (1) as mentioned in [5]

$$h(c|skin) = \frac{skin(c)}{n} \tag{1}$$

Where $skin(c)$ represent the value of histogram bin for the color vector c , and n represents the sum of all values of histogram bin.

The proposed system can be defined by equation (2)

$$h(c|skin) = \max_{i \in I} h_i(c) \tag{2}$$

Where l represent the number of color models used (which considered three color models in this study), h_i represents the histogram probability of the color model i , $h(c|skin)$ represent the probability of color c being a skin color pixel.

The skin color c is classified into skin or non-skin pixel using a thresholding technique. Empirically the value of the threshold is specified.

IV. EVALUATION OF SEGMENTATION RESULTS

For the proposed method, metric have been adopted to evaluate the result [1]. The same data base applied in Hasan [1] are utilized in this work 35 images are used for training the system with their ground truth images, the number of skin pixels used for system training is 757883, and 100 images are used for the testing phase. The first metric as described in [1]:

Correct Detection Rate (CDR): Represents the number of pixels that are correctly classified as skin pixel by the algorithm.

$$CDR = \frac{C_s^a}{T_s^g} \times 100\% \tag{3}$$

False Detection Rate (FDR): Represents the number of pixels that are wrongly classified as non-skin pixel by the algorithm.

$$FDR = \frac{W_{ns}^a}{T_{ns}^g} \times 100\% \tag{4}$$

Classification Rate (CR): The number of skin pixels that are correctly classified by the algorithm and ground truth divided by the maximum value from either the number of skin pixels classified by the algorithm or the number of skin pixels classified by the ground truth.

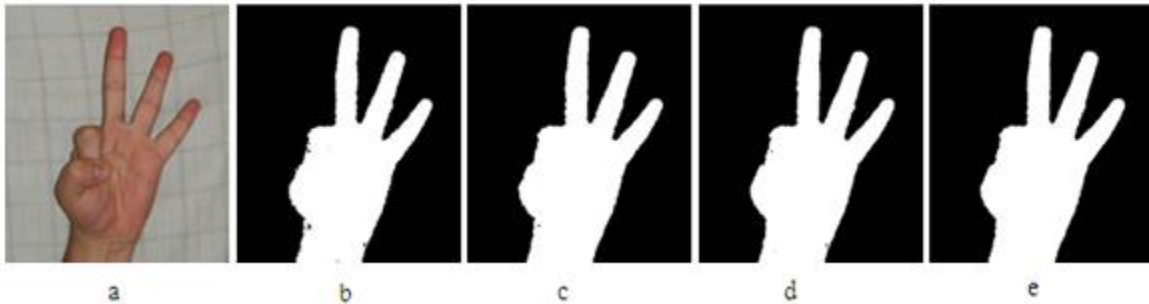
$$CR = \frac{C_s^a}{\max(T_s^a, T_s^g)} \tag{5}$$

Where C_s^a represent the total number of pixels classified correctly as skin pixels by the algorithm. T_s^g represent the total number of pixels classified correctly as skin pixels by the ground truth. W_{ns}^a represent the total number of pixels classified wrongly as non-skin pixels by the algorithm. T_{ns}^g represent the total number of pixels classified as non-skin pixels by the ground truth, and T_s^a represent the total number of pixels classified as non-skin pixels by the algorithm. Table 1 shows these metric parameters computed for the proposed algorithm and three color models.

Table 1: metric parameters for classification rate of skin color based histogram approach

parameters	Histogram of RGB	Histogram of HSV	Histogram of YCBCr	Proposed method HMCM
CDR	97.3599	98.4557	98.4743	99.1032
FDR	1.0554	0.6173	0.6099	0.3585
CR	97.3599	98.4557	98.4743	99.08507
Average	97.88813333	98.7647	98.77956667	99.2766

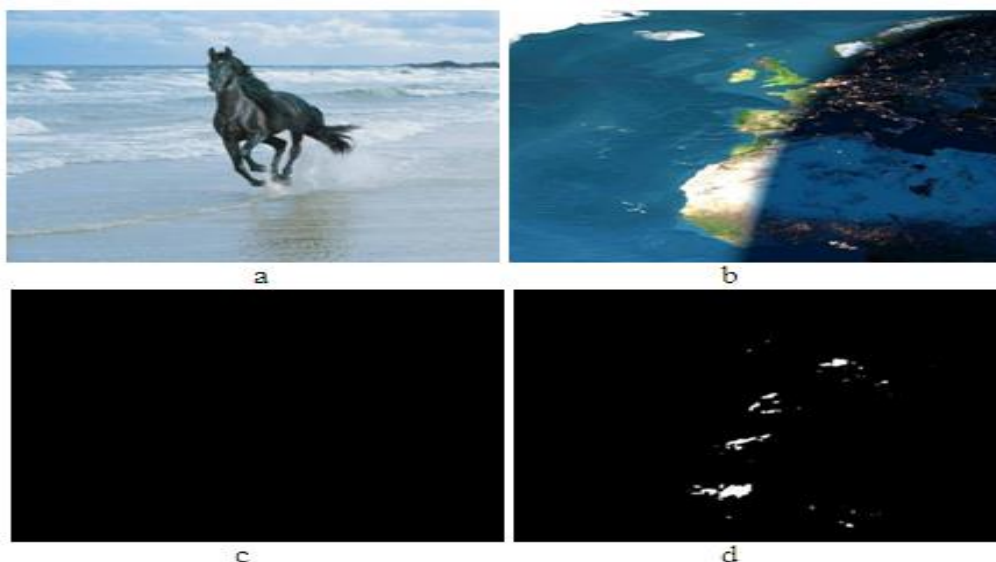
From table 1, obviously the result of the proposed algorithm is superior and outperforms on other color models when applying single color model based histogram approach comparing all the metric parameters separately. Figure 1 demonstrates some results when applying the proposed algorithm on different hand gesture images.



a) the original input image, b) rgb, c)HSV, d)YCbCr, and e) the proposed algorithm.

Figure 1: An example of implementation the histogram based skin color segmentation on the selected color models and the result of the proposed algorithm.

From the Figure 1, we can notice that the segmentation result for each of the RGB and YCbCr color models have some shortcoming in specific regions, while the results using HSV are mostly perfect, hence the proposed algorithm take the advantages of the selected color models, the result of the proposed algorithm represents the histogram based skin color applied on HSV color model results. We applied the proposed algorithm on a natural image with no kin color pixels, and the results are explained in Figure 2.



a, b) the input images, c, d) the corresponding segmented images using the proposed algorithm for each of a and b respectively.

Figure 2: the implementation of the proposed algorithm on natural scene.

V. CONCLUSION

Skin color based segmentation techniques have been widely utilized in pattern recognition and computer vision fields. Various color space are employed with skin color based segmentation algorithms depending on the application field. The separation of the chrominance components from the illumination component provides the benefit of avoiding sensitivity to illumination changes. Statistical approaches have proven its robustness in the field. In this work, we proposed a histogram based skin color segmentation system, this system take the advantage of applying histogram based skin color segmentation for several color models and combine them to unify a single modeling system. The proposed system is fast, efficient and the output results show its robustness and outperforming on other color models.

VI. FUTURE WORK

The idea of the future work are inspired also from the idea of Hasan [1] but he applied Gaussian mixture Model GMM for modeling the skin color as well, in this work we utilize histogram method for modeling the skin pixel. In this work, the maximum of histogram skin color based segmentation have been proposed as shown in equation (2). The future work is to build modeling system based histogram skin color segmentation technique by using the Mixture of multiple histogram technique (MiMHT), where each separated color model applied on histogram based approaches are evaluated by a weight value. The weights for each color model are represented by the classification rate (CR) defined in equation (5) in which it represent the exact representation of the model efficiency. Equation (6) explained the proposed system:

$$P(c|skin) = \sum_{i=1}^I W_i h_i(c) \quad (6)$$

Where W_i represents the weight's value of the i th selected color model. The value of the weight can be calculated from the normalization of the classification rates CR of the utilized color models as shown in equation (7)

$$W_i = \frac{CR_i}{\sum_{i=1}^I CR_i}, \forall i = 1, 2, \dots, I \quad (7)$$

REFERENCES

- [1]. Mokhtar M.Hasan, Pramod K. Mishra, " Superior Skin Color Model using Multiple of Gaussian Mixture Model", British Journal of Science, Vol. 6 (1), pp. 1-14, 2012.
- [2]. Moritz StÄorring, "Computer Vision and Human Skin Colour", Ph.D. Dissertation, Faculty of Engineering and Science, 2004.
- [3]. S. E. Ghobadi, O. E. Loepprich, K. Hartmann, and O. Loffeld, "Hand Segmentation Using 2D/3D Images", Conference of Image and Vision Computing New Zealand 2007, pp. 64–69, New Zealand, December 2007.
- [4]. Zhi-Kai Huang, Kwok-Wing Chau, "A New Image Thresholding Method Based on Gaussian Mixture Model", Applied Mathematics and Computation, Vol. 205(2), pp 899-907, 2008.
- [5]. Vladimir Vezhnevets, Vassili Sazonov, and Alla Andreeva, "A Survey on Pixel-Based Skin Color Detection Techniques", International Conference Graphicon, Moscow, 2003.
- [6]. Leonid Sigal, Stan Sclaroff, and Vassilis Athitsos, "Skin Color-Based Video Segmentation under Time-Varying Illumination", IEEE Transactions on Pattern Analysis and Machine Intelligence, Vol. 26(7), 2004.
- [7]. Jeff A. Bilmes, "A Gentle Tutorial of the EM Algorithm and its Application to Parameter Estimation for Gaussian Mixture and Hidden Markov Models", International Computer Science Institute. Gokalp, D.: Learning Skin Pixels in Color Images Using Gaussian Mixture. Available http://www.cs.bilkent.edu.tr/~guvenir/courses/cs550/Workshop/Demir_Gokalp.pdf Skin Color Segmentation
- [8]. Reiner Lenz, Pedro Latorre Carmona, "Transform Coding Of Rgb- Histograms" <http://scien.stanford.edu/pages/labsite/2002/psych221/projects/02/sojeong/>
- [9]. Qiong Liu, Guang-zheng Peng, " A robust skin color based face detection algorithm", 2nd International Asia Conference on Informatics in Control, Automation and Robotics (CAR), Vol. 2, pp. 525 – 528, 2010 Chia-Feng Juang , Hwai-Sheng Perng , and Shin-Kuan Chen, " Skin color segmentation by histogram-based neural fuzzy network", Proceedings IEEE International Joint Conference on Neural Networks (IJCNN '05), Vol 5, pp. 3058-3062, 2005.
- Jörg Appenrodt, Ayoub Al-Hamadi, and Bernd Michaelis, "Data Gathering for Gesture Recognition Systems Based on Single Color-, Stereo Color- and Thermal Cameras", International Journal of Signal Processing, Image Processing and Pattern Recognition, Vol. 3(1), pp. 37-49, 2010.
- [10]. Phung, S. L., Bouzerdoum, A., , Chai, D.: Skin Segmentation using Color Pixel Classification: Analysis and Comparison. IEEE Transactions on Pattern Analysis and Machine Intelligence, pp. 148-154, Vol. 27(1), (2005). Doi: [10.1109/TPAMI.2005.17](https://doi.org/10.1109/TPAMI.2005.17)

Strength of Blended Cement Sandcrete & Soilcrete Blocks Containing Cassava Waste Ash and Plantain Leaf Ash

L. O. Ettu¹, M. S. W. Mbajiorgu², and J. I. Arimanwa³

^{1,3}Department of Civil Engineering, Federal University of Technology, Owerri, Nigeria

²Department of Civil Engineering, Enugu State University of Science and Technology, Enugu, Nigeria

Abstract: This work investigated the compressive strength of binary and ternary blended cement sandcrete and soilcrete blocks containing cassava waste ash (CWA) and plantain leaf ash (PLA). 135 solid sandcrete blocks and 135 solid soilcrete blocks of 450mm x 225mm x 125mm were produced with OPC-CWA binary blended cement, 135 with OPC-PLA binary blended cement, and 135 with OPC-CWA-PLA ternary blended cement, each at percentage OPC replacement with pozzolan of 5%, 10%, 15%, 20%, and 25%. Three sandcrete blocks and three soilcrete blocks for each OPC-pozzolan mix and the control were crushed to obtain their compressive strengths at 3, 7, 14, 21, 28, 50, 90, 120, and 150 days of curing. Sandcrete and soilcrete block strengths from binary and ternary blended cements were found to be higher than the control values beyond 90 days of hydration. The 150-day strength values for OPC-CWA-PLA ternary blended cement sandcrete and soilcrete blocks were respectively 5.90N/mm² and 5.10N/mm² for 5% replacement, 5.80N/mm² and 4.95N/mm² for 10% replacement, 5.65N/mm² and 4.85N/mm² for 15% replacement, 5.60N/mm² and 4.75N/mm² for 20% replacement, and 5.25N/mm² and 4.65N/mm² for 25% replacement; while the control values were 5.20N/mm² and 4.65N/mm². Thus, OPC-CWA and OPC-PLA binary blended cements as well as OPC-CWA-PLA ternary blended cement could be used in producing sandcrete and soilcrete blocks with sufficient strength for use in building and minor civil engineering works where the need for high early strength is not a critical factor.

Keywords: Binary blended cement, ternary blended cement, sandcrete block, soilcrete block, pozzolan, cassava waste ash, plantain leaf ash.

I. INTRODUCTION

Sandcrete and soilcrete blocks are cement composites commonly used as walling units in buildings all over South Eastern Nigeria and many other parts of Africa. Many researchers have investigated various aspects of these important construction materials. Baiden and Tuuli (2004) confirmed that mix ratio, materials quality, and mixing of the constituent materials affect the quality of sandcrete blocks. Afolayan, Arum, and Daramola (2008) tested the compressive strength values of sandcrete blocks produced by different block industries in Ondo State, Nigeria and found that they were very much lower than those stipulated by the relevant Codes and Standards. The blocks also had high coefficient of variation that indicate very poor quality control in the production processes. Wenapere and Ephraim (2009) found that the compressive strength of sandcrete blocks increased with age of curing for all mixes tested at the water-cement ratio of 0.5. The strength at ages 7, 14, and 21 days were 43%, 75%, and 92% of the 28-day strength respectively. Much of the focus of researchers in this field within the past decade has been to find ways of reducing the cost of cement used in sandcrete and soilcrete block production so as to provide low-cost buildings in the suburbs and villages of South Eastern Nigeria. Agricultural by-products regarded as wastes in technologically underdeveloped societies are increasingly being investigated as partial replacement of Ordinary Portland Cement (OPC). Blended cements are already used in many parts of the world since it has been established that supplementary cementitious materials prove to be effective to meet most of the requirements of durable cement composites (Bakar, Putrajaya, and Abdulaziz, 2010). Incorporating agricultural by-product pozzolans such as rice husk ash (RHA) calcined at high temperatures has been studied with positive results in the manufacture and application of blended cements (Malhotra and Mehta, 2004). Agbede and Obam (2008) have investigated the strength properties of OPC-RHA

blended sandcrete blocks. They replaced various percentages of OPC with RHA and found that up to 17.5% of OPC can be replaced with RHA to produce good quality sandcrete blocks. Ganesan, Rajagopal, and Thangavel (2008) assessed the optimal level of replacement of OPC with RHA for strength and permeability properties of blended cement concrete. Nair, Jagadish, and Fraaij (2006) found that RHA could be a suitable alternative to OPC for rural housing. Cisse and Laquerbe (2000) reported that sandcrete blocks obtained with unground Senegalese RHA as partial replacement of OPC had greater mechanical resistance than 100% OPC sandcrete blocks. Their study also revealed that the use of unground RHA enabled production of lightweight sandcrete block with insulating properties at a reduced cost. Elinwa and Awari (2001) found that groundnut husk ash could be suitably used as partial replacement of OPC in concrete making. Oyekan and Kamiyo (2011) reported that sandcrete blocks made with RHA-blended cement had lower heat storage capacity and lower thermal mass than 100% OPC sandcrete blocks. They explained that the increased thermal effusivity of the sandcrete block with RHA content is an advantage over 100% OPC sandcrete block as it enhances human thermal comfort. Several other researchers have also investigated the combination of OPC with different percentages of a pozzolan in making binary blended cement composites (Adewuyi and Ola, 2005; De Sensale, 2006; Saraswathy and Song, 2007). Wada et al. (2000) demonstrated that RHA mortar and concrete exhibited higher compressive strength than the control mortar and concrete. Mehta and Pirtz (2000) investigated the use of rice husk ash to reduce temperature in high strength mass concrete and concluded that RHA is very effective in reducing the temperature of mass concrete compared to OPC concrete. Malhotra and Mehta (2004) reported that ground RHA with finer particle size than OPC improves concrete properties as higher substitution amounts result in lower water absorption values and the addition of RHA causes an increment in the compressive strength. Sakr (2006) investigated the effects of silica fume and rice husk ash on the properties of heavy weight concrete and found that these pozzolans gave higher concrete strengths than OPC concrete at curing ages of 28 days and above. Cordeiro, Filho, and Fairbairn (2009) investigated Brazilian RHA and rice straw ash (RSA) and demonstrated that grinding increased the pozzolanicity of RHA and that high strength of RHA, RSA concrete makes production of blocks with good bearing strength in a rural setting possible. Their study showed that combination of RHA or RSA with lime produces a weak cementitious material which could however be used to stabilize laterite and improve the bearing strength of the material. Rukzon, Chindaprasirt, and Mahachai (2009) studied the effect of grinding on the chemical and physical properties of rice husk ash and the effects of RHA fineness on properties of mortar and found that pozzolans with finer particles had greater pozzolanic reaction. Cordeiro, Filho, and Fairbairn (2009) further investigated the influence of different grinding times on the particle size distribution and pozzolanic activity of RHA obtained by uncontrolled combustion in order to improve the performance of the RHA. The study revealed the possibility of using ultrafine residual RHA containing high-carbon content in high-performance concrete. Habeeb and Fayyadh (2009) also investigated the influence of RHA average particle size on the properties of concrete and found that at early ages the strength was comparable, while at the age of 28 days finer RHA exhibited higher strength than the sample with coarser RHA. Pioneer researches have also been carried out on the possibility of ternary blended systems whereby OPC is blended with two different pozzolans. The ternary blended system has two additional economic and environmental advantages. First, it makes it possible for two pozzolans to be combined with OPC even if neither of them is available in very large quantity. Second, it enables a further reduction of the quantity of OPC in blended cements. Elinwa, Ejeh, and Akpabio (2005) investigated the use of sawdust ash in combination with metakaolin as a ternary blend with 3% added to act as an admixture in concrete. Tyagher, Utsev, and Adagba (2011) found that sawdust ash-lime mixture as partial replacement for OPC is suitable for the production of sandcrete hollow blocks. They reported that 10% replacement of OPC with SDA-lime gave the maximum strength at water-cement ratio of 0.55 for 1:8 mix ratio. Fri'as et al. (2005) studied the influence of calcining temperature as well as clay content in the pozzolanic activity of sugar cane straw-clay ashes-lime systems. All calcined samples showed very high pozzolanic activity and the fixation rate of lime varied with calcining temperature and clay content. Rukzon and Chindaprasirt (2006) investigated the strength development of mortars made with ternary blends of OPC, ground RHA, and classified fly ash (FA). The results showed that the strength at the age of 28 and 90 days of the binary blended cement mortar containing 10 and 20% RHA were slightly higher than those of the control, but less than those of FA. Ternary blended cement mixes with 70% OPC and 30% of combined FA and RHA produced strengths similar to that of the control. The researchers concluded that 30% of OPC could be replaced with the combined FA and RHA pozzolans without significantly lowering the strength of the mixes. Fadzil et al. (2008) have also studied the properties of ternary blended cementitious (TBC) systems containing OPC, ground Malaysian RHA, and fly ash (FA). They found that compressive strength of concrete containing TBC gave low strength at early ages, even lower than that of OPC, but higher than binary blended cementitious (BBC) concrete containing FA. Their results suggested the possibility of using TBC systems in the concrete construction industry and that TBC systems could be particularly useful in reducing the volume of OPC used. Much of the previous works by researchers on ternary

blended cements were based on the ternary blending of OPC with an industrial by-product pozzolan such as FA or silica fume (SF) and an agricultural by-product pozzolan, notably RHA. Tons of agricultural and plant wastes such as cassava waste (the peelings from cassava tubers) and plantain leaf are generated in the various local communities in South Eastern Nigeria due to intensified food production and local economic ventures. Very little literature is available on the possibility of binary combination of these Nigerian agricultural by-products with OPC in developing blended cements and no literature exists on the possibility of ternary blending of two of them with OPC. This work is part of a pioneer investigation of the suitability of using two Nigerian agricultural by-products in ternary blend with OPC for sandcrete and soilcrete block making. The compressive strength of binary and ternary blended cement sandcrete and soilcrete blocks containing cassava waste ash and plantain leaf ash was specifically investigated. It is hoped that the successful utilization of cassava waste ash and plantain leaf ash in binary and ternary combination with OPC for making sandcrete and soilcrete blocks would go a long way in reducing the cost of building and minor civil engineering projects that make much use of sandcrete and soilcrete blocks as well as add economic value to these agricultural by-product wastes.

II. METHODOLOGY

Cassava waste (the peelings from cassava tubers) was obtained from Ihiagwa in Imo State and plantain leaf from Ogbunike in Anambra State, all in South Eastern Nigeria. These materials were air-dried and calcined into ashes in a locally fabricated furnace at temperatures generally below 650°C. The cassava waste ash (CWA) and plantain leaf ash (PLA) were sieved and large particles retained on the 600µm sieve were discarded while those passing the sieve were used for this work. No grinding or any special treatment to improve the quality of the ashes and enhance their pozzolanicity was applied. The CWA had a bulk density of 820 Kg/m³, specific gravity of 1.95, and fineness modulus of 1.88. The PLA had a bulk density of 750 Kg/m³, specific gravity of 1.80, and fineness modulus of 1.35. Other materials used for the work are Ibeto brand of Ordinary Portland Cement (OPC) with a bulk density of 1650 Kg/m³ and specific gravity of 3.13; river sand free from debris and organic materials with a bulk density of 1590 Kg/m³, specific gravity of 2.68, and fineness modulus of 2.82; laterite also free from debris and organic materials with a bulk density of 1450 Kg/m³, specific gravity of 2.30, and fineness modulus of 3.30; and water free from organic impurities.

A simple form of pozzolanicity test was carried out for each of the ashes. It consists of mixing a given mass of the ash with a given volume of Calcium hydroxide solution [Ca(OH)₂] of known concentration and titrating samples of the mixture against H₂SO₄ solution of known concentration at time intervals of 30, 60, 90, and 120 minutes using Methyl Orange as indicator at normal temperature. For each of the ashes the titre value was observed to reduce with time, confirming the ash as a pozzolan that fixed more and more of the calcium hydroxide, thereby reducing the alkalinity of the mixture. A standard mix ratio of 1:6 (blended cement: laterite) was used for both the sandcrete and the soilcrete blocks. Batching was by weight and a constant water/cement ratio of 0.6 was used. Mixing was done manually on a smooth concrete pavement. For binary blending with OPC, each of the ashes was first thoroughly blended with OPC at the required proportion and the homogenous blend was then mixed with the sand in the case of sandcrete blocks and with laterite in the case of soilcrete blocks, also at the required proportions. For ternary blending, the two ashes were first blended in equal proportions and subsequently blended with OPC at the required proportions before mixing with the sand or laterite, also at the required proportions. Water was then added gradually and the entire sandcrete or soilcrete heap was mixed thoroughly to ensure homogeneity.

One hundred and thirty-five (135) solid sandcrete blocks and one hundred and thirty-five (135) solid soilcrete blocks of 450mm x 225mm x 125mm were produced with OPC-CWA binary blended cement, one hundred and thirty-five (135) with OPC-PLA binary blended cement, and one hundred and thirty-five (135) with OPC-CWA-PLA ternary blended cement, each at percentage OPC replacement with pozzolan of 5%, 10%, 15%, 20%, and 25%. Twenty seven (27) sandcrete blocks and twenty seven (27) soilcrete blocks were also produced with 100% OPC or 0% replacement with pozzolan to serve as control. This gives a total of 432 sandcrete blocks and 432 soilcrete blocks. All the blocks were cured by water sprinkling twice a day in a shed. Three sandcrete blocks and three soilcrete blocks for each OPC-pozzolan mix and the control were tested for saturated surface dry bulk density and crushed to obtain their compressive strengths at 3, 7, 14, 21, 28, 50, 90, 120, and 150 days of curing.

III. RESULTS AND DISCUSSION

The pozzolanicity test confirmed both the CWA and the PLA as pozzolans since they fixed some quantities of lime over time. The particle size analysis showed that both ashes were much coarser than OPC, the reason being that they were not ground to finer particles. This implies that the compressive strength values obtained using them could still be improved upon if the ashes are ground to finer particles. The compressive

strengths of the OPC-CWA and OPC-PLA binary blended cement sandcrete and soilcrete blocks as well as the OPC-CWA-PLA ternary blended cement sandcrete and soilcrete blocks are shown in tables 1, 2, and 3 for 3-14 days, 21-50 days, and 90-150 days of curing respectively.

Table 1. Compressive strength of blended OPC-CWA-PLA cement sandcrete and soilcrete blocks at 3-14 days of curing

OPC Plus	Compressive Strength of sandcrete blocks (N/mm ²)						Compressive Strength of soilcrete blocks (N/mm ²)					
	0% Poz.	5% Poz.	10% Poz.	15% Poz.	20% Poz.	25% Poz.	0% Poz.	5% Poz.	10% Poz.	15% Poz.	20% Poz.	25% Poz.
	Strength at 3 days						Strength at 3 days					
CWA	0.90	0.65	0.60	0.55	0.45	0.40	0.80	0.60	0.55	0.50	0.40	0.35
PLA	0.90	0.65	0.55	0.50	0.45	0.40	0.80	0.55	0.50	0.45	0.35	0.30
CWA&LA	0.90	0.65	0.55	0.50	0.45	0.40	0.80	0.60	0.55	0.45	0.35	0.30
	Strength at 7 days						Strength at 7 days					
CWA	1.50	1.30	1.25	1.15	1.05	0.90	1.25	1.15	1.00	0.90	0.80	0.70
PLA	1.50	1.25	1.20	1.15	1.00	0.90	1.20	1.05	0.95	0.85	0.75	0.65
CWA&LA	1.50	1.25	1.20	1.15	1.00	0.90	1.20	1.10	0.95	0.85	0.75	0.65
	Strength at 14 days						Strength at 14 days					
CWA	2.70	2.30	2.25	2.20	2.00	1.80	2.30	2.00	1.85	1.80	1.70	1.60
PLA	2.70	2.30	2.20	2.10	1.95	1.80	2.30	1.95	1.80	1.75	1.65	1.55
CWA&LA	2.70	2.30	2.20	2.15	1.95	1.80	2.30	1.95	1.85	1.75	1.65	1.55

Table 2. Compressive strength of blended OPC-CWA-PLA cement sandcrete and soilcrete blocks at 21-50 days of curing

OPC Plus	Compressive Strength of sandcrete blocks (N/mm ²)						Compressive Strength of soilcrete blocks (N/mm ²)					
	0% Poz.	5% Poz.	10% Poz.	15% Poz.	20% Poz.	25% Poz.	0% Poz.	5% Poz.	10% Poz.	15% Poz.	20% Poz.	25% Poz.
	Strength at 21 days						Strength at 21 days					
CWA	3.50	3.20	3.10	3.00	2.90	2.75	3.10	2.75	2.60	2.50	2.40	2.30
PLA	3.50	3.15	3.05	2.90	2.85	2.70	3.10	2.70	2.55	2.45	2.35	2.25
CWA&LA	3.50	3.15	3.05	2.90	2.90	2.75	3.10	2.70	2.55	2.45	2.35	2.25
	Strength at 28 days						Strength at 28 days					
CWA	4.40	4.10	4.00	3.90	3.80	3.65	3.90	3.55	3.40	3.35	3.25	3.15
PLA	4.40	4.05	3.90	3.80	3.75	3.55	3.90	3.50	3.40	3.25	3.20	3.20
CWA&LA	4.40	4.05	3.95	3.85	3.80	3.60	3.90	3.50	3.40	3.30	3.20	3.20
	Strength at 50 days						Strength at 50 days					
CWA	4.70	4.60	4.50	4.40	4.45	4.30	4.30	4.40	4.25	4.15	4.05	3.95
PLA	4.70	4.60	4.45	4.40	4.35	4.20	4.30	4.35	4.30	4.15	4.00	3.95
CWA&LA	4.70	4.60	4.45	4.40	4.35	4.25	4.30	4.35	4.30	4.15	4.00	3.95

Table 3. Compressive strength of blended OPC-CWA-PLA cement sandcrete and soilcrete blocks at 90-150 days of curing

OPC Plus	Compressive Strength of sandcrete blocks (N/mm ²)						Compressive Strength of soilcrete blocks (N/mm ²)					
	0% Poz.	5% Poz.	10% Poz.	15% Poz.	20% Poz.	25% Poz.	0% Poz.	5% Poz.	10% Poz.	15% Poz.	20% Poz.	25% Poz.
	Strength at 90 days						Strength at 90 days					
CWA	4.90	5.00	4.90	4.80	4.75	4.50	4.50	4.70	4.65	4.55	4.35	4.25
PLA	4.90	5.00	4.95	4.80	4.70	4.40	4.50	4.70	4.60	4.55	4.30	4.20
CWA&LA	4.90	5.00	4.90	4.80	4.75	4.45	4.50	4.70	4.60	4.55	4.30	4.20
	Strength at 120 days						Strength at 120 days					
CWA	5.10	5.65	5.55	5.45	5.30	5.20	4.60	5.00	4.90	4.80	4.70	4.60
PLA	5.10	5.60	5.55	5.40	5.20	5.10	4.60	5.00	4.90	4.75	4.60	4.50
CWA&LA	5.10	5.60	5.55	5.40	5.20	5.10	4.60	5.00	4.90	4.80	4.75	4.55
	Strength at 150 days						Strength at 150 days					
CWA	5.20	5.95	5.80	5.70	5.65	5.30	4.65	5.10	5.00	4.90	4.80	4.70
PLA	5.20	5.80	5.70	5.60	5.55	5.20	4.65	5.05	4.90	4.80	4.70	4.60
CWA&LA	5.20	5.90	5.80	5.65	5.60	5.25	4.65	5.10	4.95	4.85	4.75	4.65

The results in tables 1 to 3 show that the values of soilcrete block strength are consistently less than the corresponding values of sandcrete block strength for all percentages of OPC replacement with pozzolans and at all curing ages. This confirms the superiority of sand over laterite as fine aggregate material in making cement composites. Nonetheless, a close examination of the results shows that the values of the soilcrete block strengths are not much different from those of sandcrete block strengths. For example, the 50-day strengths are 4.70N/mm² for sandcrete block and 4.30N/mm² for soilcrete block at 100% OPC and 4.45N/mm² for sandcrete block and 4.30N/mm² for soilcrete block at 10% replacement of OPC with CWA-PLA in ternary blending. This also confirms that laterite could be used as sole fine aggregate in making cement composites for low-cost houses in communities where sharp sand is difficult to obtain at affordable prices.

The strength values for OPC-CWA and OPC-PLA binary blended cement sandcrete and soilcrete blocks as well as those of OPC-CWA-PLA ternary blended cement sandcrete and soilcrete blocks were all less than the equivalent control values at 3-50 days of hydration for all percentage replacements of OPC with pozzolans. The strength values of the binary and ternary blended cement sandcrete and soilcrete blocks were the same with the equivalent control values at about 90 days of hydration and greater than the control values at curing ages beyond 90 days. The 150-day strength values for OPC-CWA-PLA ternary blended cement sandcrete and soilcrete blocks were respectively 5.90N/mm² and 5.10N/mm² for 5% replacement, 5.80N/mm² and 4.95N/mm² for 10% replacement, 5.65N/mm² and 4.85N/mm² for 15% replacement, 5.60N/mm² and 4.75N/mm² for 20% replacement, and 5.25N/mm² and 4.65N/mm² for 25% replacement; while the control values were 5.20N/mm² and 4.65N/mm². The lower strength values of blended cement sandcrete and soilcrete blocks at earlier days of hydration shows that pozzolanic reaction was not yet much at those earlier periods; the pozzolanic reaction became higher at later ages and this accounts for the much increase in strength of blended cement sandcrete and soilcrete blocks compared to the control specimens.

It can also be seen from tables 1-3 that the strength values of OPC-CWA binary blended cement sandcrete and soilcrete blocks were consistently marginally greater than those of OPC-PLA binary blended cement sandcrete and soilcrete blocks for all percentage replacements of OPC with pozzolans and at all curing ages. The strength of the OPC-CWA-PLA ternary blended cement sandcrete and soilcrete blocks was consistently in-between the values of the OPC-CWA and OPC-PLA binary blended cement sandcrete and soilcrete blocks. This suggests that more CWA than PLA should be utilized if the two pozzolans were to be used in unequal proportions to optimize the strength of the OPC-CWA-PLA ternary blended cement sandcrete and soilcrete blocks. Moreover, the closeness in strength values of OPC-CWA and OPC-PLA binary blended cement sandcrete and soilcrete blocks and the fact that the strength of the OPC-CWA-PLA ternary blended cement sandcrete and soilcrete blocks was in-between these values suggests that the two agricultural by-product pozzolans could be combined in any available proportions individually in binary blending or together in ternary blending with OPC in making blended cement sandcrete and soilcrete blocks.

IV. CONCLUSIONS

The strength values of soilcrete blocks were found to be less than those of sandcrete blocks for all percentages of OPC replacement with pozzolans and at all curing ages. Therefore, sand should be used in preference to laterite for cement blocks making. However, since the soilcrete block strengths were not much less than the equivalent sandcrete block strengths, good quality laterite is still suitable for block making in the various communities where sand is scarce and unaffordable to the rural populace. OPC-CWA and OPC-PLA binary blended cement sandcrete and soilcrete blocks as well as OPC-CWA-PLA ternary blended cement sandcrete and soilcrete blocks have compressive strength values less than those of 100% OPC sandcrete and soilcrete blocks for 5-25% replacement of OPC with pozzolans at 3-50 days of hydration. The blended cement sandcrete and soilcrete block strength values become equal to the control values at about 90 days of curing and greater than the control values beyond 90 days of hydration. Thus, OPC-CWA and OPC-PLA binary blended cements as well as OPC-CWA-PLA ternary blended cement could be used in producing sandcrete and soilcrete blocks with sufficient strength for use in building and minor civil engineering works where the need for high early strength is not a critical factor.

The strength of OPC-CWA binary blended cement sandcrete and soilcrete blocks is consistently greater than that of OPC-PLA binary blended cement specimens for all percentage replacements of OPC with pozzolans and at all curing ages. The strength values of OPC-CWA-PLA ternary blended cement sandcrete and soilcrete blocks were consistently in-between the values of OPC-CWA and OPC-PLA binary blended cement sandcrete and soilcrete blocks. This suggests that more CWA should be used than PLA if the two pozzolans were to be used in unequal proportions to optimize the strength of the OPC-CWA-PLA ternary blended cement sandcrete and soilcrete blocks. Moreover, the closeness in strength values of OPC-CWA and OPC-PLA binary blended cement sandcrete and soilcrete blocks and the fact that the strength of the OPC-CWA-PLA ternary blended cement sandcrete and soilcrete blocks was in-between these values suggests that the two agricultural by-product

pozzolans could be combined in any available proportions individually in binary blending or together in ternary blending with OPC in making blended cement sandcrete and soilcrete blocks for use in various Nigerian communities.

REFERENCES

- [1]. Adewuyi, A.P., & Ola, B. F. (2005). Application of waterworks sludge as partial replacement for cement in concrete production. *Science Focus Journal*, 10(1): 123-130.
- [2]. Agbede, I. O., & Obam, S. O. (2008). Compressive Strength of Rice Husk Ash-Cement Sandcrete Blocks. *Global Journal of Engineering Research*, Vol. 7 (1), pp. 43-46.
- [3]. Afolayan, J. O., Arum, C., and Daramola, C. M. (2008). Characterization of the Compressive Strength of Sandcrete Blocks in Ondo State, Nigeria. *Journal of Civil Engineering Research and Practice*, 5 (1): 15-28.
- [4]. Bakar, B. H. A., Putrajaya, R. C., & Abdulaziz, H. (2010). Malaysian Saw dust ash –Improving the Durability and Corrosion Resistance of Concrete: Pre-review. *Concrete Research Letters*, 1 (1): 6-13, March 2010.
- [5]. Baiden, B. K. and Tuuli, M. M. (2004). Impact of quality control practices in sandcrete blocks production. *Journal of Architectural Engineering*, 10 (2): 53-60.
- [6]. Cisse, I. K., & Laquerbe, M. (2000). Mechanical characterization of sandcretes with rice husk ash additions: study applied to Senegal. *Cement and Concrete Research*, 30 (1): 13– 18.
- [7]. Cordeiro, G. C., Filho, R. D. T., & Fairbairn, E. D. R. (2009). Use of ultrafine saw dust ash with high-carbon content as pozzolan in high performance concrete. *Materials and Structures*, 42: 983–992. DOI 10.1617/s11527-008-9437-z.
- [8]. De Sensale, G. R. (2006). Strength development of concrete with rice-husk ash. *Cement & Concrete Composites*, 28: 158–160.
- [9]. Elinwa, A. U., & Awari, A. (2001). Groundnut husk ash concrete. *Nigerian Journal of Engineering Management*, 2 (1), 8 - 15.
- [10]. Elinwa, A. U., Ejeh, S. P., & Akpabio, I. O. (2005). Using metakaolin to improve sawdust-ash concrete. *Concrete International*, 27 (11), 49 - 52.
- [11]. Fadzil, A. M., Azmi, M. J. M., Hisyam, A. B. B., & Azizi, M. A. K. (2008). Engineering Properties of Ternary Blended Cement Containing Rice Husk Ash and Fly Ash as Partial Cement Replacement Materials. *ICCBT, A* (10): 125 – 134.
- [12]. Frias, M., Villar-Cocina, E., Sanchez-de-Rojas, M. I., & Valencia-Morales, E. (2005). The effect that different pozzolanic activity methods has on the kinetic constants of the pozzolanic reaction in sugar cane straw-clay ash/lime systems: Application of a kinetic-diffusive model. *Cement and Concrete Research*, 35: 2137 – 2142.
- [13]. Ganesan, K., Rajagopal, K., and Thangavel, K. (2008). Rice husk ash blended cement: assessment of optimal level of replacement for strength and permeability properties of concrete. *Constr. Build. Mater.*, 22(8):1675-1683.
- [14]. Habeeb, G. A., & Fayyadh, M. M. (2009). Saw dust ash Concrete: the Effect of SDA Average Particle Size on Mechanical Properties and Drying Shrinkage. *Australian Journal of Basic and Applied Sciences*, 3(3): 1616-1622.
- [15]. Malhotra, V. M., & Mehta, P. K. (2004). *Pozzolanic and Cementitious Materials*. London: Taylor & Francis.
- [16]. Mehta, P. K. & Pirtz, D. (2000). Use of rice husk ash to reduce temperature in high strength mass concrete. *ACI Journal Proceedings*, 75:60-63.
- [17]. Nair, D. G., Jagadish, K. S., and Fraaij, A. (2006). Reactive pozzolanas from rice husk ash: An alternative to cement for rural housing. *Cem Concr. Res.*, 36 (6): 1062-1071.
- [18]. Oyekan, G. L. and Kamiyo, O. M. (2011). A study on the engineering properties of sandcrete blocks produced with rice husk ash blended cement. *Journal of Engineering and Technology Research*, 3(3): 88-98.
- [19]. Rukzon, S., & Chindapasirt, P. (2006). Strength of ternary blended cement mortar containing Portland cement, rice husk ash and fly ash. *J. Eng. Inst. Thailand*, 17: 33-38 (547-551).
- [20]. Rukzon, S., Chindapasirt, P., & Mahachai, R. (2009). Effect of grinding on chemical and physical properties of saw dust ash. *International Journal of Minerals, Metallurgy and Materials*, 16 (2): 242-247.
- [21]. Sakr, K. (2006). Effects of Silica Fume and Rice Husk Ash on the Properties of Heavy Weight Concrete. *Journal of Materials in Civil Engineering*, 18(3): 367-376.
- [22]. Saraswathy, V., & Song, H. (2007). Corrosion performance of rice husk ash blended concrete. *Construction and Building Materials*, 21 (8): p.1779–1784.
- [23]. Tyagher, S. T., Utsev, J. T., and Adagba, T. (2011). Suitability of Sawdust Ash-Lime Mixture for Production of Sandcrete Hollow Blocks. *Nigerian Journal of Technology*, 30 (1): 79-84.
- [24]. Wada, I., Kawano, T., & Mokotomaeda, N. (2000). Strength properties of concrete incorporating highly reactive rice-husk ash. *Transaction of Japan Concrete Institute*, 21 (1): p. 57–62.
- [25]. Wenapere, D. A. and Ephraim, M. E. (2009). Physico-mechanical behaviour of sandcrete block masonry units. *Journal of Building Appraisal* 4: 301–309. doi:10.1057/jba.2009.8.

Distribution of Arsenic and Heavy Metals from Mine Tailings dams at Obuasi Municipality of Ghana

Crentsil Kofi Bempah*^{1,6}, Anthony Ewusi², Solomon Obiri-Yeboah¹, Stephen Boahen Asabere⁴, Francis Mensah³, Juliana Boateng⁵, Hans-Jürgen Voigt¹

¹Faculty of Environmental Sciences and Process Engineering, Chair of Environmental Geology Erich-Weinert-Straße 1, 03046, Brandenburgische Technische Universität, Cottbus, Germany

²Department of Geology, University of Mines, Tarkwah

³Faculty of Environmental Sciences and Process Engineering, Chair of General Ecology, P.O. Box 101344, 03013, Brandenburgische Technische Universität, Cottbus, Germany

⁴Department of Forest and Environment, Hochschule für nachhaltige Entwicklung, Friedrich-Ebert-Strasse 28, D-16225, Eberswalde Germany

⁵Environmental Protection Agency, P.O. Box M 326, Ministries, Accra, Ghana

⁶Nuclear Chemistry and Environmental Research Centre, National Nuclear Research Institute, Ghana Atomic Energy Commission, P.O. Box LG 80, Legon, Accra-Ghana

Abstract: This present study investigated the issue of gold mine tailings dams as a potential source of arsenic and other trace elements contamination and their dissolution into the adjoining environmental media in Obuasi Municipality of Ghana. One active (Sanso tailings dam) and two abandoned (Pompura and Dokyiwa) mine tailings dams in Obuasi gold mine site, were selected for the collection and analysis of the tailings. The concentrations of As, Fe, Mn, Cu and Zn were determined using an atomic absorption spectrometer (AAS, Varian Models 240FS). The total concentrations of elements in the mine tailings were up to 1752 mg/kg As, 75.16 wt.% Fe, 1848.12 mg/kg Mn, 92.17 mg/kg Cu and 7850 177.56 mg/kg Zn. Sulfate was the dominant anion throughout the leachate, reaching a maximum dissolved concentration of 58.43 mg/L. The mine tailings were contaminated with much higher concentrations of As and heavy metals than the Netherlands soil protection guideline values. Leaching levels of As were in the range of 0.04–0.56 %, presenting high proportions for the total arsenic content in the mine tailings.

Keywords: Arsenic, heavy metals, mine tailings, gold mining, Obuasi, Ghana

I. INTRODUCTION

Ghana, formerly the Gold Coast, is an important gold mining country located in the western part of Africa. Commercial scale gold mining predates the late 19th century. The Ashanti and Western regions are the major gold mining locations. The gold (Au) is associated with sulphide mineralization, particularly arsenopyrite (Griffis et al., 2002). The belief is that the Birimian formation has over ten times the average crystal abundances of gold and arsenic (Kesse, 1985). Due to the nature of the gold ore and the previous method of mining and processing of the metal, environmental degradation and metal pollution are restricted to only mining areas especially Obuasi, Prestea, and Tarkwa. Hence arsenic mobilizes in the environment as a result of arsenopyrite oxidation induced by mining activities (especially dispersal of tailings). The degeneration of the Ghanaian mining environment by mine chemical wastes is principally the consequence of poor management of mine spoil facilities and the reckless manner in which alluvial and open pit activities are carried out.

Mining operations generally produce many types of mine wastes, including mine tailings, waste rock and slag. Mine tailings out of those, in particular, act as a main source of environmental contamination (Roussel et al., 2000). Arsenic (As) and heavy metals may be released from the mine wastes to the ground and surface water systems, as well as the geological environment due to their solubility and mobility (Jang et al., 2005). A large amount of mine wastes including mine tailings, slag, and waste rock were also produced by the mining

operation and are usually passed into the tailings. Also, flood damages and ground subsidence have occurred at the mine several times because it was not equipped with any facility for the prevention of the damage. During the year 2005, there were three recorded incidents of tailings spillage, each of it resulted in serious environmental problems at Obuasi. This spillage from the dams would be the cause of reduced production levels of farm products and reddish color of vegetation in the area as well as the bare nature of some portions of the land (Kumi-Boateng, 2007). Arsenic in mine tailings usually exists in sulfide minerals such as pyrite (FeS_2), arsenopyrite (FeAsS), galena (PbS), chalcopyrite (CuFeS_2), and sphalerite [$(\text{Fe}, \text{Zn})\text{S}$] (Roussel et al., 2000). Oxidation, dissolution, precipitation, adsorption, and desorption mainly occur in mine tailings exposed to the air. Oxidation of sulfide minerals results in contamination of the surrounding soil and groundwater by allowing release of As and heavy metals in sulfide-bearing minerals (Kim et al., 2004; Lim et al., 2009). Furthermore, As and heavy metals from mine tailings may cause fatal diseases in humans through crops and water due to the characteristic easy accumulation in internal organs (Lee et al., 2007). Hence, tailings need to be properly managed because they constitute a major source of release of many trace elements into the environment. Gold mine tailings at Obuasi, for instance, contain very high amount of As, averagely 8305 mg/kg (Ahmad and Carboo, 2000). The preferred approach to tailings management is to pump the tailings, usually in slurry form, into impoundments or dams designed to hold the tailings and perform a number of functions, including treatment functions. Around the town of Obuasi, Prestea and Tarkwa studies in these locations revealed high As concentration in water, soil, fruits, food crops, biological tissues, rivers, school compounds, farmlands and settlements close to the mine sites (Smedley et al., 1996; Amonoo-Neizer et al., 1996; Golow et al., 1996; Carboo and Sarfor-Armah, 1997; Ahmad and Carboo, 2000; Boadu et al., 2001; Akabzaa et al., 2005; Asklund and Eldvall, 2005; Ansong Asante et al., 2005). In cognizance of the above, it is apparent that, the As research in the Ghanaian environment focused primarily on surface waters, soils, food crops, fruits and biological samples with limited studies on mine tailings, identified as one of major source of As poisoning. More so, the few studies performed in some parts of Obuasi were restricted to only few sites with most communities unattended. Unfortunately, gold mining is progressing steadily in Obuasi environment known to have geology rich in arsenopyrite. Yet, the impact of this element in the Ghanaian environment has not received the fullest attention.

This present study investigated the issue of gold mine tailings dams as a potential source of arsenic and other trace elements contamination and their dissolution into the adjoining environmental media in Obuasi Municipality. The study considered two types of tailings dams - one active and two decommissioned - and assessed the distribution of these heavy metals. In addition, leaching test was conducted with rain water to ascertain a way to preserve arsenic species without change of their oxidation states and to prevent added chemicals from affecting dissolution process.

II. PHYSIOGRAPHY, GEOLOGY AND HYDROGEOLOGY

Obuasi is located in the Ashanti region of Ghana (Fig. 1) and is about 64 km south of Kumasi, the regional capital and 300 km north-west of Accra, the capital of Ghana. It is situated at latitude $6^\circ 12' 00''$ North and longitude $1^\circ 40' 00''$ West. It is located in the tropical evergreen rain forest belt. It covers an area of about 162.4 km^2 and is bounded on the south by Upper Denkyira District of the Central Region, east by Adansi South District, west by Amansie Central District and north by Adansi North District (Mensah, 2012). The climate is of the semi-equatorial type with a double rainfall regime. Total annual rainfall is about 1700 mm. Mean average annual temperature is 25.5°C and relative humidity is 75-80 % in the wet season (Fig. 2).

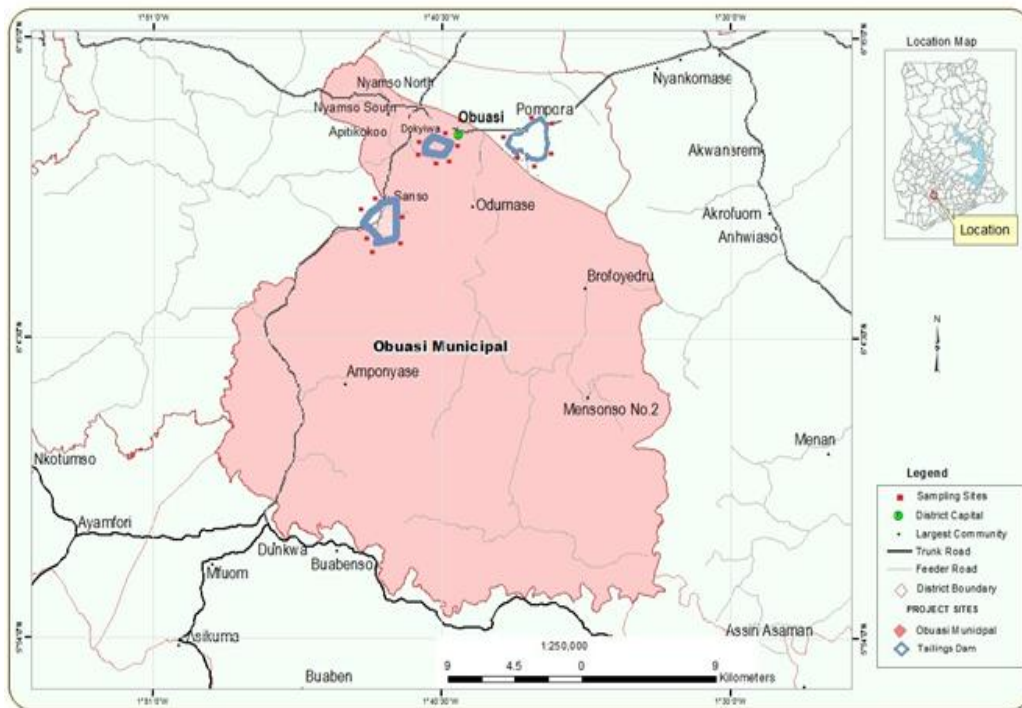


Fig. 1 Map of Obuasi Municipality showing the Sansu, Dokyiwa and Pompورا tailing dams

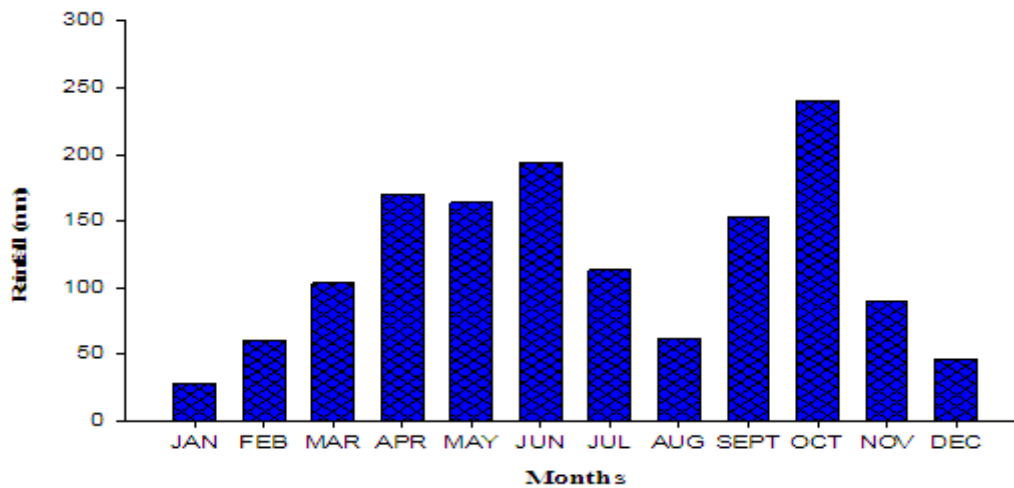


Fig. 2 Monthly rainfall pattern in Obuasi Municipality of Ghana

The area is underlain by metavolcanic, pyroclastic and metasedimentary rocks (Fig. 3). The metavolcanic rocks are of basaltic and gabbroic in compositions whereas the metasedimentary rocks are mainly tuffaceous and carbonaceous phyllites, tuff, cherts and manganeseiferous sediments. These two units are contemporaneous and separated by a major shear zone. Intruding the metavolcanic and metasedimentary rocks are magmatic bodies and porphyritic granitoids consisting of hornblende-rich varieties that are closely associated with the volcanic rocks, and mica-rich varieties which are found in the metasediment units (Kesse, 1985). The Birimian is overlain by the Tarkwaian rocks made up of sedimentary units and also recent alluvial deposits. Gold ores contain high sulphide minerals, made up mainly of arsenopyrite and pyrite (Osae et al., 1995). The top 30-80 m of the subsurface is made up of porous rocks that mark the water table in the area (Foli and Nude, 2012). Rock porosity ranges from $1.0-5.0 \times 10^{-7}$ m/s (Kumapley, 1993). These rocks have undergone some degree of weathering and consist mainly of clay deposits which have subsequently been hardened and altered. A cross section of the hills along the roads reveals the presence of an uneven distribution of quartz veins injected into the phyllites which break up on weathering to give rise to pisolithic and gravelly pebbles (Boateng et al., 2012). The topography of Obuasi and its environs varies from gently undulating to hilly. There

are moderately high-elevated lands with lowlands and valleys between them. The highlands trend in different directions; they have flat and plateau tops and are generally amorphous in their shapes.

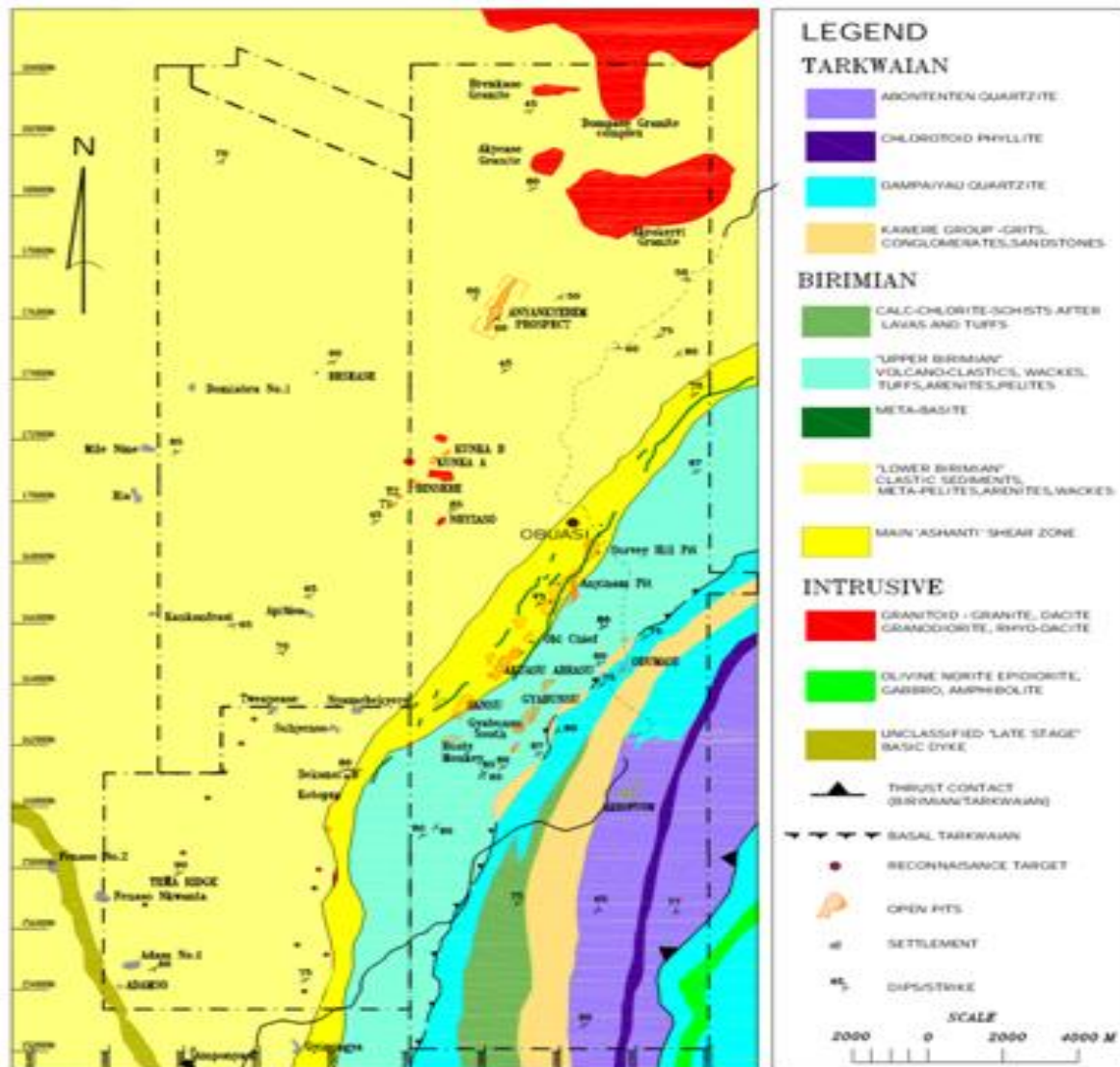


Fig 3 The geological map of Obuzasi.

III. MATERIALS AND METHODS

Sample Collection

Active and abandoned gold mine tailings dams (Fig. 1) were selected for the sample collection and analysis in the present study: they are Sansu active tailings dam, abandoned tailings dams at Pompora and Dokyiwa communities, respectively. The active tailings dams were built some two decades ago with the decommissioning of the old dam, which was used for several decades. Six spots were selected randomly at each study site for sampling using soil auger and chisel hoe. Mini pits were dug at selected points, the soils were identified by the series name and sampled at a depth of 0-20 cm. At each demarcated selected point within every site, three 1 kg soil samples were collected at a depth of 20 cm from six different locations apart by about 15 m (Fig. 1). Samples were however, not taken from locations that were difficult to access. The samples were placed into plastic bag, and then stored in a cooler in the field. The samples were transported to the laboratory for analysis. The concentrations of As, Fe, Mn, Cu and Zn were determined using an atomic absorption spectrometer (AAS, Varian Models 240FS). Particle size distribution was determined using the modified Bouyoucos hydrometer (Day, 1965). Soil pH and electrical conductivity (EC) were also determined by glass electrode in a soil-water ratio of 1:2.5. Dissolved oxygen (DO, YSI model 58) was measured. The values of several anions (Cl^- , F^- , NO_3^- , and SO_4^{2-}) were determined by an ion chromatography (as described below).

Laboratory Analysis

In order to determine the total concentrations of arsenic and metals (Fe, Cu, Mn and Zn) in the mine tailings, the samples were dried using a freeze-drier for 3–4 days and homogenized by thorough mixing. The homogenized dried samples were sieved through a 0.2 mm sieve and were digested using EPA method 6010 (Roy-Keith, 1998). A total of 18 samples were digested separately and replicate results for each sample were obtained by repeating the same process on two different days. The final suspended mixture was filtered through a 0.45 μm membrane filter. The same procedure was performed with a blank and a standard reference material (2711, Montana Soil Moderately Elevated Traces) in each batch of digestion. The concentrations of arsenic and the trace metals in the leachate were determined using atomic absorption spectrometer (AAS) whereas those of anions were by ion chromatograph (IC).

Lastly, leaching concentrations of arsenic from the mine tailings were evaluated. Leaching tests of the mine tailings were performed to indirectly evaluate release and mobility of contaminants to the surrounding environment by normal rainwater (approx. pH 5.8). The leaching test was conducted with rainwater in order to preserve arsenic species without change of their oxidation states and to prevent added chemicals from affecting As dissolution process.

Quality Control Parameter for Mine Tailings Arsenic Determination

Quality control measures were incorporated into the analytical scheme. Instrumental calibration, replicates and field blanks were prepared according to Knödel et al., (2007). A quality control (QC) standard was run routinely during the sample analysis to monitor instrument drift and overall quality of the analysis. For instrument calibration, a 100 $\mu\text{g/L}$ As standard was prepared from serial dilutions of a 1000 $\mu\text{g/L}$ stock standard. A calibration curve of 0.1, 0.5, 1.0, 1.5 and 2.0 ppm was prepared from that 100 $\mu\text{g/L}$ arsenic standard. To detect possible interferences and matrix effects, which are considered important for arsenic determinations, the standard addition method was used with five arbitrarily chosen samples (Table 1).

Table 1 Calibration plots corresponding to the standard of arsenic and the standard addition method of different samples

Standard of As	<i>r</i> (correlation coefficient)	a (intercept)	b (slope)	Slope ratios of As standard/sample
Standard of As	0.9998	0.0001	0.049	1.000
BK1	0.9979	0.0390	0.045	1.365
OB2	0.9999	0.0026	0.040	1.333
AW3	0.9995	0.0135	0.041	1.304
AC4	0.9993	0.0860	0.014	4.305
AN5	0.9989	0.0018	0.026	2.000

$$\text{Absorbance} = a + b (\text{As, ppb}).$$

The analytical characteristics for arsenic determination in mine tailings leachate samples were done by spiking three leachate samples from their respective tailings dam with 10 μg arsenic to three equal fractions of leachate samples, respectively. A matrix modifier of 5 μg of Pd and 3 μg of $\text{Mg}(\text{NO}_3)_2$, was used for each 20 mL of sample and was added into the blank, standard and samples. All samples and blanks were digested and diluted using the same procedure as described above. Reagent blank determinations were used to correct the instrument readings which were usually very low for this method.

Table 2 shows the analytical characteristics for arsenic determination in mine tailings leachate samples by AAS.

Table 2 Analytical recoveries (%) \pm SD of As metal in mine tailings leachate samples at 10.0 $\mu\text{g/L}$ fortification levels (n=3)

Leachate samples	SpikedAs (mgL^{-1})	Recovered As (%)
Dokyiwa	10	98.4 \pm 0.3 ^a
Pompora	10	94.9 \pm 1.7
Sansu	10	88.3 \pm 1.2

^a Average \pm standard deviation.

Mean recovery for the several added samples considered was 97.21 \pm 2.83 % (n=6). Mean relative standard deviations were lower than 7.00 %.

The arsenic concentrations determined in the certified reference material NIST CRM 1643d (National Institute of Standard and Technology) containing trace elements in water and total arsenic at a certified

concentration of $56.02 \pm 0.73 \mu\text{g/L}$, was also analyzed ($n=10$) and was not significantly different from certified levels ($p > 0.05$) (Table 3).

Table 3 Accuracy and precision of the proposed method for arsenic determination against standard reference materials.

Reference material	Mean total As \pm SD ($\mu\text{g/L}$)		Accuracy (%)	Precision RSD (%)
	Certified value ^a	Measured value ^a		
NIST CRM 1643d	56.02 ± 0.73	54.67 ± 0.89	96.41	5.33

IV. RESULTS AND DISCUSSION

Data on particle size distribution are presented in Table 4. Generally mine tailings from Sanso, Pompora and Dokyiwa tailings dams were reddish-brown to dark-gray coloration and sticky. The samples were in a slightly wet state containing 9.6 %, 6.2 % and 4.5 % water from the mine tailings from Sanso, Pompora and Dokyiwa tailings dam, respectively. The texture of the mine tailings at Sanso is silty clay loam whereas those of Pompora and Dokyiwa are clay.

Table 4 Particle size distribution (mean of three samples) and texture of the tailings mud

Sampling location	Depth (cm)	Particle size distribution (%)			Texture	Moisture content
		Sand	Silt	Clay		
Sanso	0-20	12	56	32	Silty clay loam	9.6
Pompورا	0-20	20	29	51	Clay	6.2
Dokyiwa	0-20	30	20	50	Clay	4.5

Data represent means of 6 samples per site

Table 5 shows pH, DO and the concentrations of fluoride, chloride, nitrate and sulfate in the leachate of mine tailings. The pHs of leachate in the analyzed samples were alkaline in nature which are not so low (not so acidic). In many cases, the mine leachate where acid mine drainage occurs would show very low pH values such as 2-4 (Jambor et al., 2003; Alvarez, et al., 2006). These neutral or slightly alkaline conditions greatly affected mobility of arsenic in the tailings mud. Relatively high pH values in this tailings mud may be derived from deficiency or less abundance of sulfide minerals in the tailings dam. Thus not much sulfate was generated from oxidation of the sulfide minerals, which did not substantially lower the pHs of the tailings mud, however, sulphate was the dominant anion among the other anions determined, reaching a maximum dissolved concentration of 58.43 mg/L. The high concentration of sulfate indicates that the oxidation of sulfide minerals had occurred in the mine tailings, so that sulfate had been produced.

Table 5 Values of several chemical constituents in leachate of mine tailings ($n=18$)

Sampling location	Chemical constituent (mg/L)						
	pH	EC ($\mu\text{S/cm}$)	DO	F ⁻	Cl ⁻	NO ₃	SO ₄ ⁻²
Sanso 1	7.13 ± 1.23^a	686 ± 48.36	3.32 ± 1.12	0.04 ± 0.02	1.42 ± 0.96	0.35 ± 0.09	53.17 ± 7.74
Sanso 2	7.53 ± 0.98	690 ± 52.68	3.76 ± 1.42	0.06 ± 0.03	0.39 ± 0.13	0.57 ± 0.36	58.43 ± 9.64
Pompورا 1	6.12 ± 2.34	798 ± 79.22	3.83 ± 1.08	0.28 ± 0.14	0.19 ± 0.07	0.48 ± 0.84	32.73 ± 6.46
Pompورا 2	7.85 ± 2.02	$773 \pm 0.74.64$	3.67 ± 1.03	0.15 ± 0.09	0.23 ± 0.17	0.76 ± 0.62	40.13 ± 7.15
Dokyiwa 1	7.17 ± 1.42	665 ± 35.46	4.95 ± 1.72	0.78 ± 0.16	4.44 ± 1.24	0.13 ± 0.07	29.64 ± 5.33
Dokyiwa 2	7.94 ± 1.06	732 ± 42.83	5.03 ± 2.08	1.26 ± 0.84	3.97 ± 1.03	0.17 ± 0.03	56.87 ± 9.14

^aMean \pm standard deviation.

As shown in Fig. 4, the concentration of sulfate is inversely related to pH, showing that the sulfuric acid is the main source of large amounts of hydrogen ions. The EC values of the tailings mud ranged from 665 to 798 $\mu\text{S/cm}$, which were considered quite similar values compared with those in other abandoned metal mines (Kim et al., 1995). The highest EC values were measured at mine tailings (Pompورا 1=798 and Pompورا 2=773 $\mu\text{S/cm}$).

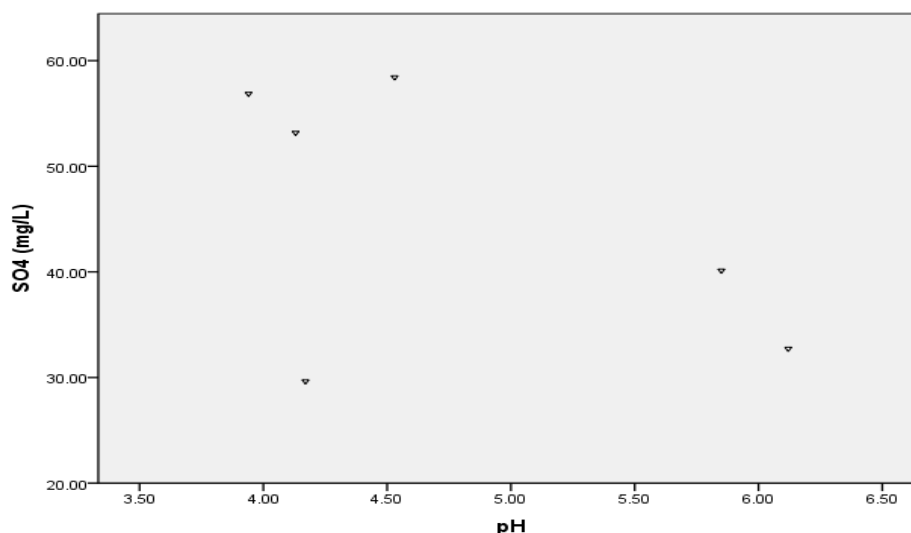


Fig. 4 Relation between pH and sulfate concentration in leachate of mine tailings.

The concentrations of other anions in the leachate were very low (<1.5 mg/L, with an exceptional value 4.5 mg/L for Cl). The values of DO were relatively low (3.32–5.03 mg/L at 25 °C).

Table 6 shows the total concentrations of arsenic and other trace metals (As, Fe, Mn, Cu and Zn) in the mine tailings and arsenic leaching rates in rainwater. The results showed that the mine tailings were heavily polluted with arsenic, and total concentrations of each element were diverse. The total concentrations of elements in the mine tailings were up to 1752 mg/kg As, 75.16 wt.% Fe, 1848.12 mg/kg Mn, 92.17 mg/kg Cu and 7850 177.56 mg/kg Zn. The order of abundance of the trace elements was Fe>As>Mn>Zn>Cu in the analyzed mine tailings (Table 6).

Table 6 Concentrations of arsenic and metals in mine tailings, and arsenic leaching rates in rainwater (n=18)

Sampling location	Concentrations of arsenic and metals in mine tailings					Leaching rate in rainwater
	As (mg/kg)	Fe (wt. %)	Mn (mg/kg)	Cu (mg/kg)	Zn (mg/kg)	As (%)
Sanso 1	542±21.34 ^a	7.87±4.34	154.63±21.35	33.42±6.32	88.67±33.58	0.04
Sanso 2	622±35.46	4.14±0.53	129.56±34.57	24.16±7.32	79.47±17.94	0.06
Pompora 1	1634±124.53	33.26±14.32	846.13±77.34	82.44±13.57	185.13±24.87	0.43
Pompora 2	1752±154.34	46.41±16.46	1204.63±127.46	79.12±18.3	204.56±43.65	0.36
Dokyiwa 1	1412±112.78	57.23±21.02	1848.12±168.96	92.17±11.35	165.48±54.86	0.56
Dokyiwa 2	1292±175.49	75.16±31.21	1653.43±143.62	88.64±7.34	177.56±33.42	0.55

^aMean ±standard deviation.

Arsenic concentrations in soils from the decommissioned tailings dam site (Pompora and Dokyiwa tailings dam) far exceeded that from the active tailings dam (Sanso tailings dam). In relation to the Netherlands soil protection guidelines, As levels in soil beyond 55 mg/kg dry weight requires remediation (VROM, 2000). At this threshold, all the soils tested, especially soils from decommissioned and active tailings dams sites, showed poor quality with respect to As and may pose environmental health concern. Potential intrusions of As from the decommissioned tailings dam was approximately three fold that from the active tailings dams.

The Fe content in all the analyzed samples was far above the soil protection guideline value of 21,000 mg/kg, which meant that the presence of the tailings dams, both active and decommissioned probably impacted the surrounding soils with significant amount of Fe. Soils in Obuasi are rich in iron, associated with gold ore deposits principally characterized by sulphide minerals in arsenopyrite form (Osae et al., 1995; Amonoo-Neizer et al., 1995; Asiam, 1996; Smedley, 1996; Smedley et al., 1996; Ahmad and Carboo, 2000; Kumi-Boateng, 2007).

Mn contamination from the active tailings dams is only marginal, as the Mn levels from the active tailings dam were within the permissible range of values of 320 mg/kg for soil protection guideline. However, the levels of Mn in the decommissioned tailings dam were far above the intervention limit of 320 mg/kg. Factors contributing to the differences in Mn concentration between soil samples from the two tailings dam sites are not clear, however, the possible cause for this might be poor mobility of Mn in soils. Mn contamination from the

dams via movement through soil might take considerably long time to manifest, probably, a reason why the Mn contamination was more pronounced in the decommissioned dam compared to the more recent active dam. Another reason might be the susceptibility of old dried tailings of the decommissioned dam to transport by air, in view of the fact that it was not capped.

The mean concentrations of Cu in soils from the active and decommissioned tailings dams exceeded the recommended limit of 36 mg/kg for a typical uncontaminated soil, however, the values were still within Cu intervention limit of 190 mg/kg for contaminated sites (VROM, 2000).

Zn contamination from the active tailings dams is also marginal, as in the Mn levels from the active tailings dam. The mean levels of Zn from the active tailing dam were within the recommended limit of 140 mg/kg for a typical uncontaminated soil. However, Zn levels of soil samples from the decommissioned tailings dam site fell short of recommended background level of 140 mg/kg, but were still within intervention limit of 720 mg/kg (VROM, 2000).

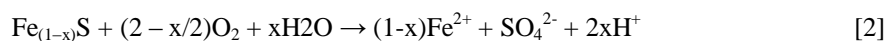
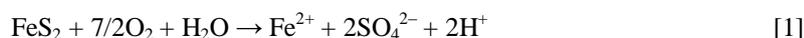
With regards to the site with the highest concentrations of trace elements, the following observation was made: decommissioned tailings dam site (Dokyiwa) > decommissioned tailings dam site (Pompura) > active tailings dam site (Sanso). The high level of trace elements contamination potentially associated with the decommissioned tailings dam in this study could be a function of dust, since the tailings were dried and uncapped, and easily prone to the effect of wind. Hence the tailings dam will release a considerable amount of these contaminants into the surrounding soils.

The low levels of As and trace metals observed in the active tailings dam might be as a result of the active tailings dams, being relatively recent (built in 1991), have benefited from substantial technological improvement over the decommissioned one, which was one of the earliest to be operated at the AngloGold Ashanti mines. Coupled with recent implementation of an environmental management system that is ISO 14001 compliant (since December 2006), there has been great institutional commitment to keep contamination from mining operations very low at the AngloGold Ashanti mines (Antwi-Agyei et al., 2009). In addition the presence of security around tailings facilities has prevented vandalization of these facilities, perhaps, constituted a network of management activities that altogether might have worked to ensure the reduced level of contamination around the active tailings dams. Indeed, provision of improved security to protect tailings facilities has substantially reduced deliberate damages to tailings transmitting lines by small-scale artisanal miners, who often seek to obtain and reprocess these tailings.

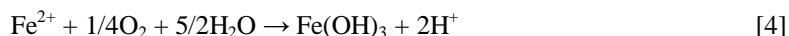
Hitherto, such damages to tailings lines resulted in spillage problems that affected land, vegetation and nearby rivers (AngloGold Ashanti, 2006). The active tailings dams are also presently equipped with facility for draining and re-treatment of effluent, which did not exist during operation of the old decommissioned dam. Leaching tests of the mine tailings were performed to indirectly evaluate release and mobility of contaminants to the surrounding environment by normal rain. Thus rain water (approx. pH 5.8) was selected for the leaching test.

Table 6 shows leaching concentrations of As from the mine tailings. Especially, the leaching levels of As were in the range of 0.04–0.56 %, presenting high proportions for the total arsenic content in the mine tailings. Kim et al., (2000) and Lim et al., (2009) reported a similar result on leaching of As from mine tailings. In their study, As leaching levels were in the range of 0.0017–0.37 % and 0.014–0.026 %, respectively, when mine tailings of six types were mixed with water for 1 hr at a ratio of 1:5 as mass and 1:10 wt:wt, respectively. Even though the test conditions such as leaching solution and shaking time do not correspond to those in our study.

This result is also comparable with results conducted elsewhere (Jang et al., 2005; Ribit et al., 1995; Johnson et al., 2000). Although the mine tailings used in this study were sampled from the surface (0–20 cm) of the uncovered mine tailings pile at active and abandoned mine tailings dam which had been allowed to be in contact with oxygen. This condition might have resulted in the oxidation of sulfide minerals in the mine tailings. The oxidation of sulfide minerals which combine with As can also result in the dissolution of As by water (Lim et al., 2009). Based on the presence of sulfide minerals, high contents of As, potential of oxygen contact, and high sulfate concentration in the mine tailings, the equations 1–3 related to dissolution of iron and arsenic, as an example, could have occurred in the mine tailings (Kim et al., 2004; Lim et al., 2009; McGregor et al., 1998; Johnson et al., 2000):



Here, ferrous ions precipitate in the form of ferric hydroxide by oxidizing or hydrating, as shown in the equation (4):



As and heavy metals released by oxidation can be re-adsorbed onto the surface of ferric hydroxide, and also adsorbed As and other heavy metals can be separated from the surface of ferric hydroxide by water (Lim et al., 2009; Holmstrom et al., 1999).

V. CONCLUSIONS

Considerable amount of As and trace elements (Fe, Cu, Mn and Zn) contamination was associated with gold mine tailings dams, irrespective of whether the dam was active or decommissioned. This potential impact was greater for decommissioned tailings dam since the tailings were dried and uncapped, and easily prone to the effect of wind. Hence the tailings dam will release a considerable amount of these contaminants into the surrounding soils. Arsenic contents of soils from the vicinity of the active and decommissioned tailings dams far exceeded recommended Netherlands intervention value of 55 mg/kg, hence, constituted significant environmental health threat. However, Cu and Fe contents of the mine tailings from both active and decommissioned tailings dams within the study area were also far above the Netherlands soil protection guideline values. Similar pattern was exhibited in the Mn and Zn levels in the abandoned tailings dams but not in the case of active tailings dam which might not present direct environmental threat, although potentially, they could remobilize (with rainfall) and affect aquatic systems. The leaching concentration level of As observed in this study indicates that easily soluble fraction of As might be already released by the oxidation of sulfide minerals with air and water for a long period at the tailings deposition site. Based on the potential that As could be already released from the mine tailings, investigations on the status of contaminants in nearby environmental media (lands, plants, nearby streams and rivers as well as groundwater) are needed. In addition, mine tailings treatment is needed to prevent additional oxidation of sulfide minerals in mine tailings by oxygen contact which releases As and heavy metals by water.

REFERENCES

- [1]. Ahmad, K., & Carboo, D. (2000). Speciation of As (III) and As (V) in some Ghanaian gold tailings by a simple distillation method. *Water, Air Soil Pollution*, 122, 317-326.
- [2]. Akabzaa, T.M., Banoeng-Yakubu, B. & Seyire, J.S. (2005). Heavy metal contamination in some mining communities within Jimi river basin in Ashanti Region. *Journal of the Ghana Science Association*, 7 no.1.
- [3]. Alvarez, R., Ordóñez, A. & Loreda, J. (2006). Geochemical assessment of an arsenic mine adjacent to a water reservoir (León, Spain). *Environmental Geology*, 50, 873-884.
- [4]. Amonoo-Neizer, E.H., Nyamah, D. & Bakiamoh, S.B. (1995). Mercury and arsenic pollution in soil and biological samples around the mining town of Obuasi, Ghana. *Water, Air Soil Pollution*, 91, 363-373.
- [5]. Amonoo-Neizer, E.H., Nyamah, D., & Bakiamoh, S.B. (1996). Mercury and arsenic pollution in soil and biological samples around the mining towns of Obuasi, Ghana. *Water and Soil Pollution*. 91, 363-373.
- [6]. AngloGold Ashanti. (2006). AngloGold Ashanti, Obuasi – Ghana, Country Report.
- [7]. Ansong Asante, O., Agusa, T., Kubota, R., Subramania, A., Ansa-Asare, O.D., & Tanbe, S. (2005). 14th symposium on Environmental chemistry, Osaka.
- [8]. Antwi-Agyei, P., Hogarh, J.N. & Foli, G. (2009). Trace elements contamination of soils around gold mine tailings dams at Obuasi, Ghana. *African Journal of Environmental Science and Technology*, 3(11), 353-359.
- [9]. APHA., AWWA., & WEF. (2005). Standard methods for the examination of water and wastewater. 20th Ed. APHA Washington, DC.
- [10]. Asiam, E.K. (1996). Environmental assessment of gold beneficiation: Arsenic audit and impact on Obuasi environs. *Ghana Mining Journal*, 2 (1), 17-20.
- [11]. Asklund, R. & Eldvall, B. (2005). Contamination of water resources in Tarkwa mining area of Ghana. Department of Engineering Geology, Lund University, Sweden.
- [12]. Boadu, M., Osa, E.K., Gollow, A.A., Serfor-Armah, Y. & Nyarko, B.J.B. (2001). Determination of arsenic in some water bodies, untreated ore and tailing samples at Konongo in the Ashanti region of Ghana and its surrounding towns and villages by instrumental neutron activation analysis. *Journal of Radioanalytical and Nuclear Chemistry*, 249 (3), 581-585.
- [13]. Boateng, E., Dowuona, G.N.N., Nude, P.M., Foli, G., Gyekye, P. & Jafaru, H.M., (2012). Geochemical assessment of the impact of mine tailings reclamation on the quality of soils at AngloGold concession, Obuasi, Ghana. *Research Journal of Environmental and Earth Sciences*, 4(4), 466-474.
- [14]. Carbo, D. & Sarfor-Armah, Y. (1997). Arsenic pollution in streams and sediments in the Obuasi Area, Proc. of UST-IDRC'97 National Symposium, Kumasi, Ghana. pp. 114.
- [15]. Day, P.R. (1965). Particle fractionation and particle size analysis. In: methods of soil analysis, No. 9 Part 2. Black, C.A., (Ed.), American Society of Agronomy, Madison, Wisconsin, pp: 545-567.
- [16]. Foli, G. & Nude, P.M. (2012). Concentration levels of some inorganic contaminants in streams and sediments in areas of pyrometallurgical and hydrometallurgical activities at the Obuasi mine, Ghana. *Environmental Earth Sciences*, 65: 753-763, DOI: 10.1007/s12665-011-1121-x.
- [17]. Golow, A.A., Schlueter, A., Amihere-Mensah, S., Granson, H.L.K. & Tetteh, M.S. (1996). Distribution of arsenic and sulphate in the vicinity of Ashanti goldmine at Obuasi, Ghana. *Bulletin of Environmental Contamination and Toxicology*, 56: 703-710.
- [18]. Griffis, R.J., Barning, K., Agezo, F.L. & Akosah, F.K. (2002). Gold deposits of Ghana. Minerals Commission of Ghana, Accra.

- [19]. Holmstrom, H., Ljungberg, J., Ekstrom, M. & Ohlander, B. (1999). Secondary copper enrichment in tailings at the Laver mine, northern Sweden. *Environmental Geology*, 1999, 38, 327-342.
- [20]. Jambor, J. L., Blowes, D. W. & Ritchie, A.I.M. (2003). Environmental aspects of mine wastes. Mineralogical Association of Canada, Ontario, pp. 430.
- [21]. Jang, M., Hwang, J.S., Choi, S.I. & Park, J.K. (2005). Remediation of arsenic-contaminated soils and washing effluents. *Chemosphere*, 60, 344-354.
- [22]. Johnson, R., Blowes, D., Robertson, W. & Jambor, J. (2000). The hydrogeochemistry of the Nickel Rim mine tailings impoundment, Sudbury, Ontario. *Journal of Contamination and Hydrology*, 41, 49-80.
- [23]. Kesse, G.O. (1985). The mineral and rock resources of Ghana. A.A. Balkema, Rotterdam.
- [24]. Kim, M. & Jung, Y. (2004). Vertical distribution and mobility of arsenic and heavy metals in and around mine tailings of an abandoned mine. *Journal of Environmental Science and Health Part A*, 39, 203-222.
- [25]. Kim, M., Ahn, K. & Jung, Y. (2000). Distribution of inorganic species in mine tailings of abandoned mines from Korea. *Chemosphere*, 49, 307-312.
- [26]. Kim, M., Ahn, K. & Jung, Y. (2002). Distribution of inorganic arsenic species in mine tailings of abandoned mines from Korea. *Chemosphere*, 49, 307-312.
- [27]. Kumapley, N.K. (1993). Some geotechnical aspects of minerals resources development in Ghana: Proceedings of the seminar on current developments in the minerals industry of Ghana: IMME KNUST Kumasi, Ghana. pp. 105 – 110.
- [28]. Kumi-Boateng, B. (2007). Assessing the spatial distribution of arsenic concentration from goldmine for environmental management at Obuasi, Ghana. MSc. Thesis. International Institute for Geo-Infomatics. Science and Earth Observation, Enschede, The Netherlands.
- [29]. Lee, M., Paik, I., Kim, I., Kang, H. & Lee, S. (2007). Remediation of heavy metal contaminated groundwater originated from abandoned mine using lime and calcium carbonate. *Journal of Hazard and Materials*, 144, 208-214.
- [30]. Lim, M., Han, G.C., Ahn, J.W., You, K.S. & Kim, H.S. (2009). Leachability of arsenic and heavy metals from mine tailings of abandoned metal mines. *International Journal of Environmental Research and Public Health*, 6, 2865-2879; doi:10.3390/ijerph6112865.
- [31]. McGregora R., Blowes, D., Jambor, J. & Robertson, W. (1998). The solid-phase controls on the mobility of heavy metals at the Copper Cliff tailings area, Sudbury, Ontario, Canada. *Journal of Contamination and Hydrology*, 33, 247-271.
- [32]. Mensah, A. (2012). Municipal Planning Officer, Obuasi Municipal Assembly [oral reference: 18.11.2012].
- [33]. Osa, S., Kase, K., Yamamoto, M., (1995). A geochemical study of the Ashanti gold deposit at Obuasi, Ghana. Okayama University, Earth Science Report, 2, 81-90.
- [34]. Ribit, I., Ptacek, C., Blowes, D. & Jambor, J. (1995). The potential for metal release by reductive dissolution of weathered mine tailings. *Journal of Contamination and Hydrology*, 17, 239-273.
- [35]. Roussel, C., Bril, H. & Fernandez, A. (2000). Heavy metals in the environment. Arsenic speciation: involvement in evaluation of environmental impact caused by mine wastes. *Journal of Environmental Quality*, 29, 182-188.
- [36]. Roy-Keith, S. (1998). Guide to environmental analytical methods. 5th Edition. Genium Publishing Corporation. River Front Center, Amsterdam, NY 12010 (518) 842-4111.
- [37]. Smedley, P.L. (1996). Arsenic in rural groundwater in Ghana. *Journal of African Earth Sciences*, 22, 459–470.
- [38]. Smedley, P.L., Edmunds, W.M. & Pelig-Ba, K.B. (1996). Mobility of arsenic in groundwater in the Obuasi area of Ghana. In: Appleton, J.D., Fuge, R., McCall, G.J.H. (Eds.), *Environmental Geochemistry and Health*, Geological Society Special Publication.113. Geological Society, London, pp. 163–181.
- [39]. VROM. (2000). Circular on target values and intervention values for soil remediation. The Ministry of Housing, Spatial Planning and Environment, Department of Soil Protection (VROM), The Hague.

Promoting best practice design intent in 3D CAD for engineers through a task analysis

Keelin Leahy¹

¹Department of Design and Manufacturing Technology, University of Limerick, Ireland

Abstract: Assessment encompasses a range of methods and techniques. At the University of Limerick, Ireland, it is an affirmed obligation to facilitate timely and useful feedback for both formative (for learning) and summative (of learning) assessment. However, the effectiveness of this feedback has raised concern and has a wide-ranging review of research findings. This paper presents research findings to build a picture of the extent to which the impact of feedback as a constructivist paradigm of teaching and learning can promote best practice design intent in 3D CAD Modelling. The resulting data set, comprised of 114 higher education students, is used to discuss the impact of assessment and feedback, comparing semesters Spring 2011/12 and Spring 2012/13. The 2012/13 cohort received formative assessment feedback from a task analysis. This evidenced an upsurge in understanding in best practice design intent in 3D CAD parametric modelling, supported by an effect size of 0.534.

Keywords: Design intent, effect size, formative assessment, task analysis, 3D CAD modelling.

I. INTRODUCTION

PT4424, 3D CAD Modelling, learning outcomes set out to develop student's application of effective parametric model building techniques, in the context of design, thereby building an understanding of design intent, creation of comprehensive product models and specifications in the context of the total development of a product, and comprehensively document designs generated from feature based models. In addition, and the focus of this paper, students must be able to apply the design process to solving a design problem using SolidWorks and explain their design solution, and demonstrate an appreciation of the importance of 3D parametric modelling in the contemporary design process. Constructive alignment ensured learning outcomes and assessment were associated. This was further promoted through the facilitation of feedback for the 2012/13 cohort.

Providing students with timely feedback is not the underpinning goal in higher education. Feedback has the implications for improving student's quality of work and developing an understanding for lifelong learning. Formative assessment aims to scaffold student's critical thinking and evaluative skills thus "*students have to be able to judge the quality of what they are producing and be able to regulate what they are doing during the doing of it*" (Sadler, 1989, p. 121). A focus on assessment can often lead to instrumentally motivated students who focus on marks rather than the value of the feedback (Bailey, 2010). This could consequently result in no feed forward for further learning and assessment as highlighted by Hounsell et al (2008) (Fig 1). Hounsell's feedback loop promotes a student-centred constructivist paradigm of teaching and learning; student's understanding and expectations of assessment is evident, student's experience and awareness of feedback is facilitated and the idioms used in the feedback are clarified if required (Hounsell et al, 2008).

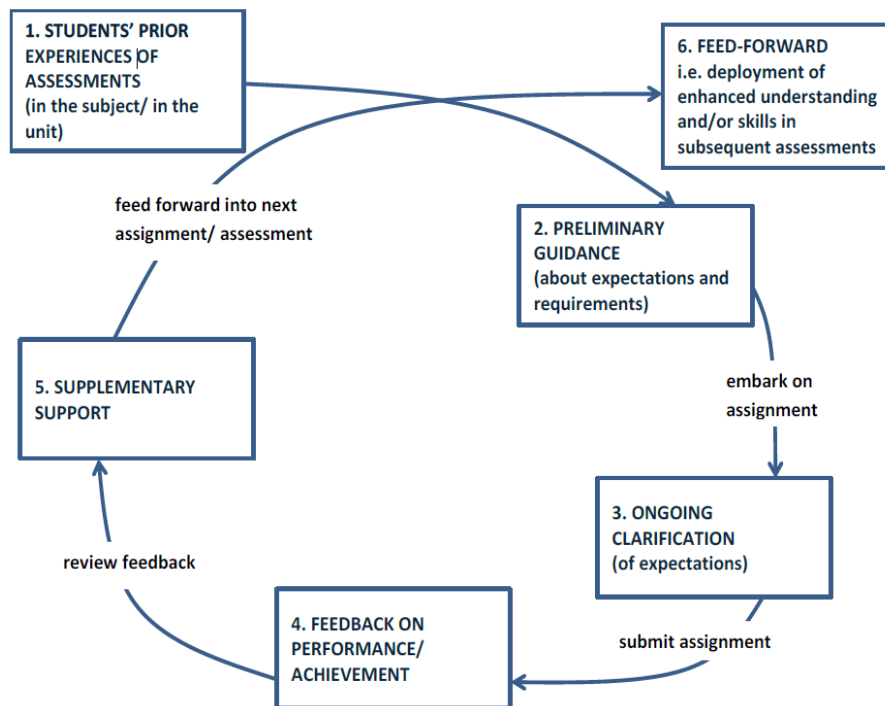


Figure I: Guidance and feedback loop – main steps (Hounsell et al, 2008)

II. METHOD

Students learning outcomes (Table I) were assessed in Spring 2011/12 through summative assessment, in contrast to PT4424 Spring 2012/13 formative and summative assessment (Table II). Hounsell’s guidance and feedback loop was applied for the 2012 cohort’s coursework assessment. At the end of Spring 2012/13 semester students were surveyed to determine the impact of the changes in relation to feedback during the 2012/13 module. The change in assessment was developed in relation to constructive alignment (Fig II). The intention of well-constructed learning outcomes enabling students to learn more effectively is evidenced in the literature (Biggs 2003, Rust et al 2003). However, there is an on-going concern that learning outcomes can also reduce student’s critical thinking ability, due to a focus on assessment (Mc Mahon and Thakore, 2006). Thus, this study set out to investigate if and how outcomes can be used to foster critical thinking in 3D CAD Modelling. This critical thinking required students to apply synthesis and evaluation through their coursework, via a task analysis, along with the module leader’s feedback via Hounsell’s guidance and feedback loop.

Table I: PT4424 Learning outcomes

Learning outcomes: By the end of the module students will be able to:
1. Construct and edit part files using the SolidWorks parametric modeller.
2. Construct assembly files from created part files.
3. Demonstrate an ability to capture and implement design intent in product design.
4. Generate fully dimensioned and annotated working drawings for created parts and assemblies.
5. Develop exploded and cutaway assembly configurations for design documentation.
6. Apply the design process to solving a design problem using SolidWorks and explain their design solution.
7. Use the SolidWorks Toolbox library of fasteners and components.
8. Create and use document templates for part, assembly and drawing documents.
9. Produce photorealistic product renderings and animations.
10. Demonstrate an appreciation of the importance of 3D parametric modelling in the contemporary design process.

Table II: Overview of PT4424 2011/12 and 2012/13

MODULE	SEM/ YEAR	LEVEL / NO. OF STUDENTS	DELIVERY STRATEGY	ASSESSMENT
PT4424 (3D CAD Modelling)	Spring 2011/12	UG 2nd yr / 36, PG / 20, Co-op 2, Erasmus 1	2 hr interactive lecture. 2 hr lab. Educator-student interaction. Two-way communication. Educator-student questions. Shared responsibility for active learning. Small group, problem-solving activities. Variety of supporting media. Limited note taking required (students have copies of lecture notes).	Coursework design project Exam
PT4424 (3D CAD Modelling)	Spring 2012/13	UG 2nd yr / 30, PG / 20, Co-op 4, Erasmus 1	2 hr interactive lecture 2 hr lab 1hr Peer Supported Learning Groupx3 Educator-student interaction. Two-way communication. Educator-student questions. Shared responsibility for active learning. Small group, problem-solving activities. Variety of supporting media. Limited note taking required (students have copies of lecture notes).	Task analysis design product Coursework design project Exam

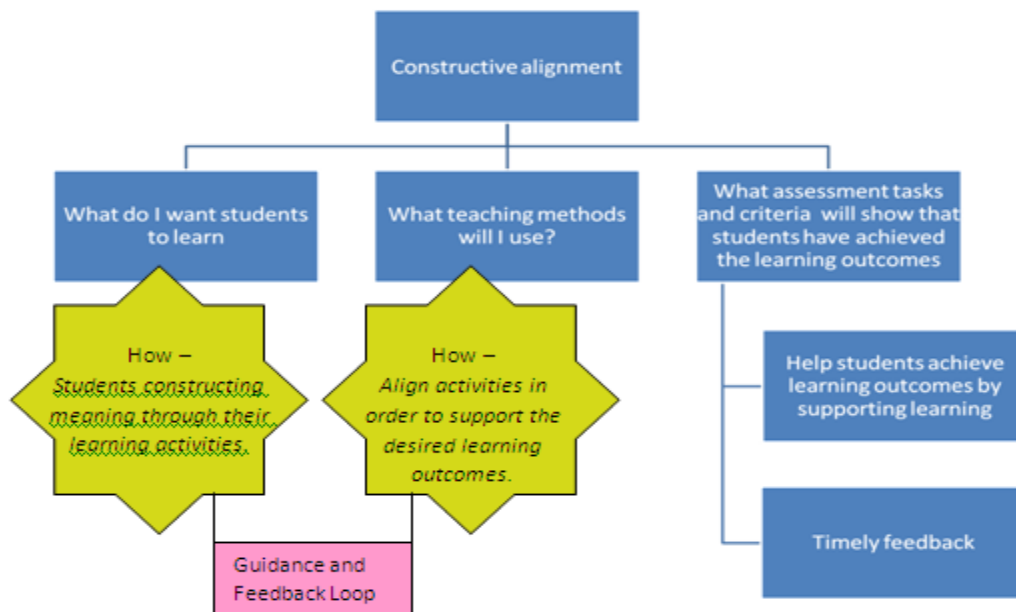


Figure II: Constructive alignment (Biggs, J., 2003)

The formative assessment in Spring 2012/13 involved a task analysis of students design intent for parametric modelling of a product (Fig III; Table III). This task analysis did not form part of the student’s final grade or mark. It was used to provide constructive feedback to improve students learning and understanding of 3D CAD Modelling. The task analysis served as preliminary guidance and on-going clarification for the assessment (Hounsell, 2008). The feedback from the task analysis helped scaffold students as they embarked on the coursework. The peer supported learning group and laboratory sessions provided supplementary support to this feedback.

Table III: PT4424 Coursework outline abridged

Coursework:
<ol style="list-style-type: none"> 1. Select the consumer product from the household product range in the file provided, or from a personal source. 2. Once your product is selected you must start planning your design intent. Create a task analysis for the design and manufacture for the production of the component. This is an essential element in the design intent and planning for parametric modelling. Task analysis is in the context of the design process for the product and design intent for SW modelling.

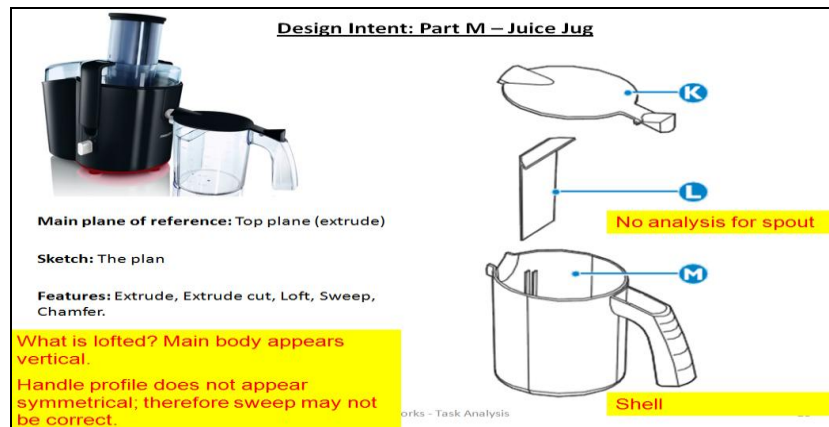


Figure III: Sample student work

In addition, as highlighted in the literature, effective feedback is ‘timely’ (Bailey & Garner, 2010). “A not uncommon fault, particularly within semester system, is that students only find out how well, or how badly, they have done when their assessed work is returned with a mark and comment at the end of the semester. By that time is it too late to take any remedial action.” (Fry, H. et al, 2008, pg 121)

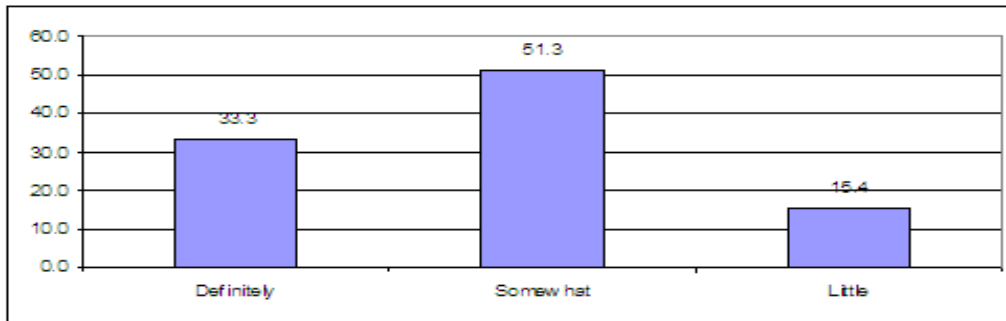
The return of this task analysis and feedback by the module leader was timely (week 6 of 13-week semester) and communicated by the module leader to individual student via email and a summary of all students feedback was uploaded to Sulis (Sulis is a set of software tools designed to help lecturers, tutors and students have spaces (web sites) for collaboration, communication, teaching and learning). The written feedback comments were clearly referenced in context or embodied on the various task analysis sheets (Figure 3), thus students were able to connect the specific elements of coursework the module leader was providing feedback for. In addition, opportunities for tutorial interactions between the module leader and the students were facilitated during ‘open office’ feedback time, peer supported learning sessions and laboratory time.

Whilst also maintaining the balance between the teacher’s role of supporting and facilitating students’ learning and that of assessing their achievement, this task analysis solely served the purpose of clarifying, supporting and facilitating students learning, thus as mentioned earlier no marking was allocated to this element of coursework. This is supported by the literature; “One of the most important aspects of supporting student learning is the feedback that students receive on their work” (Fry, H. et al, 2008, pg 121). In addition, though this task analysis was not awarded marking, 92.2% of students completed the task analysis, which is an extremely high proportion, demonstrating that the majority of students understood the benefits for the learning experience. Allocating marks for such task analysis could result in students focusing on assessment thus becoming instrumentally motivated, focusing on marks rather than the educational value (Higgins, R. et al, 2002; Bailey, 2010).

III. RESULTS

This formative assessment, (written responses noted (in yellow textbox) on students task analysis) (Fig III), provided students with more confidence and motivation to obtain a good grade. From an end of semester assessment and student feedback survey 84.6% (Graph I) of students reported that feedback (Table IV) made them more determined / motivated. Thus students were extrinsically motivated. One student commented “From the analysis I found out in advance how to draw. The feedback helped me find different ways to model the parts.

The feedback impacted on nearly everything I used. The feedback motivated me because I knew I could achieve it. However it would be good to get a grade for this. The feedback, all problems were answered. It would be good to get feedback at the end to know where I went wrong” (PT4424 Student comment, Week 12 feedback survey).

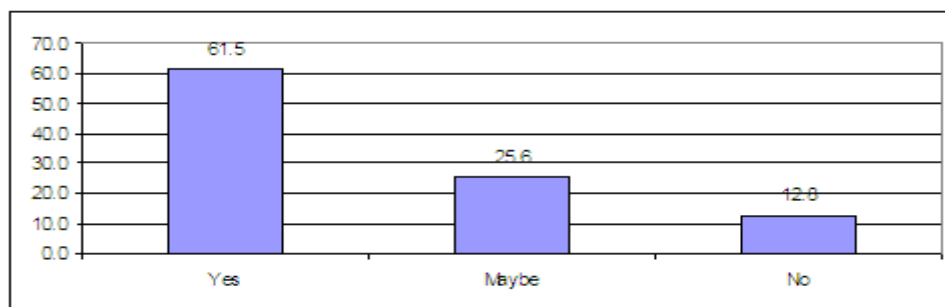


Graph I: Students more confidence and motivation (values as percentage)

Table IV: Feedback abridged

Feedback
Needs to greatly improve and incorporate advanced modeling
Excellent work! Small few bits need to be considered
Needs more advanced modelling and ensure detail is very detailed as parts appear very simple
Needs more advanced modelling and consideration of moving parts.
Needs to clarify parts and design intent not visible for main part!
Poor did not analyse in the context of each part and graphic. Few bits need clarification such as the basket!
Confusion between loft, sweep, extrude. Also watch symmetry of parts.
Need to use more advanced modeling, design intent for some parts not correct or not completed
Needs more advanced modelling. All parts not analysed.
Lacks advanced modelling. Many parts not explored in the analysis. Difficult to follow the analysis as it is not in context of supporting visuals for various parts.
Yes okay, few bits to improve; difficult to determine where featuring was referring to.

Intrinsic motivation was also addressed, 87.1% (Graph II) of students understood the benefits of the task analysis, highlighting that the feedback increased their learning and understanding of 3D CAD modelling. Student comments supporting this include; “Good idea to do the analysis and get feedback as it got you thinking of your project.” (PT4424 Student, Week 12 feedback survey); “The analysis and feedback made me think a bit harder” (PT4424 Student, Week 12 feedback survey). The teaching assistant for this module also noted the difference between the 2011 and 2012 cohort; “They seemed to have a greater grasp of some of the advanced functions, and that’s probably due to the fact that they had to start thinking about how they were going to build the parts. Most of the design intent was better to previous years and use of the programme was much better” (PT4424 Teaching Assistant).



Graph II: Understand the benefits of task analysis (values as percentage).

This motivation in students learning through feedback and assessment was not instrumentally motivated; focusing on marks rather than the educational value of written comments. Students also expressed the appreciation for feedback; in the survey only 20.5% (Graph III) of students expressed that they would like to receive a grade rather than feedback. Student’s comments include;

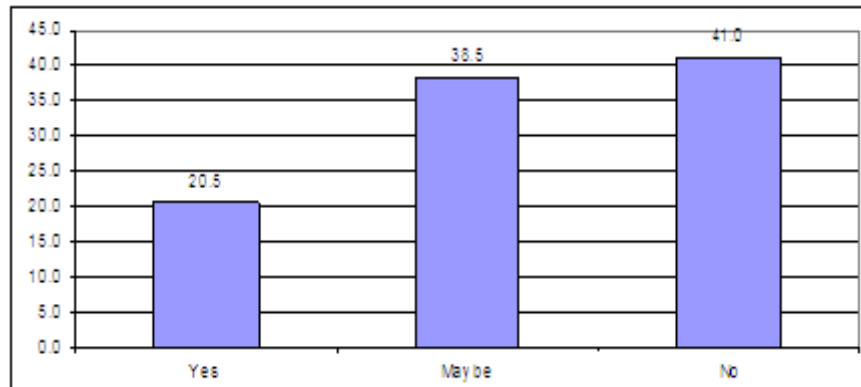
“I would like to get feedback on my final exam to see where I can improve / went wrong.”

“I would like to know where I went wrong as well as getting a grade”

“It would be good to get feedback at the end to know where I went wrong.”

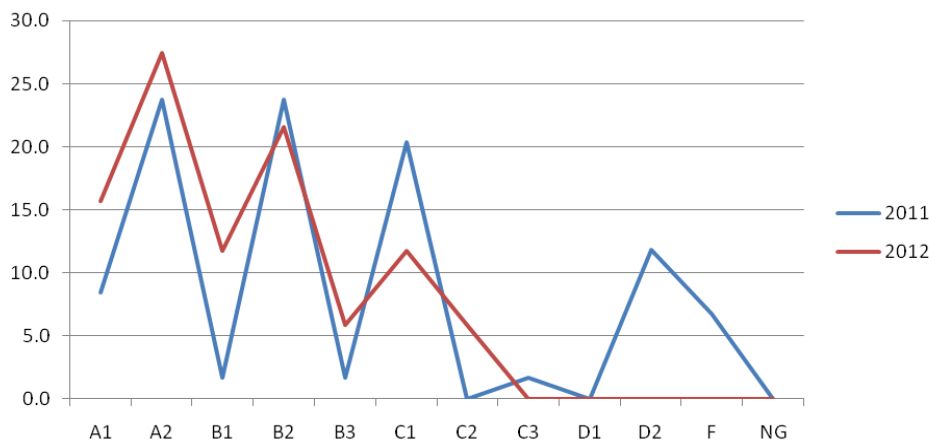
“Very good thorough feedback. Definitely want feedback on exam and project.”

“Feedback was good as it gave hints and tips on how to model your chosen product. I would want feedback if I was to do more 3D CAD modelling modules.”



Graph III: Would you like to receive a grade rather than feedback (values as percentage).

From the summative assessment, comparing end of semester coursework grades for PT4424 2011 /12 cohort and PT4424 2012 cohort, the 2012/13 cohort demonstrated a higher percentile for higher grades (Graph IV). Thus, one can deduce that the impact of the formative assessment has improved students understanding of design intent for parametric modelling by instilling greater motivation and appreciation for best practice.



Graph 4: PT4424 Coursework grades (values as percentage).

Statistically measuring the magnitude of difference between the two groups is calculated using the effect size. An effect size above 0.4 is above average for educational research. The task analysis involved in this study was carried out to reinforce best practice design intent. The task analysis also served the function of feedback, giving students positive reinforcement toward improvement and clarifying goals. From this task analysis students demonstrated the ability to self-regulate their own learning, thus increase achievement. The effect size between the two groups in this study was 0.534, medium effect (Cohen, et al, 2011), which is equivalent to one grade leap (Hattie, 2011).

IV. CONCLUSION

The feedback has acted as a constructivist paradigm of teaching and learning, whereby students demonstrated improved learning achievement through design intent, a key fundamental for parametric modelling. This paradigm shift in assessment design to promote assessment for learning rather than of learning is demonstrated through student's improved learning achievement for best practice design intent. The implementation of the task analysis was facilitative for deep learning. Assessment in PT4424 is not about the reproduction of passive incremental knowledge; assessment is active and transformational. This is evident in student's final submission of coursework assessment where students demonstrated a 'deployment of enhanced understanding and skills' thus evidencing their ability to feed forward the feedback and guidance. This correlates with Black and Wiliam (1998) statement with respect to formative assessment; "with gains in learning 'among the largest ever reported for educational interventions'" (Hounsell et al, 2008 p. 55).

REFERENCES

- [1]. Sadler, D.R., Formative assessment and the design of instructional systems. *Instructional Science*, 18(2), 1989, 119–144.
- [2]. Bailey, R., & Garner, M. Is the feedback in higher education assessment worth the paper it is written on? Teachers' reflections on their practices. [doi: 10.1080/13562511003620019]. *Teaching in Higher Education*, 15(2), 2010, 187-198.
- [3]. Hounsell, D. et al, The quality of guidance and feedback to students, *Higher Education Research & Development*, 27 (1), 2008, 55-67
- [4]. Biggs, J., *Teaching for quality learning at university – What the student does* (2nd Edition) (SRHE / Open University Press, Buckingham, 2003).
- [5]. Rust C., Price M. A., O'Donovan B., Improving students' learning by developing their understanding of assessment criteria and processes. *Assessment and Evaluation in Higher Education*, 28 (2), 2003, p. 147-164.
- [6]. McMahon. T & Thakore. H, Achieving constructive alignment: putting outcomes first the quality of higher education 3. Available at <http://www.eric.ed.gov/PDFS/EJ874250.pdf> , 2006
- [7]. Fry, H. et al., *A handbook for teaching and learning in higher education* (London: Kogan Page 2008)
- [8]. Higgins, R., Hartley, P. and Skelton, A. The conscientious consumer: reconsidering the role of assessment feedback in student learning. *Studies in Higher Education*, 27 (1), 2002, pp.53-64
- [9]. Cohen, L., Manion, L., Morrison, K., *Research methods in education*, 7th edition (Routledge, 2011)
- [10]. Hattie, J. *Visible learning for teachers: Maximizing impact on learning*, (Routledge, 2011).
- [11]. Black, P., & Wiliam, D., Assessment and classroom learning. *Assessment in Education*, 5(1), 1998, 7–74.

Implementing Short Term Scheduler and Preemptive Algorithm in Grid Computing Scheduling

CH.V.T. E.V Laxmi, K.Somasundaram,

1. Research Scholar (Karpagam University), Associate Professor, Department of Computer Science Engineering, Raghun Engineering College, Visakhapatnam, Andhra Pradesh, India.

2. Professor, Department of Computer Science and Engineering, Jaya Engineering College, CTH Road, Prakash Nagar, Thiruniravur, Thiruvallur - Dist, Tamilnadu.

Abstract: Grid Computing has emerged as an important new field focusing on resource sharing. One of the most challenging issues in Grid Computing is efficient scheduling of tasks and there is need of finding faster and cheaper solutions to solve computational problems. The deployment of Grid systems involves the efficient management of heterogeneous, geographically distributed and dynamically available resources. However, the effectiveness of a Grid environment is largely dependent on the effectiveness and efficiency of its schedulers, which act as localized resource brokers. This article provides a brief overview on grid computing and Scheduling processes, important factors considered in resource management and Scheduling, comparison of different Scheduling processes and future outlook of its resource management and Scheduling in Grid systems by implementing short term scheduling. This paper investigates the use of short term scheduling mechanism in grid computing and implementing the Shortest Remaining Time First (SRTF) algorithm for the selection of jobs from the job pool.

Keywords: Grid Computing, Resource Management, Scheduling, Resource Sharing, scheduling processes

I. INTRODUCTION

The Grid is emerging as a new paradigm for solving problems in science, engineering, industry and commerce. Increasing numbers of applications are utilizing the Grid infrastructure to meet their computational, storage and other needs. A single site can simply no longer meet all the resource needs of today's demanding applications, and using distributed resources can bring many benefits to application users. The deployment of Grid systems involves the efficient management of heterogeneous, geographically distributed and dynamically available resources. However, the effectiveness of a Grid environment is largely dependent on the effectiveness and efficiency of its schedulers, which act as localized resource brokers. Figure 1.1 shows that user tasks, for example, can be submitted via Globus to a range of resource management and job scheduling systems, such as Condor, the Sun Grid Engine (SGE), the Portable Batch System (PBS) and the Load Sharing Facility (LSF). Grid scheduling is defined as the process of mapping Grid jobs to resources over multiple administrative domains. A Grid job can be split into many small tasks. The scheduler has the responsibility of selecting resources and scheduling jobs in such a way that the user and application requirements are met, in terms of overall execution time (throughput) and cost of the resources utilized.

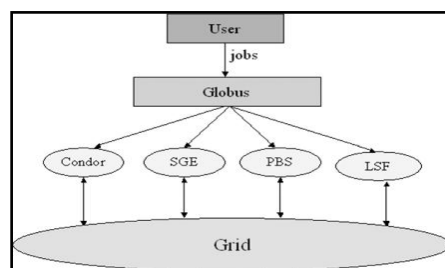


Figure 1.1

Jobs, via Globus, can be submitted to systems managed by Condor, SGE, PBS and LSF

II. RELATED WORK

Brief Description of SCHEDULING PARADIGMS

In the grid-computing system, the use of computer resources from multiple administrative domains that are applied collectively to solve a problems that has demanding requirements such as a storage space, bandwidth etc. therefore these resource has to be scheduled, present there are three scheduling paradigms– centralized, hierarchical and distributed.

Centralized scheduling

In a centralized scheduling environment, a central machine (node) acts as a resource manager to schedule jobs to all the surrounding nodes that are part of the environment. This scheduling paradigm is often used in situations like a computing centre where resources have similar characteristics and usage policies. Figure 1.2 shows the architecture of centralized scheduling. One advantage of a centralized scheduling system is that the scheduler may produce better scheduling decisions because it has all necessary, and up-to-date, information about the available resources. However, centralized scheduling obviously does not scale well with the increasing size of the environment that it manages. The scheduler itself may well become a bottleneck, and if there is a problem with the hardware or software of the scheduler's server, i.e. a failure, it presents a single point of failure in the environment.

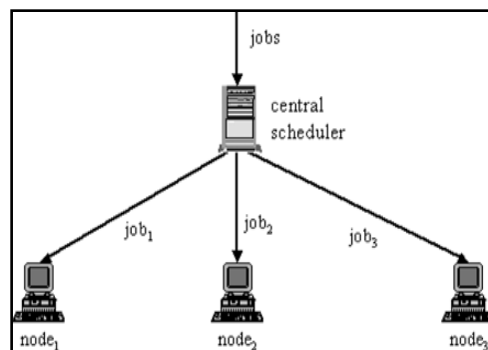


Figure 1.2 Centralized scheduling

Distributed scheduling

In this paradigm, there is no central scheduler responsible for managing all the jobs. Instead, distributed scheduling involves multiple localized schedulers, which interact with each other in order to dispatch jobs to the participating nodes. There are two mechanisms for a scheduler to communicate with other schedulers – direct or indirect communication. Figure 1.3 shows the direct communications in distributed scheduling.

Direct communication

In this scenario, each local scheduler can directly communicate with other schedulers for job dispatching. Each scheduler has a list of remote schedulers that they can interact with, or there may exist a central directory that maintains all the information related to each scheduler. Figure 1.3 shows the architecture of direct communication in the distributed scheduling paradigm.

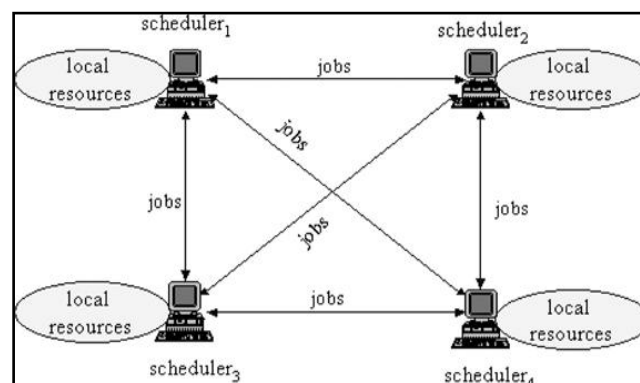


Figure 1.3 Direct communications in distributed scheduling

Communication via a central job pool

In this scenario, jobs that cannot be executed immediately are sent to a central job pool. Compared with direct communication, the local schedulers can potentially choose suitable jobs to schedule on their resources. Policies are required so that all the jobs in the pool are executed at some time. Figure 1.4 shows the architecture of using a job pool for distributed scheduling.

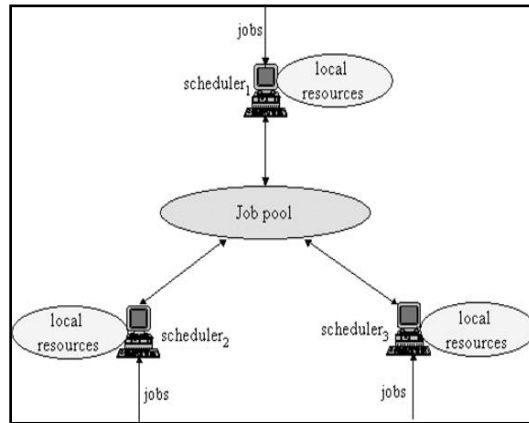


Figure 1.4 Distributed scheduling with a job pool

Hierarchical scheduling

In hierarchical scheduling, a centralized scheduler interacts with local schedulers for job submission. The centralized scheduler is a kind of a meta-scheduler that dispatches submitted jobs to local schedulers. Figure

1.4 shows the architecture of this paradigm.

Similar to the centralized scheduling paradigm, hierarchical scheduling can have scalability and communication bottlenecks. However, compared with centralized scheduling, one advantage of hierarchical scheduling is that the global scheduler and local scheduler can have different policies in scheduling jobs.

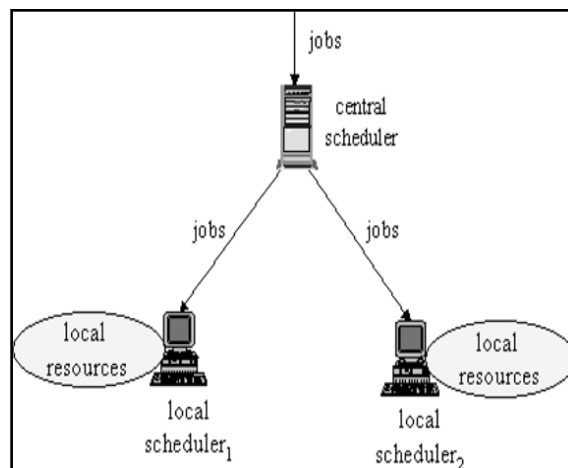


Figure 1.4 Hierarchical scheduling

III. PROPOSED APPROACH

This section explains our proposed approach of new scheduling that is hierarchical scheduling with job pool. In hierarchical scheduling, a centralized scheduler interacts with local schedulers for job submission and then it dispatches submitted jobs to local schedulers. Therefore there is no guarantee of execution of all the submitted jobs which are in the central scheduler. So aim is to execute all the jobs therefore by implementing job pool in between the central scheduler and to the local schedulers, we can give the guarantee of execution of all the jobs which are submitted at the centralized scheduler. Jobs which cannot be executed immediately such jobs are sent to the job pool. The approach aim is, all the jobs should be executed which are submitted to central schedulers by sending the jobs which cannot be executed immediately to the job pool and by implementing special policies on all those jobs which cannot be executed immediately. Figure 1.5 shows the proposed architecture of hierarchical scheduling with job pool.

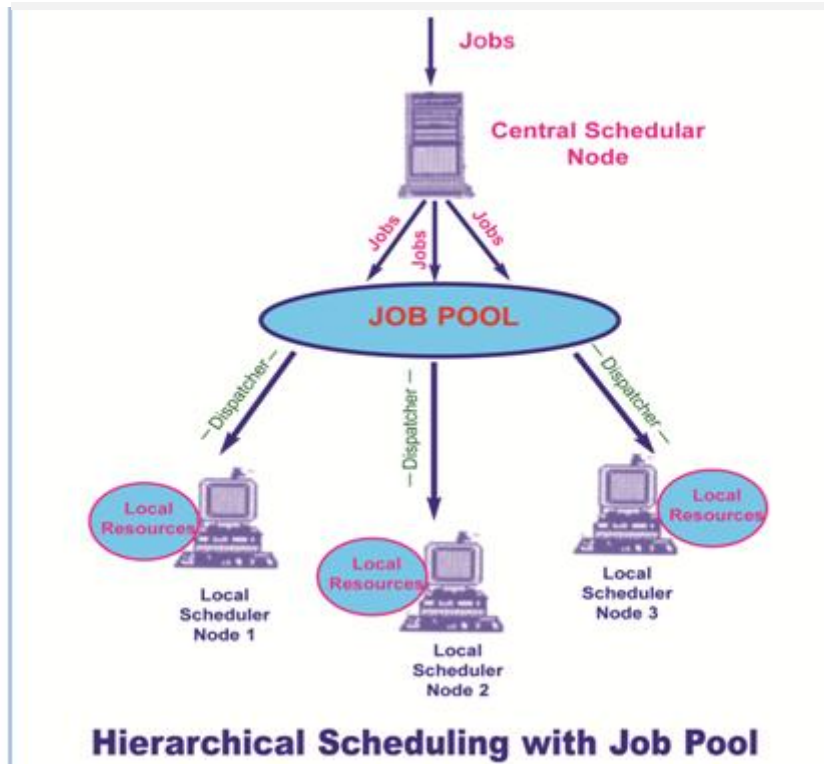


Figure 1.5 Hierarchical scheduling with job pool

3.1 Implementing Short Term Scheduler in Hierarchical scheduling with job pool

The main function of the short term scheduler is, selecting a job from the pool of jobs, which we demonstrated in the figure 1.5, as Hierarchical scheduling with job pool. The short term scheduler gives the control of the CPU of central scheduler with the help of 'Dispatcher'. A dispatcher is a module; it connects the CPU to the process selected by the short term scheduler. The main function of the dispatcher is switching, it means switching the CPU from one process to another process. The method of selecting a job from job pool is depends on the scheduling algorithm. Figure 1.5.1 shows the Queuing diagram for the hierarchical scheduling with job pool.

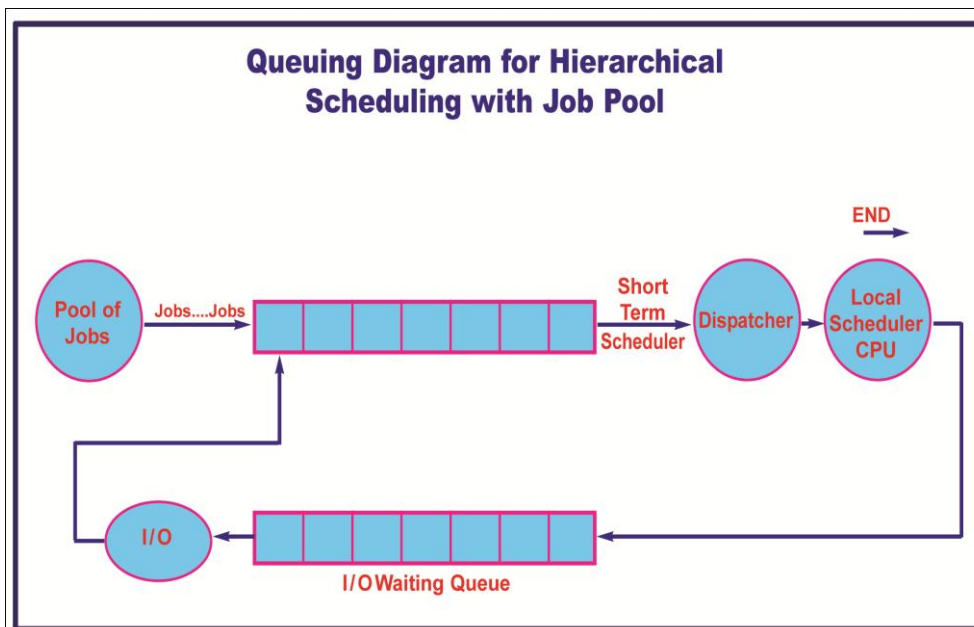


Figure 1.5.1 Queuing diagram for Hierarchical scheduling with job pool

3.2 Shortest Remaining Time First (SRTF) Algorithm

There are many grid scheduling algorithms available. Different grid scheduling algorithms have different properties, in choosing which algorithm to use in a particular situation; we must consider the properties of the various algorithms. Shortest Remaining Time First (SRTF) is the preemptive scheduling algorithm, in which the short term scheduler always chooses the process that has the shortest remaining processing time. When a new process enters, the short term scheduler compare the remaining time of executing process and new process. If the new process has the least CPU burst time, the scheduler selects that job and connects to the CPU of the local nodes; otherwise it continues the old process.

3.3 Case study and experimental Results

The idea of the above algorithm is illustrated considering the case study with the below problem.

JOBS	Local Nodes Burst Time	Arrival Time
J1	3	0
J2	2	6
J3	4	4
J4	6	5
J5	2	8

Figure 1.5.2 shows the arrival chart for the above problem

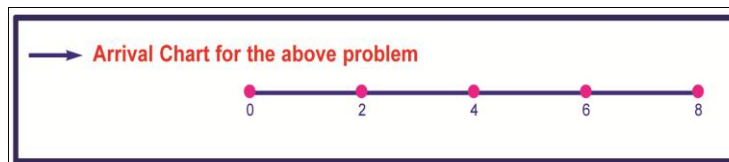
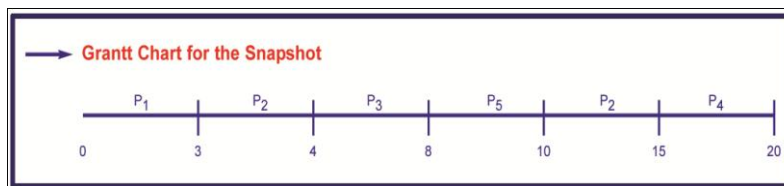


Figure 1.5.3 shows the Gantt chart for the snapshot



Job J1 arrives at time 0, so J1 executing first, J2 arrives at time 2 mi.sec, so compare the J1 remaining time (3-2=1) and J2 time (1<6) so continue the job J1. After the completion of J1, executing the process J2, at time 4 J3 arrives, so compare the reaminging time of J2(6-1=5) and burst time of J3(4),(4<5) so CPU of the local scheduler shift to job J3. At time 6 J4 arrives.

Then compare the remaining time for J3(4-2=2) and local node burst time of J4 is 5. (2<5). So continue the process J3. After the completion of J3, the central scheduler consisting of J5, J2, J4. J5 is the least out of three, so executing the J5. After that execute the J2,then next J4.

Now we have to calculate the Average Turnaround Time (ATT), Average Response Time (ART) and Average Relative Delay (ARD).

• Turn Around Time:

Turn around time =	first time-arrival time			
Turn around for J1	= 3	-	0	= 3
Turn around for J2	= 15	-	2	= 13
Turn around for J3	= 8	-	4	= 4
Turn around for J4	= 20	-	6	= 14
Turn around for J5	= 10	-	8	= 2

Average turn around time= 36/5=7.2

- Relative delay or normalized turn around time:
Relative delay= T_q/T_s =turn around time/service time
Relative delay for

J1	=	3/3	=	1.00
J2	=	13/6	=	2.17
J3	=	4/4	=	1.00
J4	=	14/5	=	2.80
J5	=	2/2	=	1.00

$$\text{Average Relative Delay} = \frac{1+2.17+1+2.80+1}{5} = \frac{7.97}{5} = 1.59$$

IV. CONCLUSION

Grid computing is an important tool that is used for both scientific and industrial purposes, which provides an environment with a high amount of resources for computational purposes to solve complex problems. These resources can be scientific instruments, storage devices, network bandwidth, sensors and processors which belong to different proprietary organizations.

This paper carries out a survey on Grid scheduling from the study of different researches carried out on this field. An algorithm of job scheduling has been proposed within this paper. In this paper a brief overview on grid computing and scheduling processes, important factors considered in resource management and scheduling has been proposed. This paper investigated the use of short term scheduling mechanism in grid computing and implementing shortest remaining time first (SRTF) algorithm for the selection of jobs from the job pool has been discussed with a case study.

REFERENCES

- [1] Ian Foster and Carl Kesselman, "The Grid: Blueprint for a New Computing Infrastructure," Elsevier Inc., Singapore, Second Edition, 2004.
- [2] Raksha Sharma, Vishnu Kant Soni, Manoj Kumar Mishra, Prachet Bhuyan A Survey of Job Scheduling and Resource Management in Grid Computing World Academy of Science, Engineering and Technology 40 2010
- [3] Edi.Laxmi Scheduling in Grid Computing International Journal of Computer Science and Management Research Vol 2 Issue 1 January 2013
- [4] Hamscher, V., Schwiegelshohn, U., Streit, A. and Yahyapour, R. Evaluation of Job-Scheduling Strategies for Grid Computing. GRID 2000, 191–202, 17–20 December 2000, Bangalore, India. Lecture Notes in Computer Science, Springer-Verlag.
- [5] Srinivasan, S., Kettimuthu, R., Subramani, V. and Sadayappan, P. Characterization of Backfilling Strategies for Parallel Job Scheduling. ICPP Workshops 2002, 514–522, August 2002, Vancouver, BC, Canada. CS Press. DAGManager, <http://www.cs.wisc.edu/condor/dagman/>.
- [6] Ghare, G. and Leutenegger, S. Improving Small Job Response Time for Opportunistic Scheduling. Proceedings of 8th International Workshop on Modeling, Analysis, and Simulation of Computer and Telecommunication Systems (MASCOTS 2000), San Francisco, CA, USA. CS Press.
- [7] Raman, R., Livny, M. and Solomon, M. Matchmaking: Distributed Resource Management for High Throughput Computing. Proceedings of the 7th IEEE International Symposium on High Performance Distributed Computing, July 1998, Chicago, IL, USA. CS Press.
- [8] Enterprise Edition policy, <http://www.sun.com/blueprints/0703/817-3179.pdf>.
- [9] N1GE 6 Scheduling, <http://docs.sun.com/app/docs/doc/817-5678/6ml4alis7?a=view>. PBS Pro, <http://www.pbspro.com/>.
- [10] Figueira, M., Hayes, J., Obertelli, G., Schopf, J., Shao, G., Smallen, S., Spring, N., Su, A. and Zagorodnov, D. Adaptive Computing on the Grid Using AppLeS. IEEE Transactions on Parallel and Distributed Systems, 14(4): 369–382 (2003). NWS, <http://nws.cs.ucsb.edu/>.
- [11] Dail, H., Berman, F. and Casanova, H. A Decoupled Scheduling Approach for Grid Application Development Environments. Journal of Parallel Distributed Computing, 63(5): 505–524 (2003).
- [12] Abramson, D., Giddy, J. and Kotler, L. High Performance Parametric Modeling with Nimrod/G: Killer Application for the Global Grid? Proceedings of the International Parallel and Distributed Processing (IPDPS 2000), May 2000, Cancun, Mexico. CS Press.
- [13] Gerasoulis, A. and Jiao, J. Rescheduling Support for Mapping Dynamic Scientific Computation onto Distributed Memory Multiprocessors. Proceedings of the Euro-Pa '97, August 1997, Passau, Germany. Lecture Notes in Computer Science, Springer-Verlag.
- [14] Goux, Jean-Pierre, Kulkarni, Sanjeev, Yoder, Michael and Linderoth, Jeff. Master-Worker: An Enabling Framework for Applications on the Computational Grid. Cluster Computing, 4(1): 63–70 (2001).
- [15] Cactus, <http://www.cactuscode.org/>. 300 GRID SCHEDULING AND RESOURCE MANAGEMENT
- [16] Spooner, D., Jarvis, S., Cao, J., Saini, S. and Nudd, G. Local Grid Scheduling Techniques using Performance Prediction, IEE Proc. – Comp. Digit. Tech., 150(2): 87–96 (2003).
- [17] Young, L., McGough, S., Newhouse, S. and Darlington, J. Scheduling Architecture and Algorithms within the ICENI Grid Middleware. Proceedings of the UK e-Science All Hands Meeting, September 2003, Nottingham, UK.
- [18] YarKhan, A. and Dongarra, J. Experiments with Scheduling Using Simulated Annealing in a Grid Environment. Proceedings of the 3rd International Workshop on Grid Computing (GRID 2002), November 2002, Baltimore, MD, USA. CS Press.

Parameter Optimization In Image Enhancement Using PSO

Nirmal Singh¹, Maninder kaur², K.V.P Singh³

1(ECE, DIET Kharar/ PTU Jalandhar, India)

2(ECE, DIET Kharar/ PTU Jalandhar, India)

3(ECE, DIET Kharar/ PTU Jalandhar, India)

Abstract: In this paper parameters of the transformation function is considered as an optimization problem and Particle Swarm Optimization (PSO) is used to solve it.(PSO) algorithms is a new approach for optimization. With intensity transformation function image enhancement is done by maximizing the information content of the enhanced image. In this work a parameterized transformation function is used, which uses local and global information of the image. Here an objective criterion for measuring image enhancement is used which considers entropy and edge information of the image. We tried to achieve the best enhanced image according to the objective criterion by optimizing the parameters used in the transformation function with the help of PSO. Results are compared with other enhancement techniques, viz. Histogram equalization, contrast stretching based image enhancement.

Keywords: Particle swarm optimization, image enhancement and histogram equalization.

I. INTRODUCTION

Image enhancement, one of the important image processing techniques, can be treated as transforming one image to another to improve the interpretability or perception of information for human viewers, or to provide better input for other automated image processing techniques. According to [16], image enhancement techniques can be divided into four main categories: point operation transformation, spatial operation, and pseudo coloring. The work done in this paper is based on spatial operation. Histogram transformation is considered as one of the fundamental processes for contrast enhancement of gray-level images [15], which facilitates subsequent higher level operations such as detection and identification. Linear contrast stretching employs a linear transformation that maps the gray-levels in a given image to fill the full range of values. Pseudo coloring is an enhancement technique that artificially "color" the gray-scale image based on a color mapping, with the extensive interactive trials required to determine an acceptable mapping [16]. Color images can be enhanced by separating the image into the chromaticity and intensity components [17]. Majority of the image enhancement work usually manipulates the image histogram by some transformation function to obtain the required contrast enhancement. Consequently, this operation also delivers the maximum information contained in the image. Evolutionary algorithms have been previously used to perform image enhancement [1] - [5]. In [1], the authors applied a global contrast enhancement technique using genetic programming (GP) [11] to adapt the color map in the image so as to fit the demands of the human interpreter. In [2] a real coded GA is used with a subjective evaluation criterion to globally adapt the gray-level intensity transformation in the image. Combination of different transformation functions with different parameters is used to produce the enhanced image by GA in [5]. In this paper we have performed gray-level image contrast enhancement by PSO. In comparison to Linear Contrast Stretching (LCS) and Histogram Equalization (HE), PSO does not require selection, crossover and mutation operations. At the same time PSO takes less time to converge to a better optima. The resulted gray-level enhanced images by PSO are found to be better compared with other automatic image contrast enhancement techniques. Both objective and subjective evaluations are performed on the resulted image which says about the goodness of PSO.

The rest of the paper is organized as follows: In Section II, functions used for the proposed work (transformation and evaluation function) are described. In Section III, theory of PSO (basic PSO, proposed methodology, parameter setting) is discussed. In Section IV, results and discussions are put, and finally in Section V, conclusion of the work is made.

II. FUNCTIONS USED

For image enhancement task, a transformation function is required which will take the intensity value of each pixel from the input image and generate a new intensity value for the corresponding pixel to produce the enhanced image.

To evaluate the quality of the enhanced image automatically, an evaluation function is needed which will tell us about the quality of the enhanced image. In this section we describe the function used for the proposed work.

A. Transformation function

Image enhancement done on spatial domain uses a transformation function which generates a new intensity value for each pixel of the $M \times N$ original image to generate the enhanced image, where M denotes the number of columns and N denotes the number of rows. The enhancement process can be denoted by :

$$g(x, y) = T(f(x, y)) \quad (1)$$

Where $f(x, y)$ is the input image, $g(x, y)$ is the output (processed) image, and T is an operator on f defined over a specified neighborhood about point (x, y) . In addition, T can operate on a set of images, such as performing the addition of K images for noise reduction.

The principal approach for defining spatial neighborhoods about a point (x, y) is to use a square or rectangular region centered at (x, y) . The center of the region is moved from pixel to pixel starting, say, at the top, left corner, and, as it moves, it encompasses different neighborhoods. Operator T is applied at each location (x, y) to yield the output, g , at that location. Only the pixels in the neighborhood centered at (x, y) are used in computing the value of g at (x, y) .

$$g(x, y) = K(x, y)[f(x, y) - c \cdot m(x, y)] + m(x, y)^a \quad (2)$$

Where, a and c are the parameters whose value is to be optimized.

$m(x, y)$ is local mean over a window of $n \times n$.

$K(x, y)$ is enhancement function which takes both local and global information into account.

Expression for local mean and enhancement function are defined as:

$$m(x, y) = \frac{1}{n \times n} \sum_{i=0}^{n-1} \sum_{j=0}^{n-1} f(i, j) \quad (3)$$

$$D = \frac{1}{M \times N} \sum_{x=0}^{M-1} \sum_{y=0}^{N-1} f(x, y)$$

The enhancement function $K(x, y)$ can be defined as:

$$K(x, y) = \frac{k \cdot D}{\sigma(x, y) + b} \quad (4)$$

Where, b and k are the parameters to optimize.

D is the Global mean of the input image.

$\sigma(x, y)$ is local Standard Deviation over a window of $n \times n$

$\sigma(x, y)$ is defined as :-

$$\sigma(x, y) = \sqrt{\frac{1}{M \times N} \sum_{i=0}^{M-1} \sum_{j=0}^{N-1} (f(i, j) - m(x, y))^2} \quad (5)$$

Hence, the complete transformation function is defined as follows:-

$$g(x, y) = \frac{k \cdot D}{\sigma(x, y) + b} [f(x, y) - c \cdot m(x, y)] + m(x, y)^a \quad (6)$$

With the transformation stated in eq. (6) contrast of the image can be stretched considering local mean as the centre of stretch. The last term $m(x, y)^a$ has brightening & smoothing effect thus smooths the output image and the four parameters introduced in the transformation function i.e. a , b , c & k are the parameters of the enhancement function and the small variation in their value produces a large variation in the processed output image and thus the value of these parameters should be precisely set. The approximate range of these parameters is defined as: a [0, 1.5]; b [0, (D/2)]; c [0, 1]; K [.5, 1.5].

A. Evaluation Criterion

In order to evaluate the performance of the proposed algorithm and the quality of an enhanced image without human intervention, we need an objective function which tells us about the quality of the output image. Many objective functions are presented in literature [45]-[47]. It is observed that compared to the original image good contrast enhanced image has more number of edgels i.e. number of edge pixels and enhanced version should have a higher intensity of the edges. But these two measures are not sufficient to test an enhanced image and that why one more performance measure is taken into account i.e. entropy value of the image. Entropy value reveals the information content in the image. If the distribution of the intensities is uniform, then we can say that histogram is equalized and the entropy of the image will be more. Thus, the objective function considered here uses three performance measures i.e. entropy value, sum of edge intensities value and number of edgels (edge pixels) and is defined as:-

$$F(I_{enh}) = \log(\log(E(I_c))) \times \frac{n(I_c)}{M \times N} \times H(I_{enh}) \quad (7)$$

In the above mentioned equation I_{enh} is the enhanced image resulted from the transformation function defined above. In eq. 4.8 the edges or edgels can be detected by many efficient edge detector algorithms such as Sobel [1], Laplacian [1], Canny [5] etc. In this study Canny is used as an automatic threshold detector [15]. Canny's edge detection algorithm is computationally more expensive compared to Sobel, Prewitt and Robert's operator. However, the Canny's edge detection algorithm performs better than all these operators under almost all scenarios and thus in this work after using Canny edge operator we produce an edge image I_c .

$E(I_c)$ is the sum of $M \times N$ pixels intensities of canny edge images. n is the number of pixels, whose intensity value is greater than a threshold in canny edge image. Entropy of the enhanced image I_{enh} is given by:-

$$H(I_{enh}) = -\sum_{i=0}^1 e_i \quad (8)$$

Where,

$$e_i = \begin{cases} h_i \log_2(h_i), & h_i \neq 0 \\ 0, & \text{otherwise} \end{cases} \quad (9)$$

III. THEORY OF PSO

PSO algorithm is a population based search algorithm based on the simulation of the social behavior of birds within a flock. The initial intent of the particle swarm concept was to graphically simulate the graceful and unpredictable choreography of a bird flock, with the aim of discovering patterns that govern the ability of birds to fly synchronously, and to suddenly change direction with a regrouping in an optimal formation.

B. PSO Algorithm

In PSO, individuals are referred to as particles, which are "flown" through hyper dimensional search space [49]. Change in the position of each particle within the search space is based on the social psychological tendency of particle to emulate the success of other particle. The change to a particle's position within the swarm is therefore influenced by the past experience, or by the knowledge of its neighbours. The search behaviour of a particle is thus affected by that of other particles within the swarm (PSO is therefore a kind of symbiotic cooperative algorithm). Particle Swarm optimization technique has mainly two primary operators:

- Velocity update
- Position update During each generation each particle is accelerated toward the particle's previous best position (pbest) and the global best (gbest) position and new velocity value for each particle is calculated based on:
 - ★ Its current velocity.
 - ★ The distance from its previous best position.
 - ★ The distance from the global best position.

The new velocity value is then used to calculate the next new position of the particle in the search space. In PSO, initially each potential solution is assigned a randomized velocity and is "flown" through the problem space. Each particle adjusts its flying according to its own flying experience and its companion flying experience.

$$v_i^{t+1} = w \cdot v_i^t + c_1 \cdot r_1^t * [pbest_i^t - X_i^t] + c_2 \cdot r_2^t [gbest - X_i^t] \quad (10)$$

$$X_i^{t+1} = X_i^t + v_i^{t+1}$$

Where;

v_i^t is velocity of i^{th} particle at iteration t ,
 w is weight inertia.

c_1, c_2 is Acceleration Constants.

r_1, r_2 is random number between 0 and 1.

x_i^t is current position of i^{th} particle at iteration t ,

$pbest_i$ is personal best of i^{th} particle,

$gbest$ is global best value of the group.

C. Proposed Methodology

In the proposed method an enhanced image produced from a transformation function which incorporates both global and local information of the input image defined in eq. 4.7 is used. The function also contains four parameters namely a, b, c, k which are used to produce diverse result and help to find the optimal one according to the objective function. These four parameters have their defined range which is described above. Now our aim is to find the best set of values for these four parameters which can produce the optimal result and to perform this work PSO is used. P number of particles are initialized, each with four parameter a, b, c and k by the random values within their range and corresponding random velocities. It means position vector of each particle X has four component a, b, c and k . Now using these parameter values, each particle generates an enhanced image. Quality of the enhanced image is calculated by an objective function defined in eq. 4.8 which is termed as fitness of the particle. Fitness value of all the enhanced images generated by all the particles is calculated. From these fitness values $pbest$ & $gbest$ are found. In PSO the most attractive property is that $pbest$ & $gbest$ are found according to their fitness values. With the help of these best values, component wise new velocity of each particle is calculated to get the new solution. In this way new positions of particles are created for generations. When the process is completed the enhanced image is created by the global best ($gbest$) particle, as it provides the maximum fitness value and the image is displayed as the final result.

Main steps for PSO algorithm is as follows:

- ★ Initialize number of particles with random position and velocity.
- ★ Evaluate the fitness value for each particle.
- ★ Evaluate $gbest$.
- ★ Evaluate $pbest$.
- ★ Update velocity & position.
- ★ Evaluate the fitness value for new position
- ★ If condition is fulfilled $gbest$ is the solution else repeat above steps

The pseudocode for the proposed methodology :

Repeat

for $i = 1$ to number of particles **do**

if $G(X_i) > G(pbest_i)$ then $G()$ evaluates goodness

for $d = 1$ to dimensions **do**

$pbest_i = X_i$ // $pbest_i$ is the best state found so far

end for

end if

$gbest = i$ // arbitrary

for $j =$ indexes of neighbours **do**

if $G(pbest_j) > G(gbest)$ then

$gbest = j$ // $gbest$ is the index of the best performer in the neighbourhood

end if

end for

for $d = 1$ to number of dimensions **do**

$V_i^t = f(X_i^{(t-1)}, V_i^{(t-1)}, pbest_i, gbest)$ //Update velocity

$V_i = (-V_{max}, + V_{max})$

$X_i^t = f(V_i^t, X_i^{(t-1)})$ //Update position

end for

end for

until stopping criteria

end procedure

D. Parameter setting

The result of PSO algorithm for image enhancement is very much parameter dependent and fine tuning of these defined parameters is required in order to get the better result than other optimization algorithms. Parameter w used in eq. 10 plays an important role in balancing the global & local search and is known as inertia weight. Maximum and minimum value for this is set to two and zero respectively, which is same for all

particles. It may have fixed value throughout the procedure but in our case we start with maximum inertia value i.e. 2 and gradually reduce it to minimum. Therefore, initially inertia component is large and explore larger area in the solution space, but gradually inertia component becomes small and exploit better solutions in the solution space. Inertia value w is calculated as follows:

$$w_t = (w_{max} - w_{min}) \times \frac{t}{t_{max}} \tag{11}$$

Where, t is the i^{th} iteration and t_{max} is the total number of iteration. Parameters c_1 & c_2 are positive acceleration constants, given a random number between 0 & 2. These parameters are fixed for each particle throughout its life. c_1 is also known as cognitive coefficient and it controls the pull to the personal best position while c_2 is known as social-rate coefficient and it control the pull to the global best position. r_1 called cognition random factor & r_2 called social learning random factor. These are random numbers in [0, 1] and varies for each component of the particles in every generation. These have important effect on balancing the global & local search.

The experiment proves that the four parameter to be optimized i.e. a, b, c & k give better results if there values are selected in the following range $a \in [0, 1.5]$; $b \in [0, (D/2)]$; $c \in [0, 1]$; $K \in [.5, 1.5]$ Where D is the global mean of the original image.

IV. RESULT AND DISCUSSION

The experimentation is done for the four images shown below. Results of the proposed method is compared with two other methods, namely (i)linear contrast stretching (LCS),(ii) histogram equalization (HE)

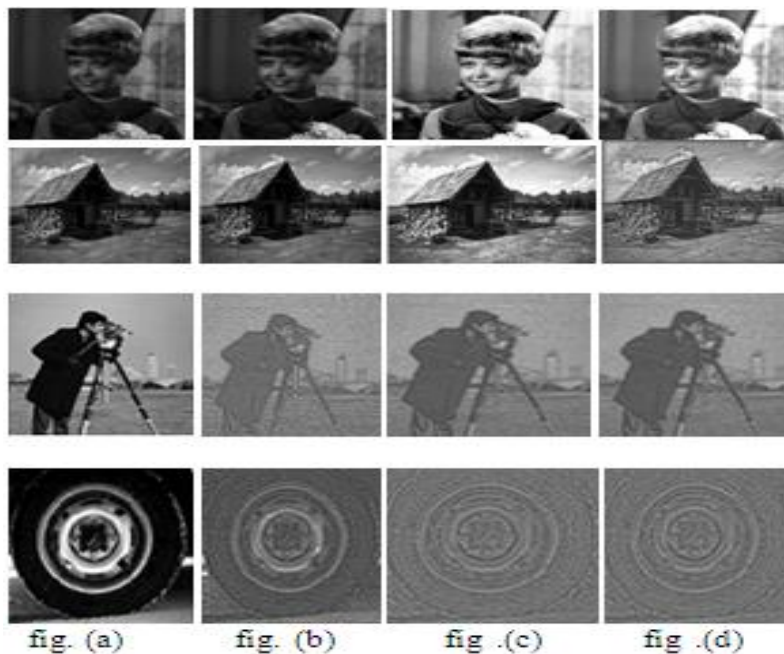


Figure (a): Original image Figure (b): Image obtained by LCS Figure (c): Image obtained by HE Figure (d): Image obtained by PSO

DETAILS ABOUT THE ORIGINAL IMAGES

TABLE 1					
IMAGE	SIZE	P/I/W	FITNESS		
			LCS	HE	PSO
Camerman	256×256	30/20/5	0.51088	1.12475	1.9363
Hut	280×272	30/20/3	1.25004	1.90515	2.03482
Tire	205×232	30/20/7	0.42902	1.61869	2.38565
Angle	291×240	40/20/7	0.85795	1.70078	1.89644

P/I/W third column of Table-1 signify the number of particles maximum number of generation and window size taken to extract the local information correspondingly.

V. CONCLUSION

Results of the proposed technique are compared with some other image enhancement techniques, like linear contrast stretching, histogram equalization based image enhancement. Most of the times it is observed that our technique is giving better result compared to other techniques mentioned above. In PSO, the most important property is that, it can produce better result with proper tuning of parameters. But in case of contrast stretching and histogram equalization, they always produce only one enhanced image for a particular. In this paper we have propose a PSO based automatic image enhancement technique for gray level images. In this paper we have propose a PSO based automatic image enhancement technique for gray level images VI .Acknowledgment

VI. ACKNOWLEDGMENT

Authors would like to thank the department of electronics and communication engineering, diet, kharar.

REFERENCES

- [1]. Cambridge University Press 978-0-521-86085-7 – “Digital Image Processing for Medical Applications”
- [2]. R. C. Gonzales and R. E. Woods, “Digital Image Processing”. Addison-Wesley, 2009.
- [3]. A. K. Jain, “Fundamentals of Digital Image Processing”. Englewood Cliffs, NJ: Prentice-Hall, 1991.
- [4]. A. Zagzebski, Essentials of Ultrasound Physics. St. Louis, Missouri: Mosby, 1996.
- [5]. J. Canny, “A Computational Approach To Edge Detection”, IEEE Trans.Pattern Analysis and Machine Intelligence., vol. 8, pp. 679-714, 1986.
- [6]. T. Peli and J. S. Liin, “Adaptive filtering for image enhancement”, Optical Eng., vol. 21, no. 1, pp. 108-112, 1982.
- [7]. S. M. Pizer, J. B.Zimmerman, and E. V. Staab, “Adaptive grey level assignment in CT scan display”, J. Comput. Assist. Tomogr.,vol. 8, pp. 300-308, 1984.
- [8]. M. I. Sezan, A. M. Tekalp, and R. Schaetzing,“Automatic anatomically selective image enhancement in digital chest radiography”, IEEE Trans. Med. Imag., vol. 8, pp. 154-162, 1989.
- [9]. Ji, T.-L., Sundareshan, M.K.; Roehrig, H., “Medical Imaging”, IEEE Transactions on Volume: 13 , Issue: 4, Page(s): 573 – 586, 1994
- [10]. B.T. Chen; Y.S. Chen; W.H. Hsu; “Automatic histogram specification based on fuzzy set operations for image enhancement”, Signal Processing Letters, IEEE Volume: 2 , Issue: 2, PP: 37 – 40, 1995
- [11]. F. Russo and G. Ramponi, “An Image Enhancement Technique Basedon the FIRE Operator”, IEEE international Conference on Image Processing, KIP-95, October 22-25, 1995
- [12]. T. K. Kim; J. K. Paik; B. S. Kang, “Contrast enhancement system using spatially adaptive histogram equalization with temporal filtering”, Consumer Electronics, IEEE Transactions on Volume: 44 , Issue: 1, PP: 82 – 87, 1998
- [13]. S.C. Matz, R.J.P Figueiredo, “A nonlinear technique for image contrast enhancement and sharpening”, Proceedings of the IEEE International Symposium on Volume: 4, PP: 175 – 178, 1999.
- [14]. K. Horio, T. Haraguchi, T. Yamakawa, “An Intuitive Contrast Enhancement of an Image Data Employing the Self-organizing Relationship”, IJCNN '99. Vol: 4, PP: 2710 – 2714, 1999.
- [15]. F. Saitoh, “Image Contrast Enhancement Using Genetic Algorithm”, IEEE International Conference on Volume: 4, PP: 899 – 904, 1999.
- [16]. U. Bidarte, J.L. Martin, A. Zuloaga, J. Ezquerria, “Adaptive Image Brightness and Contrast Enhancement Circuit for Real-Time Vision Systems”, Proceedings of IEEE International Conference on Volume: 1, PP: 421 – 426, 2000.
- [17]. F. Russo, “An image enhancement technique combining sharpening and noise reduction.”,IEEE Transactions onVolume: 51 , Issue: 4, PP: 824 – 828, 2002
- [18]. J. L. Starck, F. Murtagh, E. J. Candes, D. L. Donoho, “Gray and colour image contrast enhancement by the curvelet transform”, Image Processing, IEEE Transactions on Volume: 12 , Issue: 6, PP : 706 – 717, 2003.
- [19]. J. T. Cheng, B. Hsieh, W. S. Jyh, “Image contrast enhancement based on intensity-pair distribution”,IEEE International Conference on Volume: 1, PP : 913-916, 2005
- [20]. L. Q. Hiep, P. Smet, W. Philips,“Image interpolation using constrained adaptive contrast enhancement techniques”, IEEE International Conference on Volume: 2, PP: II - 998-1001, 2005.
- [21]. Z. Y. Chen, B. R. Abidi, D. L. Page, M. A. Abidi , “A Generalized and Automatic Image Contrast Enhancement Using Gray Level Grouping”, Acoustics, Speech and Signal Processing, IEEE International Conference on Volume: 2, 2006
- [22]. Z. Y. Chen, B. R. Abidi, D. L. Page, M. A. Abidi , “Gray-level grouping (GLG): an automatic method for optimized image contrast enhancement - part II: the variations” Image Processing, IEEE Transactions on Volume: 15 , Issue: 8, PP: 2303 – 2314, 2006.
- [23]. E. Nezhadarya, M. B. Shamsollahi, “Image Contrast Enhancement by Contourlet Transform”, Multimedia Signal Processing and Communications, 48th International Symposium ELMAR, PP: 81 – 84, 2006.
- [24]. X. Jianmao, S. Junzhong, Z. Changjiang, “Non-linear Algorithm for Contrast Enhancement for Image Using Wavelet Neural Network”, Control, Automation, Robotics and Vision, PP: 1 – 6, 2006.
- [25]. Y. Hu, B. Li, J. Zheng, B. Yu, “An Adaptive Image Enhancement Based on the Vector Closed Operations”, Image and Graphics, ICIG, Fourth International Conference, PP: 75 – 80, 2007
- [26]. K. A. Panetta, E.J. Wharton, S.S. Agaian, “Human Visual System-Based Image Enhancement and Logarithmic Contrast Measure”, Systems, Man, and Cybernetics, Part B: Cybernetics, IEEE Transactions on Volume: 38, Issue: 1, PP: 174 – 188, 2008.
- [27]. T. Chun-Ming, Y. Zong-Mu, “Contrast Enhancement by Automatic and Parameter-Free Piecewise Linear Transformation for Colour Images”, Consumer Electronics, IEEE Transactions on Volume: 54, Issue: 2, PP: 213 – 219, 2008.
- [28]. Z. Tiedong, W. Lei, X. Yuru, L. Yu, “Sonar Image Enhancement Based on Particle Swarm Optimization”, Industrial Electronics and Applications, 3rd IEEE Conference Page(s): 2216 – 2221, 2008.
- [29]. S. Te-Jen, L. Tzu-Hsiang, L. Jia-Wei, “Particle Swarm Optimization for Gray-Scale Image Noise Cancellation”, Intelligent Information Hiding and Multimedia Signal Processing, International Conference, PP: 1459 – 1462, 2008.
- [30]. A. Choudhury, G. Medioni, “Perceptually Motivated Automatic Color Contrast Enhancement”, Computer Vision Workshops, IEEE 12th International Conference, PP: 1893 – 1900, 2009.

- [31]. P. Jagatheeswari, S. S. Kumar, M. Rajaram, "Contrast Stretching Recursively Separated Histogram Equalization for Brightness Preservation and Contrast Enhancement", *Advances in Computing, Control, & Telecommunication Technologies, International Conference*, PP: 111 – 115, 2009.
- [32]. T. R. Benala, S.D. Jampala, S.H. Villa, B. Konathala, "A novel Approach to Image Edge Enhancement Using Artificial Bee Colony Optimization Algorithm for Hybridized Smoothing Filters", *Nature & Biologically Inspired Computing, World Congress*, Page(s): 1071 – 1076, 2009.
- [33]. L. Ching-Hsi, H. Hong-Yang, W. Lei, "A New Contrast Enhancement Technique by Adaptively Increasing the Value of Histogram", *Imaging Systems and Techniques, IEEE International Workshop*, PP: 407 – 411, 2009.
- [34]. T. Arici, S. Dikbas, Y. Altunbasak, "A Histogram Modification Framework and Its Application for Image Contrast Enhancement", *Image Processing, IEEE Transactions on Volume: 18*, PP: 1921 – 1935, 2009.
- [35]. J. Kennedy and R. C. Eberhart, "Particle Swarm Optimization", *Proceedings of IEEE International Conference on Neural Networks*, pp 1942-1948, 1995.
- [36]. A. P. Engelbrecht, "Computational Intelligence - An Introduction", Chichester, England: John Wiley and Sons, 2007.
- [37]. J. Kennedy and R. Eberhart. "Swarm Intelligence", Morgan Kaufmann Publishers, Inc., San Francisco, CA, 2001.
- [38]. Kennedy, J. "Small worlds and megaminds: Effects of neighborhood topology on particle swarm performance", in *Proceedings of IEEE Congress on Evolutionary Computation*, pages 1931–1938, 1999.
- [39]. R. Poli, S. Cagnoni, "Evolution of pseudo-coloring algorithms for image enhancement", Univ. Birmingham, CSRP- 97-5, 1997.
- [40]. C. Munteanu, V. Lazarescu, "Evolutionary contrast stretching and detail enhancement of satellite images", in *Proc. Mendel, Berno, Czech Rep.*, pp. 94-99, 1999.
- [41]. C. Munteanu, A. Rosa, "Evolutionary image enhancement with user behavior modeling," *ACM SIGAPP Applied Computing Review*, vol. 9, no. 1, pp. 8-14, 2001.
- [42]. F. Saitoh, "Image contrast enhancement using genetic algorithm," in *Proc. IEEE SMC, Tokyo, Japan*, pp. 899-904, 1993.
- [43]. S. K. Pal, D. Bhandari, M. K. Kundu, "Genetic algorithms for optimal image enhancement," *Pattern Recognition Letter*, vol. 15, pp. 261-271, 1994.
- [44]. T. Back, D. Fogel and Z. Michalewicz, "Handbook of Evolutionary Computation", Oxford Univ. Press, London, U.K., 1997.
- [45]. S. Jingquan, F. Mengyin, Z. Chanjian, "An image enhancement algorithm based on chaotic optimization", *Computer Engineering and Applications*, vol. 27, pp. 4-6, 2003.

Mechanism Study on Flocculating Organic Pollutants By Chitosan with Different Molecular In Wastewater

Zeng De-fang, Liu Jun, Yan Huan

School of Resource and Environmental Engineering, Wuhan University of Technology; Hubei Key Laboratory of Mineral Resource Processing and Environment; Wuhan 430070, P.R.China

Abstract: This paper presents the effect of the molecular weight of chitosan on flocculation of simulation sewage. The flocculation process of different chitosan samples were analyzed in different deacetylation degree, dosage and pH. The different molecular weight of chitosan samples and simulation sewage were all laboratories homemade. The flocculating effects of chitosan increases with the increase of deacetylation degree; the flocculating effects of chitosan decreases with the increase of viscosity-average molecular weight, the viscosity-average molecular weight in $8.5\sim 68\times 10^4$ range. Some conclusions were different from classical theory, the higher molecular weight of chitosan, the better its precipitation effect is. This discovery of the phenomenon is important to perfect the existing polymer flocculation theory.

Keywords: Chitosan, Molecular, Flocculation, Organic contaminant

I. INTRODUCTION

Chitosan(CTS) as a kind of promising natural biomaterial[1-3,4], its research and application of chitosan in the field of water treatment, which mainly used for drinking-water and water supply in American [5,4] and applied to water treatment and sewage treatment in Japan[6]. Lots of carboxyl groups and amido groups were distributed in chitosan as cationic flocculant [7-9]. The organic pollutants such as carbohydrate, protein, nucleic acid and so on in the water were effectively adsorbed and flocculating settling by adsorption, ion exchange, subsidence etc [2,3]. Up to now, which is widely studied is the removal efficiency of COD of chitosan flocculant on its dosage and its strong chelation to metal ions [10]. Due to the viscosity-average molecular weight and deacetylation degree of chitosan is the key factors [11-15] which related to the effect of flocculation. When chitosan is used in water treatment in the traditional, the viscosity-average molecular weight is greater than 1×10^6 and the removal of COD about 65% [1,3,16]. This paper, the effect of the $8.5\sim 68\times 10^4$ range of viscosity-average molecular weight of chitosan on the removal of COD was examined. Through experiment and mechanism analysis, to this kind of abnormal phenomenon demonstrated and explanation, so as to add and perfect the existing macromolecular flocculating theory provides a powerful experiment basis.

II. MATERIALS AND METHODS

2.1 Materials

2.1.1 Main experimental apparatus

BA120 type one ten thousandth digital display electronic microbalance (Shanghai Constant Balance instrument Ltd.); (0.5-0.6mm) Ubbelohde viscometer (Zhengzhou Zhongtian Experimental instrument Ltd.); Water bath (Fuhua Instrument Ltd.); Zeta potential measurement instrument (American Beckman Coulter company); Six joint electric blender (WuHan Meiyu Instrument Ltd.) etc

2.1.2 Main experimental reagents

CTSm#: white powder, moisture 6%, ash content less than 2%, insolubles less than 2%, $M_w=4.120\times 10^5$, DD(%)=70, industrial class. CTSn#: white powder, $M_w=6.108\times 10^5$, DD(%)=85, industrial class. Anhydrous alcohol, NaOH, H_2O_2 , potassium bichromate, ferrous reagent, ammonium ferrous sulfate,

sulfuric acid silver, mercury sulfate, potassium hydrogen phthalate and soluble starch were of analytical grade. Edible soybean vegetable oil and bovine serum album with biological pure.

Water sample: Choosing soluble starch as carbohydrate of organic pollutants; "Bovine serum albumin" as protein of organic pollutants; Edible soybean vegetable oil as fat class of organic pollutants in simulation material. According to the requirements of the influent water in some sewage plants in Hubei province, COD=186 mg/L.

2.2 Experimental Methods

2.2.1 Deacetylation degree determination

Double-saltation potentiometric titration method: weigh accurately 0.200g CTS in 20ml 0.1 mol/L HCl solution in a mechanical stir to completely dissolve, then titrated with 0.1 mol/L NaOH to neutralize, when the HCl in solution was completely neutralized, pH value would rise is the first saltation. The second stage for NaOH neutralized another part of HCl, which was the combination with CTS amino, when reaching the end of titration, pH value would rise named after the second mutation. The consumption of the NaOH mole number during the two saltation was equivalent to the content of amino in CTS molecules. The calculation formulas of deacetylation degree (DD) was as followed[16]:

$$DD(\%) = \frac{\Delta v \times C_{NaOH} \times 10^{-3} \times 16}{m \times 0.0994} \quad (1)$$

Δv -the difference of the consumption volume of NaOH between two saltation (mL);
 C_{NaOH} -the concentration of NaOH/mol⁻¹; m-weight of CTS/g; DD-deacetylation degree;
 16-the molecular weights of amino; 0.0994-the theoretical content of amino.

2.2.2 Molecular weight determination

Viscosity measurement of the molecular weight of CTS: the viscosity of linear polymer generally was higher, which was relevant with its molecular weight. When the polymer external physical and chemical condition is determined, according to Mark-Houwink equation ($[\eta]=KM^\alpha$ [16]) can get the sample molecular weight M value, which K and α is constant about polymer, solvent, temperature[16]. Weigh accurately 0.500g CTS in 0.2mol/L of HCl and 0.1mol/L NaCl solution, mixed to dissolve, then filter and determined the viscosity with ubbelohde viscometer.

2.2.3 Flocculation experiment

At room temperature, taking 800mL water sample in 1000mL beaker adjusting pH, added different kinds of CTS, stirred in 350r/min 2min, then 75r/min 5 min in the six league mixer, then statically settled 20 min, at last determinated COD of treated water sample. And analysis flocculation characteristics of different CTS's molecular weigh.

III. RESULTS AND DISCUSSION

3.1 CTS deacetylation degree and molecular weight

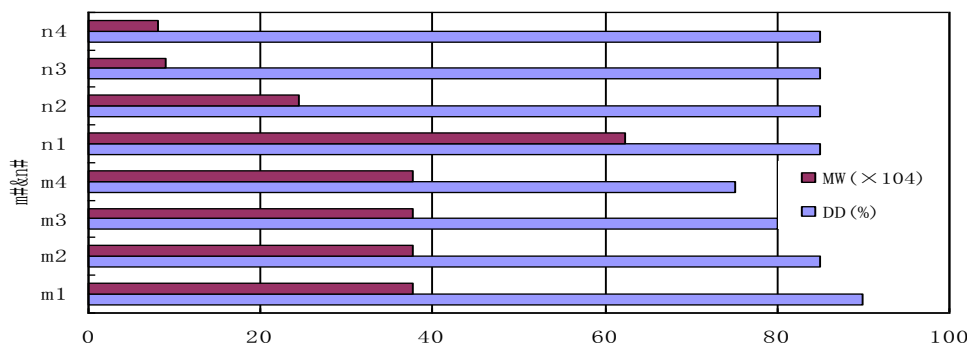


Figure 1 Deacetylation degree and molecular weight of CTS m# and n#

According to the formula (1) to deacetylation degree and molecular weight of CTS m# and n#, it can be showed in Fig.1. In Fig.1, the molecular weight of CTSm# were the same, but the deacetylation degree different; And deacetylation degree of CTSn# were the same, but the molecular weight different.

3.2 Effects of the CTS deacetylation degree on flocculation

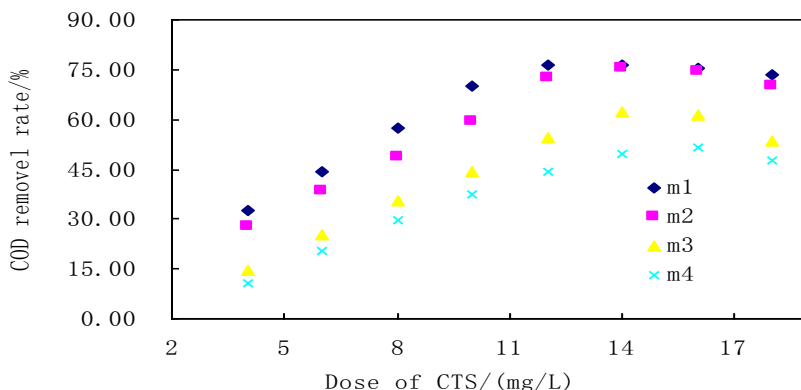


Figure 2 Effects of the CTS deacetylation degree on flocculation

Deacetylation degree is the influence factor of CTS on water purifying function, CTSm# were made into the same mass fraction of the solution, then flocculated the same amount of simulated sewage and determined the removal rate of COD. The results was showed in Fig.2, with the CTS deacetylation degree increased, the removal rate of COD in water also improved. When the deacetylation degree in 78~86.5%, the removal rate of COD reached a larger extent, and when the deacetylation degree was higher than 86%, the removal rate of COD ascending slowly and the effect is not distinct. With the increasing dosage of CTS, the removal rate of COD in water improved, but reaching a certain dosage, the removal rate of COD began to decline. Deacetylation degree was different; the best dosage was also different. The best dosage of m1, m2, m3 and m4 was 12.0-12.5mg/L, 12.3-13.0mg/L, 14.5-15.0mg/L and 16.6-17.0mg/L respectively.

3.3 Effects of the CTS molecular weight on flocculation

Molecular weight is the key index of CTS on water purifying function; CTSn# were made into the same mass fraction of the solution, then flocculated the same amount of simulated sewage and determined the removal rate of COD. The results was showed in Fig.3, with the CTS molecular weight increased, the removal rate of COD in water decreased. And with the increasing dosage of CTS, the removal rate of COD in water improved, but the removal rate of COD began to decline when reaching a certain dosage. Molecular weight was different; the best dosage was also different. The best dosage of n1, n2, n2 and n3 was 15.4mg/L, 13.5mg/L, 12mg/L and 9.5mg/L respectively. The result of the unit test indicated that the corresponding optimal dosage of low molecular weight was less than that of high one, the removal rate of COD would get the same effect.

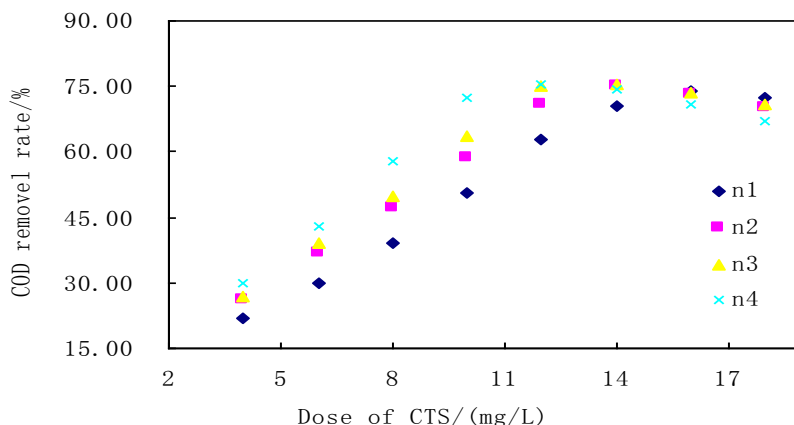


Figure 3 Effects of the CTS molecular weight on flocculation

It maybe for that low molecular weight of CTS combined blank position on the surface of particles quickly after dissolved, through an effect on electric neutralization to shorten the distance between the particles so as to flocculate. But with the increasing concentration of CTS, blank particle on the surface of particles were covered completely. At this time, CTS played a protective effect, so flocculation instead weakened. When the CTS concentration further increased, stretch structure of its molecular chain changed slowly into single chain structure, then mutually winded and form line-group structure. Mutual-winding degree of high molecular weight

was high, and its molecular internal and intermolecular formed a large amount of hydrogen bond. The stable structure made a mount of CTS was difficult to dissolve in flocculation process, and repulsive force of CTS intermolecular was stronger, and caused molecules not easy to near each other and got together. Solubility of low molecular weight CTS was better, it was easy to close to each other between molecules. So low molecular weight CTS on the removal rate of COD in water was superior to high molecular weight CTS.

3.3 Effects of pH on flocculation

CTSn# was made into the same mass fraction of the solution, then flocculated the same amount of simulated sewage and determined the removal rate of COD in different pH. The results were showed in Fig.4. The COD removal trend of different molecular weight of the CTS was roughly the same in different pH. When the pH=5.5-7.0, the removal rate of COD rose gradually and then reduced with the increase of pH in water. And when pH was 6.0 to 6.5, the removal rate of COD reached the maximum. CTS was a weak cationic electrolyte, which played mainly electric neutralization in a low pH and CTS formed granular carbide and precipitated with pH increased so as to affect the removal efficiency of COD.

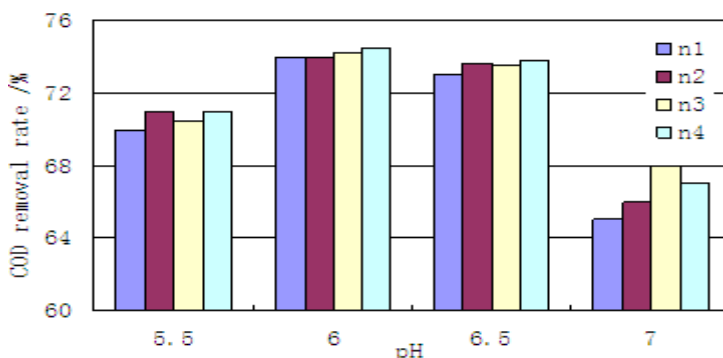


Figure 4 Effects of pH on flocculation

3.4 Effects of different viscosity-average molecular weight CTS on settling velocity in the flocculation process

The results of the settling velocity were shown in Fig.5. With the increasing dosage of CTS, settling velocity of flocs in water improved. Generally the flocs of high molecular weight CTS was bigger and faster formed, and could settle during the short time. In this test shown that n3 was the lowest, but the removal rate of COD of n3 was the best. This could be that the solubility and dissolution rate of high molecular weight CTS is relatively lower in the same concentration so that it was not easy to flocculate fully in the relatively short time and affected the removal efficiency of COD in water.

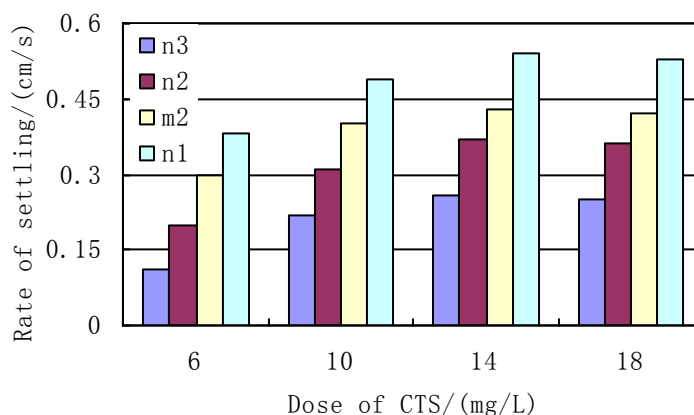


Figure 5 Effects of different viscosity-average molecular weight CTS on settling velocity in the flocculation process

3.6 Flocculation mechanism

From the above experimental results, molecular weight in $8.5-68 \times 10^4$ in a certain deacetylation degree range, low molecular weight CTS as a flocculant to treat sewage could have a better flocculation effect and a higher removal efficiency of COD, the corresponding amount will also decreased. The adsorption on the particles surface of polymer rooted in all kinds of physical and chemical action of intermolecular, such as electrostatic attraction, all kinds of coordination bond, hydrogen bond, etc. We found that a large amount of

hydrogen bond between the intramolecular and intermolecular [17] of high molecular weight CTS. The stable structure made macromolecules CTS in weak-acid to dissolve difficultly and the repulsive force of CTS intermolecular was strong, so it was hard to near each other to concentrate. And low molecular CTS after dissolving in acidic condition are more likely to spread its molecular chain [18,19], which have a faster dispersed and strong electropositive, thus the neutralized on the surface of particle making colloid stability and settlement. The repulsion of low molecular weight between the molecules CTS was weak and easier to close to play a bridging role, quick adsorb. The principles of electric neutralization and bridging cause that low molecular weight CTS could effective settle particles in water. When the CTS molecular weight up to a certain value and CTS molecular chain length reached a certain length, the bridging flocculation played a leading role, the flocculation effect would be increased with the molecular weight increased obviously.

IV. CONCLUSIONS

The self-prepared CTS flocculated in the same sewage COD. The results showed that in the same molecular weight, with the CTS deacetylation degree increased, the removal rate of COD in water also improved, when deacetylation degree in 80~85%, the removal rate of COD reached a larger extent, and when the deacetylation degree is higher than 85%, the removal rate of COD ascended slowly and the effect was not distinct. Selecting chitosan as flocculating agent, should be comprehensive consideration of the cost and benefit. Secondly, when deacetylation degree was 85% and molecular weight in $8.5-68 \times 10^4$, the removal efficiency and dosing quantity of low molecular weight CTS was superior to high molecular weight in room temperature and pH=6.5. Thirdly, choosing n# samples and m2 sample to test the effects on the pH value in its best dosing quantity. When the pH value was in 6.0~7.0, with the increase of pH, the removal rate of COD after the first rise gradually reduce. When pH was neutral and a little acid, the removal rate of COD reached the highest. In molecular weight $8.5-68 \times 10^4$, with the high molecular weight, the flocculating constituent of CTS was larger and faster formed than that of low one, could settle in short time.

REFERENCE

- [1]. Wang J. P., Clien Y. Z., Ge X. W. et al. Gamma radiation-induced grafting of a cationic monomer onto chitosan as a flocculant [J]. *Chemosphere*. Vol.66:pp.1752-1757,2007
- [2]. Jiang C. Y., Shan L. S., Chang C. Synthesis of cationic chitosan and study of flocculation performance[J]. *Journal of China University of Petroleum*. Vol 30 (2):pp.106-109,2006
- [3]. Riske F., Schroeder J., Belliveau J. et al. The use of chitosan as a flocculant in mammalian cell culture dramatically improves clarification throughput without adversely impacting monoclonal antibody recovery. *Journal of Biotechnology*. 4(128):pp.813-823,2007
- [4]. Nitayaphat W, Jiratumnukul N, Charuchinda S, Kittinaovarat S. Mechanical properties of chitosan/bamboo charcoal composite films made with normal and surface oxidized charcoal. *Carbohydrate Polymers*. 78(3): pp.444-448, 2009
- [5]. Babel S, Kurniawan T A. Cr (VI) removal from synthetic wastewater using coconut shell charcoal and commercial activated carbon modified with oxidizing agents and/or chitosan. *Chemosphere*. 54(7):pp. 951-967,2004
- [6]. Amit Bhatnagar, Mika Sillanpää. Applications of chitin-and chitosan-derivatives for the detoxification of water and wastewater-A short review [J]. *Advances in Colloid and Interface Science*. Vol 152, Iss 1-2, 30 Nov, pp.26-38,2009
- [7]. Douglas de Britto, Odilio B. G. deAssis. Synthesis and mechanical properties of quaternary salts of chitosan-based films for food application [J]. *International Journal of Biological Macro molecules*. Vol 41:pp. 198-203,2007
- [8]. Bautista-Banos S., Hernandez-Lauzardo A. N., Vela M. G., et al. Chitosan as a potential natural compound to control pre and postharvest diseases of horticultural commodities[J]. *Crop Protection*. Vol 25: pp.108, 2006
- [9]. E. Guibal, "Interactions of metal ions with chitosan-based sorbents: a review", *Separation and Purification Technology*. Vol 38, pp. 43-74,2004
- [10]. F.Renault,B.Sancey,P.-M.Badot,G.Crini, Chitosan for coagulation/flocculation processes-An eco-friendly approach. Vol 45, Iss 5,pp.1337-1348,2009
- [11]. Liu Dongying, Yu Xiongyong, Zhou Liyan. Study on Preparation of Water Soluble Chitosan Derivatives. *Food and fermentation industries editorial staff*. Vol 35, 10(262): pp.93-94,2009
- [12]. Mart W. Anthonsen, Kjell M. Varum, Olav Smidsrod. Solution properties of chitosans: Conformation and chain stiffness of chitosams with different degrees of N-acetylation [J]. *Carbohydrate Polymers*. Vol 22:pp. 193-201,1993)
- [13]. Guillaume Lamarque, Jean-michel Lucas, Christophe Viton, et al. Physicochemical behavior of homogeneous series of acetylated chitosans in aqueous solution: role of various structural parameters [J]. *Biomacromolecules*, 6: pp.131-142,2005
- [14]. Marit W, Anthonsen, Olav Smidsred. Hydrogen ion titration of chitosans with varying degrees of Nacetylation by monitoring induced 1H-NMR chemical shifts [J]. *Carbohydrate Polymers*, 26:pp. 303-305,1995
- [15]. Sabina P. Strand, Kristoffer Tommeraas, Kjell M. Varum, et al. Electrophoretic light scattering studies of chitosans with different degrees of N-acetylation [J]. *Biomacromolecules*, 2: pp.1310-1314, 2001
- [16]. Mamoni Dash, Federica Chiellini, Elizabeth G. Fernandez, etc. Statistical approach to the spectroscopic determination of the deacetylation degree of chitins and chitosans. Vol 86, Iss1, 1 Aug pp.65-71,2011
- [17]. Houbin Li, Yumin Dua, Xiaojun Wu, Huaiyu Zhan. Effect of molecular weight and degree of substitution of quaternary chitosan on its adsorption and flocculation properties for potential retention-aids in alkaline papermaking. *Colloids and Surfaces A: Physicochem. Eng.pp*.242: 1-8,2004
- [18]. Rong Xing, Song Liu, Huahua Yu, Quanbin Zhang, ect. Preparation of low-molecular-weight and high-sulfate-content chitosans under microwave radiation and their potential antioxidant activity in vitro [J]. *Carbohydrate Research* 339pp. 2515-2519,2004
- [19]. Junping Zhang, Qin Wang, Aiqin Wang, Synthesis and characterization of chitosan-g-poly(acrylic acid)/attapulgite superabsorbent composites [J], *Carbohydrate Polymers* pp.68367-374, 2007

CDMA2000 Radio Measurements at 1.9GHz and Comparison of Propagation Models in Three Built-Up Cities of South-South, Nigeria.

Isabona Joseph¹, Isaiah Gregory Peter²

1. Department of Basic Sciences, Benson Idahosa University, PMB.1100, Benin City, Nigeria

2. Department of Physics, University of Uyo, Uyo, Nigeria.

Abstract: Radio propagation measurements and prediction, realized by the mobile terminal or the base station, is needed to guarantee quality of service and to supervise the planned coverage area. A wide variety of approaches have been developed over the years to predict signal pathloss using what are known as propagation models. In this paper, we compare the measured pathloss obtained for the urban areas with seven existing propagation models, that is, SUI, Lee, Hata, ECC and COST-231 W/I and W/B. Firstly, for both areas, the results show that the path loss is not constant at various locations for a constant distance around the respective base station (BS). This shows that the terrains of studied cities are irregular. Secondly, observations show that the W/B gives better agreement for all the studied three cities; hence, it can be used to model signal coverage area of cellular networks in any region of South-South Nigeria.

Keywords: CDMA2000, Radio measurements, Signal coverage area, Pathloss.

I. INTRODUCTION

It is established that propagation phenomena can cause unexpectedly poor performance in cellular networks. These are manifested in reduced coverage, dropped calls and unexpected handovers [1]. The performance of the cellular network can be assessed, or new networks can be designed when deferent models are tested with observed measurement results.

Radio measurements, realized by the mobile terminal or the base station, are crucial to assess mobile network reliability as they are needed to guarantee quality of service and to supervise the planned coverage area. These measurements are standardized for each wireless radio technology (GSM, UMTS, EDGE, CDMA2000, HSDPA...) and are essentially used as input for Radio Resource Management (RRM) algorithms. According to current radio network standards such as (third generation partnership project (3GPP) which is the joint standardization body from Europe, Japan, Korea, USA and China, the available metrics in the network can be divided in several categories, depending on their target use:

- Intra frequency measurements: Measurements on the same frequency as the active set. An active set corresponds to the set of base stations (for example Node B in CDMA) to which the mobile terminal is connected,
- Inter RAT measurements: Measurements on channels belonging to other radio access technologies,
- Quality measurements: Measurements of quality of service and of comparison to requested QoS,
- Internal measurements: Measurements in the mobile terminal, on the transmitted and received signal level,
- Positioning measurements: Measurements of the mobile terminal position. These metrics are related to the chosen positioning technology. The widely used technique is the Global Positioning System (GPS),
- Synchronization measurements: Mainly mobile terminal synchronization measurements,
- Traffic volume measurements.

In this study, we focus on internal measurements in the mobile terminal, on the transmitted and received signal level. This type of measurements is characterized with interesting properties linked to the propagation phenomenon. The idea is to explore the hidden properties in the radio measurements of CDMA2000 1x network operating at a frequency of 1.9GHz in built-up areas, so as to obtain received signal

level information and predict pathloss between the base station (BS) transmitter and the mobile station (MS) terminal.

II. RESEARCH MOTIVATION

Academically, built-up environments are interesting to study because of the complexity they present for the radio wave propagation. The many surfaces of buildings and objects in the streets produce reflections, diffraction, and shadowing of the signal, guiding it as it propagates from transmitter to receiver. Built-up environments are also of practical interest because these areas attract great concentrations of users. In fact, the popularity of wireless services in these areas is leading to network congestion. Since adding additional base stations to extend capacity is an expensive endeavor, system operators seek ways to extend the capacities of their existing systems.

Moreover, one way to extend capacity is through improved resource allocation methods. A resource is any shared commodity that the system provides to users on demand. Examples of such resources are frequency, timeslots, transmitted power, and modulation level/bandwidth. For example, in systems that spend less time performing unnecessary handoffs in regions where two base stations serve equally well, an improved handoff algorithm can use information from the propagation characteristics in the area to better refine the handoff location point [2-4].

Signal pathloss prediction models are important in this regard since they predict the received signal strength. Although other parameters may be used in resource allocation decisions, the received signal strength is the fundamental parameter by which these decisions are made. We study propagation models since they yield predictions of signal strength. The signal strength is the primary parameter by which resource allocation decisions are made in cellular systems.

III. MATERIALS AND METHODS MATERIALS

The materials used for field measurements are:

1. Acer compatible Laptop.
2. TEMS measurement software.
3. NOKIA 1265 CDMA test phone
4. External GPS antenna.
5. USB connector.

IV. METHODS

Field measurements were performed in the built-up city of Port Harcourt, Benin and Uyo for their CDMA2000 based system. All the measurements were taken for mobile terminal the NOKIA 1265 CDMA test phone systems (TEMS) operated in the active mode which was provided by the studied CDMA network service provider, accompanied with an Acer portable laptop and a MAP76CSX GPS receiver for accurate location. Measurements were taken in all three zones/sectors of studied BS sites. For macro cellular system, the reference distance is taken as $d_0 = 100\text{m}$. Starting from 100m, measurements were taken in intervals of 0.1 km, then up to a distance of 2 km from the transmitter in the three cities. In all, 9 cellular base stations were involved in the field measurements and their configuration parameters is shown in table 1.

For confidential and legal purposes, the name of the service provider used for the study will be designated as Operator A throughout the research.

The values of the signal strength level measured were converted into pathloss using the expression in equation (1):

$$PL = P_T + G_T + G_R - L_T - L_R - RSS_{(measured)} \quad (1)$$

where P_T is BS transmitted power, $RSS_{(measured)}$ is measured received signal strength, G_T and G_R are the gain of transmitting and receiving antenna, and L_T and L_R are feeder losses of the transmitter and the receiver, all in dB scale.

Table 1: Base station and CDMA network specification

Parameter	Specification for Operator A
Carrier Frequency in the Downlink	1900MHz
Bandwidth	1.25MHz
Modulation/Data Spreading	QPSK
Antenna Height	45m
Antenna Type	Directional (3-Sectored Antenna)
Antenna Gain	17dBi
Vertical Beam width	6.5°
Transmit Power	43dBm

Table 2: Environmental parameters for the pathloss calculation in the study location

Environmental parameters	Benin	Port Harcourt	Uyo
Average Height of Building (m)	6	5	7
Average space between building (m)	2.5	3	3
Average Street width (m)	9	9	10
Average root height (m)	2	2.5	2
Environment	Built-up city	Built-up city	Built-up city
City type	Large	Large	Medium large

EXISTING PROPAGATION MODELS

Here, some key city models available in existing literature for network planning are chosen and analysed relative to actual measured path loss to see how accurate they are for path loss prediction for CDMA2000 in the different locations of study. The chosen models which are Walfisch-Bertoni (W/B), Hata, ECC, SUI, COST-231(W/I), Lee and Egli model and their input environmental parameters used are summarized in table 1 and table 2

HATA PROPAGATION MODEL

The propagation model known as Hata -model, is based on Okumura's measurements in Tokyo [5], which were fitted into a mathematical model by Hata. The original Okumura-Hata formula is given in Equation (2) [6]:

$$L = 69.55 + 26.16 \log_{10}(f) - 13.82 \log_{10}(h_{BS}) - a(h_{MS}) + [44.9 - 6.55 \log_{10}(h_{BS})] \log_{10}(d) \quad (2)$$

where a is defined as:

$$a(h_{MS}) = [1.1 \log_{10}(f) - 0.7] h_{MS} - [1.56 \log_{10}(f) - 0.8] \quad (3)$$

$$a(h_{MS}) = 3.2 [\log_{10}(11.75h_{MS})]^2 - 4.97 \quad (4)$$

Equation (2) is used for small and medium cities and Equation (3) for large cities.

Other definitions used in Equation (1) are:

L= Path loss (dB)

F= Frequency (150 - 1500 MHz)

h_{BS} = Base station effective antenna height (20 - 200 m)

h_{MS} = Mobile station antenna height (1 - 10 m)

d = Distance between base and mobile station (1 - 20 km)

The original Okumura-Hata has some limitations. The most restrictive is that Okumura's measurements were made at 1920 MHz, and Hata's formulas cover only frequencies range from 150 to 1500 MHz. Also antennas have been over average rooftop level.

The original formula has been modified by COST-231 -project, which resulted in extending Okumura-Hata formula to cover frequencies from 1500 to 2000 GHz. This makes it possible to use the formula in simulations for 3G-networks for a reasonable accuracy [7]. Constants A and B are redefined, and distance dependence parameter C is recommended to be defined by measurements, but value 44.9 is still often used. The COST-231-Hata -formula is given in Equation 2.69. Constants A and B are chosen from the Table 3 [8]. Also an additional environment dependent parameter, area type correction factor, C_m , is given. It is above 0 dB in urban areas, but in rural areas it can be even below -15 dB [7].

$$L = A + B \log_{10}(f) - 3.82 \log_{10}(h_{BS}) - a(h_{MS}) + [C - 6.55 \log_{10}(h_{BS})] \log_{10}(d) + C_m \quad (5)$$

New definitions in the formula are:

A Constant, see Table 2.2

B Constant, see Table 2.2

C User defined value for distance dependence (slope factor) C_m Area correction factor.

TABLE 3: CONSTANTS A AND B FOR HATA MODEL

	150-1000MHz	1500-2000MHz
A	69.55	46.3
B	26.16	39.9

STANFORD UNIVERSITY INTERIM (SUI) MODEL

The SUI model was developed under the institute of Electrical and Electronics Engineers (IEEE) 802.16 working group for prediction of path loss in urban, suburban and rural environments [9]. The applicability of this model in the 800 MHz and 1900MHz band has not been validated. However, due to the availability of correction factors for the operating frequency, this model is selected. The SUI models are divided into three types of terrains 1, namely, A, B, and C. Type A is associated with maximum path loss and is appropriate for hilly terrain with moderate to heavy foliage densities. Type C is associated with minimum path loss and applies to flat terrain with light trees densities. Type B is associated characterized with either mostly flat terrains with moderate to heavy three density or hilly terrains with light tree densities. The basic path loss equation with correction factors is presented in [9]:

$$L(\text{dB}) = A + 10n \log_{10} \left(\frac{d}{d_0} \right) + X_f + X_b + S \quad \text{for } d > d_0 \quad (6)$$

Where d is the distance between the Access Point (AP) and mobile station in meters, $d_0 = 100\text{m}$ and S is a log normally distributed factor that is used to account for the shadow fading owing to tree and other cluster and has a valued between 8.2 dB and 10.6dB [10]. The other parameters are defined as

$$A = 20 \log_{10} \left(\frac{4\pi d_0}{\lambda} \right) \quad (7)$$

$$n = a - bh_b + \frac{C}{h_b} \quad (8)$$

where the parameter h_b is the base station height above the ground in metres and should be between 10m and 80m. The constants used a , b , and c is given in Table 4. The parameter n in (8) is equal to the pathloss exponent. For a given terrain type the pathloss exponent is determined by h_b

TABLE 4: SUI MODEL PARAMETERS IN DIFFERENT TERRAIN [10]

Model arameter	Terrain A	Terrain B	Terrain C
a	4.6	4.0	3.6
b (m^{-1})	0.0075	0.0065	0.005
c (m)	12.6	17.1	20

The correction factors for the operating frequency and the mobile station antenna height for the model are [10].

$$X_f = 6.0 \log_{10} \left(\frac{f}{2000} \right) \quad (9)$$

and

$$X_h = -10.8 \log_{10} \left(\frac{hr}{2000} \right) \quad \text{for Terrain A and B} \quad (10)$$

$$= -20.0 \log_{10} \left(\frac{hr}{2000} \right) \quad \text{for Terrain type C} \quad (11)$$

where, f is the frequency in MHz and hr is the mobile antenna height above the ground in metres. The SUI model is used to predict the path loss in all three environments, namely rural, suburban and urban.

THE LEE MODEL

This is a power law model, with parameters taken from measurements in a number of locations, together with a procedure for calculating an effective base station antenna height which takes account of the variations in terrain. It can be expressed in the simplified form [11]:

$$L = 10n \log(d) - 20 \log(h_{BS}) - P_o - 10 \log(h_{MS}) + 29 \quad (12)$$

where n and P_o are given in table 5 below

TABLE 5: PARAMETERS FOR LEE'S PATH LOSS MODEL

Environment	P_o	n
Free space	80	2.0
Open Area	89	4.35
North American Suburban	101.7	3.85
North American Urban	110	3.68
North American Urban	104	4.31
Japanese Urban	124	3.05

THE EGLI FACTOR MODEL

The Egli Model is a terrain model for radio frequency propagation. This model consists of the plane earth loss plus an extra loss component called the clutter factor. An example of clutter factor model is the method due to Egli, which is based upon a large number of measurements taken around American cities.

The formulas for the Egli's propagation loss prediction model are as below [12]:

For $hms \leq 10$,

$$PL (dB) = 20 \log_{10} f_c + 40 \log_{10} R + 20 \log_{10} hbs + 76.3 - 10 \log_{10} hms \tag{13}$$

For $hms \geq 10$,

$$PL (dB) = 20 \log_{10} f_c + 40 \log_{10} R + 20 \log_{10} hbs + 85.9 - 10 \log_{10} hms \tag{14}$$

ECC-33 MODEL

ECC-33 is a model from Electronic Communication Committee based on analysis in 3.4 and 3.8 GHz band. The path loss is obtained from the following equations [13]:

$$L = A_{fs} + A_{bm} - G_b - G_r \tag{15}$$

A_{fs} : Free space attenuation (dB)

A_{bm} : Basic median path loss (dB)

G_b : Transmitter antenna height gain factor

G_r : Receiver antenna height gain factor

$$A_{fs} = 92.4 + 20 \log(d) + 20 \log(f) \tag{16}$$

$$A_{bm} = 20.41 + 9.83 \log(d) + 7.894 \log(f) + 9.56 [\log(ff)^2] \tag{17}$$

When dealing with gain of the cities, G_b and G_r is expressed as [13]:

$$G_b = \log_{10}(h_b/200) \{13.958 + 5.8 [\log(d)]^2\} \tag{18}$$

$$G_r = 42.57 + 13.17 \log(f) [\log(h_{MS}) - 0.585] \tag{19}$$

Where d : Distance between transmitter and receiver antenna (km)

f : Frequency (GHz)

h_{BS} : Transmitter antenna height (m)

h_{MS} : Receiver antenna height (m)

COST 231(WALFISCH - IKEGAMI)

The parameters, excess path loss from Walfisch-Bertoni model and final building path loss from Ikegami Model are combined in this model with a few empirical correction parameters. This model is statistical and not deterministic because you can only insert a characteristic value, with no considerations of topographical database of buildings. The model is restricted to flat urban terrain.

The parameters used in Cost 231 Walfisch- Ikegami are denoted figure 1

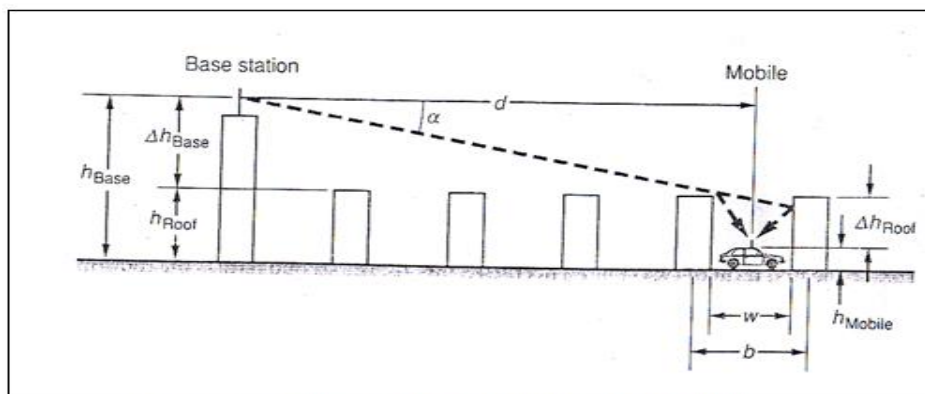


Figure 1: Geometry of Cost 231 Walfisch- Ikegami

The formulation of the model is given as follow

If a free LOS exists in a street canyon then, path loss defined as[2] :

$$L_{los}=42.6+26\log d+20\log f \quad d \geq 20m \tag{20}$$

WALFISCH IKEGAMI (NLOS)

Restrictions of the model are given as follow [2]:

TABLE 6 RESTRICTIONS OF THE COST 231 W-I MODEL

Frequency (MHz)	800-2000 MHz
Base Station Height (h_{base})	4-50 m
Mobile Height (h_{mobile})	1-3 m
Distance d,km	0.02-5 km

If a non-LOS exists, path loss defined as follow:

$$L_b = \begin{cases} L_{FS} + L_{rts} + L_{msd} \\ L_{FS} \end{cases} \quad \text{If } L_{rts} + L_{msd} < 0 \tag{21}$$

L_{FS} represents free space loss, L_{rts} is rooftop to street diffraction and scatter loss, L_{msd} is the multi-screen loss. The rooftop to street diffraction and scatter loss L_{rts} represents the coupling of wave propagating along the multi-screen path into the street mobile located.

$$L_{rts} = \begin{cases} -16.9 - 10\log w + 10 \log f + 20 \log \Delta h_{mobile} + \dots \\ 0 \end{cases} \quad \begin{matrix} h_{roof} > h_{mobile} \\ L_{rts} < 0 \end{matrix} \tag{22}$$

$$L_{ori} = \begin{cases} -10 + 0.354 (\varphi/\text{deg}) & 0 \leq \varphi < 35 \\ 2.5 + 0.075 [(\varphi/\text{deg}) - 35] & 35 \leq \varphi < 55 \\ 4 - .114[(\varphi/\text{deg}) - 55] & 55 \leq \varphi \leq 90 \end{cases} \tag{23}$$

Where φ is the angle between incidences coming from base station and road, in degrees shown in following figure 2.

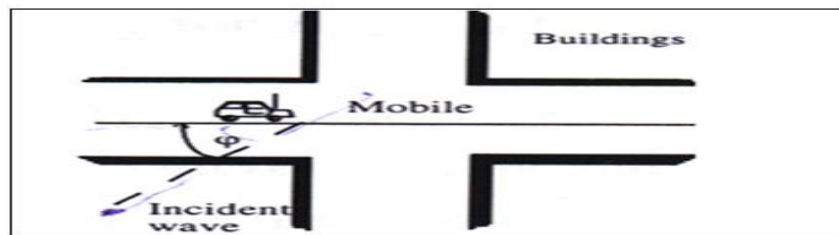


Figure 2: Definition of Street Orientation angle φ .

$$\Delta h_{mobile} = h_{roof} - h_{mobile}$$

$$\Delta h_{Base} = h_{base} - h_{roof}$$

The multiscreen diffraction loss L_{msd} is an integral for which Walfisch-Bertoni model approximate a solution to this for the cases base station antenna height is greater than the average rooftop. COST 231 extended this solution to the cases base station antenna height is lower than the average rooftop by including empirical functions.

$$L_{msd} = L_{bsh} + k_a + k_d \log (d/\text{km}) + k_f \log (f/\text{MHz}) - 9 \log (b/\text{m}) \tag{24}$$

$$L_{bsh} = \begin{cases} -18 \log (1 + \Delta h_{base}) \\ 0 \end{cases} \quad \begin{matrix} \text{for } h_{base} > h_{roof} \\ \text{for } h_{base} \leq h_{roof} \end{matrix} \tag{25}$$

$$k_f = -4 + \begin{cases} 0.7 [(f/925)-1] & \text{Medium sized cities and suburban centers with moderate tree density} \\ 1.5 [(f/925)-1] & \text{Metropolitan centers} \end{cases} \tag{26}$$

$$k_a = \begin{cases} 54 & \text{for } h_{base} > h_{roof} \\ 54 - 0.8\Delta h_{base} & \text{for } d \geq 0.5 \text{ km and } h_{base} \leq h_{roof} \end{cases} \tag{27}$$

$$k_d = \begin{cases} 54 - 0.8\Delta h_{base} R/0.5 & \text{for } d < 0.5 \text{ km and } h_{base} \leq h_{roof} \\ 18 & \text{for } h_{base} > h_{roof} \\ 18 - 15 \Delta h_{base} / h_{roof} & \text{for } h_{base} \leq h_{roof} \end{cases} \quad (28)$$

The term k_a denotes the increase of the path loss for base station antennas below the rooftops of adjacent buildings. The terms k_d and k_f control the dependence of the multi screen diffraction loss versus distance and radio frequency.

In case of that data on the structure of buildings and roads are not available; following values could be taken as default [14]:

$$\begin{aligned} b &= 20 \sim 50\text{m} \\ w &= b/2 \\ h_{roof} &= 3\text{m} \times (\text{number of floors}) + \text{roof height} \\ \text{roof} &= 3\text{m for pitched } 0\text{m for flat} \\ \varphi &= 90^\circ \end{aligned}$$

WALFICSH-BERTONI MODEL

Bertoni and Walfisch [15] proposed a semi-empirical model that is applicable to propagation through buildings in built-up environments. The model assumes building heights to be uniformly distributed and the separation between buildings are equal. Propagation is then equated to the process of multiple diffractions past these rows of buildings. The Walfisch-Bertoni reduces path loss model to three elements: Free space loss, PL_{fs} , diffraction from the rooftops, $PL_{rooftops}$ and diffraction and scatter loss from rooftop down the street, PL_{down}

Free space loss,

$$PL_{fs} = -10 \log_{10} \left(\frac{\lambda}{4 \pi r} \right)^2 \quad (29)$$

Diffraction and scatter loss from rooftop down the street, PL_{down}

$$PL_{down} = \frac{\lambda \rho_1}{2\pi^2 (H_b - h_m)} \quad (30)$$

Diffraction from the rooftops, $PL_{rooftops}$

$$PL_{rooftops} = P(g)^2 = \left[0.1 \left(\frac{\sin \delta \sqrt{\frac{d}{\lambda}}}{0.03} \right)^{0.9} \right]^2 \quad (31)$$

Here, $\sin \delta$ can be written in terms of BS height h_T , the building height H_B , and the distance R as,

$$\sin \delta = \frac{h_T - H_B}{R} \quad (32)$$

Equation (31) becomes,

$$PL_{rooftops} = P(g)^2 = 0.01 \left(\frac{h_T - H_B}{0.03R} \right)^{1.8} \left(\frac{d}{\lambda} \right)^{0.9} \quad (33)$$

The total loss is thus given by:

$$\begin{aligned} PL_{total} &= \log \left(\frac{\lambda}{4 \pi R} \right)^2 P(g)^2 \frac{\lambda \rho_1}{2\pi^2 (H_b - h_m)} \\ &= \frac{5.51}{32\pi^4} \frac{(h_r - H_g)^{1.8} \rho_1 d^{0.9}}{(H_B - h_m)^2} \frac{\lambda^{21}}{E^{3.8}} \end{aligned} \quad (34)$$

Equation (34) can be expressed in decibels as:

$$PL_{total} = 89.5 - 10 \log \left[\frac{\rho_1 d^{0.9}}{(H_B - h_m)^2} \right] + 21 \log f_m - 18 \log (h_T - H_B) + 38 \log R_k \quad (35)$$

Where

$$\rho_1 = \sqrt{\left(\frac{d}{2}\right)^2 + (H_B - h_m)^2} \tag{36}$$

and

f_m : Frequency in MHz.

h_T : Antenna Height in meters.

H_b : Building height in meters.

h_m : Mobile height in meters.

d : Space between buildings in meters.

R : Distance between base station transmitter and mobile station in meters.

Given in table 5 and 6 are the definition of the basic parameters/ specification of the CDMA networks of the two operators in the chosen area of study.

V. RESULTS AND DISCUSSION

In figure 3-5, the measurement pathloss data is examined with the existing models based on the separation distance between the mobile and base station, for comparison.

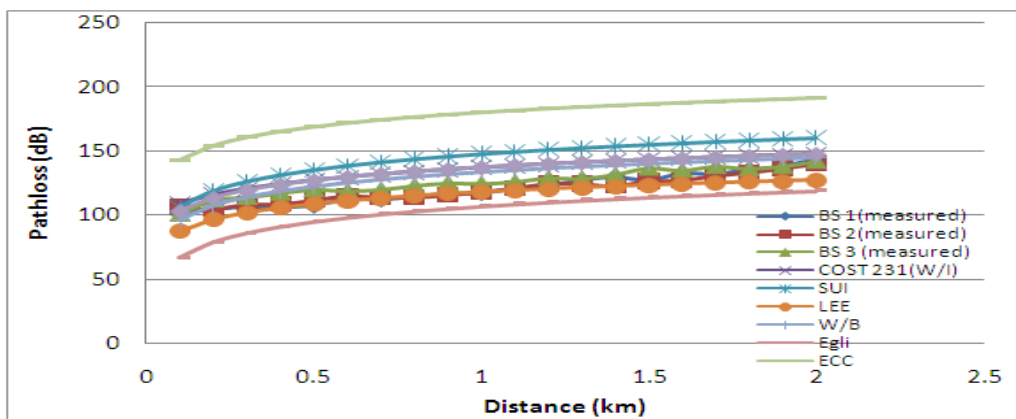


Figure 3: Comparative pathloss model for operator A, location 1

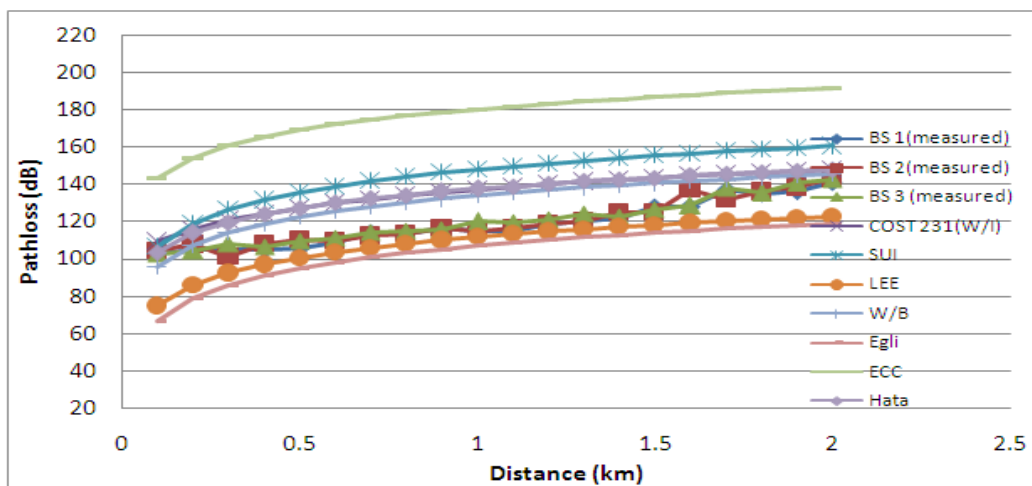


Figure 4: Comparative pathloss model for operator A, location 2

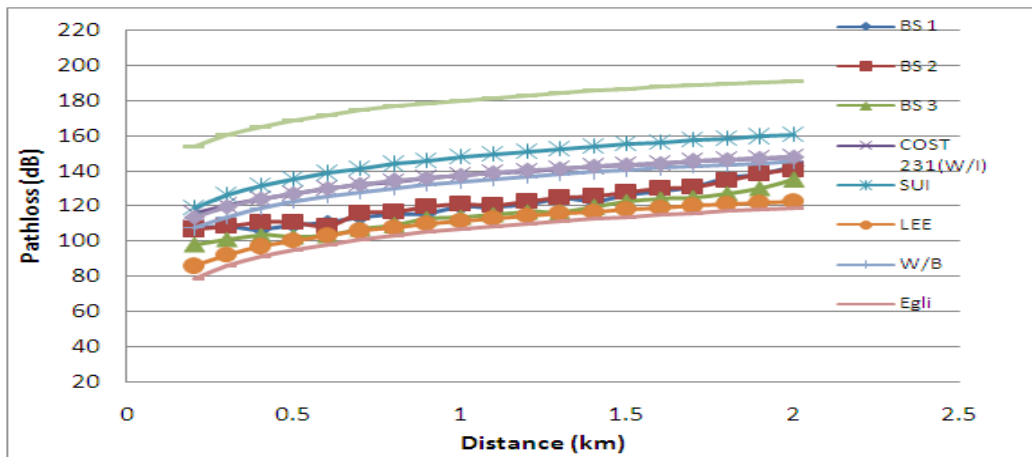


Figure 5 : Comparative pathloss model for operator A, location 3

As can be clearly observed from the above plots, the measured path loss is over predicted by W/B, Hata, ECC, SUI, and COST-231(W/I) models and under predicted by Lee and Egli model. Such performances can be ascribed to the differences in city structures and local terrain profiles.

For instance, the LEE pathloss model was designed based empirical data chosen from a flat terrain. Large errors arise when the model is applied to a non flat terrain. Also, Hata model, which is based on extensive empirical measurements taken by OKumura in city of Tokyo, Japan does not account for clutter factors [2]. In general, such outsized differences between the measured and predicted values can be explained by the fact the expression for pathloss calculation by the existing models were designed in an environment where the definition for urban, suburban and rural areas is not the same in Nigeria. Also, choosing the appropriate propagation model for application depends on system and terrain parameters. Thus, the accuracy of pathloss models suffers when they are used in an environment other than for which they have been developed. Therefore, performing in-field measurements in the environment of interest, and applying necessary corrections to the existing models, or developing a new model from the site-specific measured data is the only solution.

THE MODEL’S GOODNESS OF FIT STATISTICS

In order to examine the goodness of logarithmic fit of existing pathloss model to field data, root mean squared error (RMSE) and relative error (RE) have been calculated. These two statistical parameters are defined as:

Rmse: This statistic gives a quantitative measure on how close (on the average) are the predicted pathloss values, which are estimated using the existing models, to the measured pathloss values. RMSE value closer to 0 indicates a better fit.

Re: This statistic measures the largest error in predictions

Mathematically, the following equations define RMSE and RE:

$$RMSE = \sqrt{\frac{\sum(P_m - P_r)^2}{N}} \tag{37}$$

$$RE = \frac{\sum(P_m - P_r)}{P_m} \times 100 \tag{38}$$

where,

- P_m = measured Pathloss (dB)
- P_r = Predicted Pathloss (dB)
- N = Number of measured data points
- \bar{y} = Mean of measured pathloss (dB)

The deduced errors are summarized in figure 6-8.

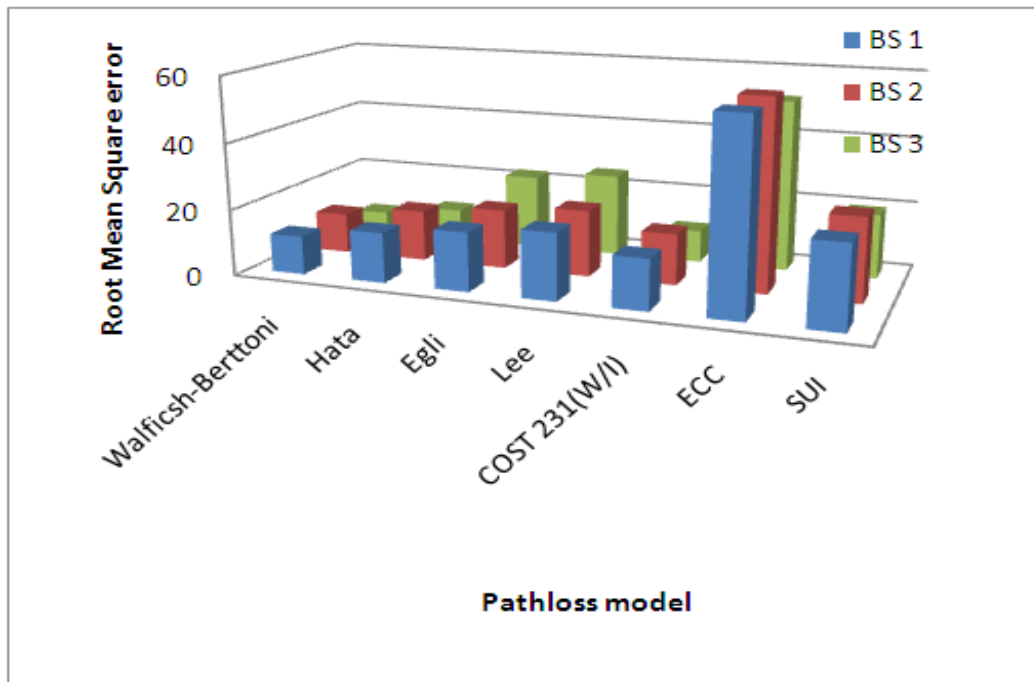


Table 6: The relative errors of the measurement path loss to the path loss of the existing path loss models for operator A, location 1

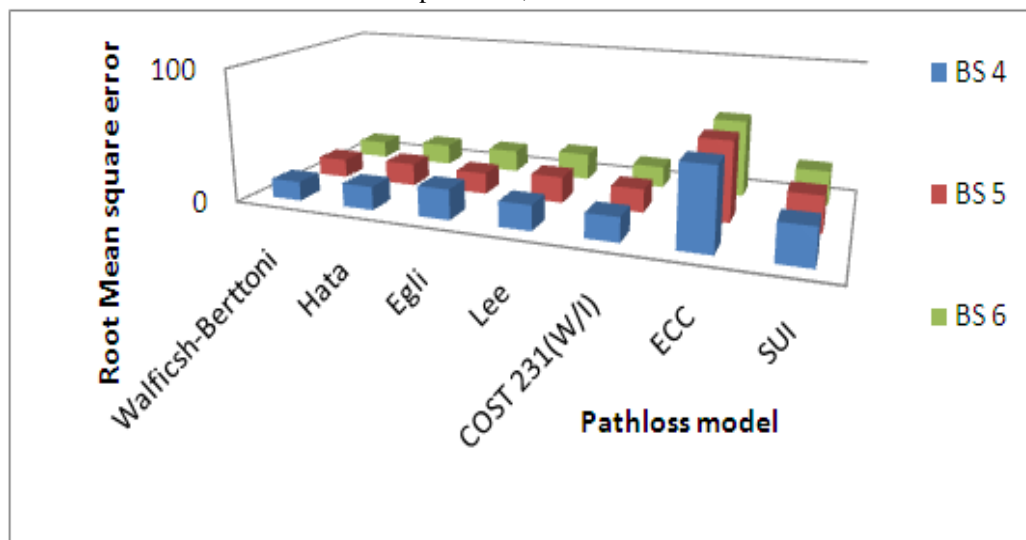


Table 7): The relative errors of the measurement path loss to the path loss of the existing path loss models for operator A, location 2

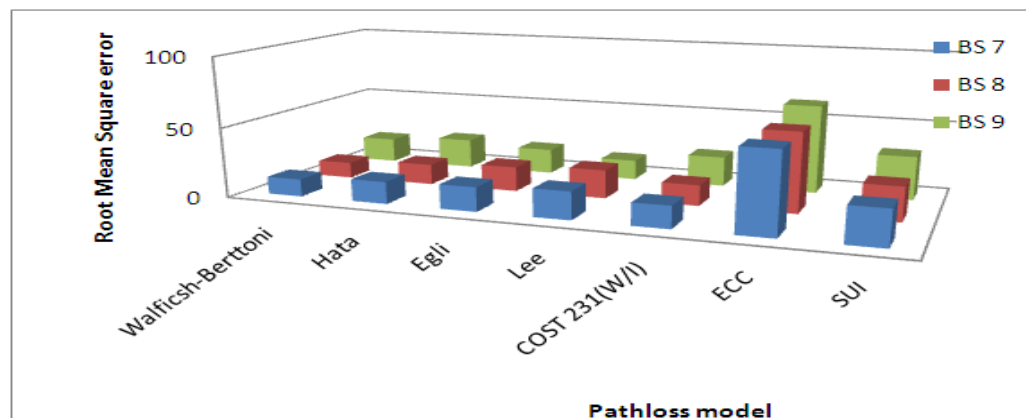


Table 8: The relative errors of the measurement path loss to the path loss of the existing path loss models for operator A, location 3

From the plots in figure 6-8, the measurement data are more close to the Walficsh-Bertoni (W/B) model with RMSE and RE of 6.5279- 17.6577 and 5.4965-15.4049 and more far from ECC model with RMSE and RE of 43.67169-63.26773 and 35.79981-54.20873 respectively. Based on closest agreement to field data, the W/B model is selected as the best model for signal coverage prediction for the studied environment.

VI. CONCLUSION

This study aims to measure and predict the signal path loss for built-up areas of South-South, Nigeria and to compare with different empirical models. The practical measurements that are collected over different distances from the base stations are used to estimate the path loss. Though propagation models are available to predict the losses, they are not very accurate in determining the coverage area of a system. This is due to the fact that these models have been designed based on measurements elsewhere. Therefore, in-field measurements must support the path loss prediction models for better and accurate results. Firstly, the effects of different parameters, such as distance from base stations have been studied and it is observed that path loss increases with distance due to a corresponding decrease in field strength. Secondly, observations show that the W/B gives better agreement for all the studied three cities; hence, it can be used to model any region in South-South Nigeria. Based on the obtained results, a proposal for future works can consider an adjustment of W/B Model by changing some parameters or adding a term which is related to some new environment feature.

REFERENCES

- [1]. Kwakkernaat, M. R. J. A. E. and M. H. A. J. (2011) Herben, Diagnostic analysis of radio propagation in UMTS networks using high resolution angle-of-arrival measurements," IEEE Antennas and Propagation Magazine, 53: 1, pp 66-75.
- [2]. Mukubwa, W.E. (2006). "Statistical Per Cell Model Tuning Approaches for Cellular Networks Multiple Access (CDMA) System in Malaysia".[.http://liserv5.tut.ac.za:7780/pls/eres/wpgg](http://liserv5.tut.ac.za:7780/pls/eres/wpgg)., 2006
- [3]. Narasimhan, R (1999) "Estimation of Mobile Speed and Average Received Power with Application to corner Detection and Handoff", Ph.D. dissertation, Stanford University.
- [4]. William M. S, (2004) Urban Propagation Modeling for Wireless systems, Ph.D Thesis, department of electrical Engineering, Stanford University.
- [5]. Okumura, Y., Ohmori, E., Kawano, T., and Fukada, K (1968). "Field Strength and its Variability in VHF and UHF Land-Mobile Radio Service", Review of the Electrical Communication Laboratory, 16, p 9-10.
- [6]. Hata, M "Empirical formula for propagation loss in land mobile radio services", IEEE Transactions Vehicular. Technology, 29: 3; pp 317– 325.
- [7]. Lempiainen, J., and Manninen, M (2003). UMTS Radio Network Planning, Optimization and QoS Management. Dordrecht: Kluwer Academic Publishers, Dordrecht, Netherlands
- [8]. Laiho J, Wacker A, and Novosad T. (2002) Radio Network Planning and Optimisation for UMTS. John Wiley & Song Ltd
- [9]. Erceg, V. and Hari, K. V. S. (1999) Channel models for fixed wireless applications. tech. rep., IEEE 802.16 Broadband Wireless Access Working Group, 1999.
- [10]. Erceg, V. and Greenstein, L. J(1999). "An empirically based path loss model for wireless channels in suburban environments" IEEE Journal on Selected Areas of Communications, 17, pp 1205–1211.
- [11]. Armoogum, V., and Munnee, R (2010). "Path Loss Analysis for 3G Mobile Networks for Urban and Rural Regions of Mauritius". Sixth International Conference on Wireless and mobile communications (ICWMC), pp 164-169
- [12]. http://en.wikipedia.org/wiki/Egri_Model
- [13]. Abhayawardhana, V.S., Wassel, I. J., Crosby, D., Sellers, M. P., and Brown, M.G. (2005) "Comparison of empirical propagation path loss models for fixed wireless access systems". 61th IEEE Technology Conference, Stockholm, pp 73-77
- [14]. Rappaport, T.S (2002) "Wireless Communications Principles and Practice", Second Edition,
- [15]. Prentice Hall, Free Space Propagation Model, pp 107-109.
- [16]. Walfisch, J. and Bertoni, H.L (1998) "Theoretical Model of UHF Propagation in Urban Environments' IEEE Transaction on Antenna and Propagation 36:12, pp 1788-1796.

Invention of the plane geometrical formulae - Part II

Mr. Satish M. Kaple

Asst. Teacher Mahatma Phule High School, Kherda Jalgaon (Jamod) - 443402 Dist- Buldana,
Maharashtra (India)

Abstract: In this paper, I have invented the formulae for finding the area of an Isosceles triangle. My finding is based on pythagoras theorem.

I. INTRODUCTION

A mathematician called Heron invented the formula for finding the area of a triangle, when all the three sides are known. Similarly, when the base and the height are given, then we can find out the area of a triangle. When one angle of a triangle is a right angle, then we can also find out the area of a right angled triangle. Hence forth, We can find out the area of an equilateral triangle by using the formula of an equilateral triangle. These some formulae for finding the areas of a triangles are not exist only but including in educational curriculum also.

But, In educational curriculum. I don't appeared the formula for finding the area of an isosceles triangle with doing teaching – learning process . Hence, I have invented the new formula for finding the area of an isosceles triangle by using Pythagoras theorem.

I used pythagoras theorem with geometrical figures and algebraic equations for the invention of the new formula of the area of an isosceles triangle. I Proved it by using geometrical formulae & figures, 20 examples and 20 verifications (proofs).

Here myself is giving you the summary of the research of the plane geometrical formulae- Part II

II. METHOD

First taking an isosceles triangle ABC

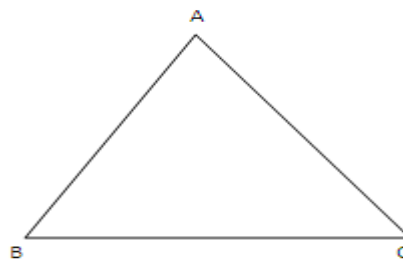


Fig. No. -1

Now taking a, a & b for the lengths of three sides of $\triangle ABC$

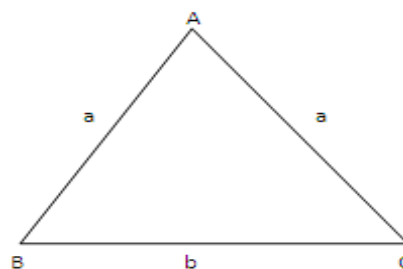


Fig. No. – 2

Draw perpendicular AD on BC.

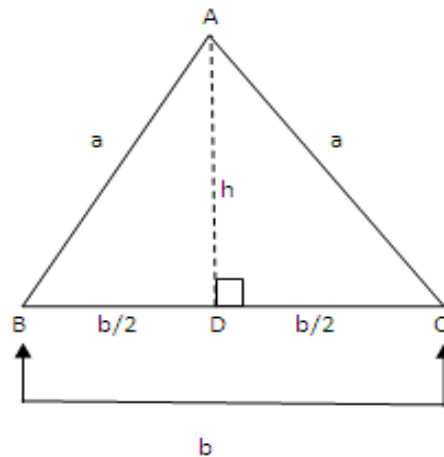


Fig. No. - 3

$\triangle ABC$ is an isosceles triangle and it is an acute angle also.

In $\triangle ABC$,

Let us represent the lengths of the sides of a triangle with the letters a,a,b. Side AB and side AC are congruent side. Third side BC is the base. AD is perpendicular to BC.

Hence, BC is the base and AD is the height.

Here, taking $AB=AC = a$

Base , $BC = b$ Height, $AD = h$

In $\triangle ABC$, two congruent right angled triangle are also formed by the length of perpendicular AD drawn on the side BC from the vertex A. By the length of perpendicular AD drawn on the side BC, Side BC is divided into two equal parts of segment. Therefore, these two equal segments are seg DB and seg DC. Similarly, two a right angled triangles are also formed, namely, $\triangle ADB$ and $\triangle ADC$ which are congruent.

Thus,

$$DB = DC = 1/2 \times BC$$

$$DB = DC = 1/2 \times b = b/2$$

$\triangle ADB$ and $\triangle ADC$ are two congruent right angled triangle.

Taking first right angled $\triangle ADC$,

In $\triangle ADC$, Seg AD and Seg DC are both sides forming the right angle. Seg AC is the hypotenuse.

Here, $AC = a$

Height , $AD = h$

$DC = b/2$ and $m \angle ADC = 90^\circ$

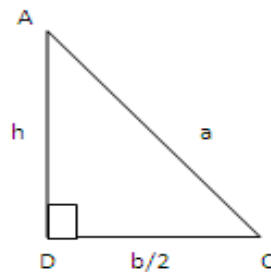


Fig. No - 4

According to Pythagoras Theorem,

$$(\text{hypotenuse})^2 = (\text{one side forming the right angle})^2 + (\text{second side forming the right angle})^2$$

In short,

$$(\text{Hypotenuse})^2 = (\text{one side})^2 + (\text{second side})^2$$

$$AC^2 = AD^2 + DC^2$$

$$AD^2 + DC^2 = AC^2$$

$$h^2 + (b/2)^2 = a^2$$

$$h^2 = a^2 - (b/2)^2$$

$$h^2 = a^2 - \frac{b^2}{4}$$

$$h^2 = \frac{a^2 \times 4}{4} - \frac{b^2}{4}$$

$$h^2 = \frac{4a^2}{4} - \frac{b^2}{4}$$

$$h^2 = \frac{4a^2 - b^2}{4}$$

Taking the square root on both side,

$$\sqrt{h^2} = \sqrt{\frac{4a^2 - b^2}{4}}$$

$$\sqrt{h^2} = \sqrt{\frac{1 \times (4a^2 - b^2)}{4}}$$

$$\sqrt{h^2} = \sqrt{\frac{1}{4}} \times \sqrt{4a^2 - b^2}$$

The square root of h^2 is h and the square root of $\frac{1}{4}$ is $\frac{1}{2}$

$$\therefore h = \frac{1}{2} \times \sqrt{4a^2 - b^2}$$

$$\therefore \text{Height, } h = \frac{1}{2} \sqrt{4a^2 - b^2}$$

$$\therefore AD = h = \frac{1}{2} \sqrt{4a^2 - b^2}$$

Thus,

$$\text{Area of } \triangle ABC = \frac{1}{2} \times \text{Base} \times \text{Height}$$

$$= \frac{1}{2} \times BC \times AD$$

$$= \frac{1}{2} \times b \times h$$

$$\therefore \text{Area of } \triangle ABC = \frac{1}{2} \times b \times \frac{1}{2} \sqrt{4a^2 - b^2}$$

$$\therefore \text{Area of } \triangle ABC = \frac{b \times 1}{2 \times 2} \sqrt{4a^2 - b^2}$$

$$= \frac{b \times 1}{2 \times 2} \times \sqrt{4a^2 - b^2}$$

$$= \frac{b}{4} \sqrt{4a^2 - b^2}$$

$$\therefore \text{Area of an isosceles } \triangle ABC = \frac{b}{4} \sqrt{4a^2 - b^2}$$

For example-

Now consider the following examples:-

Ex. (1) If the sides of an isosceles triangle are 10 cm, 10 cm and 16 cm.

Find it's area

$\triangle DEF$ is an isosceles triangle.

In $\triangle DEF$ given alongside,

l (DE) = 10 cm.

l (DF) = 10 cm.

l (EF) = 16 cm

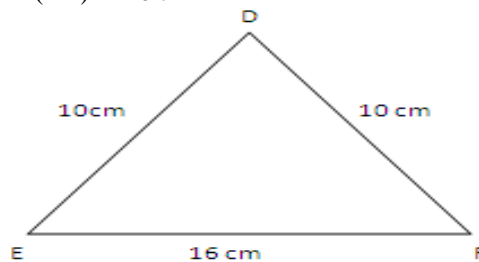


Fig No- 5

Let,

a = 10 cm

Base, b = 16 cm.

By using The New Formula of an isosceles triangle,

\therefore Area of an isosceles $\triangle DEF = A (\triangle DEF)$

$$= \frac{b}{4} \sqrt{4a^2 - b^2}$$

$$= \frac{16}{4} \times \sqrt{4(10)^2 - (16)^2}$$

$$= 4 \times \sqrt{4 \times 100 - 256}$$

$$= 4 \times \sqrt{400 - 256}$$

$$= 4 \times \sqrt{144}$$

The square root of 144 is 12

$= 4 \times 12 = 48 \text{ sq.cm.}$

\therefore Area of an isosceles $\triangle DEF = 48 \text{ sq.cm}$

Verification :-

Here,

$\angle (DE) = a = 10 \text{ cm.}$

$\angle (EF) = b = 16 \text{ cm.}$

$\angle (DF) = c = 10 \text{ cm.}$

By using the formula of Heron's

Perimeter of $\triangle DEF = a + b + c$

$= 10 + 16 + 10 = 36 \text{ cm}$

Semiperimeter of $\triangle DEF,$

$$S = \frac{a + b + c}{2}$$

$$S = \frac{36}{2}$$

$S = 18 \text{ cm.}$

$$\begin{aligned} \therefore \text{Area of an isosceles } \triangle DEF &= \sqrt{s(s-a)(s-b)(s-c)} \\ &= \sqrt{18 \times (18 - 10) \times (18 - 16) \times (18 - 10)} \\ &= \sqrt{18 \times 8 \times 2 \times 8} \\ &= \sqrt{(18 \times 2) \times (8 \times 8)} \\ &= \sqrt{36 \times 64} \\ &= \sqrt{36} \times \sqrt{64} \end{aligned}$$

The square root of 36 is 6 and the square root of 64 is 8

$= 6 \times 8 = 48 \text{ sq.cm}$

\therefore Area of $\triangle DEF = 48 \text{ sq.cm}$

Ex. (2) In $\triangle GHI,$ l (GH) = 5 cm, l (HI) = 6 cm and l (GI) = 5 cm.

Find the area of $\triangle GHI.$

$\triangle GHI$ is an isosceles triangle.

In $\triangle GHI$ given alongside,

$\angle (GH) = 5 \text{ cm.}$

$\angle (HI) = 6 \text{ cm.}$

$\angle (GI) = 5 \text{ cm}$

Let,

$a = 5 \text{ cm}$

Base, $b = 6 \text{ cm}$

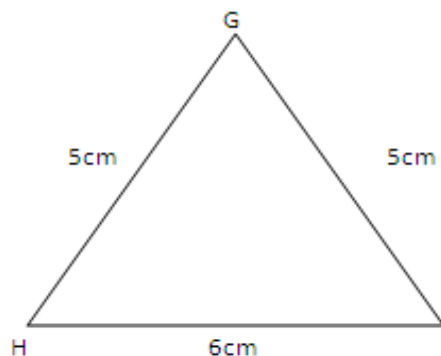


Fig No- 6

By using The New Formula of area of an isosceles triangle,

$$\begin{aligned} \therefore \text{Area of an isosceles } \triangle GHI &= \frac{b}{4} \sqrt{4a^2 - b^2} \\ &= \frac{6}{4} \times \sqrt{4 \times (5)^2 - (6)^2} \end{aligned}$$

The simplest form of $\frac{6}{4}$ is $\frac{3}{2}$

$$\begin{aligned} &= \frac{3}{2} \times \sqrt{(4 \times 25) - 36} \\ &= \frac{3}{2} \times \sqrt{100 - 36} \\ &= \frac{3}{2} \times \sqrt{64} \end{aligned}$$

The square root of 64 is 8

$$\begin{aligned} &= \frac{3 \times 8}{2} = \frac{3 \times 8}{2} = \frac{24}{2} \\ &= 12 \text{ sq.cm.} \end{aligned}$$

\therefore Area of an isosceles $\triangle GHI = 12 \text{ sq.cm.}$

Verification :-

Here,

$$\angle(GH) = a = 5 \text{ cm.}$$

$$\angle(HI) = b = 6 \text{ cm.}$$

$$\angle(GI) = c = 5 \text{ cm.}$$

By using the formula of Heron's

Perimeter of $\triangle GHI = a + b + c$

$$= 5 + 6 + 5$$

$$= 16 \text{ cm}$$

Semiperimeter of $\triangle GHI$,

$$S = \frac{a + b + c}{2}$$

$$S = \frac{16}{2}$$

$$S = 8 \text{ cm.}$$

$$\begin{aligned} \therefore \text{Area of an isosceles } \triangle GHI &= \sqrt{s(s-a)(s-b)(s-c)} \\ &= \sqrt{8 \times (8-5) \times (8-6) \times (8-5)} \\ &= \sqrt{8 \times 3 \times 2 \times 3} \\ &= \sqrt{(8 \times 2) \times (3 \times 3)} \\ &= \sqrt{16 \times 9} \\ &= \sqrt{144} \end{aligned}$$

The square root of 144 is 12

$$= 12 \text{ sq.cm}$$

\therefore Area of an isosceles $\triangle GHI = 12 \text{ sq.cm.}$

III. EXPLANATION

We observe the above solved examples and their verifications, it is seen that the values of solved examples by using the new formula of an isosceles triangle and the values of their verifications are equal.

Hence, The new formula of the area of an isosceles triangle is proved

IV. CONCLUSIONS

$$\text{Area of an isosceles triangle} = \frac{b}{4} \times \sqrt{4a^2 - b^2}$$

REFERENCES

- [1]. Geometry concepts and Pythagoras theorem.

Adsorption of Copper by Ethylenediamine-modified cross-linked magnetic chitosan resin (EMCMCR)

Miss Priwiya Peter, Prof .S. Gopalakrishnan, Dr.T.Kannadasan

M. Tech Scholar, Department of Chemical Engineering, Coimbatore Institute of Technology
Associate Professor, Department of Chemical Engineering, Coimbatore Institute of Technology
Professor and Head, Department of Chemical Engineering, Coimbatore Institute of Technology

Abstract: The adsorption of Copper (II) ions from aqueous solution by ethylenediamine modified cross linked magnetic chitosan resin (EMCMCR) was studied in a batch adsorption system. For 100 ppm, maximum removal of copper (II) was observed at a contact time of 4hours. Copper (II) removal is pH dependant and the maximum removal was observed at pH 6.0 and temperature of 25⁰C for 200 ppm. The adsorption could be well interpreted by Langmuir adsorption model.

Keywords: Adsorption of Copper, Ethylene diamine, Effect of parameters

I. INTRODUCTION

Chitosan (Fig.1) is a modified carbohydrate polymer derived industrially by hydrolyzing the amino acetyl groups of chitin. It is a natural, biodegradable, biocompatible, non-toxic, and anti-bacterial poly-saccharide available in different forms such as solution, powder, flake, fibre and film. Due to its wide range of physical forms, chitosan has broad applications in different fields. Chitosan, a naturally occurring polysaccharide, is a cationic polysaccharide composed of [α 2-amino-2-deoxy- β -D-glucan] (Figure 1) obtained by the alkaline deacetylation of chitin. This chitin is present in shells of insects and marine crustacean such as shrimps and crabs. The unique properties of chitosan including availability, biodegradability, biocompatibility, bioactivity, non-toxicity as well as good adhesion and sorption are the major reasons for its multiple applications. Another main reason for this increasing interest of chitosan is its wide range of physical forms which can be obtained by using an appropriate technological process. Chitosan has already been used in a variety of fields such as wastewater treatment, medicine, agriculture, food, paper industry and cosmetics.

Due to the importance of the physical forms of chitosan in various fields of science and technology, this short review attempts to present the recent studies involved with chitosan as well as its blends in different physical forms. Finally the most important applications of the physical forms of chitosan and its blends in different fields are also depicted.

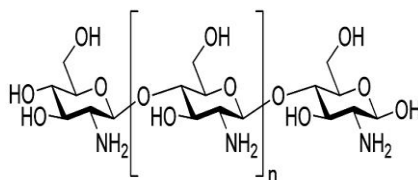


Fig.1. Chitosan-Structure

In the present work, we prepared ethylenediamine-modified glutaraldehyde-crosslinked magnetic chitosan resin (EMCMCR) and used it to adsorb Cu (II) ions in a batch system. The effects of the process parameters such as pH, temperature, dosage of EMCMCR, initial Cu (II) concentration on Cu (II) removal were investigated. In order to better understand the adsorption characteristic, some isotherm models were investigated.

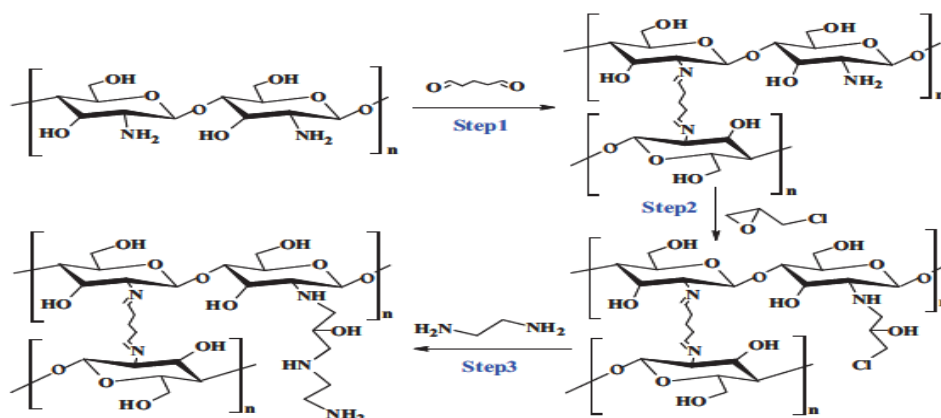


Fig. 2.1 Scheme for the synthesis of EMCMCR: (step1) expected cross-linking mechanism for chitosan using glutaraldehyde; (step2) expected mechanism of action for cross-linked chitosan using Epichlorohydrin; (step3) expected mechanism for aminated chitosan beads.

II. MATERIALS AND METHODS

2.1 Materials

Chitosan, Glutaraldehyde, Epichlorohydrin, Ethylenediamine. All reagents above were of chemical grade. Stock solutions (1000 mg L^{-1}) of Cu(II) was prepared by dissolving 392.682 g in 1000 ml distilled water. Acetic acid, Glutaraldehyde, Epichlorohydrin, Tween 80, Ethylenediamine, Aloe-vera extract powder, Hydrochloric acid, Sodium hydroxide pellets.

2.2. Preparation of EMCMCR

2.2.1 Preparation of Magnetic fluid

Magnetic fluid was prepared at a temperature of 45°C , a mixture of FeCl_3 (15 ml, 0.6 mol.L^{-1}) and FeSO_4 (15 ml, 0.4 mol.L^{-1}) was stirred in a beaker. Sodium hydroxide was added into the mixture quickly to keep the pH value 10.0. After stirring for 10 minutes the temperature rises to 55°C by setting the mixture in a water bath, thereafter surfactant (Tween 80) is added to modify the surface of $\text{Fe}_3 \text{O}_4$ and kept for 30 minutes and then the pH was adjusted to 7.0.

EMCMCR was prepared by dissolving chitosan in acetic acid solution with stirring until completely dissolved at 50°C and then the magnetic fluid was added to the solution slowly. Glutaraldehyde and ethylenediamine were used to form the gel. Meanwhile, ethylenediamine was introduced into the mixture to modify the resin of EMCMCR. Fig. 3 shows the photos of the chitosan and EMCMCR.

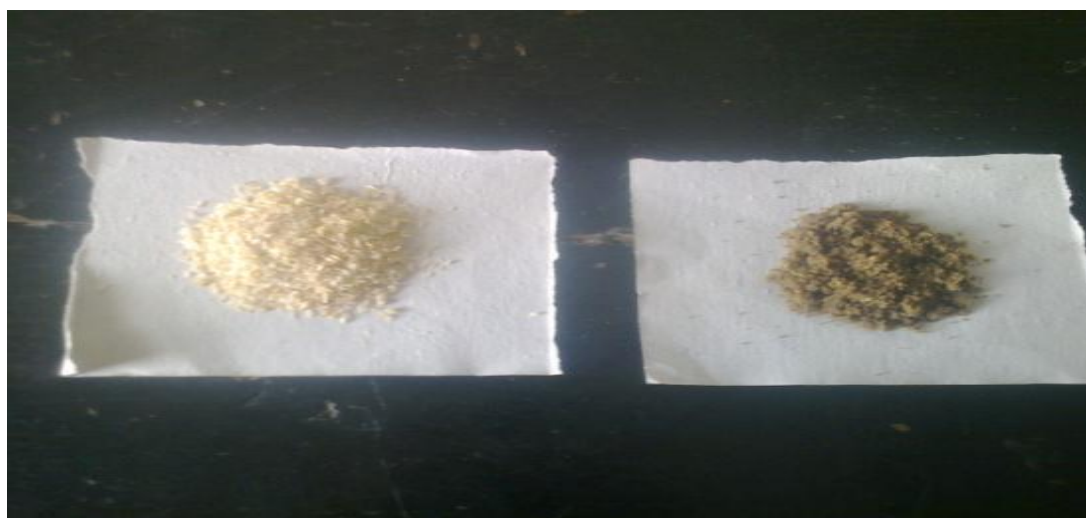


Fig.2.2. Photos of Chitosan and EMCMCR

2.3. Batch adsorption experiments

All batch experiments were carried out with adsorbent samples in a 250 mL beaker with 100 ppm Cu (II) aqueous solutions on a mechanical stirrer at slow speed. The 100 ppm solution was contacted i.e; stirred for various hours (1 hr,2 hr,3 hr,4 hr,5 hr,6 hr etc.) The concentration of Cu (II) ions was determined spectrophotometrically at 820 nm .At the end of 4 hrs there was maximum adsorption (i.e: 100%) .

The study of the pH (1.0–8.0) dependency of Cu (II) adsorption onto EMCMCR was carried out in Cu (II) solutions with different initial concentration of 100, 200 and 300 mg L⁻¹ at a temperature (25^o C).Since at 100ppm we got 100% for 4 hrs of stirring, we use 200 ppm Cu(II) solution with varying pH(1.0-10.0) The pH value was adjusted by 1 M NaOH or 1 M HCl.

Isotherm studies were conducted by contacting 1 g EMCMCR with 100 mL of Cu (II) solution at different initial concentration (100, 200, and 300 mg L⁻¹) stirring for 240 min. The experiments were performed at different temperature (25, 35 and 45 and 55 ° C). Adsorption isotherms are plots of the equilibrium adsorption capacity (q_e) (according to Eq. (1)) versus the equilibrium concentration of the residual Cu (II) in the solution (C_e).

$$q_e = \frac{(C_0 - C_e)V}{W} \tag{1}$$

Where q_e is the equilibrium adsorption capacity (mg g⁻¹), C₀ and C_e are the initial and equilibrium liquid phase solute concentration (mg L⁻¹), respectively. V is the liquid phase volume (L) and W (or m) is the amount of adsorbent (g).

Table 1

Sl.No	Isotherm	Nonlinear form	Linear form	Plot	Reference
1	Langmuir	$q_e = Q_0 b C_e / (1 + b C_e)$	$C_e/q_e = 1/b Q_0 + C_e/Q_0$ $1/q_e = 1/Q_0 + 1/b Q_0 C_e$ $q_e = Q_0 - q_e/b C_e$ $q_e/C_e = b Q_0 - b q_e$	C_e/q_e vs C_e $1/q_e$ vs $1/C_e$ q_e vs $q_e/b C_e$ q_e/C_e vs q_e	[11]
2	Freundlich	$q_e = K_F C_e^{1/n}$	$\log q_e = \log K_F + 1/n \log C_e$	$\log q_e$ vs $\log C_e$	[12]
3	Tempkin	$q_e = RT/b_T \ln A_T C_e$	$q_e = RT/b_T \ln A_T + (RT/b_T) \ln C_e$	q_e vs $\ln C_e$	[13]

Lists of adsorption isotherms models

III. RESULTS AND DISCUSSION

3.1.1 Effect of Contact time on Cu (II) adsorption by EMCMCR (for 100 ppm)

Initial Concentration: 100 ppm (39.268 mg/l), Dosage m : 1 gm, Temperature:25 °C
pH: 4.85

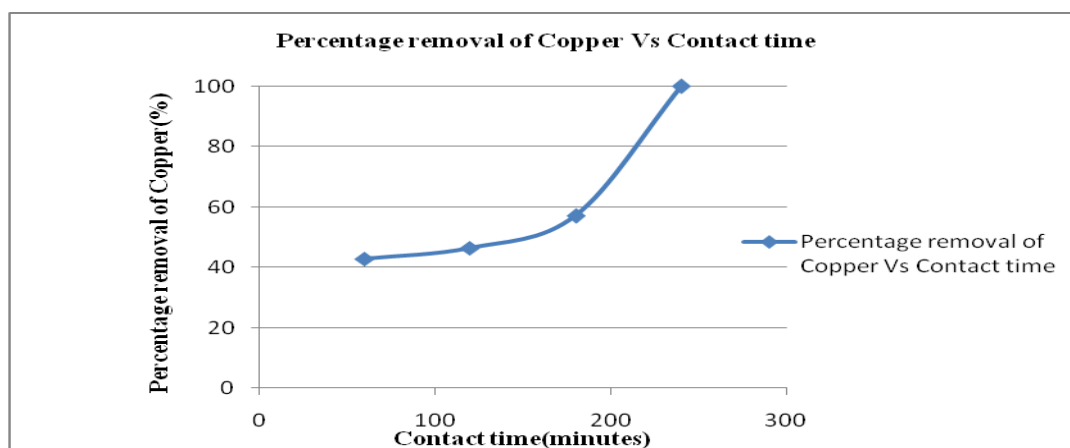


Fig 3.1 Graph of Percentage of removal of Copper vs Contact Time(For 100 ppm)

Percentage removal of copper increases with increase in contact time .The maximum removal resulted in 100% for 100 ppm for stirring it for 4 hours at temperature 25⁰C. The pH was 4.85

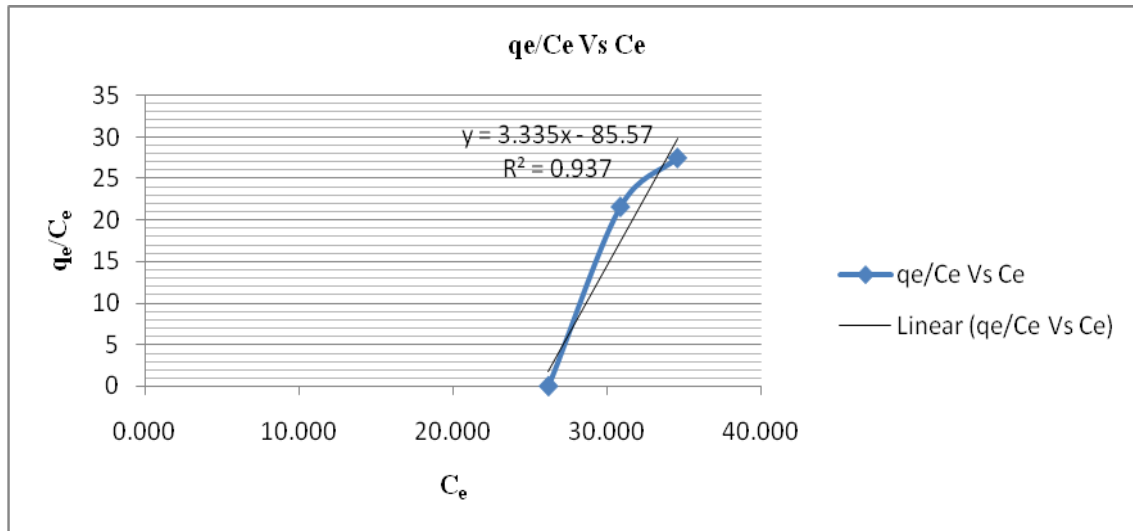


Fig 3.2 Graph of q_e/C_e vs C_e (For 100 ppm)

From the above graph with R-square(R²).Langmuir adsorption isotherm have R² =0.937.Since Langmuir adsorption is having highest R² value and close to 1.This parameter follows Langmuir adsorption isotherm .The R-square values of the linear regression performed were used to determine whether the isotherm was a good fit for the given experimental adsorption data. The R-square value close to 1 indicates a good fit by the model for the given experimental data whereas R-square value near 0 indicates that the model is not a good fit for the given experimental data.

3.1.2 For 200 ppm

Initial Concentration: 200 ppm (78.536 mg/l), Dosage m : 1 gm, Temperature:25 ⁰C
pH :4.85

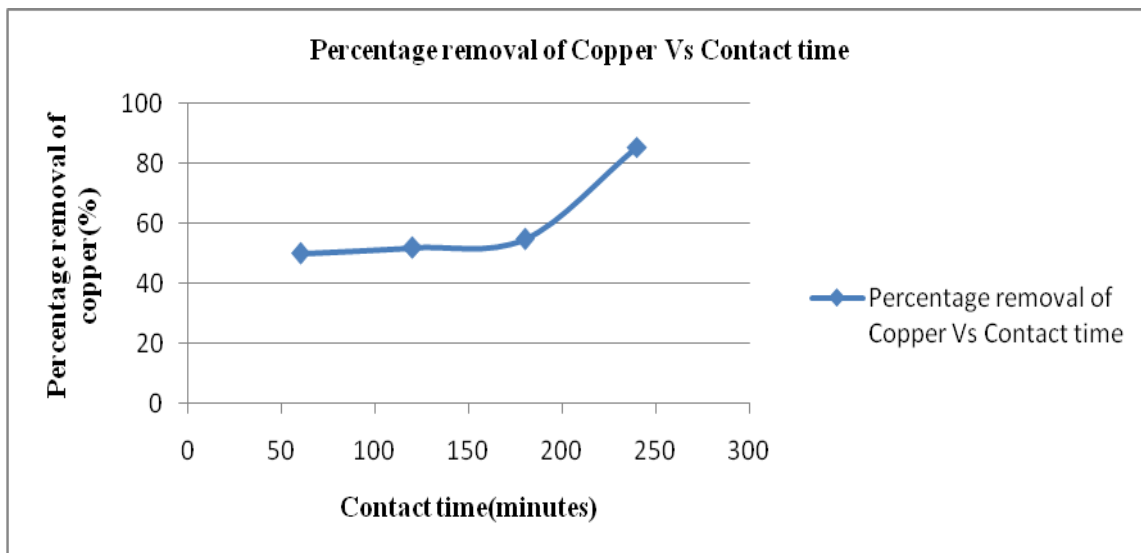


Fig 3.3 Graph of Percentage of removal of Copper vs Contact Time(For 200 ppm)

Percentage removal of copper increases with increase in contact time .The maximum removal resulted in 85.29% for 200 ppm by keeping 4hours as constant temperature 25⁰C .The pH was 4.85

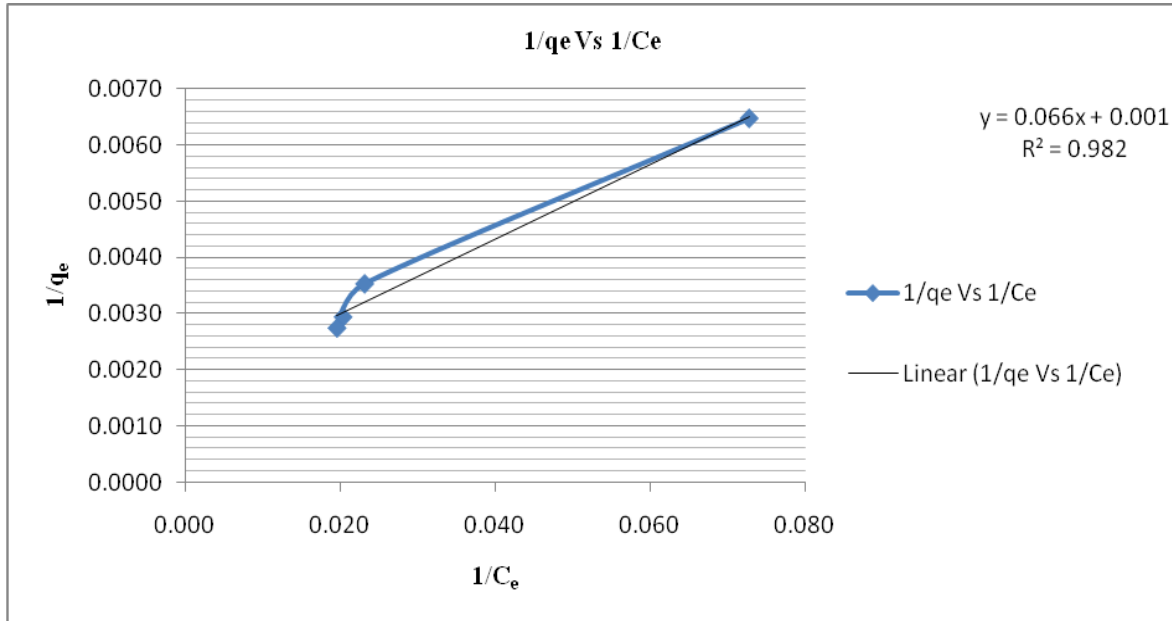


Fig 3.4 Graph of 1/q_e vs 1/C_e(For 200ppm)

For 200 ppm it follows Langmuir Adsorption model since it has highest R² value and is equal to 0.982

3.1.3 For 300 ppm

Initial Concentration: 300 ppm(117.8 mg/l), Dosage m : 1 gm, Temperature:25 °C,pH : 4.85

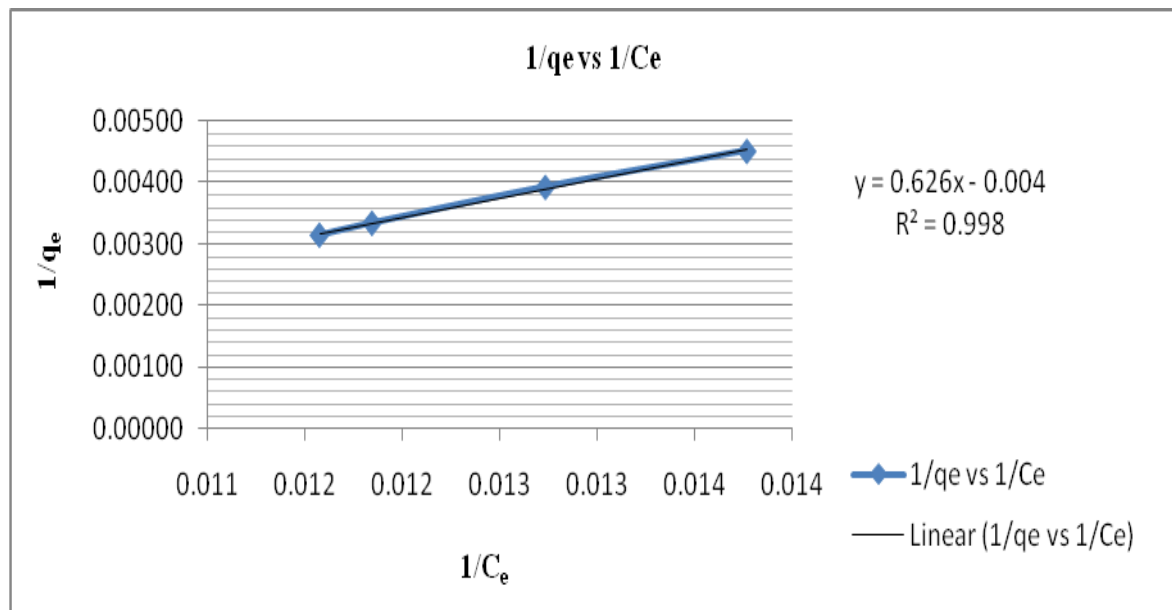


Fig 3.5 Graph of 1/q_e vs 1/C_e(For 300ppm)

Percentage removal of copper increases with increase in contact time .The maximum removal of copper resulted in 36.29% for 300 ppm by keeping 4hours as constant at temperature 25°C.For 300ppm too it follows Langmuir adsorption Isotherm with R² =0.998

3.2 For 200ppm
pH Variation

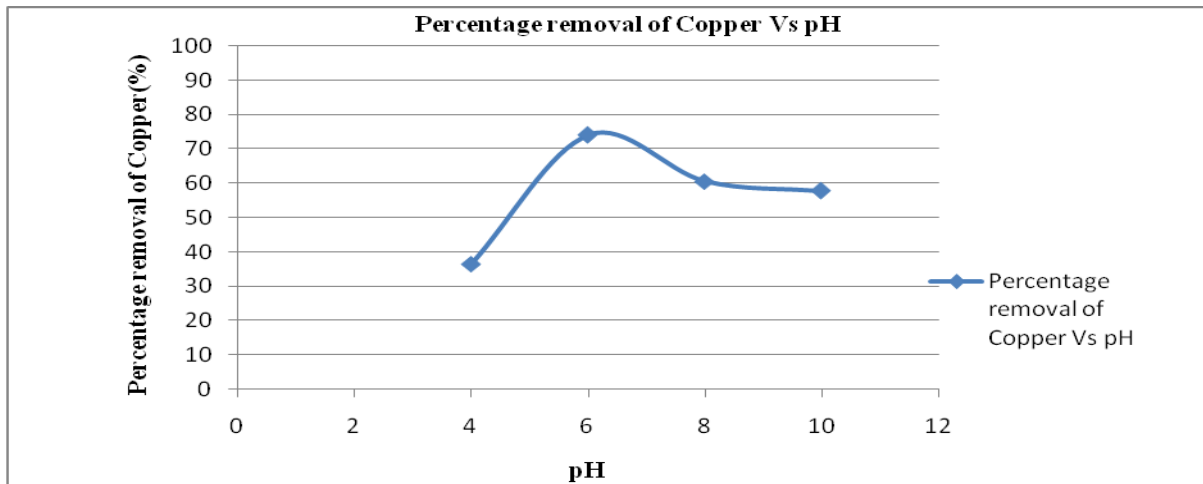


Fig 3.7 Graph of Percentage of removal of Copper vs pH (For 200 ppm)

Maximum percentage of copper removal is attained at pH 6 at concentration 200 ppm and temperature 25°C. The percentage removal resulted in 74.038 %

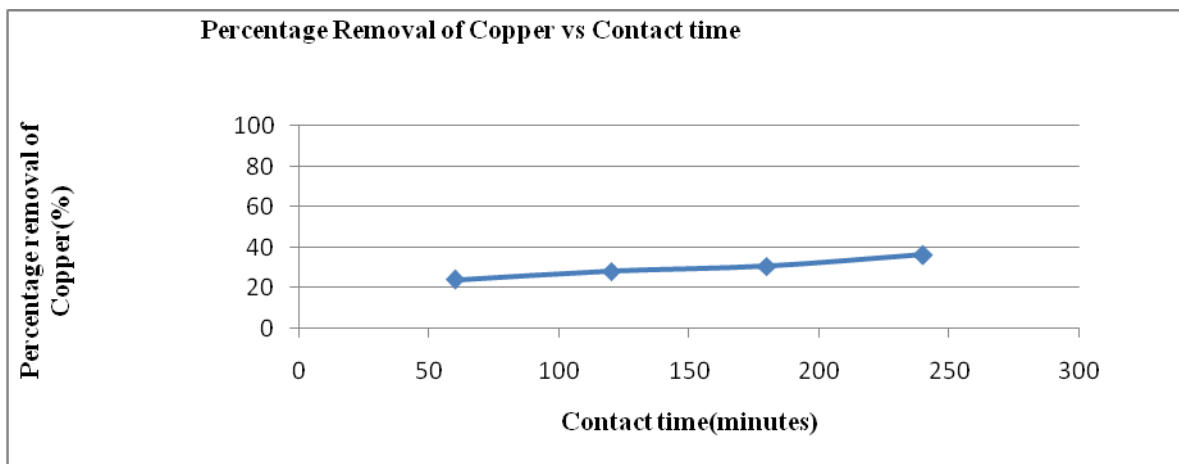


Fig 3.6 Graph of Percentage of removal of Copper vs Contact Time (For 300 ppm)

3.3 Temperature Variation

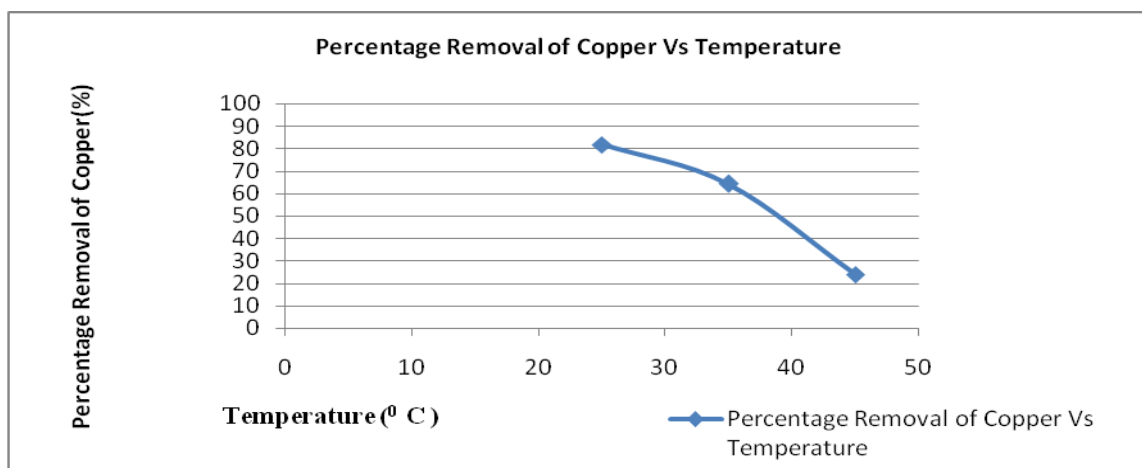


Fig 3.8 Graph of Percentage of removal of Copper vs Temperature (For 200 ppm)

As the temperature increases percentage removal of copper reduces. Maximum percentage removal is attained at 25°C and pH 4.85. The percentage removal of copper resulted in 81.73% at an initial concentration 200 ppm.

3.4 Concentration variation

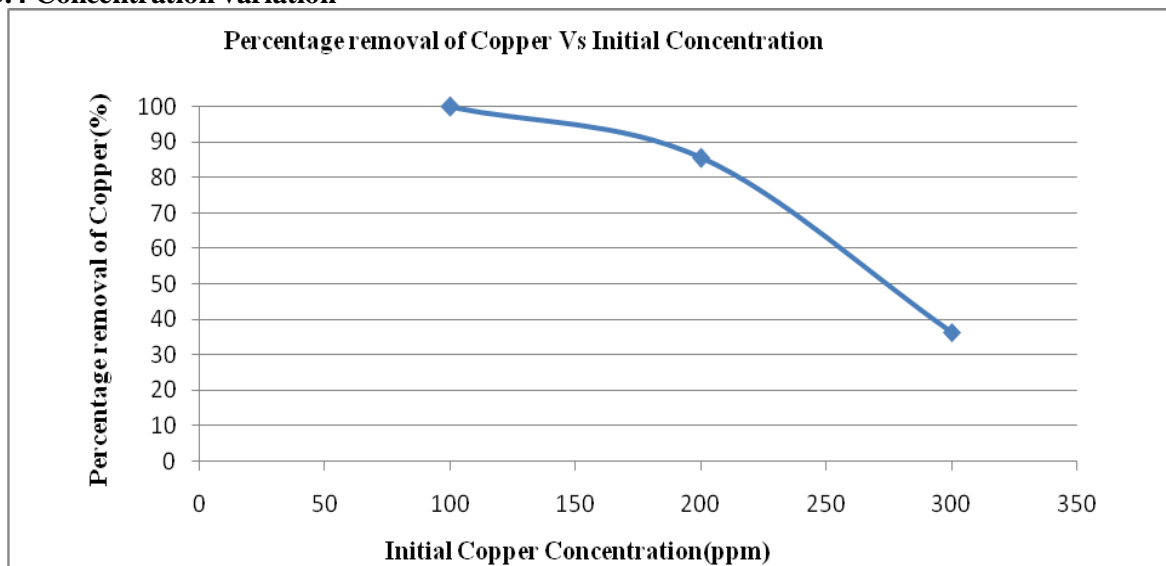


Fig 3.9 Graph of Percentage of removal of Copper vs Initial Concentration

Percentage removal of copper is maximum for 100ppm for four hours of stirring time(contact time).It resulted in 100% removal of copper. Now keeping 4 hours of contact time as constant, percentage removal of copper reduces to 85.29% for 200 ppm .For 300ppm it reduced to 36.29 % for 4 hours of contact time

3.5 Maximum Equilibrium Isotherm

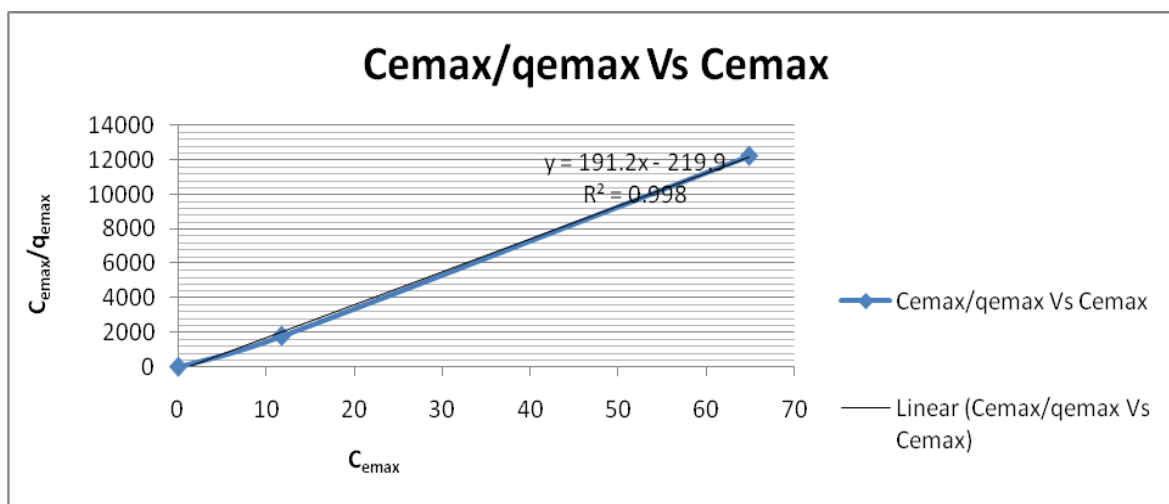


Fig 3.10 Graph of C_{emax}/q_{emax} vs C_{emax}

Since the mean square value R^2 has value and is equal to 0.998 and is very close to 1 it best fits Langmuir adsorption isotherm .Hence the plot C_{emax}/q_{emax} Vs C_{emax} follows a linear curve and have maximum mean square value equal to 1.Hence our study of batch adsorption of copper by ethylene-di-amine modified cross-linked chitosan resin is best described by Langmuir Adsorption Isotherm.

The below given graph shows decrease in percentage of copper removal with respect to increase in concentration (ppm)

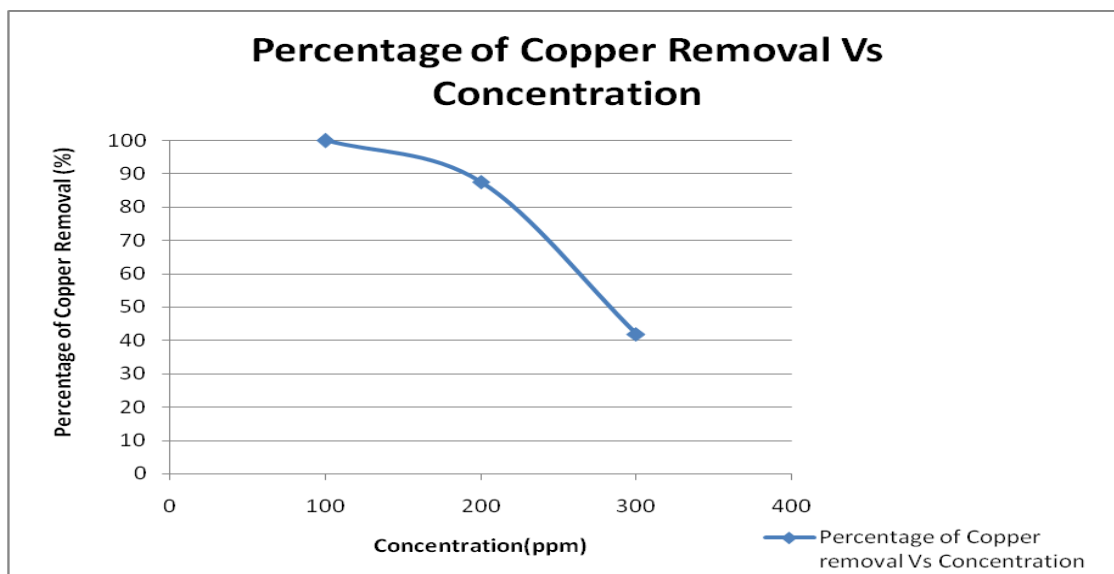


Fig 3.11 Graph of Percentage of removal of Copper vs Initial Concentration for maximum equilibrium adsorption

IV. CONCLUSION

Ethylenediamine modified crosslinked magnetic (EMCMCR) chitosan resins were prepared. From the above results it is obvious that adsorption efficiency was dependent on various factors or operating conditions such as pH, contact time, initial concentration, temperature and dosage of the adsorbent.

The optimum concentration and pH for maximum removal of Cu (II) ions was found to 100ppm and pH 6 for EMCMCR. Increase of adsorbent dose prominently increased the adsorption due to an increase in the surface area. With the increase in temperature adsorption efficiency gradually decreased and was found to have maximum percentage of removal of Cu (II) at 25°C.

The equilibrium data were analyzed by Langmuir, Freundlich and Tempkin isotherm models. The Langmuir adsorption isotherm provided the best fit by giving maximum R^2 value i.e; 0.998 suggesting a monolayer adsorption on a homogenous surface.

The obtained results showed the prepared EMCMCR proves its high efficiency in removing the copper (II) ions from aqueous solution. On the economical front application of EMCMCR for heavy metal removal could be tested in industrial environments.

REFERENCES

- [1] Basha .S, Murthy Z.V.P, Jha.B, Biosorption of hexavalent chromium by chemi-cally modified seaweed, *Cystoseira indica*, *J.Chem. Eng.* 137 (2008) 480–488.
- [2] Karthikeyan.T, Rajgopal.S, Miranda.L.R, Chromium (VI) adsorption from aque-ous solution by Hevea Brasilinesis sawdust activated carbon, *J. Hazard. Mater.* B124 (2005) 192–199.
- [3] Kandile.N.G, Nasr.A.S, Environment friendly modified chitosan hydrogels as a matrix for adsorption of metal ions, synthesis and characterization, *Carbohydr. Polym.* 78 (2009) 753–759.
- [4] Ruiz.M, Sastre.A.M, Guibal.E, Palladium sorption on glutaraldehyde-crosslinked chitosan, *React. Funct. Polym.* 45 (2000) 155–173.
- [5] Ngah.W.S.W, Endud C.S, Mayanar.R, Removal of copper(II) ions from aqueous solution onto chitosan and cross-linking chitosan beads, *React. Funct. Polym.* 20 (2002) 181–190.
- [6] Li.N, Bai.R, Development of chitosan-based granular adsorbents for enhanced and selective adsorption performance in heavy metal removal, *Wat. Sci. Technol.* 54 (2006) 103–113.
- [7] Martinez.L, Agnely.F, Leclerc.B, Siepmann.J, Cotte.M, Deiger.S, Couarraze.S, Cross-linking of chitosan and chitosan poly(ethylene oxide) beads: a theoretical treatment, *Eur. J. Pharm. Biopharm.* 67 (2007) 339–348.
- [8] Ramesh.A, Hasegawa.H, Sugimoto.W, Maki.T, Ueda.K, Adsorption of gold(III), platinum(IV) and palladium(II) onto glycine modified crosslinked chitosan resin, *Bioresour. Technol.* 99 (2008) 3801–3809.
- [9] Rutnakornpituk.M, Ngamdee.P, Phinyocheep.P, Preparation and proper-ties of polydimethylsiloxane-modified chitosan, *Carbohydr. Polym.* 63 (2006) 229–237.
- [10] Zhou.L, Wang.Y, Liu.Z, Huang.Q, Characteristics of equilibrium, kinetics stud-ies for adsorption of Hg(II), Cu(II), and Ni(II) ions by thiourea-modified magnetic chitosan microspheres, *J. Hazard. Mater.* 161 (2009) 995–1002.
- [11] I. Langmuir, The constitution and fundamental properties of solids and liquids, *J. Am. Chem. Soc.* 38 (11) (1916) 2221–2295.
- [12] H.M.F. Freundlich, Over the adsorption in solution, *J. Phys. Chem.* 57 (1906) 385–471.
- [13] M.I. Tempkin, V. Pyzhev, Kinetics of ammonia synthesis on promoted iron catalyst, *Acta Phys. Chim. USSR* 12 (1940) 327–356.

Some Fixed Point and Common Fixed Point Theorems in 2-Banach Spaces

A.S.Saluja, Alkesh Kumar Dhakde

Govt. J.H. P.G. College Betul (M.P.), India

IES College of Technology Bhopal (M.P.), India

Abstract: In the present paper we prove some fixed point and common fixed point theorems in 2-Banach spaces for new rational expression. Which generalize the well known results.

AMS: 47H10, 54H25.

Keywords: Banach Space, 2-Banach Spaces, Fixed point, Common Fixed point.

I. INTRODUCTION

The study of non-contraction mapping concerning the existence of fixed points draws attention of various authors in non-linear analysis. It is well known that the differential and integral equations that arise in physical problems are generally non-linear, therefore the fixed point methods specially Banach's contraction principle provides a powerful tool for obtaining the solutions of these equations which were very difficult to solve by any other methods. Recently Verma [9] described about the application of Banach's contraction principle [2]. Ghalar [5] introduced the concept of 2-Banach spaces. Recently Badshah and Gupta [3], Yadava, Rajput and Bhardwaj [10], Yadava, Rajput, Choudhary and Bhardwaj [11] also worked for Banach and 2-Banach spaces for non contraction mappings. In present paper we prove some fixed point and common fixed point theorems for non-contraction mappings, in 2-Banach spaces motivated by above, before starting the main result first we write some definitions.

Definition (1.2A), 2-Banach Spaces:

In a paper Gähler [5] define a linear 2-normed space to be pair $(L, \|\cdot, \cdot\|)$ where L is a linear space and $\|\cdot, \cdot\|$ is non negative, real valued function defined on L such that $a, b, c \in L$

(i) $\|a, b\| = 0$ if and only if a and b are linearly dependent

(ii) $\|a, b\| = \|b, a\|$

(iii) $\|a, \beta b\| = |\beta| \|a, b\|$, β is real

(iv) $\|a, b+c\| \leq \|a, b\| + \|a, c\|$

Hence $\|\cdot, \cdot\|$ is called a 2-norm.

Definition (1.2B):

A sequence $\{x_n\}$ in a linear 2-normed space L , is called a convergent sequence if there is, $x \in L$, such that

$$\lim_{n \rightarrow \infty} \|x_n - x, y\| = 0 \text{ for all } y \in L.$$

Definition (1.2C):

A sequence $\{x_n\}$ in a linear 2-normed space L , is called a Cauchy sequence if there exists $y, z \in L$, such that y and z are linearly independent and

$$\lim_{m,n \rightarrow \infty} \|x_m - x_n, y\| = 0$$

Definition (1.2D):

A linear 2-normed space in which every Cauchy sequence is convergent is called 2-Banach spaces.

II. MAIN RESULTS

Theorem 1.1:

Let T be a mapping of a 2-Banach spaces into itself. If T satisfies the following conditions:

$$T^2 = I, \text{ where } I \text{ is identity mapping} \tag{1.1}$$

$$\|Tx - Ty, a\| \geq \alpha \frac{\|x - Tx, a\| \|y - Ty, a\|}{\|x - y, a\|} + \beta \frac{\|y - Ty, a\| \|y - Tx, a\| \|x - Ty, a\| + \|x - y, a\|^3}{\|x - y, a\|^2} \tag{1.2}$$

$$+ \gamma \left[\frac{\|x - Tx, a\| + \|y - Ty, a\|}{2} \right] + \delta \left[\frac{\|x - Ty, a\| + \|y - Tx, a\|}{2} \right] + \eta \|x - y, a\|$$

Where $x \neq y, a > 0$ is real with $8\alpha + 10\beta + 4\gamma + 2\delta + 3\eta > 4$. Then T has unique fixed point.

Proof: Suppose x is any point in 2-Banach space X .

$$\text{Taking } y = \frac{1}{2}(T + I)x, \quad z = T(y)$$

$$\|z - x, a\| = \|Ty - T^2x, a\| = \|Ty - T(Tx), a\|$$

$$\geq \alpha \frac{\|y - Ty, a\| \|Tx - T(Tx), a\|}{\|y - Tx, a\|} + \beta \frac{\|Tx - T(Tx), a\| \|Tx - Ty, a\| \|y - T(Tx), a\| + \|y - Tx, a\|^3}{\|y - Tx, a\|^2}$$

$$+ \gamma \left[\frac{\|y - Ty, a\| + \|Tx - T(Tx), a\|}{2} \right] + \delta \left[\frac{\|y - T(Tx), a\| + \|Tx - Ty, a\|}{2} \right] + \eta \|y - Tx, a\|$$

$$\geq \alpha \frac{\|y - Ty, a\| \|Tx - x, a\|}{\frac{1}{2}\|x - Tx, a\|} + \beta \frac{\|Tx - x, a\| [\|Tx - y, a\| + \|y - Ty, a\|] \|y - x, a\| + \|y - Tx, a\|^3}{\frac{1}{4}\|x - Tx, a\|^2}$$

$$+ \gamma \left[\frac{\|y - Ty, a\| + \|Tx - x, a\|}{2} \right] + \delta \left[\frac{\|y - x, a\| + \|Tx - y, a\| + \|y - Ty, a\|}{2} \right] + \eta \|y - Tx, a\|$$

$$\geq 2\alpha \|y - Ty, a\| + \beta \frac{\|Tx - x, a\| \left[\frac{1}{2}\|x - Tx, a\| + \|y - Ty, a\| \right] \frac{1}{2}\|x - Tx, a\| + \frac{1}{8}\|x - Tx, a\|^3}{\frac{1}{4}\|x - Tx, a\|^2}$$

$$+ \gamma \left[\frac{\|y - Ty, a\| + \|Tx - x, a\|}{2} \right] + \delta \left[\frac{\frac{1}{2}\|x - Tx, a\| + \frac{1}{2}\|x - Tx, a\| + \|y - Ty, a\|}{2} \right] + \frac{\eta}{2} \|x - Tx, a\|$$

$$\geq 2\alpha \|y - Ty, a\| + \frac{\beta}{2} \left\{ 4 \left[\frac{1}{2}\|x - Tx, a\| + \|y - Ty, a\| \right] + \frac{\|x - Tx, a\|^3}{\|x - Tx, a\|^2} \right\}$$

$$+ \gamma \left[\frac{\|y - Ty, a\| + \|Tx - x, a\|}{2} \right] + \delta \left[\frac{\|x - Tx, a\| + \|y - Ty, a\|}{2} \right] + \frac{\eta}{2} \|x - Tx, a\|$$

$$\begin{aligned}
 &\geq 2\alpha\|y - Ty, a\| + \frac{\beta}{2}[2\|x - Tx, a\| + 4\|y - Ty, a\| + \|x - Tx, a\|] \\
 &+ \frac{\gamma}{2}[\|y - Ty, a\| + \|Tx - x, a\|] + \frac{\delta}{2}[\|x - Tx, a\| + \|y - Ty, a\|] + \frac{\eta}{2}\|x - Tx, a\| \\
 &\geq \|x - Tx, a\|\left(\frac{3\beta}{2} + \frac{\gamma}{2} + \frac{\delta}{2} + \frac{\eta}{2}\right) + \left(2\alpha + 2\beta + \frac{\gamma}{2} + \frac{\delta}{2}\right)\|y - Ty, a\| \\
 &\geq \frac{1}{2}\|x - Tx, a\|(3\beta + \gamma + \delta + \eta) + \frac{1}{2}\|y - Ty, a\|(4\alpha + 4\beta + \gamma + \delta)
 \end{aligned}$$

Now for

$$\begin{aligned}
 \|u - x, a\| &= \|2y - z - x, a\| = \|Tx - Ty, a\| \\
 &\geq \alpha \frac{\|x - Tx, a\|\|y - Ty, a\|}{\|x - y, a\|} + \beta \frac{\|y - Ty, a\|\|y - Tx, a\|\|x - Ty, a\| + \|x - y, a\|^3}{\|x - y, a\|^2} \\
 &+ \gamma \left[\frac{\|x - Tx, a\| + \|y - Ty, a\|}{2} \right] + \delta \left[\frac{\|x - Ty, a\| + \|y - Tx, a\|}{2} \right] + \eta\|x - y, a\| \\
 &\geq \alpha \frac{\|x - Tx, a\|\|y - Ty, a\|}{\frac{1}{2}\|x - Tx, a\|} + \beta \frac{\|y - Ty, a\|\frac{1}{2}\|x - Tx, a\|\left[\frac{1}{2}\|x - Tx, a\|\right] + \frac{1}{8}\|x - Tx, a\|^3}{\frac{1}{4}\|x - Tx, a\|^2} \\
 &+ \gamma \left[\frac{\|x - Tx, a\| + \|y - Ty, a\|}{2} \right] + \delta \left[\frac{\frac{1}{2}\|x - Tx, a\| + \frac{1}{2}\|x - Tx, a\|}{2} \right] + \frac{\eta}{2}\|x - Tx, a\| \\
 &\geq 2\alpha\|y - Ty, a\| + \beta\|y - Ty, a\| + \frac{\beta}{2}\|x - Tx, a\| + \gamma \left[\frac{\|x - Tx, a\| + \|y - Ty, a\|}{2} \right] \\
 &+ \frac{\delta}{2}\|x - Tx, a\| + \frac{\eta}{2}\|x - Tx, a\| \\
 &\geq \|x - Tx, a\|\left(\frac{\beta}{2} + \frac{\gamma}{2} + \frac{\delta}{2} + \frac{\eta}{2}\right) + \|y - Ty, a\|\left(2\alpha + \beta + \frac{\gamma}{2}\right) \\
 &\geq \frac{1}{2}\|x - Tx, a\|(\beta + \gamma + \delta + \eta) + \frac{1}{2}\|y - Ty, a\|(4\alpha + 2\beta + \gamma)
 \end{aligned}$$

Now

$$\begin{aligned}
 \|z - u, a\| &= \|z - x, a\| + \|x - u, a\| \\
 &\geq \frac{1}{2}\|x - Tx, a\|(3\beta + \gamma + \delta + \eta) + \frac{1}{2}\|y - Ty, a\|(4\alpha + 4\beta + \gamma + \delta) + \frac{1}{2}\|x - Tx, a\|(\beta + \gamma + \delta + \eta) \\
 &+ \frac{1}{2}\|y - Ty, a\|(4\alpha + 2\beta + \gamma) \\
 &\geq \frac{1}{2}\|x - Tx, a\|(3\beta + \gamma + \delta + \eta + \beta + \gamma + \delta + \eta) + \frac{1}{2}\|y - Ty, a\|(4\alpha + 4\beta + \gamma + \delta + 4\alpha + 2\beta + \gamma) \\
 &\geq \frac{1}{2}\|x - Tx, a\|(4\beta + 2\gamma + 2\delta + 2\eta) + \frac{1}{2}\|y - Ty, a\|(8\alpha + 6\beta + 2\gamma + \delta)
 \end{aligned}$$

(1.3)

On the other hand

$$\begin{aligned}
\|z - u, a\| &= \|T(y) - (2y - z), a\| \\
&= \|T(y) - 2y + T(y), a\| \\
&= 2\|Ty - y, a\|
\end{aligned} \tag{1.4}$$

$$\text{So } 2\|Ty - y, a\| \geq \frac{1}{2}\|x - Tx, a\|(4\beta + 2\gamma + 2\delta + 2\eta) + \frac{1}{2}\|y - Ty, a\|(8\alpha + 6\beta + 2\gamma + \eta)$$

$$\Rightarrow [4 - (8\alpha + 6\beta + 2\gamma + \eta)]\|y - Ty, a\| \geq (4\beta + 2\gamma + 2\delta + 2\eta)\|x - Tx, a\|$$

$$\Rightarrow \|x - Tx, a\| \leq \frac{4 - (8\alpha + 6\beta + 2\gamma + \eta)}{4\beta + 2\gamma + 2\delta + 2\eta}\|y - Ty, a\|$$

$$\Rightarrow \|x - Tx, a\| \leq k\|y - Ty, a\| \quad \text{as } (8\alpha + 10\beta + 4\gamma + 2\delta + 3\eta > 4)$$

$$\text{Where } k = \frac{4 - (8\alpha + 6\beta + 2\gamma + \eta)}{4\beta + 2\gamma + 2\delta + 2\eta} < 1$$

Let $R = \frac{1}{2}(T + I)$, then

$$\begin{aligned}
\|R^2(x) - R(x), a\| &= \|R(R(x)) - R(x), a\| \\
&= \|R(y) - y, a\| = \frac{1}{2}\|y - Ty, a\| \\
&< \frac{k}{2}\|x - Tx, a\|
\end{aligned}$$

By the definition of R we claim that $\{R^n(x)\}$ is a Cauchy sequence in X , $\{R^n(x)\}$ converges to some element x_0 in X . So $\lim_{n \rightarrow \infty} \{R^n(x)\} = x_0$. So $\{R(x_0)\} = x_0$. Hence $T(x_0) = x_0$

So x_0 is a fixed point of T .

Uniqueness:

If possible let $y_0 \neq x_0$ is another fixed point of T . Then

$$\begin{aligned}
\|x_0 - y_0, a\| &= \|Tx_0 - Ty_0, a\| \\
&\geq \alpha \frac{\|x_0 - Tx_0, a\| \|y_0 - Ty_0, a\|}{\|x_0 - y_0, a\|} + \beta \frac{\|y_0 - Ty_0, a\| \|y_0 - Tx_0, a\| \|x_0 - Ty_0, a\| + \|x_0 - y_0, a\|^3}{\|x_0 - y_0, a\|^2} \\
&+ \gamma \left[\frac{\|x_0 - Tx_0, a\| \|y_0 - Ty_0, a\|}{2} \right] + \delta \left[\frac{\|x_0 - Ty_0, a\| + \|y_0 - Tx_0, a\|}{2} \right] + \eta \|x_0 - y_0, a\| \\
&\geq \beta \|x_0 - y_0, a\| + \delta \|x_0 - y_0, a\| + \eta \|x_0 - y_0, a\| \\
&\geq (\beta + \delta + \eta) \|x_0 - y_0, a\|
\end{aligned}$$

Which is contradiction so $x_0 = y_0$. Hence fixed point is unique.

Theorem 2.1:

Let T and G be two expansion mappings of a 2-Banach space X into itself. T and G satisfy the following conditions:

(2.1) T and G commute

(2.1) $T^2 = I$ and $G^2 = I$, where I is identity mapping.

(2.3)

$$\|Tx - Ty, a\| \geq \alpha \frac{\|Gx - Tx, a\| \|Gy - Ty, a\|}{\|Gx - Gy, a\|} + \beta \frac{\|Gy - Ty, a\| \|Gy - Tx, a\| \|Gx - Ty, a\| + \|Gx - Gy, a\|^3}{\|Gx - Gy, a\|^2}$$

$$+ \gamma \left[\frac{\|Gx - Tx, a\| + \|Gy - Ty, a\|}{2} \right] + \delta \left[\frac{\|Gx, Ty, a\| + \|Gy - Tx, a\|}{2} \right] + \eta \|Gx - Gy, a\|$$

For every $x, y \in X, \alpha, \beta, \gamma, \delta, \eta \in [0, 1]$ with $x \neq y$ and $\|Gx - Gy\| \neq 0$ and $\beta + \delta + \eta > 1$.

Then there exists a unique common fixed of T and G such that $T(x_0) = x_0$ and $G(x_0) = x_0$.

Proof: -

Suppose x is point in 2-Banach space X it is clear that $(TG)^2 = I$

$$\|TG.G(x) - TG.G(y), a\| \geq \alpha \frac{\|G(G^2x) - T(G^2x), a\| \|G(G^2y) - T(G^2y), a\|}{\|G(G^2x) - G(G^2y), a\|}$$

$$+ \beta \frac{\|G(G^2y) - T(G^2y), a\| \|G(G^2y) - T(G^2x), a\| \|G(G^2x) - T(G^2y), a\| + \|G(G^2x) - G(G^2y), a\|^3}{\|G(G^2x) - G(G^2y), a\|^2}$$

$$+ \gamma \left[\frac{\|G(G^2x) - T(G^2x), a\| + \|G(G^2y) - T(G^2y), a\|}{2} \right] + \delta \left[\frac{\|G(G^2x) - T(G^2y), a\| + \|G(G^2y) - T(G^2x), a\|}{2} \right]$$

$$+ \eta \|G(G^2x) - G(G^2y), a\|$$

$$\geq \alpha \frac{\|Gx - TG(Gx), a\| \|Gy - TG(Gy), a\|}{\|Gx - Gy, a\|^2} + \beta \frac{\|Gy - TG(Gy), a\| \|Gy - TG(Gx), a\| \|Gx - TG(Gy), a\| + \|Gx - Gy, a\|^3}{\|Gx - Gy, a\|^2}$$

$$+ \gamma \left[\frac{\|Gx - TG(Gx), a\| + \|Gy - TG(Gy), a\|}{2} \right] + \delta \left[\frac{\|Gx - TG(Gx), a\| + \|G(y) - TG(Gx), a\|}{2} \right]$$

$$+ \eta \|Gx - Gy, a\|$$

Taking $G(x) = p, G(y) = q$, where $p \neq q$

$$\geq \alpha \frac{\|p - TG(p), a\| \|q - TG(q), a\|}{\|p - q, a\|} + \beta \frac{\|q - TG(q), a\| \|q - TG(p), a\| \|p - TG(q), a\| + \|p - q, a\|^3}{\|p - q, a\|^2}$$

$$+ \gamma \left[\frac{\|p - TG(p), a\| + \|q - TG(q), a\|}{2} \right] + \delta \left[\frac{\|p - TG(q), a\| + \|q - TG(p), a\|}{2} \right] + \eta \|p - q, a\|$$

Taking $TG = R$ we get

$$\|R(p) - R(q), a\| \geq \alpha \frac{\|p - R(p), a\| \|q - R(q), a\|}{\|p - q, a\|} + \beta \frac{\|q - R(q), a\| \|q - R(p), a\| \|p - R(q), a\| + \|p - q, a\|^3}{\|p - q, a\|^2}$$

$$+ \gamma \left[\frac{\|p - R(p), a\| + \|q - R(p), a\|}{2} \right] + \delta \left[\frac{\|p - R(q), a\| + \|q - R(p), a\|}{2} \right] + \eta \|p - q, a\|$$

It is clear by theorem (1.1); that $R = TG$ has at least one fixed point say x_0 in K that is

$$R(x_0) = TG(x_0) = x_0$$

$$\text{And so } T.(TG)(x_0) = T(x_0)$$

$$\text{Or } T^2(Gx_0) = T(x_0)$$

$$G(x_0) = T(x_0)$$

Now

$$\begin{aligned}
& \|Tx_0 - x_0, a\| = \|Tx_0 - T^2(x_0), a\| = \|Tx_0 - T.T(x_0), a\| \\
& \geq \alpha \frac{\|G(x_0) - T(x_0), a\| \|GT(x_0) - T(Tx_0), a\|}{\|G(x_0) - G(Tx_0), a\|} \\
& + \beta \frac{\|G(Tx_0) - T(Tx_0), a\| \|G(Tx_0) - T(x_0), a\| \|G(x_0) - T(Tx_0), a\| + \|G(x_0) - G(Tx_0), a\|^3}{\|G(x_0) - G(Tx_0), a\|^2} \\
& + \gamma \left[\frac{\|G(x_0) - T(x_0), a\| + \|G(Tx_0) - T(Tx_0), a\|}{2} \right] + \delta \left[\frac{\|G(x_0) - T(Tx_0), a\| + \|G(Tx_0) - T(x_0), a\|}{2} \right] \\
& + \eta \|G(x_0) - G(Tx_0), a\| \\
& = (\beta + \delta + \eta) \|Tx_0 - x_0, a\| \\
& \text{So } T(x_0) = x_0 \quad (\beta + \gamma + \eta > 1)
\end{aligned}$$

That is x_0 is the fixed point of T .

But $T(x_0) = G(x_0)$ so $G(x_0) = x_0$.

Hence x_0 is the fixed point of T and G .

Uniqueness:

If possible let $y_0 \neq x_0$ is another common fixed point of T and G .

$$\begin{aligned}
\text{Then } & \|x_0 - y_0, a\| = \|T^2(x_0) - T^2(y_0), a\| = \|T(T(x_0)) - T(T(y_0)), a\| \\
& \geq \alpha \frac{\|G(Tx_0) - T(Tx_0), a\| \|G(Ty_0) - T(Ty_0), a\|}{\|G(Tx_0) - G(Ty_0), a\|} \\
& + \beta \frac{\|G(Ty_0) - T(Ty_0), a\| \|G(Ty_0) - T(Tx_0), a\| \|G(Tx_0) - T(Ty_0), a\| + \|G(Tx_0) - G(Ty_0), a\|^3}{\|G(Tx_0) - G(Ty_0), a\|^2} \\
& + \gamma \left[\frac{\|G(Tx_0) - T(Tx_0), a\| + \|G(Ty_0) - T(Ty_0), a\|}{2} \right] + \delta \left[\frac{\|G(Tx_0) - T(Ty_0), a\| + \|G(Ty_0) - T(Tx_0), a\|}{2} \right] \\
& + \eta \|G(Tx_0) - G(Ty_0), a\| \\
& \geq \beta \|x_0 - y_0, a\| + \delta \|x_0 - y_0, a\| + \eta \|x_0 - y_0, a\| \\
& \geq (\beta + \delta + \eta) \|x_0 - y_0, a\|
\end{aligned}$$

But $\beta + \delta + \eta > 1$

So $x_0 = y_0$. So common fixed point is unique.

REFERENCES:

- [1]. Ahmad, and Shakil, M. "Some fixed point theorems in Banach spaces" Nonlinear Funct. Anal. & Appl. 11 (2006) 343-349.
- [2]. Banach, S. "Sur les operation dans les ensembles abstraits et leur application aux equations integrals" Fund. Math.3 (1922) 133-181.
- [3]. Badshah, V.H. and Gupta, O.P. "Fixed point theorems in Banach and 2-Banach spaces" Jnanabha 35(2005) 73-78.
- [4]. Goebel, K. and Zlotkiewics, E. "Some fixed point theorems in Banach spaces" Colloq Math 23(1971) 103-106.
- [5]. Gahlar, S. "2-metrche raume and ihre topologisce structure" Math.Nadh.26 (1963-64) 115-148.
- [6]. Isekey, K. "fixed point theorem in Banach space" Math.Sem.Notes, Kobe University 2 (1974) 111-115.
- [7]. Jong, S.J. Viscosity approximation methods for a family of finite non expansive in Banach spaces" nonlinear Analysis 64 (2006) 2536-2552.
- [8]. Sharma, P.L. and Rajput S.S. "Fixed point theorem in Banach space" Vikram Mathematical Journal 4 (1983) 35-38.
- [9]. Verma, B.P. "Application of Banach fixed point theorem to solve non linear equations and its generalization" Jnanabha 36 (2006) 21-23.
- [10]. Yadava, R.N., Rajput, S.S. and Bhardwaj, R.K. "Some fixed point and common fixed point theorems in Banach spaces" Acta Ciencia Indica 33 No 2 (2007) 453-460.
- [11]. Yadava, R.N., Rajput, S.S., Choudhary, S. and Bhardwaj, R.K. "Some fixed point and common fixed point theorems for non-contraction mapping on 2-Banach spaces" Acta Ciencia Indica 33 No 3 (2007) 737-744.

Mathematical Modelling of Cassava Wastewater Treatment Using Anaerobic Baffled Reactor

A.O. Ibeje¹, B.C. Okoro²

Department of Civil Engineering, Imo State University, Owerri, Nigeria;

Department of Civil Engineering, Federal University of Technology, Owerri, Nigeria.

Abstract: The performance of an anaerobic baffled reactor (ABR) was evaluated in the treatment of cassava wastewater as a pollutant residue. An ABR divided in four equal volume compartments (total volume 4L) and operated at 35°C was used in cassava wastewater treatment. Feed tank chemical oxygen demand (COD) was varied from 2000 to 7000mg L⁻¹. The objective of the study was to formulate an improved mathematical model to describe cassava wastewater treatment without taking into account its inhibition characteristic. In the study, Kincannon-Stover model constants μ_{max} and K_s , were found to be 0.8803mg/L.d and 0.2113COD/m³.day respectively and Monod Model constants μ_{max} and K_s , were found to be 100mg/L.d and 98mgCOD respectively. The coefficient of determinations (R^2) of Kincannon-Stover and Monod Models were evaluated as 0.634 and 0.986. This showed that the Monod model is a more applicable model for describing the kinetics of the organic removal in anaerobic baffled reactor for treating cassava wastewater.

Keyword: *Mathematical Modeling; Anaerobic Baffled Reactor (ABR); Cassava Wastewater; COD Removal; Treatment*

I. INTRODUCTION

Wastewater treatment in developing countries is a problem to manage. The major components of the effluents from garri processing industries is cyanide and starch, and in most cases, these effluents are channeled into pits where they continue to accumulate and gradually percolate into the surrounding soils thereby posing serious health and environmental hazard. The wastewater from cassava processing or its derivative (garri) ends up with domestic sewage if processed in small quantities while others end up being carried with industrial wastes if processed in large industrial quantities. Lastly, others percolate into the soil depending on the processors. Wastewater from cassava processing, if released directly into the environment before proper treatment, is a source of pollution. In many areas where traditional processing is practiced, wastewater is normally discharged beyond the “factory” wall into roadside ditches or fields and allowed to flow freely, settling in shallow depressions. Eventually this will percolate into the subsoil or flow into streams. Cassava roots contain cyanogenic glucosides (the precursors of HCN) in various concentrations depending on the variety and growing conditions (Bolhuis, 1954). This cyanide is released during peeling, slicing and crushing. The bound cyanide is converted to free cyanide during the milling operation. About 40% to 70% of the total cyanide appears in the water used to wash the starch from the disintegrated tissue (Maduagwu and Umoh, 1988). The press water, although produced in relatively low volumes (250 – 300 litres per tonne of roots), is the main problem because of its high biological oxygen demand (BOD) of 25,000 – 50,000 mg/l with a typical cyanide concentration in excess of 400 mg/l (Gomez et al., 1984). Cyanide, being an acidic component will naturally have an inhibiting action on the biological degradation of cassava wastewater. Cassava wastewaters are often discharged into sewers or allowed to percolate into the soil causing environmental degradation. This effect on the environment is significant as the air we breathe becomes contaminated with the odor emanating from it, an effect yet to be addressed properly in developing countries due to inadequate equipment and lack of research materials. The cassava wastewater may introduce some toxic elements e.g. cyanide in sewage which may inhibit the usual degradation processes. It is therefore very important to establish the pathway of degradation, the level of inhibition and the extent of treatability of cassava wastewater. The objective of this study is to formulate an

improved mathematical model to describe cassava wastewater treatment without taking into account its inhibition characteristic.

Materials and Method

The laboratory scale ABR was constructed from 6mm thick stainless steel, with external dimensions of lengths, widths, depths and working volumes as shown in Table 1. Figure 1 shows a schematic diagram of the reactor. The reactor was divided into 4 equal compartments by vertical baffles with each compartment of each the reactors having down-comer and riser regions created by a further vertical baffle.

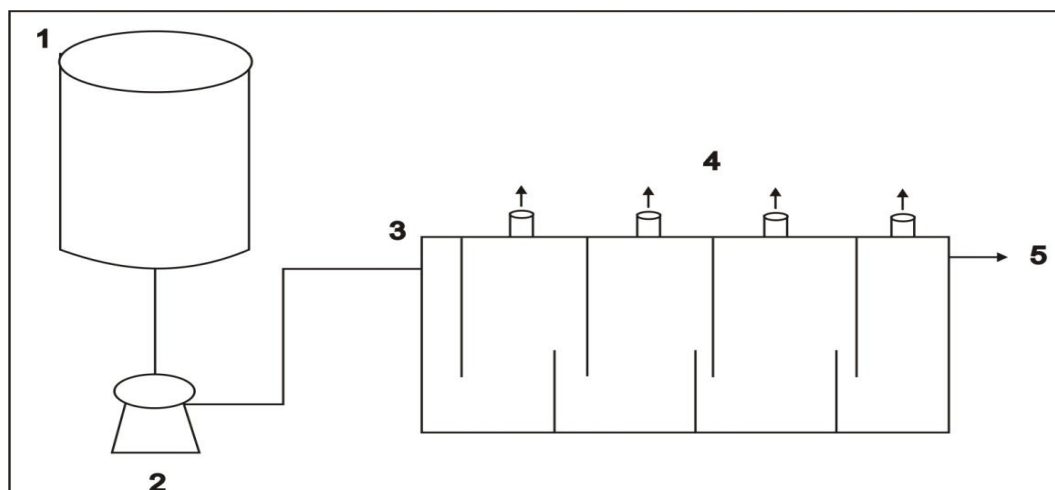


Figure 1: The Reactor - Scheme of the ABR. 1. Feed Tank; 2. Peristaltic Pump; 3. Influent; 4. Sampling Ports; 5. Effluent.

For each of the reactors, the widths of up-comers were multiples of the widths of down-comer (Fernanda et al., 2001). The lower parts of the down-comer baffles were angled at 45° in order to direct the flow evenly through the up-comer. This produced effective mixing and contact between the wastewater and anaerobic sludge at the base of each riser. Each compartment was equipped with sampling ports that allowed biological solids and liquid samples to be withdrawn. The operating temperature was maintained constant at $35 \pm 0.5^{\circ}\text{C}$ by putting the reactor in a water bath equipped with a temperature regulator (Movahadyan et al., 2007). The influent feed was pumped using variable speed peristaltic pump.

Table 1: Dimensions of the Reactor

Dimensions	Reactor 1
Length (cm)	53
Width (cm)	16
Depth (cm)	30
Working Volume (L)	13.57
Up-comer Width/ Down-comer Width	2.6
No of Compartments	5
Volume of Each Compartment (L)	2.7

Start-up of ABR

Start-up without seed sludge was rather difficult and time consuming for suspended growth anaerobic reactors. The following 3 steps were taken: (i) the reactor was filled with cassava wastewater and allowed to rest for 15 d (ii) the sludge bed was allowed through a process of sludge accumulation by settling and sludge improvement and (iii) after 15 d, feeding of the wastewater was resumed (Movahadyan et al., 2007). The resumed wastewater feeding helped the development of sludge bed at the bottom of individual chambers of the ABR. This process of feeding the system followed by two weeks rest is based on the experiment made in Kanpur (India) for the start-up of a UASB plant without inoculum (Draaijer et al., 1992).

Characterization of Wastewater

The cassava wastewater from a cassava processing factory at Imo Polytechnic Umuagwo in Eastern Nigeria was used as feed. The supernatant of the wastewater after the simple gravity settling, used in the investigation, had low TSS, as approximately 90% of the solids were removed. The supernatant wastewater was

diluted to achieve the COD concentration required for each loading rate with water. In order to achieve pH and alkalinity adjustment, the supernatant was neutralized by NaOH and NaHCO₃. A COD:N:P ratio of 300:5:1 was kept during operation using NH₄Cl and K₂HPO₄. The micro-nutrient deficiency was added occasionally to correct growth conditions.

Procedure for Experiment

The wastewater was collected twice a day from the cassava processing plant, and it was intermittently mixed to feed the reactor with a consistent quality. The wastewater was fed to the reactor with the help of a variable speed peristaltic pump. The ABR was operated at various hydraulic retention times (HRTs) by varying the flow rate of influent wastewater (Q_{inf}), thereby varying the organic loading rate (OLR). The wastewater flow from the down-comer to the up-comer within an individual chamber through the sludge bed formed at the bottom of the individual chambers. After receiving treatment in the particular chamber, wastewater entered the next chamber from the top. Due to the specific design and positioning of the baffle, the wastewater is evenly distributed in the up-comer and the vertical up-flow velocity (V_{up}) could be significantly reduced. The treated effluent was collected from the outlet of the 3rd compartment. The reactor was kept in a temperature controlled chamber maintained at 35 °C.

Mathematical Modeling of Cassava Wastewater Treatment

Nomenclature:

S_i = Substrate concentration in the influent (mg/l)

S_e = Substrate concentration in the effluent (mg/l)

k_s = Half saturation constant (mg/l)

μ = Specific growth rate of organism (per day)

μ_{max} = Maximum specific growth rate of organism (per day)

V = Volume of reactor (L)

r_A = Rate of utilization of substrate (mg/l.day)

Kincannon-Stover Model for ABR

Equation (1) is Kincannon-Stover model. This equation was first used for RBC (Rotating Biological Contactor) systems. In that model the disc surface area (A) is used to represent some relationship to the total attached-growth active biomass concentration in a RBC. Where ds/dt is the substrate removal rate (mg/1. day). In the equation it was assumed that the suspended solid in the RBC system is negligible in comparison to the attached biomass (Broch-De et al., 1994).

$$r_A = \frac{ds}{dt} = \frac{\mu_{max}^1 \left(\frac{QS_i}{A} \right)}{K_s^1 + \left(\frac{QS_i}{A} \right)} \quad (1)$$

Previous studies (Broch-De et al., 1994) have shown that suspended biomass in the reactor is a significant factor in producing high and stable removal efficiency in moving bed biofilm reactors. It was demonstrated that the suspended biomass in the reactor contributed approximately one half of the total waste removal. This is extendable to ABR system because majority biomass of ABR is suspended and ABR reactors perform almost similar to plug flow reactor and it was predicted that Kincannon-Stover model was better for performance description of ABR reactor. Therefore in equation (1) volume (V) of the reactor instead of the surface area of the carrier elements can be used. By this modification results in:

$$r_{v\text{ COD}} = \frac{ds}{dt} = \frac{\mu_{max} \frac{QS_i}{V}}{K_s + \left(\frac{QS_i}{V} \right)} \quad (2)$$

A mass balance of substrate into and out of the volume can be made as follows:

$$\frac{ds}{dt} = \frac{Q}{V} (S_i - S_e) \quad (3)$$

By equation (2), (3) we have the following relationship:

$$\frac{ds}{dt} = \frac{Q}{V} (S_i - S_e) = \frac{\mu_{max} \frac{QS_i}{V}}{K_s + \left(\frac{QS_i}{V} \right)} \quad (4)$$

By linearization of equation (4), equation (5) is obtained as follows

$$\left(\frac{ds}{dt} \right) = \frac{V}{Q(S_i - S_e)} = \frac{K_s}{\mu_{max}} \left(\frac{V}{QS_i} \right) + \frac{1}{\mu_{max}} \quad (5)$$

By plotting $V/Q (S_i - S_e)$, the inverse of the loading removal rate, against V/QS_i , the inverse of total organic loading rate, a straight line was obtained. By measuring the intercept and slope of this line the μ_{max} and K_s was determined.

By substituting equation (5) in equation (3) the following equation is obtained:

$$QS_i = QS_e + \left(\frac{\mu_{max} \left(\frac{QS_i}{V} \right)}{K_s + \left(\frac{QS_i}{V} \right)} \right) V \quad (6)$$

This equation can then be solved for either the volume of reactor or the effluent substrate concentration. Thus:

$$V = \frac{QS_i}{\left(\frac{\mu_{max} S_i}{S_i - S_e} \right) - K_s} \quad (7)$$

$$S_e = S_i - \frac{\mu_{max} S_i}{K_s + \frac{QS_i}{V}} \quad (8)$$

Monod Model for ABR

The Monod model is described as

$$r_A = \frac{ds}{dt} = \frac{Q}{V} (S_i - S_e) = \mu \cdot X \quad (9)$$

$$\frac{Q}{V} (S_i - S_e) = \frac{\mu_{max} S_e}{K_s + S_e} X \quad (10)$$

By linearization of equation (10), equation (11) is obtained as follows

$$\frac{XV}{Q(S_i - S_e)} = \frac{K_s}{\mu_{max}} \frac{1}{S_e} + \frac{1}{\mu_{max}} \quad (11)$$

Experimental results were applied to Equations (11) in order to plot a graph. In this, graph $XV/Q(S_i - S_e)$ was plotted against $1/S_e$

Kincannon-Stover Model for ABR Treatment Cassava Wastewater

From the regression equation: $y = mx + c \equiv y = 0.240x + 1.136$

$$\frac{1}{\mu_{max}} = c = \text{intercept}; \quad \mu_{max} = \frac{1}{c} = \frac{1}{1.136} = 0.8803 \text{mg/L.d}$$

$$\frac{K_s}{\mu_{max}} = m = \text{slope}; \quad K_s = \mu_{max} * m$$

$$K_s = 0.8803 * 0.240 = 0.2113 \text{COD/m}^3 \cdot \text{day}$$

Substituting μ_{max} and K_s into equation 8 gives: $S_e = S_i - \frac{0.8803 S_i}{\left(1.136 + \frac{QS_i}{V} \right)}$

Monod Model for ABR Treatment Cassava Wastewater

From the regression equation: $y = mx + c \equiv y = 0.98x + 0.01$

$$\frac{1}{\mu_{max}} = c = \text{intercept}; \quad \mu_{max} = \frac{1}{c} = \frac{1}{0.01} = 100 \text{mg/L.d}$$

$$\frac{K_s}{\mu_{max}} = m; \quad K_s = K * m$$

$$K_s = 100 * 0.98 = 98 \text{mgCOD/L.day}$$

Substituting μ_{max} and K_s into equation 8 gives: $r_A = \frac{ds}{dt} = \frac{Q}{V} (S_i - S_e) = \frac{\mu_{max} X S_e}{K_s + S_e} = \frac{100 X S_e}{98 + S_e}$

II. CONCLUSION

The state-of-the-art in the field of ABR for treatment of wastewater is reviewed in this paper, based on a substantial number of relevant references published recently; it can be concluded that the ABR could be applied to treat various wastewaters with satisfactory results if integrated with proper technology. As a high-rate anaerobic reactor, ABR has considerable potential for wastewater treatment. By Kincannon-Stover model the reactor volume and effluent substrate concentration can be determined if the model constants are available. In the study, Kincannon-Stover model constants μ_{max} and K_s , were found to be 0.8803mg/L.d and $0.2113 \text{COD/m}^3 \cdot \text{day}$ respectively and Monod Model constants μ_{max} and K_s , were found to be 100mg/L.d and 98mgCOD

respectively. The coefficient of determinations (R^2) of Kincannon-Stover and Monod Models were evaluated as 0.634 and 0.986. This showed that the Monod model is a more applicable model for describing the kinetics of the organic removal in anaerobic baffled reactor for treating cassava wastewater.

Table 2: Non-Inhibited Cassava Wastewater Treatment (Kincannon– Stover Model)

S/N	$\frac{Q(S_i - S_e)}{V}$ (mg/L.d)	$\frac{Q S_i}{V} \times 10^9$ (mg/L.d)	$y = \frac{V}{Q(S_i - S_e)} \times 10^{-4}$ (/L.d/mg)	$x = \frac{V}{Q S_i} \times 10^{-10}$ (L.d/mg)
1	250.00	1.40	40.00	7.10
2	500.00	1.40	20.00	7.10
3	400.00	1.40	25.00	7.10
4	500.00	1.40	20.00	7.10
5	500.00	1.40	20.00	7.10
6	300.00	1.40	33.00	7.10
7	600.00	1.40	17.00	7.10
8	600.00	1.40	17.00	7.10
9	700.00	1.40	14.00	7.10
10	600.00	1.40	17.00	7.10
11	900.00	1.80	11.00	5.50
12	1000.00	2.40	10.00	4.20
13	1500.00	2.40	6.70	4.20
14	1600.00	2.40	6.30	4.20
15	1700.00	2.40	5.90	4.20
16	1700.00	2.40	5.90	4.20
17	1900.00	5.00	5.30	0.20
18	2700.00	5.00	3.70	0.20
19	2800.00	5.00	3.60	0.20
20	2500.00	5.00	4.00	0.20
21	2200.00	10.00	4.50	0.10
22	4200.00	10.00	2.40	0.10
23	4000.00	10.00	2.50	0.10
24	4100.00	10.00	2.40	0.10

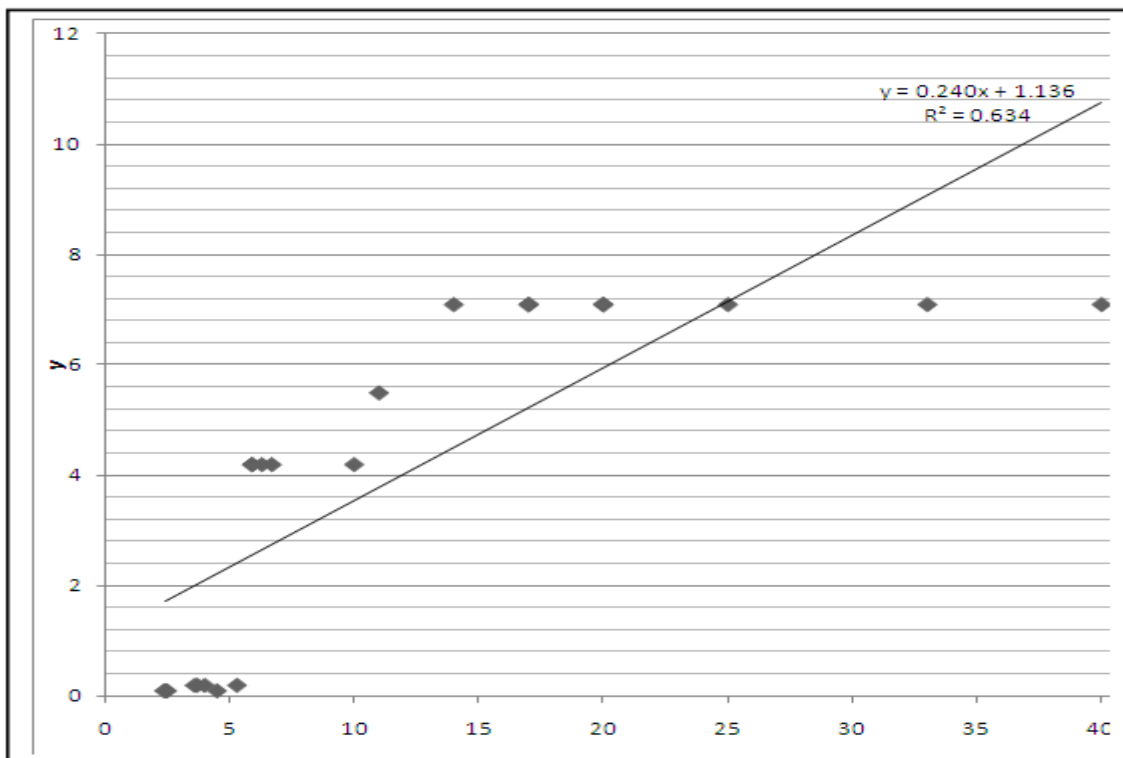


Figure 2: A Scatter Plot of Inverse of Substrate Removal Rate ($y = \frac{V}{Q(S_i - S_e)}$ (/L.d/mg)) Versus Inverse of Total Loading Rate ($x = \frac{V}{Q S_i}$ (L.d/mg)) (Kincannon– Stover Model)

Table 3: Non-Inhibited Cassava Wastewater Treatment (Monod Model)

S/N	$x_i = \frac{SV_i - SV_e}{V}$ (mg/L.d)	$\frac{Q(S_i - S_e)}{V}$ (mg/L.d)	$\frac{V}{Q(S_i - S_e)}$ (mg/L.d)	$y = \frac{x \cdot V}{Q(S_i - S_e)}$ (mg/L.d)	S_e (mg/L)	$x = \frac{1}{S_e}$ (L/mg)
1	2.60	250.00	0.004	0.0104	96.15	0.01
2	2.20	500.00	0.002	0.0044	227.27	0.004
3	1.40	400.00	0.0025	0.0035	285.71	0.004
4	0.60	500.00	0.002	0.0012	833.33	0.001
5	0.00	500.00	0.002	0	0	0
6	0.20	300.00	0.003333333	0.000666667	1500.00	7E-04
7	0.60	600.00	0.001666667	0.001	1000.00	0.001
8	1.00	600.00	0.001666667	0.001666667	600.00	0.002
9	1.40	700.00	0.001428571	0.002	500.00	0.002
10	1.70	600.00	0.001666667	0.002833333	352.94	0.003
11	2.00	900.00	0.001111111	0.002222222	450.00	0.002
12	2.20	1000.00	0.001	0.0022	454.55	0.002
13	2.40	1500.00	0.000666667	0.0016	625.00	0.002
14	2.60	1600.00	0.000625	0.001625	615.38	0.002
15	3.10	1700.00	0.000588235	0.001823529	548.39	0.002
16	3.30	1700.00	0.000588235	0.001941176	515.15	0.002
17	3.30	1900.00	0.000526316	0.001736842	575.76	0.002
18	3.40	2700.00	0.00037037	0.001259259	794.12	0.001
19	3.40	2800.00	0.000357143	0.001214286	823.53	0.001
20	3.40	2800.00	0.000357143	0.001214286	823.53	0.001
21	3.40	2200.00	0.000454545	0.001545455	647.06	0.002
22	3.50	2200.00	0.000454545	0.001590909	628.57	0.002
23	3.50	400.00	0.0025	0.00875	114.29	0.009
24	3.50	4100.00	0.000243902	0.000853659	1171.43	9E-04

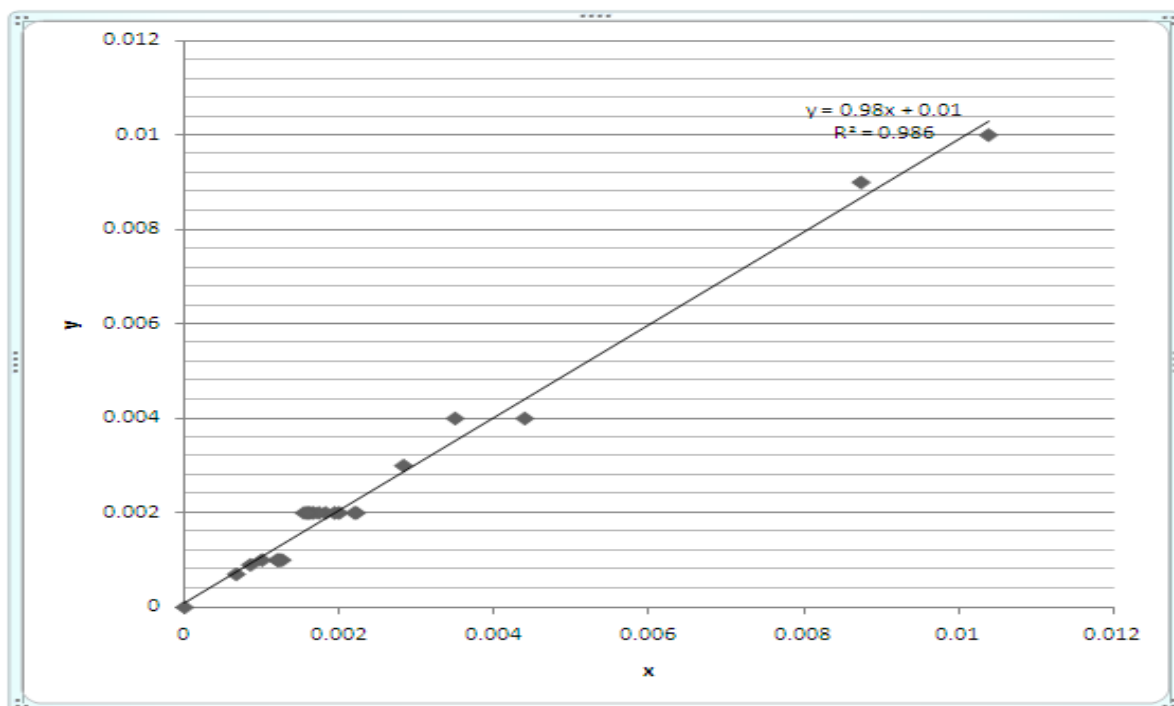


Figure 3: A Scatter Plot of $y = \frac{xV}{Q(S_i - S_e)}$ (L.d/mg) Versus $x = \frac{1}{S_e}$ (L/ mg) (Monod Model)

REFERENCES

- [1] Bolhuis, G.G. 1954. The toxicity of cassava root: *Netherlands Journal of Agriculture Science* 2:176-185.
- [2] Broch-De A., Andersen R. Kristoffersen O., (1994) Pilot plant experience with an aerobic moving bed biofilm reactor for treatment of NSSC wastewater. *Wat. Sci.*, 29, 283-294.
- [3] Draaijer, H, Maes, J.A., Schaapman, J.E, Khan, A. 1992. Performance of 5MLD UASB Reactor For Sewage Treatment at Kanpor, India, *Water Sci, Technol.* 23(7), 123-133
- [4] Fernanda, M.F., Aline, T.B, and Vanildo L., D.B. 2001. Performance of Anaerobic Baffled Reactor (ABR) in Treatment of Cassava Wastewater. *Brazilian Journal of Microbiology.* 40, 48-53. ISSN 1517-8382.
- [5] Gomez, G., and Valdivieso, m. 1988. The effects of ensiling whole root chips on cyanide elimination. *Nutrition Report International* 37:1161-1166.
- [6] Gomez, G., Valdivieso, M., De la Cuesta, D. and Salcedo, T.S. 1984. Effect of Variety and plant age on the cyanide content of whole root cassava chips and its reduction by sundrying. *Animal Feed science and Technology* 11: 57-65
- [7] Maduagwu, E.N., and Umoh, I.B, 1988. Dietary thiocyanate and N-nitrosation in vivo in the Wistar rat. *Annals of Nutrition and metabolism* 32: 30-37.
- [8] Movahadyan, E.K., Grobicki, D. And Stuckay, C. (2007). Performance of Anaerobic Baffled Reactor under Steady-state and Shock Load Condition. *Biotechnol, BioEng.* (37), 344-355.

Geocasting and Multicasting Routing Operation in Mobile Ad Hoc Network

R.Kruthika, Smitha Shekar.B, Harish.G

IVth sem, M.Tech, Department of Computer Science & Engineering, Dr.A.I.T, Bangalore, India.

Assistant Professor, Department of Computer Science & Engineering, Dr.A.I.T, Bangalore, India.

Abstract: The paper considers, the different multicasting routing protocols in wireless mobile Ad hoc network (MANET). An Ad hoc network is composed of mobile nodes without the presence of a wired support infrastructure. In this environment routing/multicasting protocols are faced with the challenge of producing multihop router under host mobility and band constraints. Various approaches and routing protocol have been proposed to address Ad hoc networking problems and multiple standardization effort within the Internet Engineering Task Force, along with academic and industrial research projects.

In recent year, a number of new multicast protocols of different styles have been proposed for Ad hoc networks. Geocast Adaptive Mesh Environment for Routing [GAMER] is one which provides geocast communication in an Ad hoc network and it adapts to the correct network environment by dynamically changing the density of the mesh. Forwarding Group Multicast Protocol [FGMP] is based on the forward group concept and it dynamically refreshes the forward group member using a procedure to On-Demand routing.

The relative strengths, weakness and applicability of each multicast protocol to diverse situations have considered and analyzed. *Index Terms:* FGMP Protocol, GAMER Protocol, MANETs, multicast, routing.

An Ad hoc networks [1] [2], is a dynamically reconfigurable wireless network with no fixed infrastructure (or) central administration. Due to the limited radio propagation range of wireless devices, routers are often "multihop". Applications such as disaster recovery, crowd control, search, rescue and automated battlefields are typical examples of where Ad hoc networks are deployed. Nodes in these networks more arbitrary thus network topology changes frequently and unpredictably. Moreover, bandwidth and battery power are limited. These constraints, in combination with the dynamic network topology make routing and multicasting in Ad hoc networks extremely challenging.

Various multicast protocols have been newly proposed to perform multicasting in Ad hoc network. However, no operation study between them has yet been performed. The comparative analysis of Ad hoc unicast routing protocols has been reported. This paper gives a comparison study of two protocols with different characteristics: GAMER [3] and FGMP [4].

The rest of the paper is organized as follows. Section I presents an overview of the multicast protocols. The section II discusses the future enhancements, and concluding remarks are made in section III.

I. MULTICAST PROTOCOLS OPERATION REVIEW

In this section, introduction to Ad hoc wireless multicast protocols operation is explained and then the basic operation procedures are described.

A.GAMER (Geocast Adaptive Mesh Environment for Routing)

GAMER goal is a geocast routing protocol is to deliver packets to a group of nodes that are within specified geographical area i.e the geocast region. An Ad hoc network is a set of wireless mobiles nodes (MN) that co-operatively form a network without specific user administration (or) configuration.

GAMER details for Building the mesh

While a source node in GAMER has geocast packets to transmit, a JOIN-DEMAND (JD) packet is periodically sent to the geocast region. GAMER uses JOIN-DEMAND packets, instead of conventional JOIN-

REQUEST (JR) packets of multicast protocols, to insist that all MNs in the geocast region join the geocast group. In other words, the geocast group consists of all MNs that are within the geocast region; that is, GAMER provides geo-broadcasting instead of geo-multicasting. The GAMER protocol ensures that all reachable MNs in the geocast region receive each geocast packet transmitted.

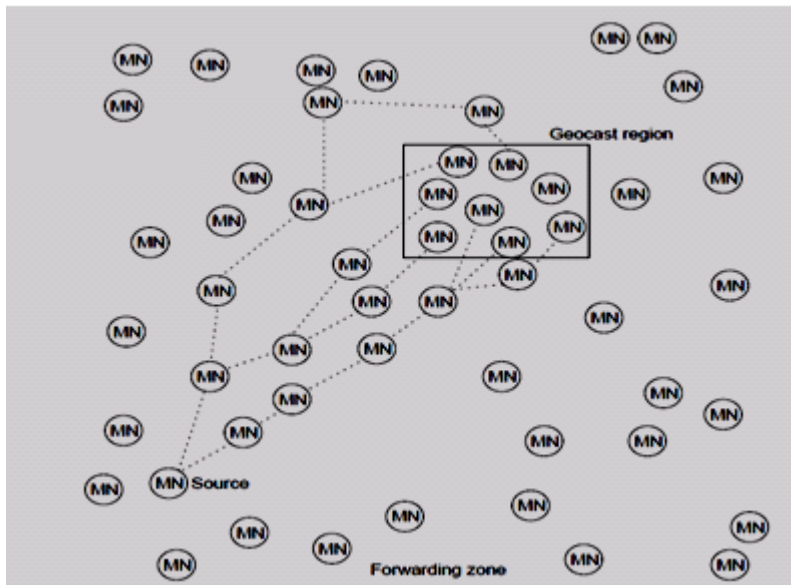


Figure 1: Mesh created by FLOOD FA

GAMER dynamically chooses (based on the current network environment) one of three different forwarding approaches (FAs) to forward JD packets to the geocast region. In one FA, JD packets are flooded throughout the entire Ad hoc network. This FA, which is similar to flooding the JR packets in ODMRP, is called FLOOD. An example of a mesh created by GAMER when using the FLOOD FA is illustrated in Figure 1. In the other two FAs, a forwarding zone is defined to reduce the area to flood the JD packets. In other words, only the MNs within the forwarding zone flood the JD packets. The other two forwarding approaches are called CORRIDOR FA and CONE FA.

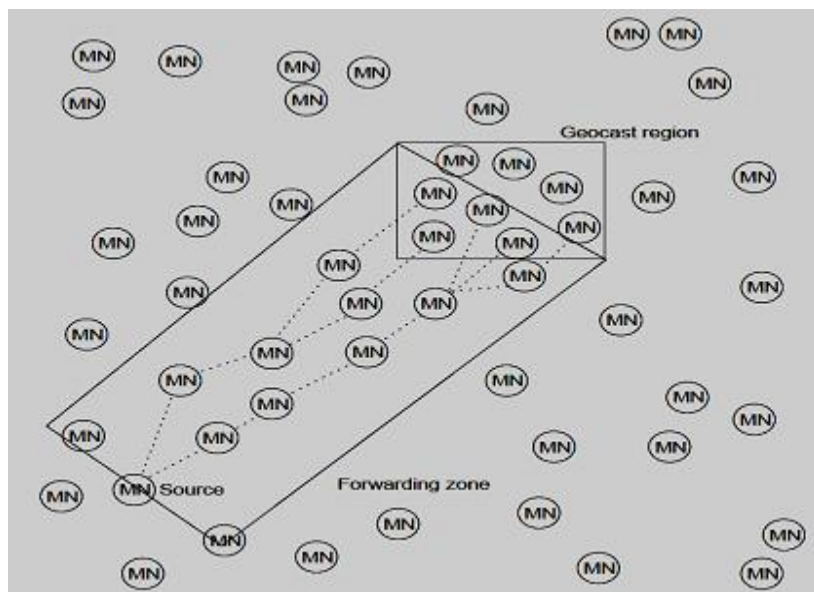


Figure 2: Mesh created by CORRIDOR FA

Figure 2, shows an example of a mesh created by GAMER when using the CORRIDOR FA. The CORRIDOR FA defines the forwarding zone as the area within two parallel lines convex to the geocast region. First, imagine a center point C in the geocast region. Then, imagine a line from the center of the source node S to C: Two of the edges in the forwarding zone defined by the CORRIDOR FA are the two parallel lines, which are parallel to the line between S and C; that cross the margins of the geocast region. The other two edges of the

forwarding zone defined by the CORRIDOR FA are perpendicular to the two parallel edges; one edge crosses S and the other edge crosses C: Thus, GAMER creates a rectangle forwarding zone when using the CORRIDOR FA. As Figure 1 and 2 illustrates, the forwarding zone of the CORRIDOR FA [5] is much smaller than the forwarding zone in the FLOOD FA which, therefore, creates a sparser mesh.

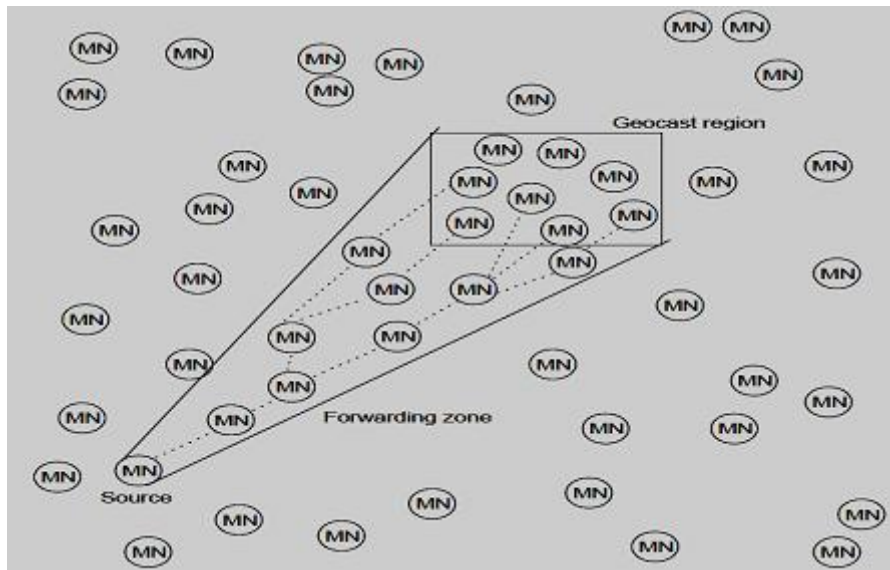


Figure 3: Mesh created by CONE FA

Figure 3, shows an example of a mesh created by GAMER when using the CONE FA. Compared to the CORRIDOR FA, the CONE FA restrains the size of the forwarding zone even further. The forwarding zone created by the CONE FA is the area enclosed by an angle whose vertex is the source node and whose sides are tangent to the geocast region. The forwarding zone created by the CONE FA is similar to the forwarding zone created in DREAM; one difference between the two is that the CONE FA does not have a minimum cone angle while the DREAM protocol has a 30% minimum cone angle.

B.FGMP (Forwarding Group Multicast Protocol)

The proposed FGMP scheme (first introduced in [6]) is reviewed here for completeness. FGMP keeps track not of links but of groups of nodes which participate in multicast packets forwarding. To each multicast group G is associated a forwarding group, FG. Any node in FG is in charge of forwarding (broadcast) multicast packets of G. That is, when a forwarding node (a node in FG) receives a multicast packet, it will broadcast this packet if it is not a duplicate. All neighbors can hear it, but only neighbors that are in FG will first determine if it is a duplicate and then broadcast it in turn

1. FG Maintenance via Receiver Advertising (FGMP-RA)

One way to advertise the membership is to let each receiver periodically and globally flood its member information (join request) formatted as in Table 1. TTL limits the scope of flooding. Each sender maintains a member table as shown in Table 2. When a sender receives the join request from receiver members, it updates its member table.

Table 1: Format of join_request/sender_info packet

Mcast Group id	Receiver/Sender member Id	Sequence #	TTL
----------------	---------------------------	------------	-----

Expired receiver entries will be deleted from the member table. Non-sender nodes simply forward the request packet. After updating the member table, the sender creates from it the forwarding table FW shown in Table 3. Next hop on the shortest path to the receiver is obtained from preexisting routing tables. The forwarding table FW is broadcast by the sender to all neighbors; only neighbors listed in the next hop list (next hop neighbors) accept this forwarding table (although all neighbors can hear it). Each neighbor in the next hop list creates its forwarding table by extracting the entries where it is the next hop neighbor and again using the

preexisting routing table to find the next hops, etc. After the FW table is built, it is then broadcast again to neighbors and so on, until all receivers are reached.

Table 2: Format of member table at the sender/receiver members

Mcast Group id	
Refresh Timer	
receiver/sender member id	timer
⋮	⋮

Table 3: Format of forwarding/joining table FW

Mcast Group id	
receiver/sender member id	next hop
⋮	⋮

Note that FW is discarded after use. The member table on the other hand is permanent. The forwarding table FW propagation mechanism essentially activates all the nodes on the source tree rooted at the sender. These nodes become part of the FG. At each step nodes on the next hop neighbor list after receiving the forwarding table enable the forwarding flag and refresh the forwarding timer. Soft state dynamic reconfiguration provides the ability to adapt to a changing topology.

Figure 4, shows an example of multicasting forwarding tables. Node 12 is the sender. Five nodes are forwarding nodes, $FG = \{4; 12; 16; 22; 25\}$, because they are in the next hop list. Only sender and internal nodes, in our case 12 and node 22, need to create a forwarding table (figure 4(a), (b)) and broadcast it. Forwarding nodes 4, 16, and 25 do not need to create their forwarding tables since they are “leaves”, i.e. all receiver members are immediate neighbors. When forwarding nodes receive new forwarding tables, their forwarding timers are refreshed; in absence of refreshes, the forwarding flag will automatically time out and the forwarding node is deleted from FG.

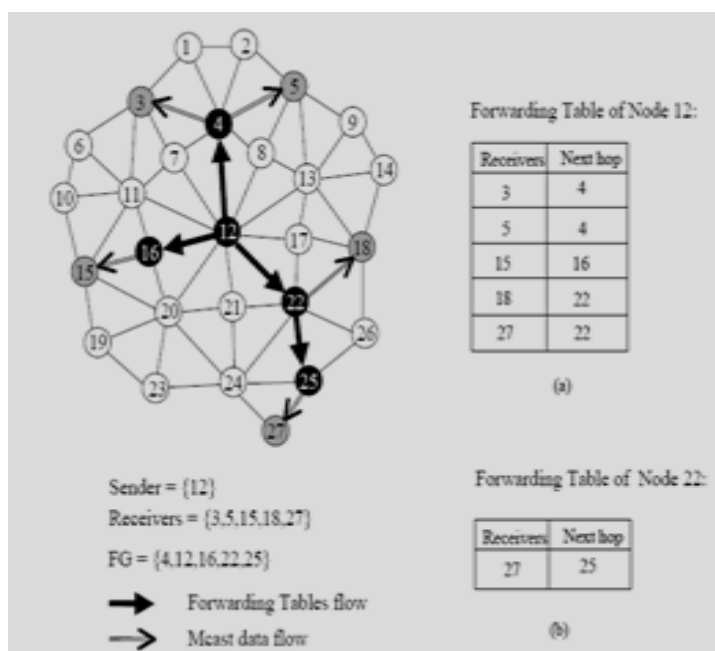


Figure 4: Example of forwarding tables for FGMP-RA

2. FG Maintenance via Sender Advertising (FGMP-SA)

Another way to advertise the membership is to let senders flood sender information. Sender advertising is more efficient than receiver advertising if the number of senders is less than the number of receivers. Most multicast applications belong to this category. Like in receiver advertising, senders periodically flood the sender information. Receivers will collect senders’ status, then periodically broadcast “joining tables” to create and maintain the forwarding group FG. The “joining table” has the same format as the “forwarding table” except

that the joining table contains the sender IDs while the forwarding table contains receiver IDs. Forwarding flag and timer are set when a node receives the joining table. Forwarding group is maintained (soft state refresh) by the senders in receiver advertising scheme and by the receivers in sender advertising scheme.

Member table and forwarding table size poses a scaling limitation when the multicast group grows to hundreds or even thousands of nodes. A possible solution (which we are currently exploring) is to dynamically (and randomly) elect a small set of "core" nodes which lie on the path between senders and receivers. These core nodes advertise (at a fairly low frequency) their presence, i.e., their ID, to all nodes. Senders and receivers alike send short join messages to each of the core nodes, activating the FG flag in all the nodes encountered along the path. The scheme scales well in both storage and channel O/H. It does not however guarantee shortest paths between all senders and receivers. It also introduces the additional complexity of core node elections. Then are evaluating some of this tradeoff in our current research.

II. FUTURE ENHANCEMENTS

As a future enhancement, an evaluation other version of GAMER that chooses the FA based on another network environment feature (e.g. the location of the source node to the Geocast region) can be considered. In addition, adding more features to GAMER, such as allowing the protocol to mark more efficient paths in the mesh as higher priority. When a path in the mesh fails, the MN's local to the failure will attempt to fix the failure locally. At low speeds, the passive GAMER has lower control overhead and lower network-wide data load than the active GAMER.

The FGMP in future defined Quality of service (Qos) extension for AODV to enable route establishment between nodes that have certain well defined traffic flow. The solution includes large membership size and methods for the integration of the multicast-On-Demand route search with existing On-Demand unicast routing protocol.

III. CONCLUSION

In the work, the performance of the Geocast adaptive mesh environment for Routing (GAMER) protocol has been investigated. GAMER dynamically chooses one of three forwarding approaches based on the current network environment by dynamically changing the density of the mesh.

Thus, when nodes are highly mobile, a dense mesh is created ;when the nodes are moving slowly ,a sparse mesh is created .Two version of GAMER exist; the passive GAMER and the active GAMER. The active GAMER is more active in increasing the size of its forwarding zone than the passive GAMER.

In FGMP novel approaches to wireless, Ad hoc multicasting is based on forwarding groups and On-Demand routing. Preliminary simulation results show that the proposed scheme is much more robust to mobility than the forwarding group version based on a global routing structure. It also outperforms conventional tree based multicast schemes such as DVMRP and shared tree. The reasons for this superior performance must be sought in lower control overhead and in more agile recovery from path breakage. Storage scalability is also greatly enhanced by On-Demand routing, especially in large networks.

REFERENCES

- [1]. Internet Engineering Task Force (IETF) Mobile AD Hoc Networks (MANET) Working Group Charter. <http://www.ietf.org/html.charters/manet-charter.html>.
- [2]. J. Jubin and J.D. Tornow, "The DARPA Packet Radio Network Protocols," Proceedings of the IEEE, vol. 75, no. 1, Jan. 1987, pp. 21-32.
- [3]. Tracy Camp and Yu Liu "An Adaptive mesh-based protocol for geocast, routing" Dept. of Math. And Computer Science, Colorado School of Mines, Golden<CO 80401, USA.
- [4]. Ching-Chuan Chiang and Mario Gerla Computer Science Department University of California, Los Angeles about " On-Demand Multicast in Mobile Wireless Networks".
- [5]. Y. Liu, A hybrid forwarding approach for the mesh-based geocast routing protocol in an ad hoc network, Master's Thesis, Colorado School of Mines, 2001.
- [6]. C.-C. Chiang, M. Gerla, and L. Zhang. Forwarding group multicast protocol (FGMP) for multihop, mobile wireless networks. Cluster Computing: Special Issue on Mobile Computings, to appear at Vol.1, No. 1, 1998.

Technical Review of peephole Technique in compiler to optimize intermediate code

Vaishali Sanghvi¹, Meri Dedania², Kaushik Manavadariya³, Ankit Faldu⁴

¹(Department of MCA/ Atmiya Institute of Technology & Science-Rajot, India)

²(Department of MCA/ Atmiya Institute of Technology & Science-Rajot, India)

³(Department of MCA/ Atmiya Institute of Technology & Science-Rajot, India)

⁴(Department of MCA/ Atmiya Institute of Technology & Science-Rajot, India)

Abstract: Peephole optimization is a efficient and easy optimization technique used by compilers sometime called window or peephole is set of code that replace one sequence of instructions by another equivalent set of instructions, but shorter, faster. Peephole optimization is traditionally done through String pattern matching that is using regular expression. There are some the techniques of peephole optimization like constant folding, Strength reduction, null sequences, combine operation, algebraic laws, special case instructions, address mode operations.

The peephole optimization is applied to several parts or section of program or code so main question is where to apply it before compilation, on the intermediate code or after compilation of the code. The aim of this dissertation to show the current state of peephole optimization and how apply it to the IR (Intermediate Representation) code that is generated by any programming language.

Keywords: Compiler, peephole, Intermediate code, code generation, PO (peephole optimization)

I. INTRODUCTION

Compilers take a source code as input, and typically produce semantically correspondent target machine instructions as output. A compiler (or a language translator) performs two operations: analysis and synthesis. The analysis phase determines the meaning of the source text, and the synthesis phase creates an equivalent program in a different language.

In the case of compilers, automatic generation of language translation tools requires and facilitates understanding of language translation. Syntactic analysis especially is well understood, encompasses a sizeable formal literature, and is habitually done mechanically by programs like **yacc** and **lex**.

A common method for implementing a group of languages on a collection of machines is to have one front end per language and one back end per machine. Each front end translates from its source language to a common intermediate code, called an UNCOL, and each back end translates from the common intermediate code to a specific target machine's assembly language.

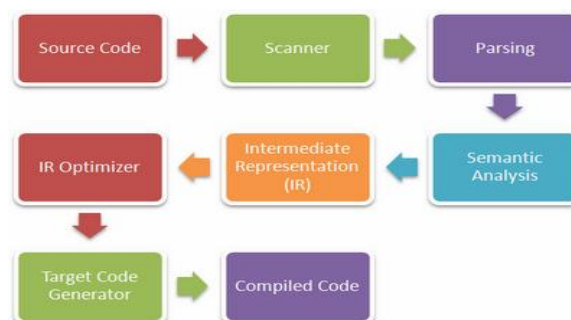


Fig 1: Compiler Process

Thus a "compiler" consists of a front end, a back end, and possibly programs that optimize the

intermediate code. When this model has been adopted, adding a new language or new machine only requires writing one new program (front end or back end) to maintain the property that all languages are available on all machines.

The question of where to perform the optimization arises. There are three theoretical possibilities:

1. in the front ends;
2. on the intermediate code;
3. in the back ends.

If the first option is chosen, many common optimizations will have to be programmed into each front end, increasing development effort.

Similarly, putting the optimizations in the back ends will also require a duplication of effort.

Though, any optimizations that can be performed on the intermediate code itself only need be done once, with the results being applicable to all front ends and all machines being used.

The compiler's task is to provide the translation. An '*optimal translation*' would ideally require minimal CPU time and memory.

This is usually not possible. But optimizing compilers can approach this by improving generated code with various techniques. Therefore, code optimization aims at producing more proficient, faster, and shorter code without changing its effects.

The problem with naive code generation is that resulting code often contains redundancies when juxtaposed. These can easily be reduced with an effective optimization technique – **peephole optimization**.

The peephole optimizer is repeatedly passed over the Modified assembly code, performing optimizations until no further changes are possible.

Peephole optimization is an effective technique for locally improving the target code. small sequences of target code instructions are examined and replacement by faster sequences wherever possible. Common techniques applied in peephole optimization.

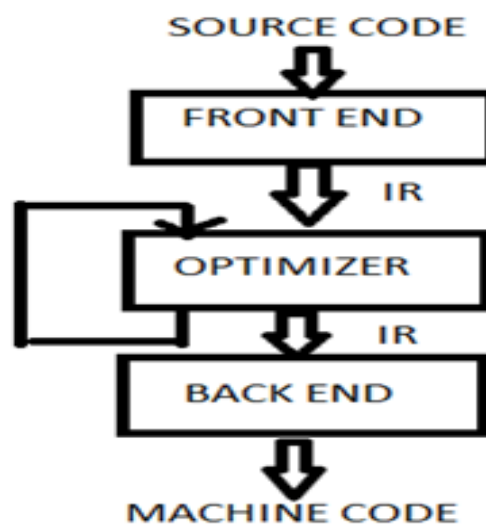


Fig 2: Optimization Level

- 1) Constant Folding
- 2) Strength Reduction
- 3) Null sequences
- 4) Combine Operations
- 5) Algebraic Laws
- 6) Special Case Instructions
- 7) Address Mode Operations
- 8) Copy Propagation

II. STRATEGIES

In peephole optimization technique, this part presents a formal analysis of the pattern matching strategies that have been implemented

1.1 Strategy Part



Fig 3: Peephole optimization as information processing problem

The main focus of this work is the strategy part shown in Fig 3, which is divided into two parts:

1.1.1 Pattern matching strategy:

This component particularly deals with the nature of the application of a single optimization rule to the input. Matching strategies that have been implemented in this work is the more primitive declarative, regular Expressions-based matching strategy, and a more abstract, object-oriented generic matching strategy.

1.1.2 Rule application strategy:

For this component, the grouping and ordering of the rules is analyzed as for a certain aim. In the implementation, the *backwards strategy* has been employed for both the *regular expressions strategy* and the *generic matching strategy*. The general matching policy has been extended with the ability to cascade rules, i.e. to control a number of rule application sequences.

III. CODE GENERATION STRATEGY

In order to understand the significance of the optimizations, it is necessary to understand something about typical code sequences produced by front ends for EM.

The traditional way to generate good code for commonly occurring statements is to build a myriad of special cases into all the front ends. For example, the statement $N := N + 1$ occurs often in many programs; so EM has a special INCREMENT VARIABLE instruction.

The normal approach would be to have the front end check all assignments to see if they can use this instruction. It is our belief that this approach is a mistake and that recognition and replacement of important instruction sequences should be done by the optimizer.

In fact, our basic intermediate file optimizer performs only this kind of peephole optimization; data flow and other optimizations can and should be done by other programs, cascading them in the manner of UNIX filters.

Coming back to the case of assignment statements, in general, assignment statements can be hard, such as $A[I + 1].FIELD1 := B[J * K].FIELD2[M]$

Although such statements measure rare, front ends should be ready to handle them consequently, the common strategy used by our front ends is to judge the address of the right-hand side, shove this address onto the stack, and then do a LOAD INDIRECT n instruction, which fetch the address through pop the address and pushes the n bite-long object starting at the address.

After that, the address of the left-hand part is also evaluated and pushed onto the stack, and then a STORE INDIRECT n instruction, which fetches the intended address and n-byte object from the stack and performs the store operation, is executed.

There are many special cases of the assignment statement that can be optimized, but the front ends ignore most of them, leaving the work to the optimizer.

Next to assignment statements, if statements are most common. Statements of the form if $A = B$ then. Occur far more frequently than other types; so the obvious EM code sequence consists of instructions to push A and B onto the stack followed by a BNE instruction, which pops 2 operands and branches to the else part if they are unequal.

At first look it might appear that six Bxx directions would be required within the EM architecture, for

xx = EQ, NE, LT, LE, GT, and GE, but fact is that many more are needed, since a entire set is needed for single-precision integers, pointers, floating-point numbers, double precision integers, unsigned integers, sets, etc.

To avoid this large number, EM has one compare instruction for each data type that pops two operands and replaces them with a -1, 0, or +1, depending on whether the first is greater than, equal or less than the second.

Then there are six Txx instructions for replacing this number with true (represented by 1) or false (represented by 0), it is based on the relational operator.

IV. OPTIMIZATION PATTERNS

The optimizer is driven by a pattern/substitute table consisting of a collection of lines. Each line contains a pattern part and a replacement part. A pattern or substitute part is composed of a consecutive sequence of EM instructions, all of which designate an opcode and some of which designate an operand. (By design, no EM instruction has more than one operand.)

The operands can be constants, references to other operands within the line, or expressions involving both
Pattern Replacement

- (1) LOV A INC STV A ~ INV A
- (2) LOV A LOV A + 2 ~ LDV A
- (3) LOC A NEG ~ LOC -A

It often occurs that the output of one optimization produces a pattern that itself can be optimized. In reality, this principle has been extensively used in the design of the optimization table to reduce its size. By repeating the matching process until no more matches can be found, patterns much longer than the longest optimization table entry can ultimately be replaced. After a replacement, the code pointer is moved back a distance equal to the longest pattern to make sure that no newly created matches are missed.

V. MEASURED RESULT

To measure the effect of the peephole optimizer, we have run two tests. In the first we compared the number of machine instructions in each optimized EM program with the number in the unoptimized EM program. Thus, for each program we have a number between 0.00 and 1.00 giving the number of instructions in the optimized program as a fraction of the original. This metric was chosen since it is independent of both the source language and the target machine and directly measures what the optimizer primarily attempts to do, namely, eliminate EM instructions. This metric can also be protected on theoretical grounds. EM code is really just glorified reverse Polish, in other words, the parse tree linearized into postfix order. Removal of an EM instruction typically corresponds to a removal of a node in the parse tree. Since object code size is typically proportional to parse tree size, such elimination normally has a straight impact on the final object code size. The dimensions presented below bear this out.

The occurrence frequencies per 1000 optimizations are shown in Table III which is labeled column EM. The median saving is 16 percent: one in six EM instructions is eliminated. The second test consisted of translating the optimized and unoptimized EM code into PDP-11 object code and comparing the number of bytes produced in each case. These results are given in Table III in the column labeled PDP-11.

The median reduction in the object code is 14 percent, close to the EM result. This closeness suggests that nearly all the EM optimizations are indeed reflected in the final object code. In 2 test programs, the optimized PDP-11 code was increased by 2 percent over the unoptimized code due to optimization 50; this was traced to a design error in the (original) EM to PDP-11 back end. (With the optimization the operands were actually stacked, whereas without it they were not.) This fault can merely be fixed, however.

On the basis of these results, we believe peep holing the intermediate code to be worthwhile, since the optimizer need only be written once, for all languages and every machines, and it in no way inhibits extra, more sophisticated optimizers, either on the source code, on the EM code, or on the target code. Moreover, the peephole optimizer is fast: 1140 EM instructions per CPU second on a PDP-11/ 45 excluding certain overhead not related to peephole optimization and 650 instructions per CPU second including all overhead. This speed was achieved without any special effort to tune the program.

It could easily be made faster still by hashing the pattern table instead of examining all patterns starting with the current op code

TABLE 4: DISTRIBUTION OF AMOUNT OF REDUCTION IN SIZE

Ratio	EM	PDP-11
<0.60	0	12
0.60-0.64	3	6
0.65-0.69	22	25
0.70-0.74	24	35
0.75-0.79	205	71
0.80-0.84	283	191
0.85-0.89	298	333
0.90-0.94	126	181
0.95-1.00	39	141
>1.00	0	4
Total	1,000	999a

a Not 1000 due to round off.[19].

VI. SUGGESTED RESEARCH SCHOP

Further suggestions for interesting extensions and improvements:

5.1 Labels table:

Since the labels table has proven to be useful, it should be utilized more. The current implementation of the look ahead matching procedure using the labels table covers two cases only.

These should be extended and more should be added. Then, as generic matching is currently employed at level 1 only, 'deeper' generic matching by means of the labels table might help finding complex structures like chains of jump instructions and label definitions, or other constructions.

Since this 'table' approach is a good way of accessing information quickly, another extension might consist of researching other constructs than jump instructions and label definitions for which a table might be useful. The aim here is to do more intelligent matching.

5.2 Extended generic strategy:

Basic improvements can be made concerning the maintenance of the options. For more challenging improvements first the look-ahead behavior should be analyzed closer with a good rules set and suitable test files. An extension might then attempt to automatically find the best look-ahead setting (or cascade) for the given assembly input before applying it. This would be a 'cascade of rule sequences'

5.3 New strategies:

The analysis of pattern matching strategies does not end with the generic ones. Other rule application and pattern matching strategies might be explored: it would be particularly interesting to combine generic matching with AI methods as a next step.

REFERENCE

- [1]. McKee man, W. M. (1965) Peephole optimization. CACM 8(7):443-444.
- [2]. Lamb, D. A. (1981) Construction of a Peephole Optimizer. Software-Practice & Experience 11(6):639-647
- [3]. Fraser, C. W. (1982) Copt, a simple, retargetable peephole optimizer. Software, available at <ftp://ftp.cs.princeton.edu/pub/lcc/contrib/copt.shar> (up 24/02/2005).
- [4]. Davidson, J. W., Fraser, C. W. (1980) The design and application of a retargetable peephole optimizer. ACM TOPLAS 2(2):191-202.
- [5]. Fraser, C. W. (1979) A compact, machine-independent peephole optimizer. POPL'79:1-6.
- [6]. Tanenbaum, A. S., van Staveren, H., Stevenson, J. W. (1982) Using Peephole Optimization on Intermediate Code. ACM TOPLAS 4(1):21-36.
- [7]. Davidson, J. W., Fraser, C. W. (1987) Automatic Inference and Fast Interpretation of Peephole Optimization Rules. Software - Practice & Experience 17(11):801-812.
- [8]. Davidson, J. W., Fraser, C. W. (1984) Automatic generation of peephole E optimizations. CC84:111-116.
- [9]. Kessler, P. B. (1986) Discovering machine-specific code improvements. CC86:249-254.
- [10]. Kessler, R. R. (1984) Peep - An architectural description driven peephole optimizer. CC84:106-110.
- [11]. STEEL, T.B., JR. UNCOL: The myth and the fact. Annu. Rev. Autom. Program. 2 (1960), 325-344.
- [12]. Warfield, J. W., Bauer, III, H. R. (1988) An Expert System for a Retargetable Peephole Optimizer. ACM SIGPLAN Notices 23(10):123-130.
- [13]. Davidson, J. W., Fraser, C. W. (1984) Register allocation and exhaustive peephole optimization. Software - Practice & Experience 14(9):857-865.
- [14]. Davidson, J. W., Fraser, C. W. (1984) Register allocation and exhaustive peephole optimization. Software - Practice & Experience 14(9):857-865.
- [15]. Aho, A. V., Ganapathi, M., Tjiang, S. W. K. (1989) Code Generation Using Tree Matching and Dynamic Programming. ACM TOPLAS11(4):491-516.
- [16]. Fraser, C. W., Wendt, A. L. (1986) Integrating Code Generation and Optimization. Proceedings of the SIGPLAN'86 symposium on Compiler Construction, pp. 242-248.

ICT Practice in Morocco's innovative teachers

Ahmed Lablidi, Brahim Nachit, Abdelmjid Abourriche, Abdelwahed Namir,
Mohammed Talbi

¹The National Center of Educational Innovation and Experimentation (NCEIE)
TVI. Av. Mehdi Ben Barka. Souissi.1200 Rabat.

²Laboratory of Information Technology and Modeling (LTIM), University Hassan -II- Mohammedia,
Casablanca, Morocco.

³Observatory for Research in Didactics and University Pedagogy (ORDUP), University Hassan -II-
Mohammedia, Casablanca, Morocco.

⁴College of Sciences Ben M'Sik, University Hassan II-Mohammedia, Casablanca, Morocco.

Abstract: The integration of Information and communication technology (ICT) in Moroccan schools forms one of the strategic levers of Ministry of National Education (MNE) to improve the quality of teaching and learning. Thus, the training teacher actions to the use of ICT in the classroom, the creation of institutional structures and the introduction of incentives for innovation in ICT accounted for the actions taken by the MNE to support teachers and help them to appropriate ICT tools and using them in their courses. Some teachers have more or less successful betting. This observation led us to question ourselves about the integration process of ICT which enabled them to distinguish themselves from the masses. The laid hypothesis is that the ICTs appropriation and their use in teaching practices is the result of a process that is located on a continuum ranging from non-use of ICT in their regular use.

Keywords: *ICT, appropriation, innovation, ICT integration, innovative teachers*

I. INTRODUCTION

The ICT enter the world of education and work. Their use requires knowledge, new skills and therefore the development of other routines in teaching and learning. Consequently, needed efforts are to deploy training capable persons to raise the innovation challenge that can negotiate the turn of the desired change. Thus, the Moroccan Educational System has focused on ICT for its potential benefit teaching and learning in order to make learning more attractive and to develop skills in information literacy and its modes of access and treatment. Therefore, the strategy of the Education Ministry, regarding the introduction of ICT at schools in particular, has focused on three different axes but complementary. It is the training, equipment and digital content. We mainly devoted this study from the latter axis representing the interest part in the action of teaching and learning.

II. PROBLEMATIC

If it's currently acquired, especially with Web 2.0, that the digital contents are accessed via the Internet and in large quantities, it does not remain less than their quality and adaptability are not always satisfactory and their integration is very slow [1]. Most teachers who use the Internet for pedagogical purposes, when they find resources, do not use them in class, these resources are in French or English and often incompatible with the Moroccan program. The teachers need to have available digital resources that are consistent with the learning objectives and consistent with the curriculum and existing programs. Then, the Ministry of National Education has initiated two actions:

The first consists of the creation of digital laboratory resources whose mission is the acquisition of

digital resources through private providers in international and national level.

The second encourages teachers to the production of digital content in the various disciplines and the best projects are awarded each year through a national competition called "Innovatice".

Only, it was found that during the seven years of the competition, the participation of teachers is very limited in terms of their workforce (more than three hundred thousand teachers). This leads us to the following question: Why some teachers do innovate teaching practices through ICT and other do not? The assumption is that the appropriation of ICT in teaching practice is the result of an integration process of ICT on a continuum ranging from non-use to a regular use one.

III. CONCEPTUAL FRAMEWORK

3.1 The concept of ICT integration

In Education, several studies have approached the phenomenon of the ICT integration at schools to study the role of ICT tools in teaching and learning, and analyze the process of their integration into practice teachings [2-3-4].

Thus, the concept of ICT integration has been associated with various meanings, including that we found in [2] and for the continuous and regular use of ICT tools in the classroom by teachers than by students. Dias (quoted in [2]) suggests, in addition to regular use, the context that will encourage active learning and support teaching.

Moreover, some studies have dealt with the integration of ICT in terms of change induced by technological innovations. Thus, the integration of ICT was considered as the process of realizing the changing levels of ICT use in personal, professional and educational practice of teachers [5-2-3].

3.2 The concept of appropriation

When the appropriation concept is associated with ICT, it has a positive connotation in the literature, because it is generally desirable to try appropriating ICT to make of it the best possible use. However, if the positive appropriation connotation of ICT does not seem uncontroversial, a common definition of the concept is far from being achieved.

Some define it as the result of a process, for example, Proulx [7-8-9], who considers appropriation as the result of a sequential process, requiring as Breton and Proulx, meeting three social conditions: to appropriate for a technical object, the individual must actually demonstrate a minimum technical and cognitive mastery of this tool. This mastery will creatively incorporate its current practices. In addition, the appropriation must give rise to opportunities for diversion, reinventions and direct contributions from users in the design.

While other researchers consider the appropriation as the process itself, for example, De Vaujany considers appropriation as a long process that begins long before the use phase of the technical object and continues after for a long time "first routinization use." [10]. So he divided the appropriation process in three phases: "Pre-appropriation" which refers to the initial discussions on the evocation of a technical object, followed by the phase of "original appropriation" where multiple socio-political processes and psycho cognitive are active in the organization, with emergence possibility of a strained relationship, then mitigated by the introduction of new routines, and finally, the final phase of the process with final installation routines.

IV. METHODOLOGY

The theoretical framework has distinguished a number of stages in the integration of ICT from non-use to the exemplary and routine use [5-2-6]. Thus, it is possible to broadly categorize teachers' practices in relation to the levels of ICT integration. Here, the purpose of this study is to determine what level of integration are the Moroccan teachers with respect to innovative uses of ICT.

We opted for the qualitative analysis of ICT use in connection with the innovative practices of teachers to highlight information that shows how ICT is used by innovative teachers. The interview technique was used as a tool for data collection.

4.1 Search tool: the interview

We chose to use the interview, because it is a way for the researcher to obtain the information that appears elsewhere [11]. For Mayer and Ouellet [12] "We speak of semi-directive interview when the researcher uses an interview guide that allows to focus on some of the narrators about limited topics by the research object" (p.456). For this, we developed an interview guide for innovative teachers. The choice of the semi-directive interview seem the best suited to the exploration of respondents' reports with predefined themes in the interview guide.

4.2 Context and Sample constitution

Inspired by the work of Raby [2] on the ICT exemplary integration to primary school teachers, we selected a sample of teachers who received awards contest "Innovatice" to maintain their relationship with ICT, their path in the use of technology in the classroom, personal, social and professional factors which enabled them to succeed and to collect their views on how to integrate ICT in teaching.

The identification of innovative teachers was facilitated by our professional position and our network contacts within the Innovative Teachers Association and at the level of central service dealing with contest.

4.3 Brief overview of "Innovatice"

The project "Innovatice" is the Moroccan version of the program "Innovative Teachers" that Microsoft worldwide launched. As part of this program, it is organized every year and for each country "Innovative Teachers Forum" known in Morocco under the same name "Innovative Teachers Forum". In the context of educational reform and the emergency program, the Ministry of National Education and Microsoft organize the annual Innovative Teachers Forum. This is a national competition of innovative projects in the use of information and communication technology in education. This contest is open to all teachers who have realized pedagogical projects aimed at improving the quality of their teaching. It has as an objective to "Strengthen the capacity of human resources working in the education sector, particularly teachers, to encourage teachers to embrace a conducive attitude to innovation. Assist teachers with ICT skills to better prepare their students. "

The first forum was held in 2005 and since then a hundred teachers from elementary, middle and high schools participate yearly in the competition by submitting their ICT projects to a national committee that chooses the best. The table below shows the evolution of the participation level of 16 Regional Academies for Education and Training (RAET). The National Center of Educational Innovation and Experimentation (NCEIE) recorded that the winning projects for all disciplines concerns Arabic, Physics-Chemistry, Mathematics and French.

Table 1: Evolution of participation in the Innovative Teachers Forum

Year	Teachers	Academy
2005	227	14
2006	235	14
2007	159	16
2008	207	16
2009	197	16
2010	261	16

Source: NCEIE

On the six editions that account the forum to its credit, 71 teachers were awarded. According to NCEIE sources, the number of participants is a little higher among primary school teachers and the participation of female teachers is far below than that of male teachers. Winners share on all RAET and the event history clearly shows that some RAET are more present than others and their share award is higher.

4.4 Constitution Sample

We used the randomly probabilistic sampling technique since we have the list of the award-winning teachers. "The use of this sampling probabilistic technique cannot be done if the researcher has a list of all the units of the parent population and each unit is numbered." [13], (p: 217). Thus, using this technique, we ended up with the following sample:

Table 2: Sample Characteristics

Teachers	RAET	Cycle	Discipline	Award year
E1	L'oriental-Oujda	Secondary school	Technology	2006
E2		Secondary school	Music Education	2010
E3	Sous-Massa- Draa	Primary school	Amazigh	2009
E4		Primary school	French	2010
E5	Meknes-Tafilalt	High school	Physics	2005
E6	Chaouia-	High school	History and Geography	2008
E7	Grand Casablanca	Primary school	Mathematics	2009

The individual interviews were conducted depending on the participants' availability that we contacted in advance regarding the appointment, sending the interview guide and agree with the communication tool to use during the interview. On our proposal, the teachers agreed that we use the tool of the audio conference «SKYPE" allowing to converse by text and phone. The duration of each interview was 30 min.

The interview guide questions the variables of our research related to the ratio of innovative teachers to ICT, their careers in ICT, personal experience, professional and pedagogical use of ICT in life, at school and especially in the classroom and their perception of ICT role in the teaching and necessary conditions for their integration in pedagogical practice

4.5 Methodology Limits

The study we conducted took place with teachers that are interested in ICT issues. Among these earned teachers due to the use of ICT in the classroom, we went to see teachers who are recognized by the Ministry as good example user of ICT. Thus, the selected population is characterized by its willingness to integrate ICT into their practice; commitment and involvement of teachers facilitated the work of the researcher, and prevents the investigation to be biased by contextual considerations.

Another weakness relative to the data collection is related to the credibility of the provided information by respondents; some may just answer to satisfy us. Note, however, that a sample of seven innovative teachers only for interviews from a larger population implies limitations to the result generalization.

Lexica has facilitated the work of selection, coding, annotations, grouping and comparing data. Some functionalities have been of a great help in individual analyzes and comparisons of this research.

Thus, in the light of the literature requirements, the process of content analysis first focused on the transcripts of interviews Verbatim data [14-15] and reading the Verbatim several times, attention has been paid to this point especially on the clear and explicit aspect of content of the interviews in terms of our framework [16].

V. RESULTS

5.1 Participant profiles

The innovative teachers being accepted to participate in the survey are seven, two women and five men, their average age is 35, the youngest is 28 years old and the older is 56. They are experienced (at least 6 years teaching) and represent the three levels of education (3 of elementary, 2 of secondary school and 2 of high school). All participants have a university degree and have completed initial training preparing for the teaching profession and continuous training on the pedagogical use of ICT. All were awarded for their production of digital resources (application, tutorial, scenario ICT).

5.2 ICT Integration Context

Professional context

7 Innovative teachers practice in urban schools in which the average class size is 34 students. Students have the opportunity to exploit the hardware (fixed SMM, mobile MMS and IWB) at least once a week. The majority of participants have the administrative and pedagogical support to develop the use of ICT in teaching and to share expertise techno-pedagogical between teachers.

Technological Context

All innovative teachers have their own laptops and Internet connection at home. Schools where they work are also equipped with fixed multimedia classrooms (7 schools), IWB (4 schools) and mobile multimedia classrooms (2 schools). All classrooms are connected to the Internet. So, the 7 Innovative Teachers operate in a personal and professional environment marked by the presence of technologies they can use in their work either inside or outside school and thus have more time access to ICT.

5.3 Place of ICT in teachers practices

5.3.1 Personal practices of ICT

It is understood by the ICT personal practices, all activities that the teacher leads outside school, on personal time using ICTs to realize those activities. Thus, it is possible to quote homework when the teacher uses ICT to communicate with others, seeks information and produces personal documents (home financial management, pays bills online, shopping on commercial sites ...).

The seven participants felt that personal use of ICT is an inescapable reality dictated by the demands of today's society. They believe that ICTs are now a part of the social landscape of individuals and communities.

Invested time

Encountered innovative teachers affect an average of two hours per day for personal use of ICT. Without exception, the seven participants reported regular use of ICT outside the school. Encouraged in this by the spread of Wi-Fi in cafes in most urban areas. Thus, teachers have the opportunity to use ICT in public areas (cafes, libraries...) are more likely to provide access points to the network. At home, the operating time is proportional to the number of activities and their nature. In addition to personal activities listed above, the teacher is sometimes forced to use ICT to review with his children, help them to provide evidence or support in the effective use of research tools, treatment or storage.

It is obvious that the invested time in the personal use of ICT is growing under the leadership of social environments that give to the citizen the means of access to ICT, in addition to the fact that the teachers' houses are increasingly equipped with computer and internet.

Levels of ICT personal practices

The data analysis revealed that the interviewed teachers justify a long experience in personal use of ICT (minimum 6 years). 4 teachers have begun to use innovative ICT before they integrate professional life. For two of them, the interest in ICT began at the university. The other two teachers state that the first contact with ICT has been in a personal use.

The analysis showed that the motivations behind ICT personal practices of 4 teachers are different. Thus, if the curiosity motivated one of them, the second was motivated by the discovery need. So the need for development has motive the two other teachers.

Considering of the experience of teachers in ICT, they all have gone through all stages of ICT integration process. The regular use of ICT in personal practices of the seven teachers put them in the stage of appropriation-routinization [5]. Indeed, this use shows that these teachers have the technical mastery and frequent use in daily life.

5.3.2 ICT Professional Practices

It is good to recall that the ICT professional practices refers to the use of ICT tools in information and communication activities, documentary research, production and storage of documents for professional purposes.

It stands out the results of the data analysis that three teachers on seven had their first contact with ICT in a professional setting. The trigger point was the ICT training they attended.

Levels of ICT Professional Practice

Some teachers have gone directly to the stage of "motivation to stage of appropriation-routinization." Lack of familiarization stage in four teachers is explained by the fact that they all started to use ICT before they integrate teaching. Remaining three, with no personal experience of ICT, they began to take an interest in ICT in professional practice; their practices have evolved step by step to arrive at the current appropriation-routinization.

The seven teachers used ICT in different ways. All have used ICT to communicate with colleagues, administrators and with students, to plan courses to prepare pedagogical materials, to find information on professional topics and manage student assessment.

As the seven teachers were awarded in the national competition "Innovative", they believe that their consecration is recognition of MNE of their ICT use skills. Asked about their feelings after the competition results, the majority of them highlight aspects of personal development and improving self-image.

The award-winning productions of innovative teachers indicate a desire to improve teaching practices by exploiting the ICT potential. If the tools are diversified and contents differ from one teacher to the other, the goal remains common and shared: the adoption of the posture of reflexive teacher changing its personal practice to the light of changes observed and takes advantage of the technological context to bring more value to our professional services. This goal was realized through websites, pedagogical scenarios and simulation applications or interactive exercises. We will quote some examples below:

The first example is an educational site for Mathematics activities offering activities of support online and outside school hours. It also includes information for teachers and some practices for sharing.

Three other teachers have also developed websites; 2 sites for each disciplinary learning Amazigh and the other for arts education (music).

The third deals with pedagogical and technological content that might interest the teachers.

A female primary school teacher preferred to work on the production of a pedagogical scenario dealing with the

integration of ICT in the course of scientific openness.

And production of a different nature were realized, it was simulation of physical phenomena, or interactive exercises in electronics.

VI. CONCLUSION

Teachers who have better integrated ICT tools in their teaching practice are often teachers who have completed one or more training on the use of ICT. Motivated, and having a direct and permanent access to ICT (school, home ...) innovative teachers have become producers of quality digital resources. Thus, it is clear that the right technical level of teachers is the result of a process of ICT appropriation which has enabled them to run frequent and regular use of technology in personal and professional practices.

The results of the study have also shown that the levels of ICT integration in teaching practices vary depending on whether they are personal, professional and pedagogical. In other words, teachers use ICT more regularly especially in personal practices and have a great mastery of the software and related applications (digital photos, business transaction, personal blog ...).

VII. ACKNOWLEDGEMENTS

We thank Mr. Mostafa BAHAT and the staff of The National Center for Educational Innovation and Experimentation (NCEIE) for their help in the realization of this work.

REFERENCES

- [1]. Combes, M.-C., Guin, D., Noguès, M. & Trouche, L. (2005). Formation à distance des professeurs de mathématiques, vers de nouvelles pratiques professionnelles. In J. Morego, C. Rocardembosch & M. Vendrell (Eds.), Rapport TRANSFORMA. Barcelone : UOC.
- [2]. Raby, C. (2004). Analyse du cheminement qui a mené des enseignants du primaire à développer une utilisation exemplaire des technologies de l'information et de la communication (TIC) en classe. Thèse de doctorat, Université du Québec à Montréal. Consulté en ligne: <http://archive-edutice.ccsd.cnrs.fr/edutice-00000750>
- [3]. Savoie-Zajc, L. (1993). Les modèles de changement planifié en éducation. Montréal: Les Editions Logiques Inc.
- [4]. Karsenti, T., Savoie-Zajc, L. et Larose, F. (2001). Les futurs enseignants confrontés aux TIC : Changements dans l'attitude, la motivation et les pratiques pédagogiques. *Éducation et Francophonie*, 29 (1). Document électronique accessible par Internet : www.uqah.quebec.ca/karsenti/karsenti-savoie-larvf.pdf.
- [5]. Depover, C. Strebelle, A. (1997). Un modèle et une stratégie d'intervention en matière d'intégration des TIC dans le processus éducatif. In : Pochon, L. -O. Blanchet, A. (dir). *L'ordinateur à l'école: De l'introduction à l'intégration*. Neuchâtel: Institut de recherche et de documentation pédagogique (IRDPA), p.73-98).
- [6]. Coen, PF. Schumacher, J. (2006) Construction d'un outil pour évaluer le degré d'intégration des TIC dans l'enseignement. *Revue internationale des technologies en pédagogie universitaire*, 3. 7-17. En ligne consulté le 12/01/2013. www.profetic.org/revue.
- [7]. Proulx, S. (2001b). Usages de l'Internet: la 'pensée-réseaux' et l'appropriation d'une culture numérique. *Comprendre les usages de l'Internet*. G. E. Paris, Presses de l'Ecole Normale Supérieure: 139-145.
- [8]. Proulx, S. (2001a). Les formes d'appropriation d'une culture numérique comme enjeu d'une société du savoir. *Gouvernance et usages d'Internet: vers un nouvel environnement normatif?* G. E. Montréal, Université de Québec à Montréal: 139-145.
- [9]. Proulx, S. (2002). Trajectoires d'usages des technologies de communication: les formes d'appropriation d'une culture numérique comme enjeu d'une société du savoir. *Annales des Télécommunications* 57(Mars - Avril): 180-189.
- [10]. De Vaujany, F.X. (2005). De la pertinence d'une réflexion sur le management de l'appropriation des objets et outils de gestion. De la conception à l'usage: vers un management de l'appropriation des outils de gestion. Paris, Editions Management.
- [11]. Mace, FC. Hock, ML. Lalli, JS. West, BJ. Belfiore, P. Pinter, P. (1988). Dynamique comportementale dans le traitement de non-conformité *Journal of Applied Behavior Analysis*. 21:123-141
- [12]. Mayer, R. Ouellet, F. (1991). *Méthodologie de recherche pour les intervenants sociaux*, Éd. Gaëtan Morin. Boucherville. 537 p.
- [13]. Dépelteau, F. (2011). La démarche d'une recherche en sciences humaines - De la question de départ à la communication des résultats. Bruxelles. Ed. De Boeck.
- [14]. Tesch, R. (1990). *Qualitative Research: Analysis types and software tools*, New York, Falmer
- [15]. Savoie-Zajc, L. (2000). La recherche qualitative/interprétative en éducation. In T. Karsenti et L. Savoie-Zajc (Dir.), *Introduction à la recherche en éducation* (p. 171-198). Sherbrooke, Québec: Éditions du CRP.
- [16]. Van der Maren, J.M. (1995). *Méthodes de recherche pour l'éducation*. Montréal : Les Presses de l'Université de Montréal.

Biodergradable Polymers in Food Packaging

P.A.Pawar, Aachal.H.Purwar

Department of Chemical Technology, Sant Gadge Baba Amravati University, Amravati.

Abstract: In recent years, there has been a marked increase in the interest in use of biodegradable materials in packaging. The principal function of packaging is protection and preservation of food from external contamination. This function involves retardation of deterioration, extension of shelf life, and maintenance of quality and safety of packaged food. Biodegradable polymers are the one which fulfill all these functions without causing any threat to the environment. The belief is that biodegradable polymer materials will reduce the need for synthetic polymer production (thus reducing pollution) at a low cost, thereby producing a positive effect both environmentally and economically.

Keywords: *Biodegradable · Deterioration · Shelf life · Synthetic polymer*

I. INTRODUCTION

As well known, synthetic polymer materials have been widely used in every field of human activity during the last decades. These artificial macromolecular substances are usually originating from petroleum and most of the conventional ones are regarded as non-degradable. However, the petroleum resources are limited and the blooming use of non-biodegradable polymers has caused serious environmental problems. In addition, the non-biodegradable polymers are not suitable for temporary use such as sutures. Thus, the polymer materials which are degradable and/or biodegradable have being paid more and more attention since 1970s. Food is the necessity of our day to day life. Now a day's most of the food items are packed. In everyday life, packaging is an important area where biodegradable polymers can be used. The primary factors driving development of the biodegradable packaging market include the increase in crude oil prices, which has narrowed the price differential; consumer demand; the proliferation of convenience packaging; development of new applications for bioplastics; increased economic viability as production ramps up and unit costs decrease, and development of the composting infrastructure for optimal disposal of bioplastic products. Even so, consumer demand for products that are environmentally friendly, safer and nontoxic, as well as, a currently favorable economic scenario leads to the conclusion that biodegradable packaging products will become increasingly popular.

In order to reduce the volume of waste, biodegradable polymers are often used. Besides their biodegradability, biopolymers have other characteristics as air permeability, low temperature sealability, availability and low price. Several biopolymers such as starch, cellulose, chitosan, PLA, PCL, PHB etc. are used for packaging purposes. The current trend in food packaging is the use of blends of different biopolymers like starch-PLA blends, starch-PCL blends etc. Bottles, jars, vials; drums, pails, cans, barrels, buckets; caps, closures, aerosol parts, packaging films, food containers, disposable cups; coating for all types of packaging, packaging bags, household and institutional refuse bags and film; boxes and baskets etc. are being manufactured by using biodegradable polymers. Many companies like Novamont, BASF, Biomer, National starch, DuPont etc. are producing biopolymers.

What are Polymers?

Polymer materials are solid, non-metallic compounds of high molecular weights (Callister 1999). They are comprised of repeating macromolecules, and have varying characteristics depending upon their composition. Each macromolecule that comprises a polymeric material is known as a mer unit. A single mer is called a monomer, while repeating mer units are known as polymers. A variety of materials (both renewable and non-renewable) are employed as feedstock sources for modern plastic materials. Plastics that are formed from non-renewable feedstocks are generally petroleum based, and reinforced by glass or carbon fibers (Williams et al.

2000). Renewable resource feedstocks include microbial-grown polymers and those extracted from starch. It is possible to reinforce such materials with natural fibers, from plants such as flax, jute, hemp, and other cellulose sources (Bismarck et al. 2002).

What are Biopolymers?

Biopolymers are long chain compounds made up of long chain molecule subunits. A biopolymer is any organic polymer. Biopolymers have been around for billions of years longer than synthetic polymers like plastics. Well

Known biopolymers include starch, proteins and peptides, DNA, and RNA. Together these make up much of our bodies and the majority of the biosphere. These are biodegradable, ecofriendly and are obtained from natural sources.

Biopolymers are polymers that are generated from renewable natural sources, are often biodegradable, and not toxic to produce. They can be produced by biological systems (i.e. micro-organisms, plants and animals), or chemically synthesized from biological starting materials (e.g. sugars, starch, natural fats or oils, etc.). Biopolymers are an alternative to petroleum-based polymers (traditional plastics).

Origin and description of biobased polymers

Biobased polymers may be divided into three main categories based on their origin and production:

Category 1: Polymers directly extracted/removed from biomass. Examples are polysaccharides such as starch and cellulose and proteins like casein and gluten.

Category 2: Polymers produced by classical chemical synthesis using renewable biobased monomers. A good example is polylactic acid, a biopolyester polymerized from lactic acid monomers. The monomers themselves may be produced via fermentation of carbohydrate feedstock.

Category 3: Polymers produced by microorganisms or genetically modified bacteria. To date, this group of biobased polymers consists mainly of the polyhydroxyalkanoates, but developments with bacterial cellulose are in progress.

The three categories are presented in schematic form in Figure.1 below:

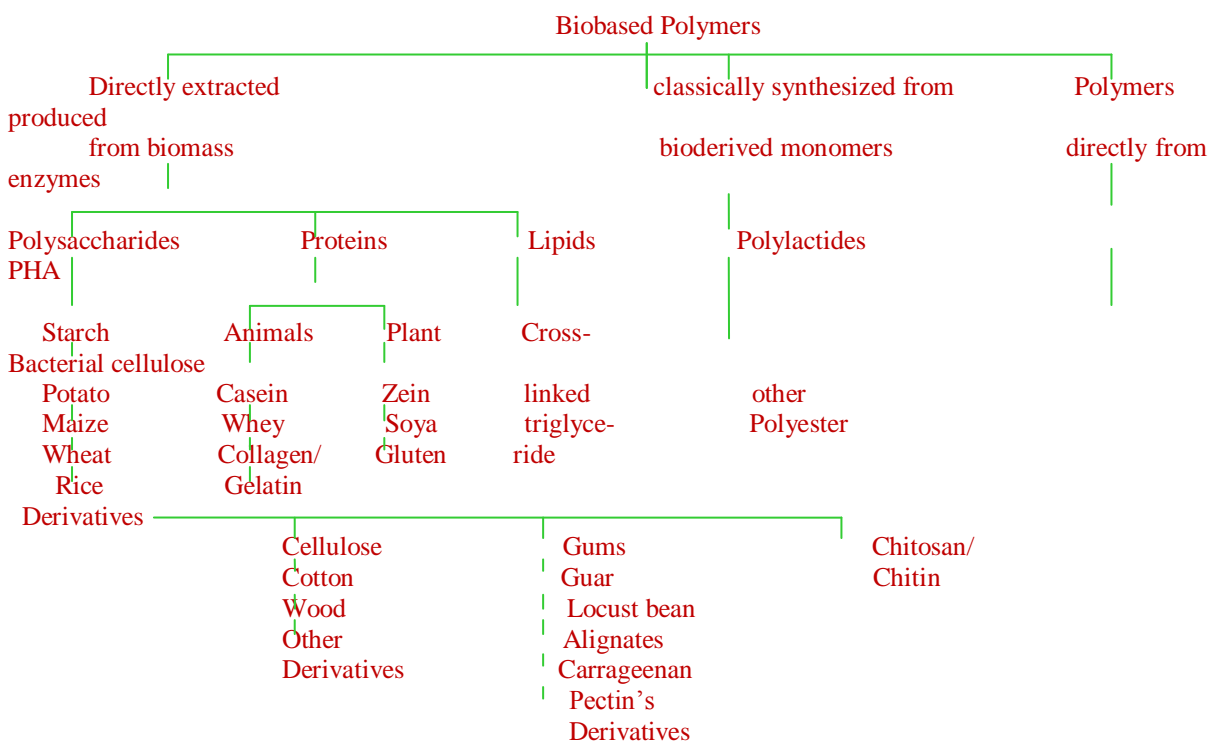


(Figure.1: Categories of biopolymers)

Starch

Starch is a well-known hydrocolloid biopolymer. It is a low cost polysaccharide, abundantly available and one of the cheapest biodegradable polymers.

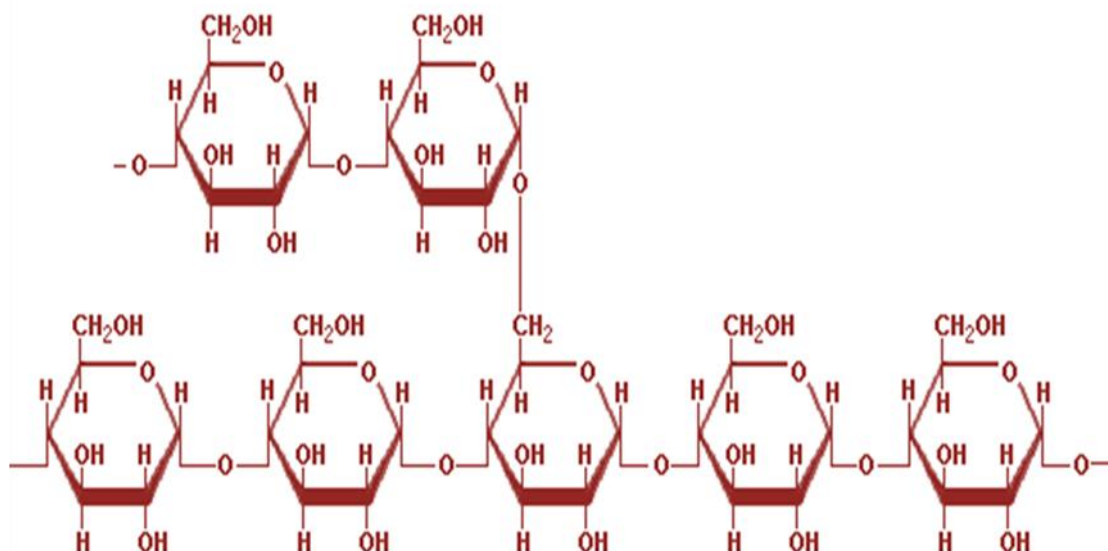


(Figure.2 : Molecular structure of starch)

Starch is produced by agricultural plants in the form of granules, which are hydrophilic. Starch is mainly extracted from potatoes, corn, wheat and rice. It is composed of amylose (poly- α -1, 4-D-glucopyranoside), a linear and crystalline polymer and amylopectin (poly- α -1, 4-D-glucopyranoside and α -1, 6-D-glucopyranoside), a branched and amorphous polymer. Starch has different proportions of amylose and amylopectin ranging from about 10–20% amylose and 80–90% amylopectin depending on the source. Amylose is soluble in water and forms a helical structure. The relative amounts and molar masses of amylose and amylopectin vary with the starch source, yielding to materials of different mechanical properties and biodegradability (Fredrikson et al. 1998, Ratnayake et al. 2001). As the amylose content of starch increases, the elongation and strength increase too. The stability of starch under stress is not high. The glucoside links start to break at 150 °C and above 250 °C the granules collapse. Retrogradation, i.e. reorganization of hydrogen bonds, is observed at low temperatures, during cooling. In its applications starch can be mixed, kept intact, and used in various resins as a filler or melt for blending compounds. In the former form, fillers are starch whiskers used with polymer resins.

Starch is usually used as a thermoplastic. It is plasticized through destructureation in presence of specific amounts of water or plasticizers and heat and then it is extruded. Thermoplastic starch (TPS) has a high sensitivity to humidity. Thermal properties of TPS have been shown to be more influenced by the content of water than the starch molecular weight. TPS thus obtained is almost amorphous. Biodegradation of starch is achieved via hydrolysis at the acetal link by enzymes (Chandra and Rustgi 1998, Claus 2000). The α -1, 4 link is attacked by amylases while glucosidases attack the α -1, 6 link. The degradation products are non toxic.

Polylactic acid

PLA is usually obtained from polycondensation of D- or L-lactic acid or from ring opening polymerization of lactide, a cyclic dimer of lactic acid. Two optical forms exist: D-lactide and L-lactide. The natural isomer is L-lactide and the synthetic blend is DL-lactide. Other different synthetic methods have been studied too. PLA is a hydrophobic polymer due to the presence of $-\text{CH}_3$ side groups. It is more resistant to hydrolysis than PGA because of the steric shielding effect of the methyl side groups. The typical glass transition temperature for representative commercial PLA is 63.8 °C, the elongation at break is 30.7% and the tensile strength is 32.22 MPa (Briassoulis 2004). Regulation of the physical properties and biodegradability of PLA can be achieved by employing a hydroxy acids co monomer component or by racemization of D- and L- isomers (Sodegard and Stolt 2002). A semi-crystalline polymer (PLLA) (crystallinity about 37%) is obtained from L-lactide whereas poly (DL-lactide) (PDLLA) is an amorphous polymer (Vert 2002). Their mechanical properties are different as are their degradation times (Auras et al. 2004). PLLA is a hard, transparent polymer with an elongation at break of 85%-105% and a tensile strength of 45-70 MPa. It has a melting point of 170-180 °C and

a glass transition temperature of 53 °C (Mochizuki and Hirami 1997). PDLLA has no melting point and a T_g around 55 °C. It shows much lower tensile strength (Rutot and Dubois 2004).

PLA has disadvantages of brittleness and poor thermal stability. PLA can be plasticized to improve the chain mobility and to favor its crystallization. Plasticization is realized with oligomeric acid, citrate ester or low molecular polyethylene glycol (Jacobsen and Fritz 1999). High molecular weight PLAs are obtained through ring opening polymerization. This route allows also the control of the final properties of PLA by adjusting the proportions of the two enantiomers (Okada 2002). Other routes are melt/solid state polymerization (Maharana et al. 2009), solution polymerization or chain extension reaction (Zeng et al. 2009). High molecular weight PLA has better mechanical properties (Perego et al. 1977).

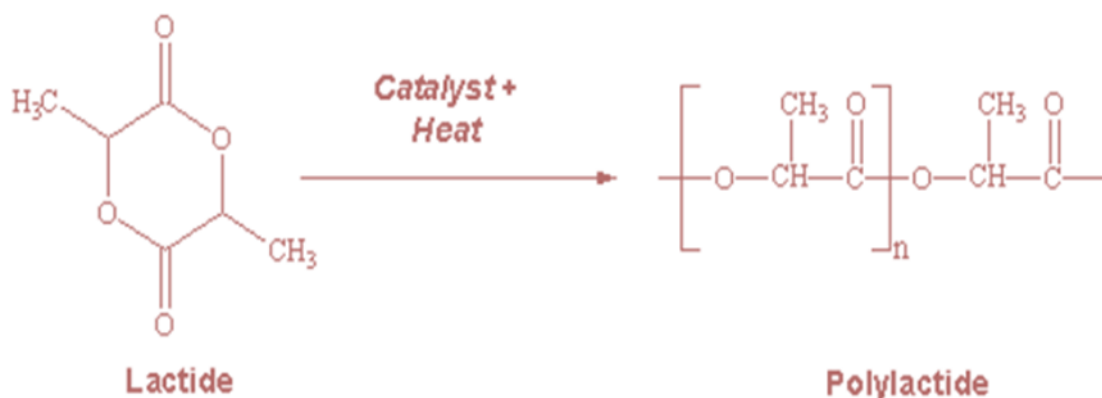


(Figure.3: Schematic view of the ring-opening polymerization reaction of poly(lactide) from lactide, a dimer of lactic acid.)

The rate of degradation of PLA depends on the degree of crystallinity. The degradation rate of PLLA is very low compared to PGA; therefore, some copolymers of lactide and glycolide have been investigated as bioresorbable implant materials (Miller et al. 1977). The biodegradability of PLA can also be enhanced by grafting. The graft copolymerization of L-lactide onto chitosan was carried out by ring opening polymerization using a tin catalyst. The melting transition temperature and thermal stability of graft polymers increase with increasing grafting percentages. As the lactide content increases, the degradation of the graft polymer decreases (Luckachan and Pillai 2006).

Poly (hydroxyalkanoates) (PHAs)

PHAs, of which poly (hydroxybutyrate) (PHB) is the most common, are accumulated by a large number of bacteria as energy and carbon reserves. Due to their biodegradability and biocompatibility these biopolyesters may easily find numerous applications. The properties of PHAs are dependent on their monomer composition, and it is, therefore, of great interest that recent research has revealed that, in addition to PHB, a large variety of PHAs can be synthesized by microbial fermentation. The monomer composition of PHAs depends on the nature of the carbon source and microorganisms used. PHB is a typical highly crystalline thermoplastic whereas the medium chain lengths PHAs are elastomers with low melting points and a relatively lower degree of crystallinity. A very interesting property of PHAs with respect to food packaging applications is their low water vapor permeability which is close to that of LDPE (Claus 2000).

Since 1925, PHB is produced biotechnologically and was attentively studied as biodegradable polyester (Zhang et al. 1997). The R alkyl substituent group is methyl. PHB is highly crystalline with crystallinity above 50%. Its melting temperature is 180 °C. The pure homopolymer is a brittle material. Its glass transition temperature is approximately of 55 °C. It has some mechanical properties comparable to synthetic degradable polyesters, as PLA (Savenkova et al. 2000). During storage time at room temperature a secondary crystallization of the amorphous phase occurs. As a result, stress and elongation modulus increase ($E = 1.7$ GPa) while the polymer becomes more brittle and hard. Elongation at break is then much lower (10%) (El.Hadi et al. 2002). Compared to conventional plastics, it suffers from a narrow processability window (Barham and Keller 1986). PHB is susceptible to thermal degradation at temperatures in the region of the melting point (Grassie et al. 1984). To make the process easier, PHB can be plasticized, with citrate ester.

PHB resembles isotactic polypropylene (iPP) in relation to melting temperature (175-180°C) and mechanical behavior. PHBs T_g is around 9°C and the elongation to break of the ultimate PHB (3- 8%), which is markedly lower than that of iPP (400%). Incorporation of 3HV or 4HB co-monomers produces remarkable

changes in the mechanical properties: the stiffness and tensile strength decrease while the toughness increases with increasing fraction of the respective co-monomer (Claus 2000). PHB is degraded by numerous microorganisms (bacteria, fungi and algae) in various environments (Kim et al. 2000). The hydrolytic degradation yields to the formation of 3-hydroxy butyric acid, a normal

constituent of blood, nevertheless with a relatively low rate. Different monomers have been grafted onto PHB to prepare biodegradable polymers to be used for wastewater treatments. The grafted monomers were either hydrophilic as acrylic acid or sodium-pstyrene sulfonate, or hydrophobic as styrene or methyl acrylate (Hsieh et al. 2009). The degree of grafting was different according to the monomers, increasing with the following order styrene, sodium-p-styrene sulfonate, methyl acrylate and acrylic acid.

Multicomponent polymeric systems containing PHB have been obtained by two ways. The first is a radical polymerization of an acrylic polymer in the presence of PHB. The second consists in melt mixing PCL with PHB. Peroxide is used in both processes to form intergrafted species responsible for compatibilization (Avella et al. 1996). These methods have been considered as reactive blending. It should be noted that apart from the bacterial synthetic way, other chemical ways have been developed for the production of PHB. The ring opening polymerization of β -butyrolactone yields to PHB too (Sheldon et al. 1971, Hori et al. 1996, Juzwa and Jedlinski 2006). Different structures are obtained according to the synthesis route. An isotactic polymer with random stereo sequences is obtained via bacterial process while a polymer with partially stereo regular block is obtained via chemical synthesis. Applications that have been developed from PHB and related materials (e.g. Biopol) can be found in very different areas and cover packaging, hygienic, agricultural, and biomedical products. Recent application developments based on medium chain length PHAs range from high solid alkyd-like paints to pressure sensitive adhesives, biodegradable cheese coatings and biodegradable rubbers. Technically, the prospects for PHAs are very promising. When the price of these materials can be further reduced, application of biopolyesters will also become economically attractive (Claus 2000).

Polycaprolactone (PCL):

Poly- ϵ -caprolactone is a relatively cheap cyclic monomer. A semi-crystalline linear polymer is obtained from ring-opening polymerization of ϵ -caprolactone in presence of tin octoate catalyst (Mochizuki and Hiramami 1997). PCL is soluble in a wide range of solvents. Its glass transition temperature is low, around -60°C , and its melting point is $60 - 65^\circ\text{C}$. PCL is a semi-rigid material at room temperature, has a modulus in the range of low-density polyethylene and high-density polyethylene, a low tensile strength of 23 MPa and a high elongation to break (more than 700%). Thanks to its low Tg, PCL is often used as a compatibilizer or as a soft block in polyurethane formulations. Enzymes and fungi easily biodegrade PCL (Chandra and Rustgi 1998, Tokiwa 1977). To improve the degradation rate, several copolymers with lactide or glycoside have been prepared (Nair and Laurencin 2007). PCL is commercially available under the trade names CAPA® (from Solvay, Belgium), Tone® (from Union Carbide, USA) or Celgreen® (from Daicel, Japan) and many others. Possible applications in packaging have been investigated.

Cellulose and derivatives

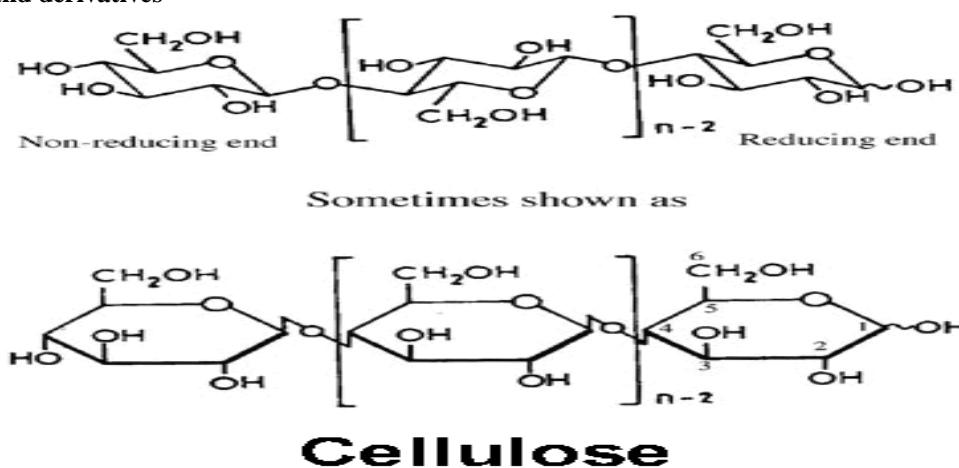


Figure.4: Cellulose structure

Cellulose is the most abundantly occurring natural polymer on earth and is an almost linear polymer of anhydroglucose. It is a linear polymer with very long macromolecular chains of one repeating unit, cellobiose. Cellulose is crystalline, infusible and insoluble in all organic solvents (Chandra and Rustgi

1998). Because of its regular structure and array of hydroxyl groups, it tends to form strongly hydrogen bonded crystalline micro fibrils and fibers and is most familiar in the form of paper or cardboard in the packaging context. Waxed or polyethylene coated paper is used in some areas of primary food packaging; however the bulk of paper is used for secondary packaging.

Cellulose is a cheap raw material, but difficult to use because of its hydrophilic nature, insolubility and crystalline structure. The cellophane produced is very hydrophilic and, therefore, moisture sensitive, but it has good mechanical properties. It is, however, not thermoplastic owing to the fact that the theoretical melt temperature is above the degradation temperature, and therefore cannot be heat-sealed.

Cellophane is often coated with nitrocellulose wax or PVdC (Poly Vinylidene Chloride) to improve barrier properties and in such form it is used for packaging of baked goods, processed meat, cheese and candies. A number of cellulose derivatives are produced commercially, most commonly carboxy-methyl cellulose, methyl cellulose, ethyl cellulose, hydroxyethyl cellulose, hydroxypropyl cellulose and cellulose acetate. Of these derivatives only cellulose acetate (CA) is widely used in food packaging's (baked goods and fresh produce). CA possesses relatively low gas and moisture barrier properties and has to be plasticized for film production (Claus 2000). Many cellulose derivatives possess excellent film-forming properties, but they are simply too expensive for bulk use. This is a direct consequence of the crystalline structure of cellulose making the initial steps of derivatization difficult and costly. Research is required to develop efficient processing technologies for the production of cellulose derivatives if this situation is to change. Tenite® (Eastman, USA), Bioceta® (Mazzucchelli, Italy), Fasal® (IFA, Austria) and Natureflex® (UCB, Germany) are some of the trade names of cellulose-based polymers.

II. BLENDS

Starch-polyvinyl alcohol: TPS and PVOH have excellent compatibility and their blends are of particular interest. TPS and starch can be blended at various ratios to tailor the mechanical properties of the final material. Compared to pure TPS materials, blends present improved tensile strength, elongation and processability (Mao and Imam 2000, Fishman and Coffin 2006). Their biodegradability has been recently investigated (Russo et al. 1998). The PVOH content has an important impact on the rate of starch degradation increasing the amount of PVOH will decrease this rate.

Starch-PLA: The mechanical properties of blends of starch with PLA using conventional processes are poor due to incompatibility. An elongation increase can be achieved by using plasticizers or reacting agents during the extrusion process. Coupling agents like isocyanates have been used. The hydroxyl groups of starch could react with the isocyanate group resulting in urethane linkages and compatibilization of these systems. The effect of gelatinization of starch was also investigated. It has been shown that in PLA/gelatinized starch blends, starch could be considered as a nucleating agent, resulting in an improvement of crystallinity in PLA blends and a greater superiority of mechanical properties. Another way to improve compatibilization is to use a compatibilizer. Maleic anhydride can be used for this purpose (Zhang 2004). An initiator was used to create free radicals on PLA and improved the reaction between maleic acid and PLA. The anhydride group on maleic acid could react with the hydroxyl groups present in starch. Interfacial adhesion between starch and PLA was then significantly improved. The mechanical properties obtained for PLA/starch blends compatibilized with maleic acid are higher than those obtained for virgin PLA/starch blends. A biodegradable PLA-grafted amylose copolymer has been synthesized, to be used as compatibilizer agent in starch/PLA blends (Ouhib et al. 2009).

Starch – PCL: To prepare films by using the film blowing technique, TPS was blended with PCL to adjust the rheological properties of the melt before the process (Matzinos et al. 2002). Novamont (Italy) produces a class of starch blend with different synthetic components. Its trade name is Mater-Bi®. Four grades are available; one of them consists of PCL (Mater-Bi® Z). The highest amount of starch allows the acceleration of the degradation of PCL. The behavior of some PCL-modified starch blends has been studied (Yavuz 2003). The addition of modified starch leads to an increase of the Young's modulus of PCL and a decrease in tensile strength and elongation at break values. The blend becomes less ductile (Shin et al. 2004). Some synthetic polymers with lower biodegradability are used to control the rate of biodegradation according to the applications. The modulus of blends of high-amylose corn starch (25% wt.) and PCL was 50% higher than that of PCL and the tensile strength 15% lower. To increase the mechanical properties of PCL/starch, blends with LDPE were prepared. The biodegradation rate of PCL, which is very low, can be significantly increased by the presence of starch (Bastioli et al. 1995).

PCL/Chitin-chitosan blends: PCL blends with chitin were prepared as biodegradable composites by melt blending (Yang et al. 2001). Increasing the amount of chitin has no effect on the melting or crystallization

temperature. This was attributed to a non miscible blend. Another blending route is solvent casting (Senda et al. 2001). The degree of crystallinity of PCL decreases upon blending with chitin. Same results are obtained with PCL/chitosan blends. These blends are expected to have good mechanical properties.

III. MATERIAL PROPERTIES

1. Gas barrier properties

Many foods require specific atmospheric conditions to sustain their freshness and overall quality during storage. Hence, increasing amounts of our foods are being packed in protective atmosphere with a specific mixture of gases ensuring optimum quality and safety of the food product in question. To ensure a constant gas composition inside the package, the packaging material needs to have certain gas barriers. In most packaging applications the gas mixture inside the package consists of carbon dioxide, oxygen and nitrogen or combinations hereof. The objective of this section is to describe the gas barriers of biobased materials using mineral oil based polymer materials as benchmarks. In Figure.5, different biobased materials are compared to conventional mineral-oil-based polymer materials. The figure is based on information from literature and on measurements of commercially available materials performed by ATO (Wageningen, NL) (Claus 2000).

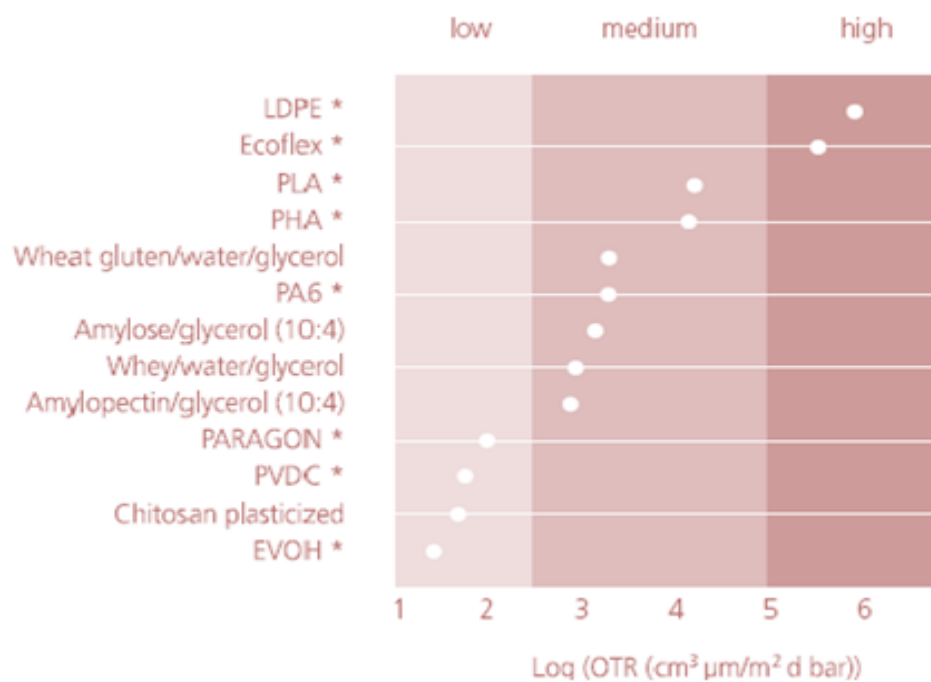


(Figure.5: Comparison of oxygen permeability of biobased materials compared to conventional mineral-oil-based materials. Permeability of materials marked with * was measured by ATO, Wageningen, NL (23°C, 50% RH), information on other materials are based on literature (Rindlav-Westling et al., 1998; Butler et al., 1996).)

Alternatives to presently available gas barrier materials like EVOH and PA6 and an equivalent biobased laminate would be an outer-layer of plasticized chitosan, a protein or starch-derived film combined with PLA or PHA. Notably, the gas barrier properties of PA6 and EVOH are sensitive towards moisture and the LDPE creates a very effective water vapor barrier ensuring that the moisture from the foodstuff does not interfere with the properties of PA6 or EVOH. In the same fashion, PLA and PHA will protect the moisture-sensitive-gas-barrier made of polysaccharide and protein (Claus 2000).

Gas barriers and humidity

As many of these biobased materials are hydrophilic, their gas barrier properties are very much dependent on the humidity conditions for the measurements and the gas permeability of hydrophilic biobased materials may increase manifold when humidity increases. Notably, this is a phenomenon also seen with conventional polymers. The gas permeability of high gas barrier materials, such as nylon and ethyl vinyl alcohol, is likewise affected by increasing humidity. Gas barriers based on PLA and PHA is not expected to be dependent on humidity (Claus 2000).

Water vapor transmittance

A major challenge for the material manufacturer is the by nature hydrophilic behavior of many biobased polymers as a lot of food applications demand materials that are resistant to moist conditions. However, when comparing the water vapor transmittance of various biobased materials to materials based on mineral oil (see Figure.6); it becomes clear that it is possible to produce biobased materials with water vapor transmittance rates comparable to the ones provided by some conventional plastics. However, if a high water vapor barrier material is required, very few biobased materials apply. Notably, developments are currently focusing on this problem and future biobased materials must also be able to mimic the water vapor barriers of the conventional materials known today (Claus 2000).

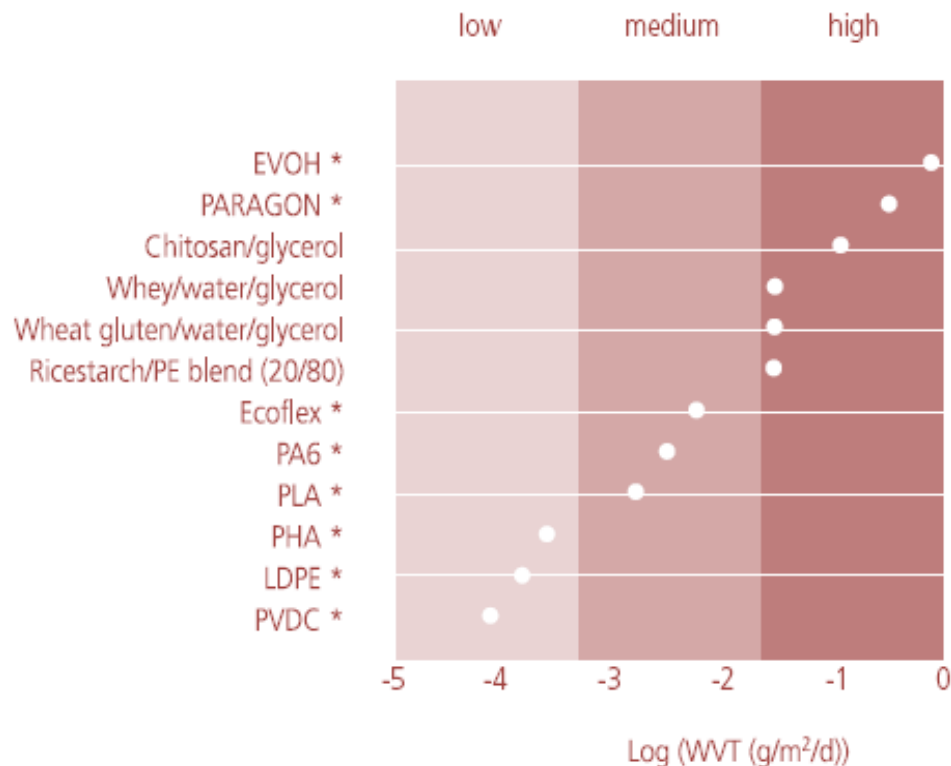


(Figure.6: Water vapor transmittance of biobased materials compared to conventional packaging materials based on mineral oil. Water vapor transmittance of materials marked with * was measured by ATO (Wageningen, NL) at 23°C, 50% RH. Transmittance of other materials are based on literature and measured at same conditions (Rindlav-Westling et al., 1998; Butler et al., 1996).)

Thermal and mechanical properties

Next to the barrier properties of the final packaging, the thermal and mechanical properties of the materials are both important for processing and also during the use of the products derived from these materials. Most biobased polymer materials perform in a similar fashion to conventional polymers. This indicates that polystyrene-like polymers (relatively stiff materials with intermediate service temperatures), polyethylene-like polymers (relatively flexible polymers with intermediate service temperatures) and PET-like materials (relatively stiff materials with higher service temperatures) can be found among the available biobased polymers. The mechanical properties in terms of modulus and stiffness are not very different compared to conventional polymers. In figure.7 a comparison of the thermal properties of biobased polymers with existing polymers is made. The modulus of biobased materials ranges from 2500-3000 MPa and lowers for stiff polymers like thermoplastic starches to 50 MPa and lower for rubbery materials like medium chain polyhydroxyalkanoates (Claus 2000).

Furthermore, the modulus of most biobased and petroleum derived polymers can be tailored to meet the required mechanical properties by means of plasticizing, blending with other polymers or fillers, cross linking or by the addition of fibers. A polymer like bacterial cellulose could for instance be used in materials which require special mechanical properties. In theory, biobased materials can be made having similar strength to the ones we use today (Iguchi et al., 2000).

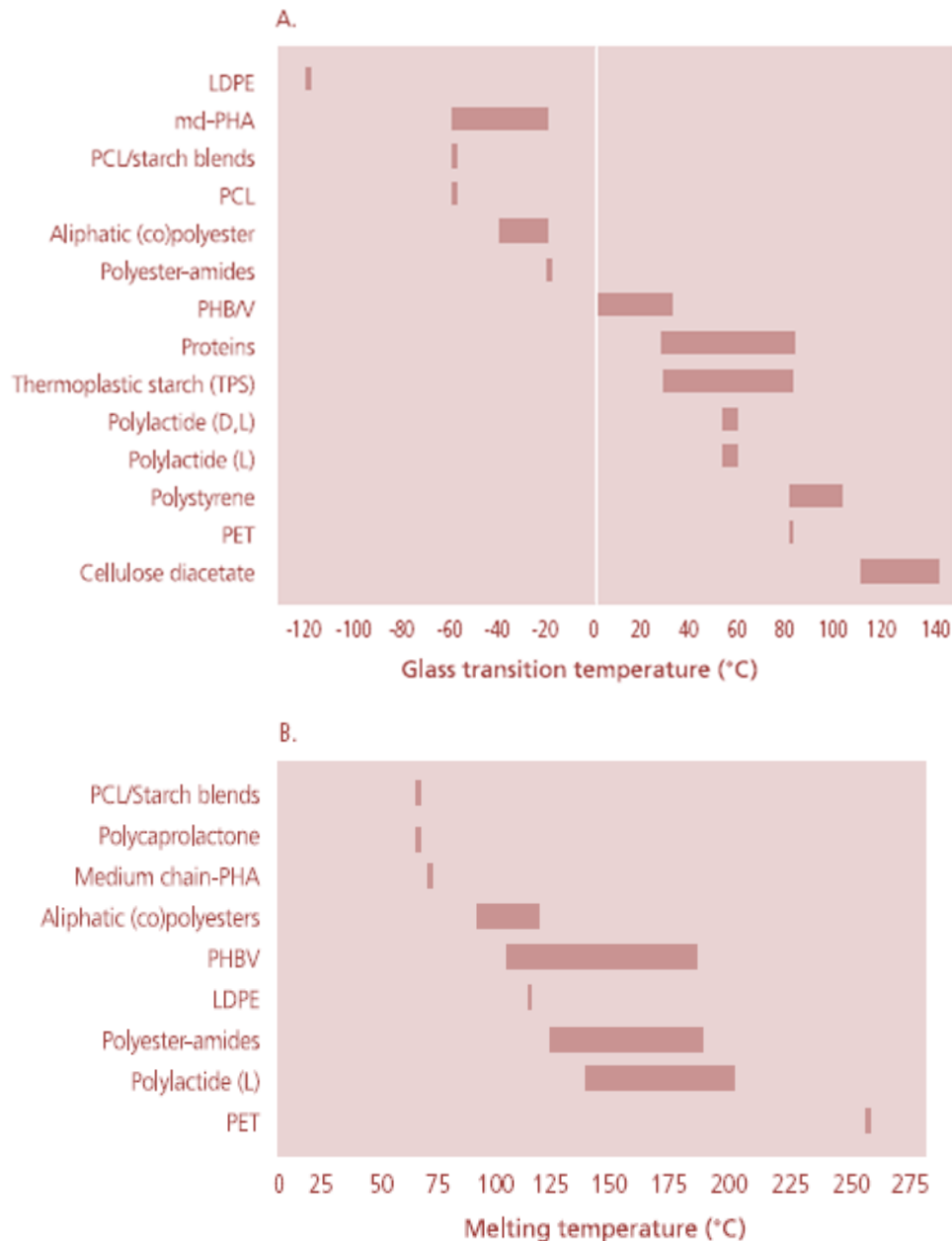


(Figure.7: Comparison of the thermal properties of biobased polymers with convectional polymers. (All data is from company information).)

IV. COMPOSTABILITY

Compostability is another important property required for biopolymers used in food packaging. Figure.8 compares the compostability of various biobased materials. Notably, the “composting time” depicted in the figure represents the approximate period of time required for an acceptable level of disintegration of the material to occur. This means that the original material should not be recognizable anymore in the final compost (fraction < 10 mm) nor in the overflow (fraction > 10 mm). The composting time does not reflect the time required for the biodegradation of the materials to be fully completed. The process could subsequently be completed during the use of the compost. The level of technology applied in the composting process highly affects the composting time needed for complete disintegration. Hence, it takes much longer to obtain a mature compost using low technology composting (e.g. passive windrow composting) than using high technology as in an intensively controlled tunnel composting process. The durations presented in figure 2.6 are based on an intermediate level of technology as observed in actively aerated and mechanically turned hall composting. Furthermore, the composting time needed for complete disintegration is also affected by the particle size of the material. For example, wood is rapidly composted in the form of sawdust and small chips. A wooden log,

however, takes more than one year to be completely disintegrated. The durations presented in this figure are based on dimensions regularly used for packaging applications (Claus 2000).

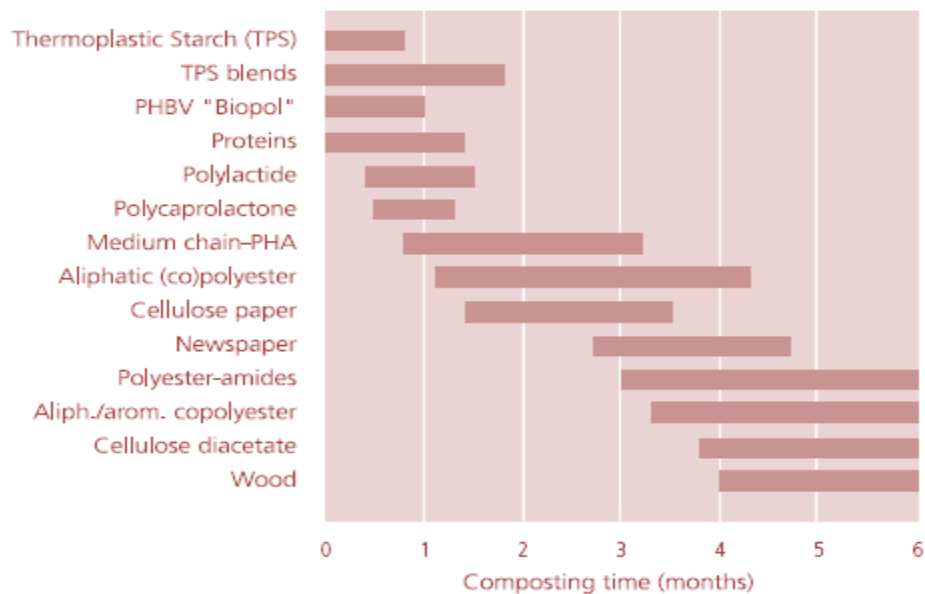


(Figure.8: Indication of the time required for composting of various biobased and synthetic polymeric materials. Measurements of composting times were performed at ATO. The durations presented in this figure are based on an intermediate level of technology as observed in actively aerated and mechanically turned hall composting.)

The compostability of the materials are highly dependent on the other properties of the materials, e.g. the first step of the composting is often a hydrolysis or wetting of the material. The rate of this step is very much related to the water vapor transmittance and the water resistance of the material. Hence, the composting rate of a material will be dependent on its other properties (Claus 2000).

Manufacturing of biobased food packaging

Engineering of a biobased package or packaging material requires knowledge of the processing and material properties of the polymers. If the properties of the native biopolymer are not identical to the required one, or if the polymer by nature is not thermoplastic, a certain modification of the polymer must take place. For very specific requirements (very low gas permeability or high water resistance) it is unlikely that one polymer will be able to provide all required properties even after modifications. Hence, it is necessary to use multiple materials in a composite, a laminate or co-extruded material (Claus 2000).

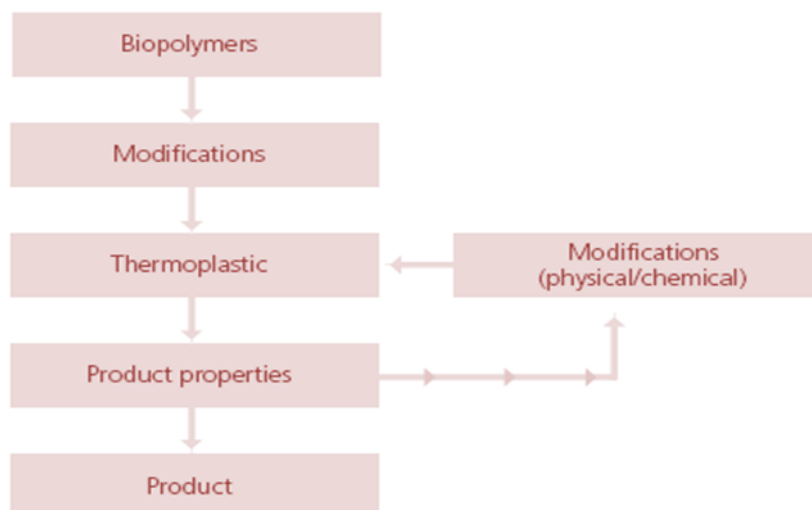


(Figure.9: Designing and manufacturing of biobased packages and packaging materials require a multistep approach)

Possible products produced of biobased materials

The fundamental repeating chemical units of the biobased materials described so far are identical to those of a significant body of the conventional plastics. Thus, in the broadest sense, poly-saccharides possessing repeating acetal functionality can be regarded as the naturally occurring analogues of the synthetic polyacetals; proteins (repeating peptide functionality) can be compared to the synthetic polyamides while polylactic acid is merely an example of the diverse group of polyesters.

Processing route	Product examples
(Co-)Extruded film	Packaging film
Cast film	Packaging film
Thermoformed sheets	Trays, cups
Blown films	Packaging film
Injection (blow-)moulding	Salad pots, cutlery, drinking beakers, cups, plates, drinks bottles, trays
Fibres and non-wovens	Agricultural products, diapers, feminine hygiene products, certain medical plastics, clothing
Extrusion coating	Laminated paper or films

(Figure.10: The major processing routes to potential biobased products.)

Clearly, however, the gross physical and chemical properties of native biobased materials and their synthetic counterparts are quite different and this is a feature of additional chemical functionality inherent in biobased materials. It should be expected that following requisite processing and product development of biobased materials resulting properties should equal or better those of the conventional alternatives. However, such processing and product development is not always trivial and is unlikely to be cost effective in all cases. It is not surprising, therefore, that the current applications of biobased materials seek not to emulate the properties of conventional plastics, but to capitalize on inherent biodegradability and on other unique properties of these polymers. Biobased plastic applications are currently targeted towards single-use, disposable, short-life packaging materials, service ware items, disposable non-wovens and coatings for paper and paperboard applications. In general, the same shapes and types of food packaging can be made from synthetic and biobased resources. The question is whether the same performance can be achieved by using the biobased materials as with the synthetic ones (Claus 2000).

Blown (barrier) films

Blown films comprise one of the first product categories to be developed based on mineral oil derived biodegradable polyesters. They have successfully been applied as garbage bags and related applications. Film blowing grades of renewable polymers have been developed based on PLA. Blown films based on these biopolyesters exhibit excellent transparency and cellophane-like mechanical properties. The sealability depends on the degree of crystallinity and good printability can also be achieved. The possibilities of film blowing PHB/V materials are at this time limited due to their slow crystallization and low melt strength. In many food packaging applications, water vapor barriers as well as gas barriers are required. No single biobased polymer can fulfill both these demands. In this case, the use of co-extrusion can lead to laminates which meet the objectives. Paragon (Avebe, NL) materials which are based on thermoplastic starch can be film blown in a co-extrusion set-up with polymers like PLA and PHB/V as coating materials, resulting in a barrier coating which, for example, proved to be successful in the packaging of cheese (Tuil et al., 2000). The use of Paragon tie-layers provides the adhesion between the coating and the base layer. In this way, starch-based materials could provide cheap alternatives to presently available gas barrier materials like EVOH and PA6 (Claus 2000).

Thermoformed containers

A next class of products is thermoformed containers for food packaging. In order to be able to thermoform a polymer it should be possible to process this material from the melt (extrusion) into sheets and consequently thermoforming these sheets just above the T_g or T_m of the material. Thermoformed products can be found based on PLA and PHB/V. Again, it is possible to produce thermoformed articles from laminates based on Paragon as well as other thermoplastically processable biopolymers (Claus 2000).

Foamed products

Starch-based foams for loose fill applications (Novamont, (I), National Starch (USA) a.o.) have been commercially introduced with success some years ago and the market for these products is still growing. Foamed products like trays and clamshells based on starch for food packaging have not yet been introduced commercially. Products based on a molding technique from a slurry phase (Earthshell (USA), APACK (D)) are close to market introduction. These products are produced from starch base slurries with inorganic and agro fiber based fillers. Other proposed techniques include loose-fill molding (Novamont (I), Biotec (D)), foam extrusion (Biotec (D)), and extrusion transfer molding (Standard Starch (USA)) and expandable bead molding (Tuil et al., (In press)). Foamed products based totally on PLA are still in a developmental phase (Claus 2000). In order to be able to use these starch-foamed products in food contact applications coatings should be applied on the starch-based foams.

Adhesion between the foam and the coating is of importance. Paraffin and other oligomer based coatings are proposed next to PLA and PHB/V based coatings. Protein and medium chain length PHA based coatings (ATO, 2000) are close to market introduction. Other proposed techniques include loose-fill molding (Novamont (I), Biotec (D)), foam extrusion (Biotec (D)), and extrusion transfer molding (Standard Starch (USA)) and expandable bead moulding (Tuil et al., (In press)). Foamed products based totally on PLA are still in a developmental phase. In order to be able to use these starch-foamed products in food contact applications coatings should be applied on the starch-based foams. Adhesion between the foam and the coating is of importance. Paraffin and other oligomer based coatings are proposed next to PLA and PHB/V based coatings. Protein and medium chain length PHA based coatings (ATO, 2000) are close to market introduction (Claus 2000).

Coated paper

It is expected that paper will stay an important biobased packaging material. Paper and board materials have excellent mechanical properties; however, the gas permeabilities are too high for many food applications. The hydrophilic nature of the paper-based materials is a major challenge of these materials when packaging moist foods. To date, the paper-based materials have been coated with a thin layer of synthetic plastic which has provided the materials with the required gas property and water resistance. Alternatively, biobased materials might be used as coating materials thus paving the way for a 100% biobased packaging material. Paper-based materials coated with PE are readily repulpable as the hydrophobic PE is easily removed in the pulping process. Hence, paper-based materials coated with biobased, hydrophobic polymeric materials are, likewise, going to be repulpable (Claus 2000).

Additional developments

To be able to produce a 100% biobased packaging development of biobased additives is needed. Additives used in the production of packaging are plasticizers, UV-stabilizers, adhesives, inks and paints, natural pigments and colorants. So far, few developments have been made in this field and it is suggested to direct research to this area (Claus 2000).

Some Biodegradable Packaging materials available in the market

<i>Biopolymers</i>	<i>Manufacturing company</i>
PHB/PHV	Monsanto, UK; Biomer, UK
Cellulose acetate	Courtaulds, USA; Mazzucchelli, Italy
PLA	Cargill Dow Polymers, USA; Mitsui, Japan; Hycail, Netherlands; Galactic, USA
Starch	National Starch, UK; Avebe, Netherlands
Starch based blends	Novamont, Italy; Biotec, Germany; Earth Shell, USA; Biop, UK

V. CONCLUSION

The food industry has seen great advances in the packaging sector since its inception in the 18th century with most active and intelligent innovations occurring during the past century. These advances have led to improved food quality and safety. While some innovations have stemmed from unexpected sources, most have been driven by changing consumer preferences. The new advances have mostly focused on delaying oxidation and controlling moisture migration, microbial growth, respiration rates, and volatile flavors and aromas. This focus parallels that of food packaging distribution, which has driven change in the key areas of sustainable packaging, use of the packaging value chain relationships for competitive advantage, and the evolving role of food service packaging. Biopolymers have highly influenced the packaging sector greatly.

Environmental responsibility is constantly increasing in importance to both consumers and industry.

For those who produce biodegradable plastic materials, this is a key advantage. Biopolymers limit carbon dioxide emissions during creation, and degrade to organic matter after disposal. Although synthetic plastics are a more economically feasible choice than biodegradable ones, an increased availability of biodegradable plastics will allow many consumers to choose them on the basis of their environmentally responsible disposal. The processes which hold the most promise for further development of biopolymer materials are those which employ renewable resource feedstocks. Time is of the essence for biodegradable polymer development, as society's current views on environmental responsibility make this an ideal time for further growth of biopolymers.

REFERENCES

- [1]. ATO, Internal communication (2000).
- [2]. Auras, R.; Harte, B.; Selke, S. An overview of polylactides as packaging materials. *Macromol. Biosci.* **2004**, *4*, 835-864.
- [3]. Avella, M.; Immirzi, B.; Malinconico, M.; Martuscelli, E.; Volpe, M.G. Reactive blending methodologies for Biopol. *Polym. Int.* **1996**, *39*, 191-204.
- [4]. Barham, P.J.; Keller, A. The relationship between microstructure and mode of fracture in polyhydroxybutyrate. *J. Polym. Sci. B-Polym. Phys* **1986**, *24*, 69.
- [5]. Bastioli, C.; Cerutti, A.; Guanella, I.; Romano, G.C.; Tosin, M. Physical state and biodegradation behavior of starch-polycaprolactone systems. *J. Environ. Polym. Degr.* **1995**, *3*, 81-95.
- [6]. Bismarck, A., Aranberri-Askargorta, I., Springer, J., Lampke, T., Wielage, B., Samboulis, A., Shenderovick, I., Limbach, H. 2002. Surface characterization of flax, hemp, and cellulose fibers; Surface properties and the water uptake behavior. *Polymer Composites*. *23*(5): 872-894.
- [7]. Briassoulis, D. An overview on the mechanical behavior of biodegradable agricultural films. *J. Poly. Environ.* **2004**, *12*, 65-81.
- [8]. Butler, B.L., Vergano, P.J. Testin, R.F., Bunn, J.M. and Wiles, J.L. (1996). Mechanical and barrier properties of edible chitosan films as affected by composition and storage. *Journal of Food Science*, *61*(5): 953 – 956.
- [9]. Callister, W.D. 1999. *Materials Science and Engineering: An Introduction*. New York, N.Y.: John Wiley and Sons.
- [10]. Chandra, R. and Rustgi, R. (1998). Biodegradable polymers. *Progress in Polymer Sciences* *23*: 1273 – 1335.
- [11]. Claus J.Weber. 2000. *Biobased packaging materials for the food industry*
- [12]. El-Hadi, A.; Schnabel, R.; Straube, E.; Muller, G.; Henning, S. Correlation between degree of crystallinity, morphology, glass temperature, mechanical properties and biodegradation of poly(3-hydroxyalkanoate) PHAs and their blends. *J. Polym. Testing* **2002**, *3*, 665-674.
- [13]. Fishman, M.L.; Coffin, D.R. Two stage extrusion of plasticized pectin/poly (vinyl alcohol) blends. *Carbohydr. Polym.* **2006**, *65*, 421-429.
- [14]. Fredriksson, H.; Silverio, J.; Andersson, R.; Eliasson, A.C.; Aman, P. The influence of amylase and amylopectin characteristics on gelatinization and retrogradation properties of different starches. *Carbohydr. Polym.* **1998**, *35*, 119-134.
- [15]. Garde, A., Schmidt, A.S., Jonsson, G., Andersen, M., Thomsen, A.B., Ahring, B.K. and Kiel, P. (2000). Agricultural crops and residuals as a basis for polylactate production in Denmark. *Proceedings of the Food Biopack Conference, Copenhagen*, 27 – 29 August 2000, pp. 45 – 51.
- [16]. Grassie, N.; Murray, E.J.; Holmes, P.A. The thermal degradation of poly (-D)- β -hydroxybutyric acid): Part 2 – Changes in molecular weight. *Polym. Degrad. Stab.* **1984**, *6*, 95.
- [17]. Guilbert, S., Gontard, N and Gorris, G.M. (1996). Prolongation of the shelf-life of perishable food products using biodegradable films and coating. *Lebensmittelwissenschaft und Technologies* *29*: 10 – 17.
- [18]. Hori, Y. Takahashi, Y.; Yamaguchi, A.; Nishishita, T. Ring-opening copolymerization of optically active β -butyrolactone with several lactones catalyzed by distannoxane complexes: Study of the mechanism. *Int. J. Biol. Macromol.* **1996**, *25*, 235-247.
- [19]. Hsieh, W.C.; Wada, Y.; Chang, C.P. Fermentation, biodegradation and tensile strength of poly (3-hydroxybutyrate-co-4-hydroxybutyrate) synthesized by *Delfia acidovorans*. *J. Tw. Inst. Chem. Eng.* 2009, doi:10.1026/jjtice.2008.11.004.
- [20]. Iguchi, M., Yamanaka, S. and Budhioni, A. (2000). Bacterial cellulose – a masterpiece of nature's arts. *Journal of Materials Science* *35*: 1 – 10.
- [21]. Jacobsen, S.; Fritz, H.G. Plasticizing polylactide – the effect of different plasticizers on the mechanical properties. *Polym. Eng. Sci.* **1999**, *39*, 1303-1310.
- [22]. Juzwa, M.; Jedlinski, Z. Novel synthesis of poly (3-hydroxybutyrate). *Macromolecules* **2006**, *39*, 4627-3460.
- [23]. Kim, M.N.; Lee, A.R.; Yoon, J.S.; Chin, I.J. Biodegradation of poly(3-hydroxybutyrate), skygreen and mater-Bi by fungi isolated from soils. *Eur. Polym. J.* **2000**, *36*, 1677.
- [24]. Krochta, J.M. and De Mulder-Johnston, C.L.C. (1997). Edible and biodegradable polymer films: Challenges and opportunities. *Food Technology* *51*: 60 – 74.
- [25]. Luckachan, G.E.; Pillai, C.K.S. Chitosan/oligo L-lactide graft copolymers: effect of hydrophobic side chains on the physico-chemical properties and biodegradability. *Carbohydr. Polym.* **2006**, *24*, 254-266.
- [26]. Maharana, T.; Mohanty, B.; Negi, Y.S. Melt-solid polycondensation of lactic acid and its biodegradability. *Progr. Polym. Sci.* **2009**, *34*, 99-124.
- [27]. Mao, L.; Imam, S. Extruded cornstarch-glycerol-polyvinyl alcohol blends: mechanical properties, morphology and biodegradability. *J. Polym. Environ.* **2000**, *8*, 205-211.
- [28]. Matzinos, P.; Tserki, V.; Kontoyiannis, A.; Panayiotou, C. Processing and characterization of starch/polycaprolactone products. *Polym. Degrad. Stab.* **2002**, *77*, 17-24.
- [29]. Miller, R.A.; Brady, J.M.; Cutright, D.E. Degradation rates of oral resorbable implants (polylactates and polyglycolates): Rate modification with changes in PLA/PGA copolymer ratios. *J. Biomed. Mat. Res.* **1977**, *11*, 711-719.
- [30]. Mochizuki, M.; Hirami, M. Structural effects on biodegradation of aliphatic polyesters. *Polym. Adv. Technol.* **1997**, *8*, 203.
- [31]. Nair, L.S.; Laurencin, C.T. Biodegradable polymers as biomaterials. *Progr. Polym. Sci.* **2007**, *32*, 762-798.
- [32]. Okada, M. Chemical synthesis of biodegradable polymers. *Progr. Polym. Sci.* **2002**, *27*, 87-133.
- [33]. Ouhib, R.; Renault, B., Mouaziz, H.; Nouvel, C.; Dellacherie, E.; Six, J.L. Biodegradable amylose-g-PLA glycopolymers from

- renewable resources. *Carbohydr. Polym.* **2009**, doi:10.1016/j.carpol.2008.11.038.
- [34]. Perego, G.; Cella, G.D.; Bastioli, C. Effect of molecular weight and crystallinity on poly (lactic acid) mechanical properties. *J. Appl. Polym. Sci.* **1996**, *59*, 37-43.
- [35]. Petersen, K., Nielsen, P.V., Bertelsen, G., Lawther, M., Olsen, M.B., Nilsson, N.H. and Mortensen, G. (1999). Potential of biobased materials for food packaging. *Trends in Food Science & Technology*, *10*(2): 52-68.
- [36]. Ratnayake, W.S.; Hoover, R.; Shahidi, F.; Perera, C.; Jane, J. Composition, molecular structure and physicochemical properties of starches from four field pea cultivars. *Food Chem.* **2001**, *74*, 189-202.
- [37]. Rindlav-Westling, A., Stading, M., Hermansson, A.M and Gatenholm, P. (1998). Structure, mechanical and barrier properties of amylose and amylopectin films *Carbohydrate Polymers* *36*: 217-224.
- [38]. Russo M.A.L.; O'Sullivan, C.; Rousefell, B.; Halley, P.J.; Truss, R. The anaerobic degradability of thermoplastic starch/polyvinyl alcohol blends: potential biodegradable food packaging materials. *Bioresour. Technol.* **2009**, *100*, 1705-1710.
- [39]. Rutot, D.; Dubois, P. Les (bio) polymères biodégradables: l'enjeu de demain? *Chim. Nouv.* **2004**, *86*, 66-75.
- [40]. Savenkova, L.; Gerçberga, Z.; Nikolaeva, V.; Dzene, A.; Bibers, I.; Kahlnin, M. Mechanical properties and biodegradation characteristics of PHB bases films. *Proc. Biochem.* **2000**, *35*, 573.
- [41]. Senda, T.; He, Y.; Inoue, Y. Biodegradable blends of poly (ϵ -caprolactone) with chitin and chitosan: Specific interactions, thermal properties and crystallization behavior. *Polym. Int.* **2001**, *51*, 33-39.
- [42]. Sheldon, J.R.; Lando, J.B.; Agostini, D.E.; Synthesis and characterization of poly (β -hydroxybutyrate). *J. Polym. Sci. Polym. Lett. B* **1971**, *9*, 173-178.
- [43]. Shin, B.Y.; Lee S.I.; Shin, Y.S.; Balakrishnan, S.; Narayan, R. Rheological, mechanical and biodegradation studies on blends thermoplastic starch and polycaprolactone. *Polym. Eng. Sci.* **2004**, *44*, 1429-1438.
- [44]. Sinclair, R.G. (1996). The case for polylactic acid as a commodity packaging plastic. *Polymeric Materials: Science and Engineering*, *72*: 133 – 135.
- [45]. Södergård, A. (2000). Lactic acid based polymers for packaging materials for the food industry. *Proceedings of the Food Biopack Conference, Copenhagen*, 27 – 29 August 2000, pp. 14 – 19.
- [46]. Södergård, A.; Stolt, M. Properties of lactic acid based polymers and their correlation with composition. *Progr. Polym. Sci.* **2002**, *27*, 1123-1163.
- [47]. Tokiwa, Y.; Suzuki, T. Hydrolysis of polyesters by lipases. *Nature* **1977**, *270*, 76-78.
- [48]. Tuil R. van, Schennink, G., Beukelaer, H. de, Heemst, J. van and Jaeger, R. (2000). Converting biobased polymers into food packaging. *Proceedings of the Food Biopack Conference, Copenhagen* 27 – 29 August 2000, Copenhagen, Denmark, pp. 28 – 30.
- [49]. Vert, M. Polymères de fermentation. Les polyacides lactiques et leurs précurseurs, les acides lactiques. *Actual. Chim.* **2002**, *11-12*, 79-82.
- [50]. Williams, G., Pool, R. 2000. Composites from natural fibers and soy oil resins. *Applied Composite Materials*. *7*(5-6): 421-432.
- [51]. Witt, U., Müller, R.-J. and Klein, J. (1997). *Biologisch abbaubare Polymere. Status und Perspektiven*. Publishers: Franz.Patatz-Zentrum Braunschweig, Germany ISBN 3-00-001529-9.
- [52]. Yang, A.; Wu, R.; Zhu, P. Thermal analysis and miscibility of chitin/polycaprolactone blends. *J. Appl. Polym. Sci.* **2001**, *81*, 3117-3123.
- [53]. Yavuz, H.; Babac, C. Preparation and Biodegradation of Starch/Polycaprolactone Films. *J Polym Environ.* **2003**, *1*, 107-113.
- [54]. Yukuta, T.; Akira, I.; Masatoshi, K. Developments of biodegradable plastics containing polycaprolactone and/or starch. *Polym. Mater. Sci. Eng.* **1990**, *63*, 742-749.
- [55]. Zeng, J.B.; Li, Y.D.; Zhu, Q.Y.; Yang, K.K.; Wang, X.L.; Wang, Y.Z. A novel biodegradable multiblock poly (ester urethane) containing poly (L-lactic acid) and poly (butylene succinate) blocks. *Polymer* **2009**, *50*, 1178-1186.
- [56]. Zhang, J.F.; Sun, X. Mechanical properties of poly (lactic acid)/starch composites compatibilized by maleic anhydride. *Biomacromolecules* **2004**, *5*, 1446-1451.
- [57]. Zhang, L.; Deng, X.; Zhao, S.; Huang, Z. Biodegradable polymer blends of poly (3-hydroxybutyrate) and starch acetate. *Polym. Int.* **1997**, *44*, 104.

ELECTROHYDRAULIC SYSTEM FOR AUTOMATIC GAGE CONTROL (AGC) FOR TANDEM COLD MILL PLANT IN SARTID SMEDEREVO

Slobodan Stefanovic¹, Radoje Cvejic², Zivoslav Adamovic³, Dusko Kostic⁴

¹High (advanced) school, Vranje, Serbia

²Faculty for strategic and operational management, Belgrade, Serbia

³Technical faculty Mihajlo Pupin, Zrenjanin, Serbia

⁴High vocational School for Entrepreneurship, Belgrade, Serbia

Abstract : Electro hydraulic servosystem for the AGC has better characteristics than electromechanical (five times greater speed of rolling, greater speed of positioning, smaller dead-zone, smaller time of roll gap adjusting start, smaller time of maximum speed reaching, greater unloading speed).

Keywords: Automatic control system, electromechanical, electrohydraulic system, mechanical system, servovalve.

I. INTRODUCTION

In Hot and Cold Mill Plants were mounted electrohydraulic servosystems for automatic gage control (instead electromechanical systems with screw thread) during modernisation. For the applications of the mostly control algorithms are necessary knowledge of mathematical models as components as complete object of automatic control. Detail analysis of these servosystems will help for better understanding and for the next optimisations by applications of modern control methods. This work is based on results from literature [1].

II. ELECTROMECHANICAL SYSTEM FOR AUTOMATIC GAGE CONTROL

Automatic control system works on the following manner: if aberration of the strip thickness at the stand exit is happened then a signal from a thickness gage 9 by converter is led to summator 14 where this signal compares with set up signal. Error signal is led to regulator and from regulator to electromotor 13. Electromotor 13 moves screw and changes rolling force and thickness of strip too. The greater disadvantage of this regulation type is the great friction between screw and screw nut which disable very quick and very precision work.

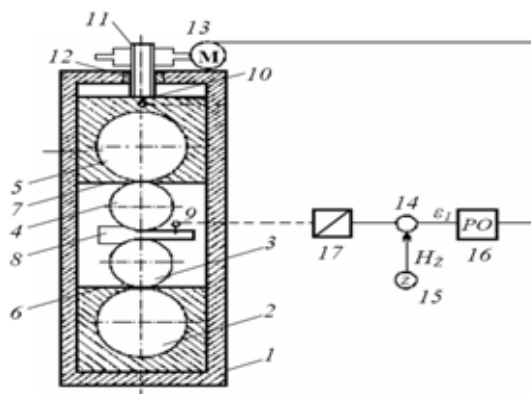


Figure 1. Mechanical system scheme for AGC

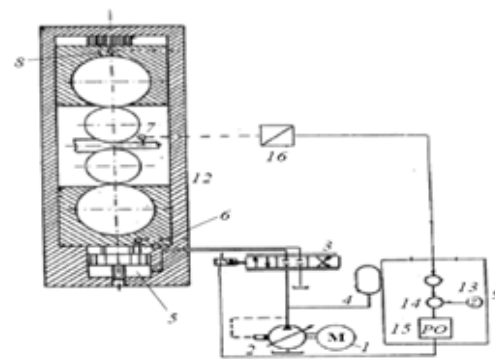


Figure 2. Electrohydraulic system scheme for AGC

III. ROLLING STANDS ELASTIC DEFORMATION AND PLASTIC DEFORMATION CURVE

Sum of elastic deformations of the all loaded rolling stand parts is rolling stand elastic deformation. Elastic deformation of rolling stand can be determined by theoretical or experimental method (theoretical method is rarely used because it is hard to determine the clearances between parts of rolling stand).

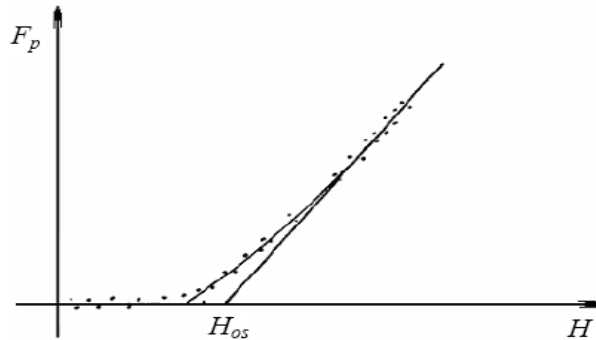


Figure 3. Curve of elastic deformation of the rolling stand

From the figure 3 is possible to write equation (1):

$$H_i = H_{os} + \frac{F_p}{E_s} \tag{1}$$

the following symbols are defined:

H_i - strip thickness at the exit from the rolling stand,

H_{os} - value of the initial gap between rolls,

F_p - modulus of rolling stand elasticity.

Therefore equation (1) contains two unknown values (rolling force and thickness of the strip at the exit from the stand) it is necessary to know dependence of rolling force from exit strip thickness for a concrete rolling conditions (entry strip thickness, friction coefficient, rolls diameters...).

Desired dependence is given by equation(2):

$$F_p = f(H_u, R, \lambda, \dots) \tag{2}$$

Curves given by equation (2) are strip plastic deformation curves (curves of plasticity and it is possible to obtain its by theoretical or experimental method. Figure 4 shows plastic deformation curve of strip.

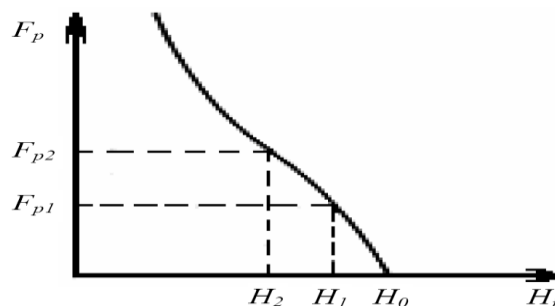


Figure 4. Plastic deformation curve of strip

From figure 4 it is obvious that greater rolling force enables smaller strip thickness at the rolling stand exit. Simultaneously equations (1) and (2) solvings give rolling force and exit strip thickness during strip deformation in real working stand. Graphic equations solution is shown on figure 5.

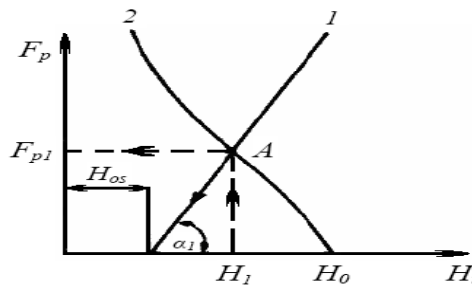


Figure 5. Graphic determination of the rolling force

Section n the straight line 1- the curve 2 determines point A. The coordinates of the point A (F_{p1} and H_1) determine rolling force F_{p1} which must act on the rolls to perform exit strip thickness H_1 . The gap between rolls increases from H_{os} to H_1 until thickness of the strip reduced from H_{os} at entry of the stand to H_1 at the exit of the stand. In the process computer are “memorized” straight line 1 and curve 2 and for demand H_1 it is possible to determinate F_{p1} and H_{os} (it is necessary to draw a vertical line from the point H_1 and point of section with the curve 2 is point A; From point A it is necessary to draw a horizontal line and obtain F_{p1} : It is necessary to draw a line through a point A with angle and obtain H_{os} . However, if the strip has the greater hardness then the rolling force F_{p1} will not be sufficient to perform H_1 and control system will increase the rolling force F_{p1} to get demand thickness of the strip at the exit of the stand.

IV. SERVOVALVE

Therefore a representation of servovalve response through the frequency range about 50 cps is sufficient (literature [1]), and a first-order expression is adequate. The time constant for the first-order transfer function is best established by 0.7 amplitude point (-3 db) (figure 6). Figure 6 shows a “Moog” servovalve dynamic response, together with the response of a first-order transfer function. The first-order approximation is a quite good through the lower frequency region. According to literature [2] and figure 6 we can write:

$$W_{sf} = \frac{1}{1 + T_1 S} \text{ while: } T_1 = \frac{1}{2\pi\omega_1} \quad (3)$$

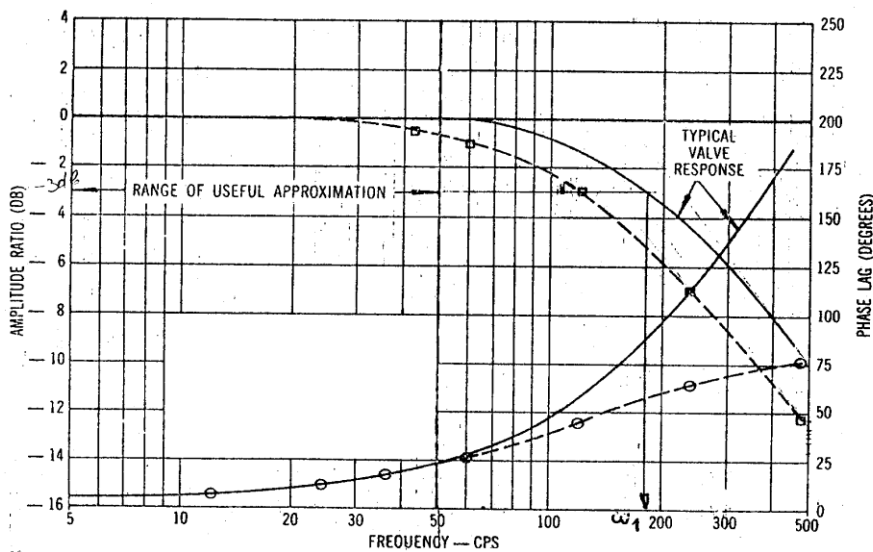


Figure 6. Bode diagram of the “Moog” servovalve

V. SERVOVALVE CONTROLLED PISTON

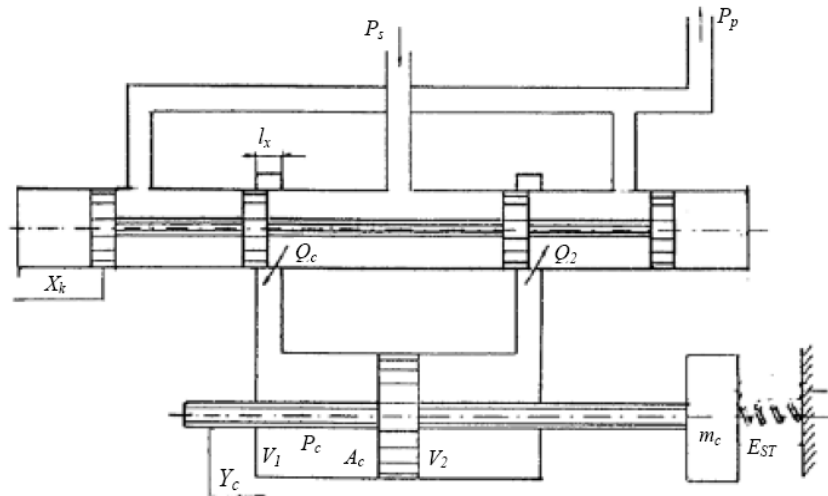


Figure7. Servovalve controlled cylinder piston

Figure 7. Servovalve controlled cylinder piston p_c ; $F_{pc} = p_c A_c$; force induced by roll stand elasticity:

$$F_x = E_{ST} Y \text{ (4)}$$

force of inertia: $F_{in} = m_c \frac{d^2 Y_c}{dt^2}$

while: $m_c = m_T + m_{kc}$;

m_T – load mass,

m_{kc} - mass of the cylinder piston,

m_c - “common” mass .

Force of friction in the gaskets is negligible because the gaskets are made from a special PTFE material. The Second Newton's law for cylinder piston is given by equation (5):

$$p_c A_c = m_c \frac{d^2 Y}{dt^2} + E_{ST} Y \text{ (5)}$$

Cylinder entry flow (Q_c) is consist of the flow for the piston moving Q_v and flow for the compressibility compensation Q_{LC} , while leakage is negligible. We can write flow equation (6):

$$Q_c = A_c \frac{dY}{dt} + \frac{V}{B} \frac{dp_c}{dt} \text{ (6)}$$

Flow which leaves servovalve is:

$$Q_{SR} = \mu_{SR} W_{SR} X_k \sqrt{\frac{2}{\rho} (p_s - p_c)} \text{ (7)}$$

We can combine equations (5) and (6) to yield equation (8):

$$\mu_{SR} W_{SR} X_k \sqrt{\frac{2}{\rho} (p_s - p_c)} = A_c \frac{dY}{dt} + \frac{V}{B} \frac{dp_c}{dt} \text{ (8)}$$

VI. GAUGES, TRANSDUCERS AND SIGNAL AMPLIFIERS

From literature [1] we can write equations for the position gage, transducer and signal amplifier:

$$W_{MP} = \frac{U_{MP}(s)}{Y_c(s)} = \frac{K_{PC}}{T_u s + 1} \tag{9}$$

$$U_y = C_1 H_{iy} \tag{10}$$

$$I = K_A (U_y - U_{MP}) \tag{11}$$

while: W_{MP} – transfer function for piston rod position gage together with the position-voltage transducer, U_{MP} – exit signal from the position gage, H_{iy} – demand piston rod position signal, C_1 – amplification of demand position signal, K_A – amplification of voltage-current transducer.

VII. MATHEMATICAL MODEL OF A ROLLING STAND

Linearisation of equation (1) gives equation (12):

$H_i = H_{osi} + \frac{F_p}{E_s}$ is given by:

$$H_i = H_{in} + (H_{osi} - H_{osin}) \frac{\partial H_i}{\partial H_{osi}} + (F_{pi} - F_{pin}) \frac{\partial H_i}{\partial F_{pi}} \tag{12}$$

From equations (1) and (12) we can write equation (13) (in relative variations):

$$h_i = \frac{H_{OSIN}}{H_{IN}} h_{osi} + \frac{F_{pin}}{H_{in} E_{si}} f_{pi} = h_i = l_{1i} h_{osi} + l_{2i} f_{pi} \tag{13}$$

We consider cylinder piston rod, bottom work roll and bottom back up roll as “common” unit and therefore piston rod position change is the same as roll gap change. Therefore we can write equation (14):

$$h_i = l_{1i} y_c + l_{2i} f_{pi} \tag{14}$$

In the literatures [1] and [3] we can find equation (14) for the any of Sartid Cold Mill stand:

$$F_{pi} = \lambda_1 F_{K_{1i}} + (1 - \lambda_1) F_{K_{2i}} - \frac{2}{3} F_{ZZi} - \frac{1}{3} F_{ZPi} \sqrt{R(H_{ui} - H_i)} \cdot 0,6 + 0,4 \sqrt{\frac{H_i}{H_{ui}} e^{\frac{\mu \sqrt{R_i}(H_{ui} - H_i)}{0,12H_i + 0,28H_{ui}}} + \frac{2}{3} a_4 \sqrt{R_i H_i} (F_{K_{2i}} - F_{ZPi})^{\frac{1}{2}}} \tag{15}$$

where:

$$F_{K_1} = a_1 \left(a_2 + \frac{H_{ui}}{H_0} \right)^{a_3}$$

$$F_{K_2} = a_1 \left(a_2 + \frac{H_{ui}}{H_5} \right)^{a_3}$$

For the soft steel are:

$$a_1 = 55,3; a_2 = 1,002; a_3 = 0,27; \lambda_1 = 0,2; a_4 = \sqrt{\frac{1 - \gamma^2}{E}}$$

F_{zzi} - force of back tension,
 F_{zpi} - force of front tension,
 R - work roll diameter,
 H_0 - thickness of the strip at the first stand entry,
 H_5 - thickness of the strip at the last stand exit.

Therefore we can write equation (16):

$$F_{pi} = (H_{ui}, H_i, F_{zzi}, F_{zpi}). \tag{16}$$

We can obtain equation (16) (in relative variations) by linearisation of equation (15):

$$f_{pi} = \frac{H_{in}}{F_{pin}} \frac{\partial F_{pi}}{\partial H_i} \Big|_{h_i} + \frac{H_{uin}}{F_{pin}} \frac{\partial F_{pi}}{\partial H_{ui}} \Big|_{h_{ui}} + \frac{F_{zzin}}{F_{pin}} \frac{\partial F_{pi}}{\partial F_{zzi}} \Big|_{f_{zzi}} + \frac{F_{zpin}}{F_{pin}} \frac{\partial F_{pi}}{\partial F_{zpi}} \Big|_{f_{zpi}} + q_{1i} h_i + q_{2i} h_{ui} + q_{3i} f_{zzi} + q_{4i} f_{zpi}. \tag{17}$$

We can combine equations (12) and (17) and write equation (18):

$$h_i = \frac{l_{li}}{1 - l_{2i} q_{li}} y_{ci} + \frac{l_{2i} q_{2i}}{1 - l_{2i} q_{li}} h_{ui} + \frac{l_{2i} q_{3i}}{1 - l_{2i} q_{li}} f_{zzi} + \frac{l_{2i} q_{4i}}{1 - l_{2i} q_{li}} f_{zpi} + a_{li} y_{ci} + a_{2i} h_{ui} + a_{3i} f_{zzi} + a_{4i} f_{zpi}. \tag{18}$$

In the literature [1] are given all values for the coefficients g, l and a . Complete calculations, experimental results and producers catalogs give conclusion that in the rolling process with the »steady rolling speeds» (without considerations of taking in (accelerating)» and »taking out (slowing down)» the strip in (out) the rolling stand), the tension forces change smaller than 5% (lit [1]). Variations of the strip thickness which enters in the Cold Rolling Mill are very small because Sartid Hot Mill has electrohydraulic system for automatic gage control, too. Coefficients a_{2i}, a_{3i} and a_{4i} are much smaller than coefficient a_1 (reference [1]) and according to these conclusions we can write equation (19):

$$h_i = a_{li} y_{ci}. \tag{19}$$

VIII. LINEAR MATHEMATICAL MODEL, BLOCK DIAGRAM AND STATE-SPACE REPRESENTATION OF THE SYSTEM

Linearisation of equations (3), (4), (5), (7), (10), (11) and equation (19) give linear mathematical model for a rolling stand:

$$\text{Regulator: } q_{sr} = K_q x_k + K_c p_c, \quad q_c = A_c \dot{y}_c + \frac{V}{B} \dot{p}_c, \quad p_c A_c = m_c \ddot{y}_c + E_{ST} y_c, \tag{20}$$

$$\dot{i} = x_k + T_1 \dot{x}_k,$$

where: $\dot{i} = K_A (u_z - u_{MP}), T_u \dot{u}_{MP} + u_{mp} = K_{pc} y_c, u_z = c_1 h_{iz}, \text{ object; } h_i = a_1 y_c.$

We can draw block diagram of the system for the automatic gage control of one rolling stand (figure 8) using system of equations (20):

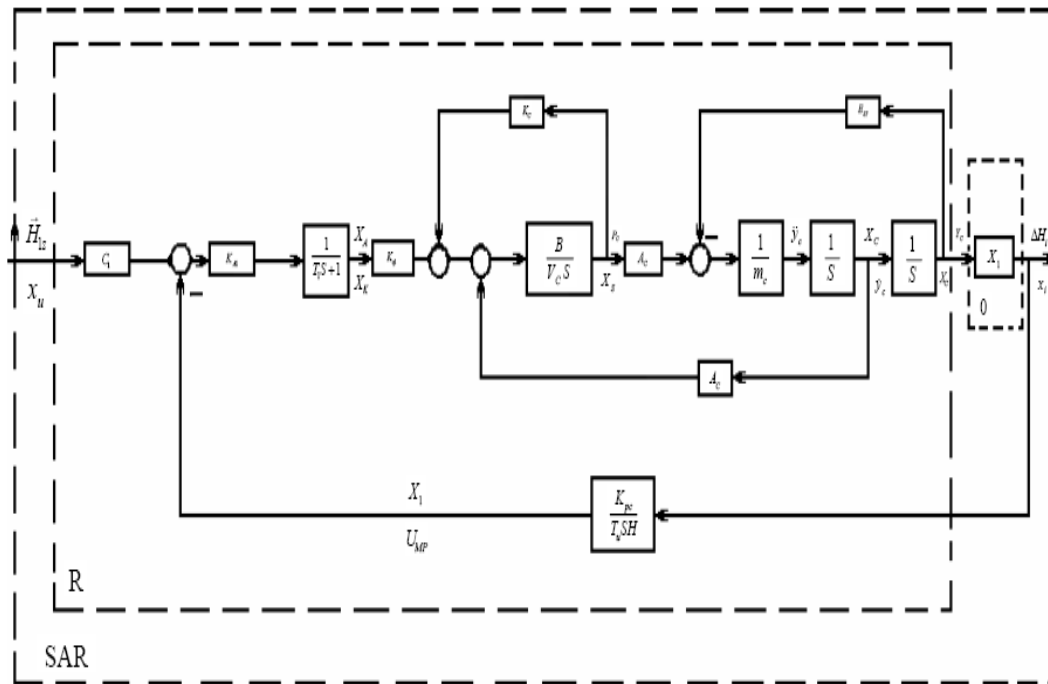


Figure 8. Automatic controlscheme- blockdiagramconnection

Define state variables:

$$x_1 = u_{MP}; x_2 = y_c; x_3 = y_c; x_4 = x_k; x_5 = p_c. (21)$$

Input and output are:

$$x_u = h_{iz}, x_i = h_i. (22)$$

Notice that all state variables are easily measurable quantities (voltage from the position gage, piston rod velocity, piston rod position, servovalve spool position and the pressure in the cylinder). Output value is the change of the strip thickness and input value is demand change of the strip thickness. Then, from the definition of the state variables (21), equations (20) and figure 9, we obtain equations (23) and (24):

$$\dot{x}_1 = \frac{1}{T_u} x_1 + \frac{K_{pc}}{T_u} a_1 x_3, \dot{x}_2 = -\frac{E_{ST}}{m_c} x_3 + \frac{A_c}{m_c} x_5, \dot{x}_3 = x_2, (23)$$

$$\dot{x}_4 = \frac{K_A}{T_1} x_1 - \frac{1}{T_1} x_4 - \frac{C_1 K_A}{T_1} x_u, \dot{x}_5 = -\frac{B A_c}{V_c} x_2 - \frac{B}{V_c} K_4 x_4 + \frac{K_c B}{V_c} x_5, (23-1)$$

$$x_i = a x_3. (24)$$

IX. SIMULATION OF THE SYSTEM WORK BY COMPUTER AND EXPERIMENTAL MEASUREMENTS IN REAL SYSTEM

According to system of equations (22) we obtain step response by computer (for the calculation of the all necessary coefficients we use dates from lit ([1,3]). For the same demand strip thickness change of 0,5-10⁻³ mm was done series of experimental testing and result of that is shown at the figure 9, too. Comparison of this curves gives conclusion that nature of this curves are the same. Small difference between these curves is induced by impossibility of exactly determination and exactly testing the system characteristics.

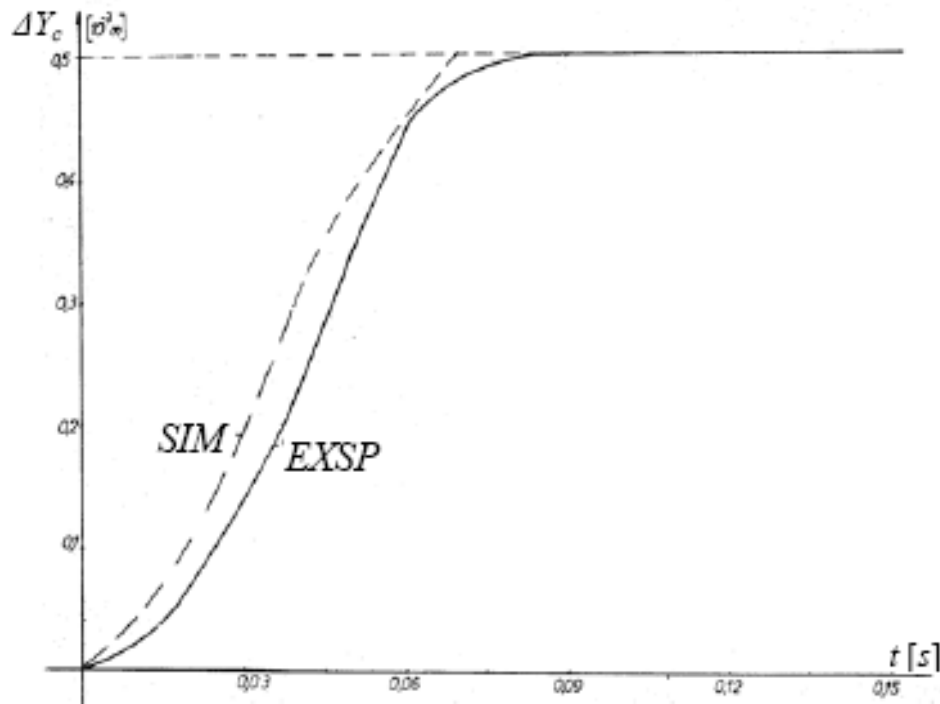


Figure 9. Step responses obtained by simulation and experimental measurements in the plant

X. CONCLUSION

Comparison of theoretical and experimental curves gives conclusion that all introduced assumptions are good. Analysis of the all system characteristics gives conclusion that system has good working. Electrohydraulic servosystem for the AGC has better characteristics than electromechanic system (five times greater speed of rolling, greater speed of positioning, smaller dead-zone, smaller time of roll gap adjusting start, smaller time of maximum speed reaching, greater unloading speed...).

REFERENCES

- [1]. "MOOG": Technical Bulletin 103, 1965
- [2]. Novica J.: Specialistic work, "Functional analysis and comparative characteristics of servovalves "PPT" and "MOOG", Technical Faculty Mihailo Pupin, Zrenjanin, 2000.
- [3]. Yun J.S.CHO.H.S "Application of an adaptive model following control technique to a hydraulic servo systems subjected to unknown disturbances" ASME Journal of DSMC, vol 113. 1991.
- [4]. Stefanovic S., Adamovic Z., Cvejic R. Petrov T. : Adaptive Control of Electrohydraulic System (Article), METALURGIA INTERNATIONAL, (2012), vol. 17 br. 11, str. 67-71.
- [5]. Adamovic Z: Maintenance of the Oilhydraulic systems, Belgrade, 1997.
- [6]. BRAYANT-AUTOMATION OF TANDEM MILLS –The Iron and Steel Institute, London 1963.
- [7]. Jokovic N.: Postgraduate work: "Electrohydraulic servosystem for AGC", Mechanical Faculty-Belgrade, 1993.

Input-Output Energy and Economic Analysis of Strawberry Production in Iran

Rasol Loghmanpor¹, Reza Tabatabaekoloor², Asadollah Akram³

^{1,3}(Department of Agricultural Machinery, College of Agricultural Engineering and Technology, University of Tehran, Iran)

²(Department of Farm Machinery, Sari Agricultural Science and Natural Resources University, Sari, Iran)

Abstract: The aim of this study was to determine the energy consumption and economic analysis for strawberry production. The data were collected from 80 farmers growing strawberry in the Babolsar zone of Iran by using a face-to-face questionnaire in May-June 2012. The plowing operation at the study area was done by two methods; manually plow and machinery plow. In addition, the irrigation operation was done by two methods; pumping irrigation and non-pumping irrigation. Total energy used in various farm operations during strawberry production was 22275.8 MJ.ha⁻¹. Total energy output was 14820 MJ.ha⁻¹, and the average annual yield of strawberry farms was 7800 kg. ha⁻¹. The energy ratio, productivities, specific and net energy gain were 0.58, 0.3 kg.MJ⁻¹, 3.33 MJ.kg⁻¹ and -9355.8 MJ.ha⁻¹, respectively. The profit/cost ratio, productivity, and net profit in the strawberry production are 1.37, 1.1 kg.\$⁻¹ and 2333.4 \$.ha⁻¹, respectively. In addition, the net return in the non-pumping and manually plow method is significantly higher than in the other methods.

Keywords: Economic analysis, energy use, input-output, renewable energy, strawberry

I. INTRODUCTION

Strawberry is an important small fruit, grown throughout the world. It is deep red in colour with unique shape and flavour. In Iran more than 20,000 tones of strawberries are produced each year. Kurdistan and Mazandaran provinces are two main regions of production with 2,000 and 500 hectares, respectively. Iran with over 3,600 hectares of strawberry cultivation has been ranked twentieth place in the world. Average Strawberry yield per unit area in Iran is 10 tons per hectare [1].

Energy is indeed the live wire of industrial, food and agricultural production, the fuel for transportation as well as for the generation of electricity in conventional thermal power plants [2]. The energy consumption for agricultural production is depended on agro-ecosystems, planting pattern, type of soil and mechanization levels [3]. For strawberry production, total energy consumptions are varied for different type of soils, farm size and level technology of machinery used. There is no reported data on strawberry energy consumption.

In developing countries like Iran, agricultural growth is essential for fostering the economic development and meeting the ever-higher demands of the growing population. Energy in agriculture is important in terms of crop production and agro processing for value adding [4]. Energy use in agriculture has been developed in response to increasing populations, limited supply of arable land and desire for an increasing standard of living. In all societies, these factors have encouraged an increase in energy inputs to maximize yields, minimize labour intensive practices or both [5].

In agriculture, a wide range of modern and traditional energy forms are used directly on the farm, e.g. as tractor or machinery fuel, and in water pumping, irrigation and crop drying, and indirectly for fertilizers and pesticides. Other energy inputs are required for post harvest processing in food production, packaging, storage, transportation and cooking [6].

Energy productivity is an important index for more efficient use of energy although higher energy productivity does not mean in general, more economic feasibility. However, the energy analysis shows the methods to minimize the energy inputs and therefore to increase the energy productivity [7]. Calculating energy inputs of

agricultural production is more difficult than in the industry sector due to the high number of factors affecting the production [8].

In order to maintain economically sustainable level of production of strawberry, it is essential to reduce the cost of production. Therefore, attempts should be made for higher efficiency of energy use.

The aim of this study was (1) to determine the amount of input-output energy used in growing strawberry, (2) to investigate the efficiency of energy consumption and (3) to make an economic analysis of strawberry production.

II. MATERIALS AND METHODS

2.1 Location and Period of the Study

The data were collected from 80 farmers growing strawberry in Babolsar zone of Iran by using a face-to-face questionnaire in May-June 2012. Babolsar zone is located in Mazandaran province of Iran. The province is located in the north of Iran, within 35° 47' and 36° 25' N latitude and 50° 34' and 54° 10' E longitude [9].

2.2 Sample Size

Random sampling of farms was done within whole population and the size of each sample was determined using equation (1) [10].

$$n = 1 \frac{\left(\sum N_h S_h\right)^2}{\left(N^2 D^2 + \sum N_h D_h^2\right)} \quad (1)$$

Where:

n = required sample size;

N = Number of holdings in target population;

N_h = Number of the population in the h stratification;

S_h = Standard deviation in the h stratification;

S_h² = Variance in the h stratification;

d = Precision where $\left(\bar{x} - \bar{X}\right) (\%5)$; and

z = Reliability coefficient (1.96, which represents the 95% reliability) ($D^2 = d^2 / z^2$)

2.3 Energy and Economic Indexes

The energy ratio (energy use efficiency), energy productivity, specific energy and net energy were calculated as per given below in (Equations 2 to 5) [11].

$$\text{Energy Ratio} = \frac{\text{Energy Output (MJ ha}^{-1}\text{)}}{\text{Energy Input (MJ ha}^{-1}\text{)}} \quad (2)$$

$$\text{Energy Productivity} = \frac{\text{Citrus Output (kg ha}^{-1}\text{)}}{\text{Energy Input (MJ ha}^{-1}\text{)}} \quad (3)$$

$$\text{Specific Energy} = \frac{\text{Energy Input (MJ ha}^{-1}\text{)}}{\text{Citrus Output (kg ha}^{-1}\text{)}} \quad (4)$$

$$\text{Net Energy} = \text{Energy Output (MJ ha}^{-1}\text{)} - \text{Energy Input (MJ ha}^{-1}\text{)} \quad (5)$$

The gross production value and productivity for economic analysis were calculated as per given below in (Equations 6 and 7).

$$\text{Gross production value (\$ ha}^{-1}\text{)} = \text{Strawberry yield (kg ha}^{-1}\text{)} * \text{price (\$ kg}^{-1}\text{)} \quad (6)$$

$$\text{Productivity (kg \$}^{-1}\text{)} = \frac{\text{Strawberry yield (kg ha}^{-1}\text{)}}{\text{Total production costs (\$ ha}^{-1}\text{)}} \quad (7)$$

Basic information on energy inputs and strawberry yields were entered into Excel and SPSS 19 spreadsheets. The plowing operation at the study area was done by two methods. At the first method, the workers did it manually, while at the second method it was done by agricultural machinery. In addition, the irrigation operation was done by two methods. In some places, the farmers used a river or spring water without using any energy for pumping the water. This was non-pumping irrigation method. In other fields there was not such a source and the farmers pumped the water from a well or a river in a lower altitude. This was pumping irrigation method.

The energy efficiency of the agricultural system has been evaluated by the energy ratio between output and input. Human labor, machinery, diesel oil, fertilizer, and ecis amounts and output yield values of strawberry crops have been used to estimate the energy ratio. The amounts of input were calculated per hectare and then, these input data were multiplied with the coefficient of energy equivalent given in table 1.

Table 1. Energy equivalents for different inputs and outputs in strawberry production in Iran.

Input	Unit	Energy Equivalent (MJ unit ⁻¹)	Reference
Labor	h	1.96	[12]
Tractor-Machinery	kg	138	[12]
Diesel fuel	L	47.8	[12]
Manure	ton	303.1	[5]
NH ₃	kg	74.2	[13]
P ₂ O ₅	kg	13.7	[13]
Disk harrow	kg	149	[12]
Eccesis	kg	0.8	[14]
Strawberry	kg	1.96	[14]

III. RESULTS AND DISCUSSION

3.1 Analysis of Input-Output Energy Use

Used inputs in the strawberry production, energy equivalences, and ratio of inputs and output are illustrated in table 2. Total energy used in various farm operations during strawberry production was 22275.8 MJ.ha⁻¹. The most of the agricultural operations was done manually in the study area, while using the agricultural machinery was limited to some areas and only for land preparation.

According to the evaluation of data in table 2 and figure 1, the average human labor required in the study area was 1204.08 h.ha⁻¹, and machine power was just 2.39 h.ha⁻¹. Total energy consumed in various farm operations during strawberry production was 22275.8 MJ.ha⁻¹. Irrigation energy consumed 30.12% of total energy followed by manure (23.11%) during production period. Machinery was the least demanding energy input for strawberry production with 330.5 MJ ha⁻¹ (only 1.48% of the total energy input), followed by eccesis with 1080 MJ. ha⁻¹ (4.84%). Total energy output was 12920 MJ.ha⁻¹, and the average annual yield of strawberry farms was 6800 kg ha⁻¹.

Table 2. Amounts of inputs and output energy in strawberry production

Inputs	Energy consumption(MJ ha ⁻¹)
Fuel	1850
Eccesis	1080
Machinery	330.5
Fertilizers	4795.3
Labor	2360
Manure	5150
Irrigation	6710
Total input energy	22275.8
Yield	12920

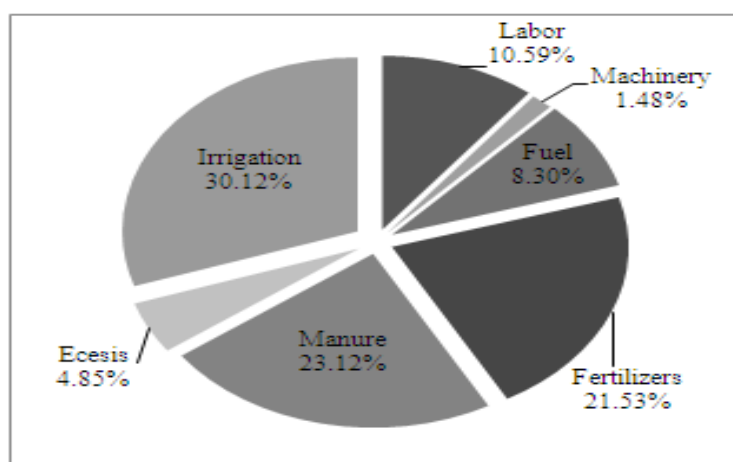


Fig. 1. Distribution of energy input ratios in the strawberry production.

Energy output-input ratio (energy efficiency) in this study was 0.58, and energy productivity calculated as 0.3 kg MJ⁻¹ (Table 3). This means that 0.3 kg of strawberry was obtained per unit of energy. This result is more than similar study in Sanandaj zone of Iran by Salami et al. in 2010 [14]. In that study, energy ratio and productivity reported 0.32 and 0.17 kg MJ⁻¹, respectively.

Table 3. Energetic parameters in strawberry production in Iran

Parameter	Unit	Value
Energy Input	MJ ha ⁻¹	22275.8
Energy Output	MJ ha ⁻¹	14820
Yield	Kg ha ⁻¹	7800
Energy Ratio	...	0.58
Energy Production	Kg MJ ⁻¹	0.3
Specific Energy	MJ kg ⁻¹	3.33
Net Energy Gain	MJ ha ⁻¹	-9355.8

The amount of 68.6% (15300 MJ.ha⁻¹) of total energy input resulted from renewable and 31.4% (6975.8 MJ.ha⁻¹) from non-renewable energy; also 8.3% (1850 MJ ha⁻¹) from direct energy and 91.7% (20425.8 MJ.ha⁻¹) indirect energy (Figure 2). Direct inputs were mainly fuel for field operations; and chemical fertilizers, manure, machinery, labor and ecesis dominated the indirect inputs. In other words, strawberry production was highly dependent on the production of indirect inputs.

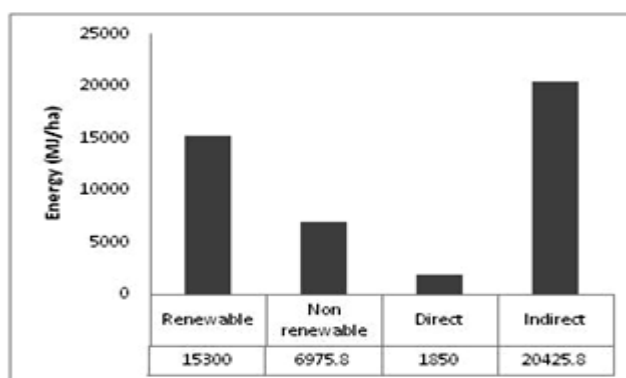


Fig. 2. Total energy input in the form of Direct, Indirect, Renewable and Non-renewable energy for strawberry production (MJ ha⁻¹).

Table 4 shows the values of total input energy for manually plow-pumping, manually plow-non-pumping, machinery plow-pumping and machinery plow-non-pumping. The least of total input energy was 11768 MJ.ha⁻¹ for manually plow-non pumping and the highest total input energy was 36755 MJ.ha⁻¹ for machinery plow-pumping.

Table 4. The values of total input energy (MJ ha⁻¹) for manually plow-pumping, manually plow-non-pumping, machinery plow-pumping and machinery plow-non-pumping.

Plow type	Irrigation type	
	Pumping	Non-Pumping
Manually plow	27223	11768
Machinery plow	36755	20235

3.2 Economic Analysis of Strawberry Production

The economic analysis is presented in table 5. The profit/cost ratio, productivity, and net profit in the strawberry production were 1.37, 1.1 kg \$⁻¹, and 3333.4 \$ ha⁻¹, respectively. Results show the net return in this study is higher than similar study in Sanandaj zone of Iran by Salami et al. in 2010 [14]. They reported the net return about 1825 \$ ha⁻¹, while in this study it was 2333.4 \$ ha⁻¹.

The net return in the non-pumping irrigation is significantly higher than in the other irrigation type (Pumping irrigation) (Table 6). This result is acceptable, because there was not any cost for production in the non-pumping

method for irrigation operation, while acquiring water in the pumping irrigation method required some cost (Electricity or Diesel cost).

Cost and return items	Value
Total production cost (\$ ha ⁻¹)	6166.6
Gross production value (\$ ha ⁻¹)	8500
Benefit/Cost ratio	1.37
Productivity (kg S ⁻¹)	1.1
Net return (\$ ha ⁻¹)	2333.4

Table 6. The mean values of net return (\$ ha⁻¹) for manually plow-Pumping, machinery plow-pumping, manually plow-non pumping and machinery plow – non pumping

Plow type	Irrigation type	
	Pumping	Non-Pumping
Manually plow	1.733	7.858
Machinery plow	4.881	2.33

IV. CONCLUSION

In this study, the total energy used in various farm operations during strawberry production was 22275.8 MJ.ha-1. The average annual yield of strawberry farms was 6800 kg.ha-1, and total energy output was 12920 MJ ha-1. Energy productivity calculated as 0.305 kg MJ-1, and energy efficiency was 0.58. The net energy gain was 9355.8 MJ.ha-1. It shows loss of energy in strawberry farms. The benefit-cost ratio, productivity, and net profit in the strawberry production were 1.37, 1.1, and 2333.4 \$ ha-1, respectively. The net return in the non-pumping and manually plow method was significantly higher than in the other methods and energy consumption in the pumping and machinery plow method was significantly higher than in the other methods.

V. ACKNOWLEDGEMENTS

The authors would like to thanks all the farmers who are participated in this research specially the strawberry growers in Babolsar zone of Mazandaran province.

REFERENCES

- [1]. FAO, 2010. <http://faostat.fao.org>. Consulted May 2010.
- [2]. Jekayinfa, S.O., Bamgboye, A.I., 2006. Estimating energy requirement in cashew nut processing operations.. Energy, 31:1305-1320.
- [3]. Hendriadi, A., Mulyantoro, L., Wahyudi, S.T., 2005. Analysis of energy consumption for paddy production in Indonesia. Proceeding of Int. Agric. Eng. Conf., Bangkok, Thailand.
- [4]. Karimi, M., Beheshti Tabar, I., Khubbakht, G.M., 2008. Energy production in Iran's agronomy. Am. Eurasian J. Agric. Environ. Sci., 4(2):172-177.
- [5]. Esengun, K., Gündüz, O., Erdal, G., 2007. Input-output energy analysis in dry apricot production of Turkey. Energy Conversation Management. 48:592-598.
- [6]. Food and Agriculture Organization (FAO), 2000. The energy and agriculture nexus. Environment and natural resources working paper No.4. Roma: FAO.
- [7]. Fluck, R.C., Baird, C.D., 1982. Agricultural Energetic. Westport, CT, AVI Publications.
- [8]. Yaldiz, O., Ozturk, H.H., Zeren, Y., Bascetomcelik, A., 1993. Energy usage in production of field crops in Turkey. In: Fifth international congress on mechanization and energy use in agriculture. 11-14 October 1993. Kusadasi. Turkey.
- [9]. Anonymous, 2009. Ministry of Interior of Mazandaran Province. Wikipedia.
- [10]. Stout, B.A., 1990. Handbook of energy for world agriculture. Elsevier Applied Science. London: pp. 21.
- [11]. Kitani, O., 1999. CIGR Handbook of Agricultural Engineering, Volume V: Energy and Biomass Engineering. ASAE publication, USA, St. Joseph, MI,
- [12]. Lockeretz, W., 1980. Energy inputs for nitrogen, phosphorus and potash fertilizers, In: Pimentel, D. (Ed.). Handbook of Energy Utilization in Agriculture. Boca Raton, FL, CRC. USA. pp. 17-20.
- [13]. Singh, S. and Mittal, J.P., 1992. Energy in production agriculture. New Delhi: Mittal Pub.
- [14]. Salami, P., Ahmadi, H., Keyhani, A., 2010. Energy use and economic analysis of strawberry production in Sanandaj zone of Iran. Biotechnol. Agn. Soc. Environ. (BASE). 14(4):653-658.

Optimization of weld bead geometry for stainless steel cladding deposited by GMAW.

P, Sreeraj¹, T, Kannan², Subhasis Maji³

¹Department of Mechanical Engineering, Valia Koonambaikulathamma College of Engineering and Technology, Kerala, 692574 India.

²Principal, SVS College of Engineering, Coimbatore, Tamilnadu, 642109 India.

³Professor, Department of Mechanical Engineering IGNOU, Delhi, 110068, India.

Abstract: The clad components quality always depends on clad bead geometry and coefficient of shape of welds and dilution. In order to obtain better quality, good corrosion resistant properties and to reduce manufacturing costs the bead parameters must be optimized. The above objectives can be achieved by developing mathematical equations to predict bead geometry. This paper presents central composite rotatable design with full replication technique was used to obtain four critical dimensions of bead geometry. The developed models have been checked for adequacy and significance. The experiments were conducted by depositing Type ER-308L stainless steel wire on to IS-2062 structural steel plates. The results of confirmation experiments showed that the developed models can be able to predict bead geometry with reasonable accuracy. This study proved that both direct and interaction effect plays a major role in determining bead dimensions and dilution. The process parameters were optimized using response surface methodology (RSM).

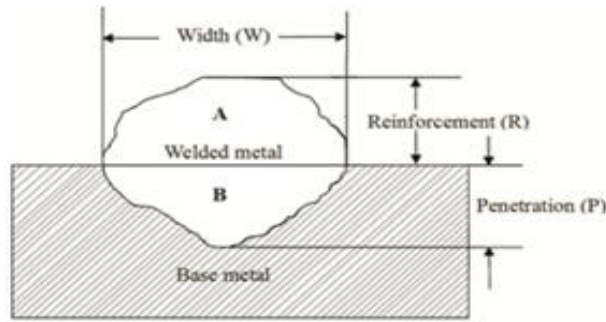
Keywords: GMAW, Weld bead geometry, RSM, Mathematical equations, stainless steel.

I. INTRODUCTION

Cladding is a process of depositing a thick layer of filler material on a low carbon steel base metal/Weld cladding finds application in repairing worn out parts for achieving good corrosion resistant surface. Usually gas metal arc welding (GMAW) has been widely used in manufacturing industries, for cladding because of its high productivity, easiness of operation and adaptability to automation. The process parameters of GMAW process must be studied in order to enhance its chance for automation and to get good quality weld. The quality of a weld depends on mechanical properties of the weld metal which in turn depends on metallurgical characteristics and chemical composition of the weld [1]. The mechanical and metallurgical feature of weld depends on bead geometry which is directly related to welding process parameters. In other words quality of weld depends on in process parameters. GMA welding is a multi objective and multifactor metal fabrication technique. The process parameters have a direct influence on bead geometry.

Fig 1 shows the clad bead geometry. Mechanical strength of clad metal is highly influenced by the composition of metal but also by clad bead shape [2]. This is an indication of bead geometry. It mainly depends on wire feed rate, welding speed, arc voltage etc. Therefore it is necessary to study the relationship between in process parameters and bead parameters to study clad bead geometry.

This study was carried out in two steps. In the first step regression models for dilution, coefficient of internal shape and coefficient of external shape were developed from the experimental data [3]. In the second stage the process parameters were optimized using response surface methodology (RSM) optimization technique to get the desired weld bead geometry.



$$\text{Percentage dilution (D)} = [B / (A+B)] \times 100$$

Fig. 1. Clad bead geometry

II. EXPERIMENTATION

The following machines and consumables were used for the purpose of conducting experiment.

- 1) A constant current gas metal arc welding machine (Invrtee V 350 – PRO advanced processor with 5 – 425 amps output range)
- 2) Welding manipulator
- 3) Wire feeder (LF – 74 Model)
- 4) Filler material Stainless Steel wire of 1.2mm diameter (ER – 308 L).
- 5) Gas cylinder containing a mixture of 98% argon and 2% of oxygen.
- 6) Mild steel plate (grade IS – 2062)

Test plates of size 300 x 200 x 20mm were cut from mild steel plate of grade IS – 2062 and one of the surfaces is cleaned to remove oxide and dirt before cladding. ER-308 L stainless steel wire of 1.2mm diameter was used for depositing the clad beads through the feeder. Argon gas at a constant flow rate of 16 litres per minute was used for shielding. The properties of base metal and filler wire are shown in Table 1. The important and most difficult parameter found from trial run is wire feed rate. The wire feed rate is proportional to current. Wire feed rate must be greater than critical wire feed rate to achieve pulsed metal transfer. The relationship found from trial run is shown in equation (1). The formula derived is shown in Fig 2.

$$\text{Wire feed rate} = 0.96742857 * \text{current} + 79.1$$

----- (1)

The selection of the welding electrode wire based on the matching the mechanical properties and physical characteristics of the base metal, weld size and existing electrode inventory [4]. A candidate material for cladding which has excellent corrosion resistance and weld ability is stainless steel. These have chloride stress corrosion cracking resistance and strength significantly greater than other materials. These have good surface appearance, good radiographic standard quality and minimum electrode wastage. Experimental design used for this study is shown in Fig 3 and importance steps are briefly explained.

Table 1: Chemical Composition of Base Metal and Filler Wire

Materials	Elements, Weight %								
	C	SI	Mn	P	S	Al	Cr	Mo	Ni
IS 2062	0.150	0.160	0.870	0.015	0.016	0.031	-	-	-
ER308L	0.03	0.57	1.76	0.021	1.008	-	19.52	0.75	10.02

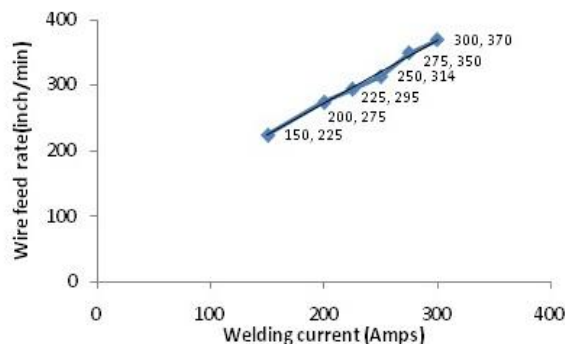


Fig. 2. Relationship between Current and Wire Feed Rate

III. PLAN OF INVESTIGATION

The research work is carried out in the following steps [5].

- Identification of important process variables and finding their upper and lower limits.
- Development of design matrix and conducting experiments as per design matrix,
- Recording responses viz; bead width (W).Penetration(P),Reinforcement(R),calculation of percentage of dilution Coefficient of internal shape and coefficient of external shape.
- development of mathematical models,
- checking adequacy of developed models,
- Conducting conformity tests.
- Optimizing the process parameters using RSM.

3.1 Identification of factors and responses

The basic difference between welding and cladding is the percentage of dilution. The properties of the cladding is the significantly influenced by dilution obtained. Hence control of dilution is important in cladding where a low dilution is highly desirable. When dilution is quite low, the final deposit composition will be closer to that of filler material and hence corrosion resistant properties of cladding will be greatly improved. The chosen factors have been selected on the basis to get minimal dilution and optimal clad bead geometry [1]. These are wire feed rate (W), welding speed (S), welding gun angle (T), contact tip to work to The following independently controllable process parameters were found to be affecting output parameters distance (N) and pinch (Ac), The responses chosen were clad bead width (W), height of reinforcement (R), Depth of Penetration. (P) and percentage of dilution (D). The responses were chosen based on the impact of parameters on final composite model.

3.2 Finding the limits of process variables

Working ranges of all selected factors are fixed by conducting trial run. This was carried out by varying one of factors while keeping the rest of them as constant values. Working range of each process parameters was decided upon by inspecting the bead for smooth appearance without any visible defects. The upper limit of given factor was coded as -2. The coded value of intermediate values were calculated using the equation (2)

$$X_i = \frac{2[X - (X_{max} + X_{min})]}{(X_{max} - X_{min})} \dots\dots\dots (2)$$

Where X_i is the required coded value of parameter X is any value of parameter from $X_{min} - X_{max}$. X_{min} is the lower limit of parameters and X_{max} is the upper limit parameters [4]. The chosen level of the parameters with their units and notation are given in Table 2.

Table 2: Welding Parameters and their Levels

Parameters	Factor Levels						
	Unit	Notation	-2	-1	0	1	2
Welding Current	A	I	200	225	250	275	300
Welding Speed	mm/min	S	150	158	166	174	182
Contact tip to work distance	mm	N	10	14	18	22	26
Welding gun Angle	Degree	T	70	80	90	100	110
Pinch	-	Ac	-10	-5	0	5	10

3.3 Development of design matrix

Design matrix chosen to conduct the experiments was central composite rotatable design. The design matrix comprises of full replication of $2^5 (= 32)$, Factorial designs. All welding parameters in the intermediate levels (o) constitute the central points and combination of each welding parameters at either is highest value (+2) or lowest (-2) with other parameters of intermediate levels (0) constitute star points. 32 experimental trails were conducted that make the estimation of linear quadratic and two way interactive effects of process parameters on clad geometry [5].

3.4 Conducting experiments as per design matrix

In this work Thirty two experimental run were allowed for the estimation of linear quadratic and two-way interactive effects of correspond each treatment combination of parameters on bead geometry as shown Table 3 at random. At each run settings for all parameters were disturbed and reset for next deposit. This is very

essential to introduce variability caused by errors in experimental set up. The experiments were conducted at SVS College of Engineering, Coimbatore, 642109, India.

3.5 Recording of Responses

For measuring the clad bead geometry, the transverse section of each weld overlays was cut using band saw from mid length. Position of the weld and end faces were machined and grinded. The specimen and faces were polished and etched using a 5% nital solution to display bead dimensions [6]. The clad bead profiles were traced using a reflective type optical profile projector at a magnification of X10, in M/s Roots Industries Ltd. Coimbatore. Then the bead dimension such as depth of penetration height of reinforcement and clad bead width were measured [6]. The profiles traced using AUTO CAD software. This is shown in Fig 4. This represents profile of the specimen (front side).The clad specimen is shown in Fig. 5. The measured clad bead dimensions and percentage of dilution is shown in Table 4.

Table 3: Design Matrix

Trial Number	Design Matrix				
	I	S	N	T	Ac
1	-1	-1	-1	-1	1
2	1	-1	-1	-1	-1
3	-1	1	-1	-1	-1
4	1	1	-1	-1	1
5	-1	-1	1	-1	-1
6	1	-1	1	-1	1
7	-1	1	1	-1	1
8	1	1	1	-1	-1
9	-1	-1	-1	1	-1
10	1	-1	-1	1	1
11	-1	1	-1	1	1
12	1	1	-1	1	-1
13	-1	-1	1	1	1
14	1	-1	1	1	-1
15	-1	1	1	1	-1
16	1	1	1	1	1
17	-2	0	0	0	0
18	2	0	0	0	0
19	0	-2	0	0	0
20	0	2	0	0	0
21	0	0	-2	0	0
22	0	0	2	0	0
23	0	0	0	-2	0
24	0	0	0	2	0
25	0	0	0	0	-2
26	0	0	0	0	2
27	0	0	0	0	0
28	0	0	0	0	0
29	0	0	0	0	0
30	0	0	0	0	0
31	0	0	0	0	0
32	0	0	0	0	0

I - Welding current; S - Welding speed; N - Contact tip to work distance; T - Welding gun angle; Ac – Pinch



Fig. 3. Traced Profile of bead geometry

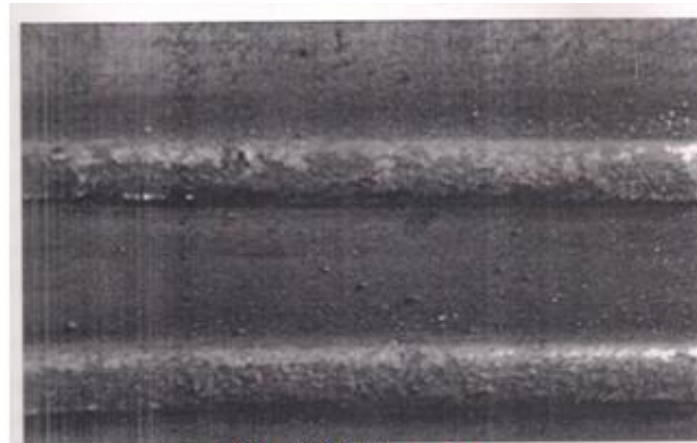


Fig. 4. Cladded specimen

3.6 Development of Mathematical Models

The response function representing any of the clad bead geometry can be expressed as [7, 8, and 9],

$$Y = f(A, B, C, D, E) \text{ ----- (3)}$$

Where,

Y = Response variable

A = Welding current (I) in amps

B = Welding speed (S) in mm/min

C = Contact tip to Work distance (N) in mm

D = Welding gun angle (T) in degrees

E = Pinch (Ac)

The second order surface response model equals can be expressed as below

$$Y = \beta_0 + \sum_{i=0}^5 \beta_i X_i + \sum_{i=0}^5 \beta_{ii} X_i^2 + \sum_{i=0}^5 \beta_{ij} X_i X_j$$

$$Y = \beta_0 + \beta_1 A + \beta_2 B + \beta_3 C + \beta_4 D + \beta_5 E + \beta_{11} A^2 + \beta_{22} B^2 + \beta_{33} C^2 + \beta_{44} D^2 + \beta_{55} E^2 + \beta_{12} AB + \beta_{13} AC + \beta_{14} AD + \beta_{15} AE + \beta_{23} BC + \beta_{24} BD + \beta_{25} BE + \beta_{34} CD + \beta_{35} CE + \beta_{45} DE \text{ ----- (4)}$$

Where, β_0 is the free term of the regression equation, the coefficient $\beta_1, \beta_2, \beta_3, \beta_4$ and β_5 is are linear terms, the coefficients $\beta_{11}, \beta_{22}, \beta_{33}, \beta_{44}$ and β_{55} quadratic terms, and the coefficients $\beta_{12}, \beta_{13}, \beta_{14}, \beta_{15}$, etc are the interaction terms. The coefficients were calculated by using MINITAB 15. After determining the coefficients, the mathematical models were developed. The developed mathematical models are given as follows.

$$\beta_0 = 0.166338 (\sum X_0 Y) + 0.05679 (\sum \sum X_{ii} Y) \text{ ----- (5)}$$

$$\beta_i = 0.166338 (\sum X_i Y) \text{ ----- (6)}$$

$$\beta_{ii} = 0.0625 (\sum X_{ii} Y) + 0.06889 (\sum \sum X_{ii} Y) - 0.056791 (\sum \sum X_0 Y) \text{ ----- (7)}$$

$$\beta_{ij} = 0.125 (\sum X_{ij} Y) \text{ ----- (8)}$$

$$\text{Clad Bead Width (W), mm} = 8.923 + 0.701A + 0.388B + 0.587C + 0.040D + 0.088E - 0.423A^2 - 0.291B^2 - 0.338C^2 - 0.219D^2 - 0.171E^2 + 0.205AB + 0.405AC + 0.105AD + 0.070AE - 0.134BC + 0.225BD + 0.098BE + 0.26CD + 0.086CE + 0.012DE \text{ ----- (9)}$$

$$\text{Depth of Penetration (P), mm} = 2.735 + 0.098A - 0.032B + 0.389C - 0.032D - 0.008E - 0.124A^2 - 0.109B^2 - 0.125C^2 - 0.187D^2 - 0.104E^2 - 0.33AB + 0.001 AC + 0.075AD + 0.005AE - 0.018BC + 0.066BD + 0.087BE + 0.058CD + 0.054CE - 0.036DE \text{ ----- (10)}$$

Table 4: Design Matrix and Observed Values of Clad Bead Geometry

Trial No.	Design Matrix					Bead Parameters				φ _e	φ _a
	I	S	N	T	Ac	W (mm)	P (mm)	R (mm)	D (%)		
1	-1	-1	-1	-1	1	6.9743	1.67345	6.0262	10.72091	4.167493	1.149547
2	1	-1	-1	-1	-1	7.6549	1.9715	5.88735	12.16746	3.88278	1.300306
3	-1	1	-1	-1	-1	6.3456	1.6986	5.4519	12.74552	3.735782	1.163263
4	1	1	-1	-1	1	7.7635	1.739615	6.0684	10.61078	4.464347	1.273122
5	-1	-1	1	-1	-1	7.2683	2.443	5.72055	16.67303	2.984928	1.270511
6	1	-1	1	-1	1	9.4383	2.4905	5.9169	15.96692	3.789721	1.599387
7	-1	1	1	-1	-1	6.0823	2.4672	5.49205	16.5894	2.443377	1.102509
8	1	1	1	-1	-1	8.4666	2.07365	5.9467	14.98494	4.082656	1.423647
9	-1	-1	-1	1	-1	6.3029	1.5809	5.9059	10.2749	3.986906	1.066553
10	1	-1	-1	1	1	7.0136	1.5662	5.9833	9.707297	4.477814	1.171354
11	-1	1	-1	1	1	6.2956	1.58605	5.5105	11.11693	3.982792	1.130716
12	1	1	-1	1	-1	7.741	1.8466	5.8752	11.4273	4.192029	1.317527
13	-1	-1	1	1	1	7.3231	2.16475	5.72095	15.29097	3.382885	1.264594
14	1	-1	1	1	-1	9.6171	2.69495	6.37445	18.54077	3.56863	1.508671
15	-1	1	1	1	-1	6.6335	2.3089	5.554	17.23138	2.873013	1.194364
16	1	1	1	1	1	10.514	2.7298	5.4645	20.8755	3.851564	1.922894
17	-2	0	0	0	0	6.5557	1.99045	5.80585	13.65762	3.29423	1.115212
18	2	0	0	0	0	7.4772	2.5737	6.65505	15.74121	2.905234	1.119526
19	0	-2	0	0	0	7.5886	2.50455	6.4069	15.77816	3.029926	1.136205
20	0	2	0	0	0	7.5014	2.1842	5.6782	16.82349	3.434392	1.321134
21	0	0	-2	0	0	6.1421	1.3752	6.0976	8.941799	4.469517	1.007298
22	0	0	2	0	0	8.5647	3.18536	5.63655	22.94721	2.688567	1.519507
23	0	0	0	-2	0	7.9575	2.2018	5.8281	15.74941	3.614088	1.401462
24	0	0	0	2	0	7.7085	1.85885	6.07515	13.27285	4.191454	1.280376
25	0	0	0	0	-2	7.8365	2.3577	5.74915	16.63287	3.298884	1.359229
26	0	0	0	0	2	8.2082	2.3658	5.99005	16.38043	3.48535	1.368228
27	0	0	0	0	0	7.9371	2.1362	6.0153	15.18374	3.714433	1.320193
28	0	0	0	0	0	8.4371	2.17145	5.69895	14.82758	3.886228	1.480695
29	0	0	0	0	0	9.323	3.1425	5.57595	22.8432	2.967218	1.672287
30	0	0	0	0	0	9.2205	3.2872	5.61485	23.6334	2.804819	1.642323
31	0	0	0	0	0	10.059	2.86605	5.62095	21.55264	3.506629	1.788256
32	0	0	0	0	0	8.9953	2.72068	5.7052	19.60811	3.306985	1.575858

W-Width; R - Reinforcement W - Width; P - Penetration; D - Dilution %

Height of Reinforcement (R), mm = 5.752 + 0.160A - 0.151B - 0.060C + 0.016D - 0.002E + 0.084A² + 0.037B² - 0.0006C² + 0.015D² - 0.006E² + 0.035AB + 0.018AC - 0.008AD - 0.048AE-0.024BC-0.062BD-0.003BE+0.012CD-0.092CE-0.095DE,------(11)

Percentage Dilution (D), % = 19.705 + 0.325A + 0.347B + 3.141C - 0.039D - 0.153E - 1.324A² - 0.923B² - 1.012C² - 1.371D² - 0.872E² - 0.200AB + 0.346 AC + 0.602 AD + 0.203AE+0.011BC+0.465BD+0.548BE+0.715CD+0.360CE+0.137DE ----- (12)

Coefficient of internal shape (φ_a)= 3.6189 - 0.08077A +0.208B + 0.1300C - 0.09460D + 0.0255E - 0.07585A² - 0.0389B² +0.044C² - 0.1239D² - 0.048E² -0.06144AB - 0.1050AC +0.07987AD-0.050AE-0.0822BC+0.12261BD-0.0045BE-0.14596CD-0.2552CE-0.08994DE ----- (13)

Coefficient of external shape (φ_e)= 1.3065 -0.04433A +0.0614B - 0.0462C + 0.01345D - 0.06922E + 0.0189A² +0.0390B² - 0.0514C² + 0.04665D² - 0.00479E² + 0.05719AB + 0.05270AC + 0.06324AD + 0.05633AE-0.05465BC-0.05404BD+0.00510BE+0.00410CD+0.05573CE-0.04192DE---(14)

Co-efficient of the above polynomial equation where calculated by regression as given by equations (5) to (8)

3.7 Checking the adequacy of the developed models

Analysis of variance (ANOVA) technique was used to test the adequacy of the model. As per this technique, if the F – ratio values of the developed models do not exceed the standard tabulated values for a desired level of confidence (95%) and the calculated R – ratio values of the developed model exceed the standard values for a desired level of confidence (95%) then the models are said to be adequate within the confidence limit [10]. These conditions were satisfied for the developed models. The values are shown in Table 5. Residual plots are shown in Fig 10.

Table 5: Analysis of variance for Testing Adequacy of the Model coefficient of internal shape (ϕ_2)

Source	DF	Seq	SS	Adj SS	MS	F	P
Regression	20	4.8722	4.8722	0.2436	0.59	0.850	
Linear	5	1.8328	1.8328	0.3666	0.89	0.518	
Square	5	0.8061	0.8061	0.1612	0.39	0.844	
Interaction	10	2.2333	2.2333	0.2233	0.54	0.826	
Residual Error	11	4.5122	4.5122	0.4102			
Lack-of-Fit	6	1.9651	1.9651	0.3275	0.64	0.699	
Pure Error	5	2.5472	2.5472	0.5094			
Total	31	9.3844					

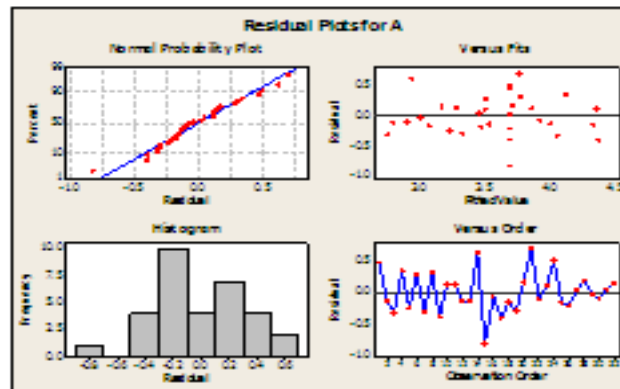


Fig. 5. Residual plots for coefficient of internal shape (A)

IV. CONFIRMATION EXPERIMENTS

Experiments were conducted to verify the regression equations 4-7. Three weld runs used at different values welding current, welding speed, contact tip to work distance, welding gun angle and pinch other than that used in the design matrix. The results obtained found to be satisfactory and the results presented Table 6

Table 6. Results of confirmation experiments

Experiment no	Measured values			Predicted values			Error		
	D (%)	ϕ_2	ϕ_3	D (%)	ϕ_2	ϕ_3	D (%)	ϕ_2	ϕ_3
CON 1	12.8	4.5	3.4	12.4	4.3	3.2	3.1	4.4	8
CON2	12.7	4.8	4.7	12.8	3.9	4.2	-8	14	11
CON3	12.9	4.3	4.2	12.8	4.8	4.1	.8	-11	.2

V. RESULTS AND DISCUSSIONS

5.1 Direct effects of welding variables on bead parameters.

Based on the mathematical models developed for predicting the bead geometry and dilution the effect of welding process parameters on the above bead parameters were calculated and have presented graphically in Fig 6-9. The effects of various process variables on the bead geometry are presented under various headings [11].

5.1.1 Effects of process variables on percent of dilution (D).

Effect of welding current and welding speed on dilution is depicted in fig 6. This shows that dilution increases first and then decreases. This may be due to the fact that weight of the deposited metal per unit of length decreases when the welding speed increases. Percentage of dilution with increase with increase in welding current but effects are not much significant.

5.1.2 Effect of process variables on coefficients of shape of welds

The weld shape coefficients give an indication of bead geometry. The coefficient of internal shape is the width to depth of penetration ratio and the coefficient of external shape is the ratio of width to height of reinforcement. Response surface graphs have been drawn to visualize the nature of response and the give satisfactory explanation about the interaction effects of process parameters on bead geometry. Fig 8 shows the interaction effect of contact tip to work distance (N) and welding current on percent of dilution (D), it is evident that when welding current is increased dilution seems to be decreasing. Fig 11 depicts the effect of welding current (I) and welding speed (S) on coefficient of internal shape. It is evident from the figure that when welding speed is increased for all values of I but at the same time for a given speed the value of coefficients of internal shape decreases as the welding current is increased. Fig 13 depicts the interaction effects of welding current and welding speed on coefficient of external shape. Coefficient of external shape is increased with the increases of welding current. Other interaction surface plots of various process parameters are shown in fig 6-9. Fig 11-12 shows interaction effect of process parameters on coefficient of external and internal shape

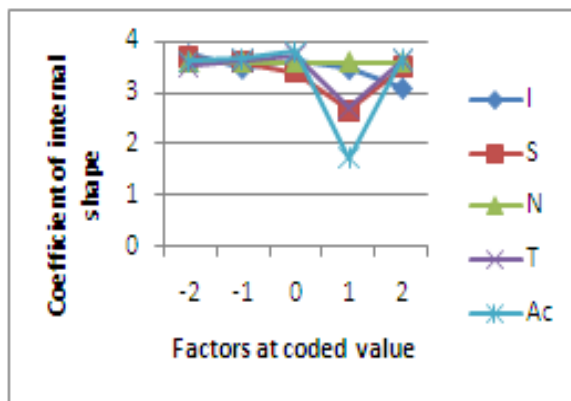


Fig. 6. Direct effects of process parameters on ϕ_i current (I), Contact tip to work distance (N) on percent of dilution (D)

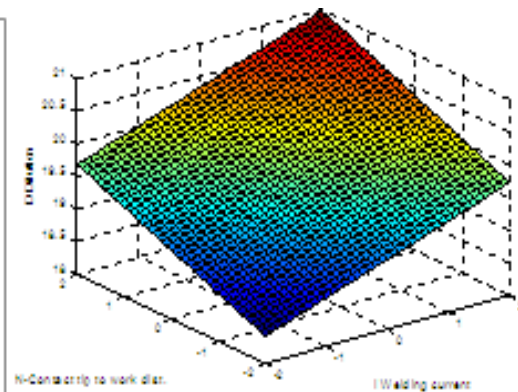


Fig 8. Surface plots for interaction effect of

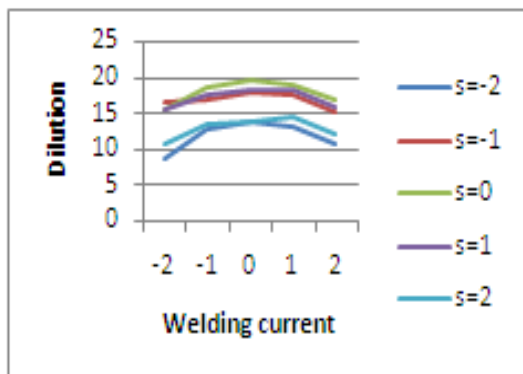


Fig. 7. Direct effect of process parameters on ϕ_i Welding speed(S) on percent of dilution (D).

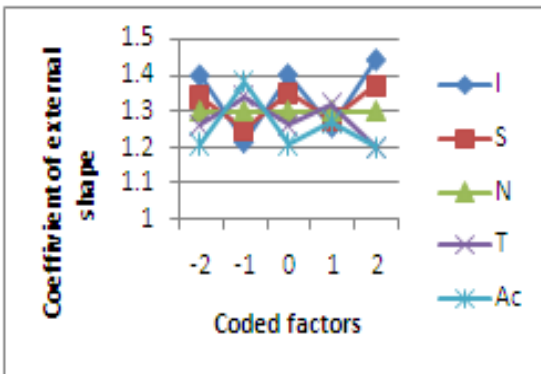


Fig 9. Interaction effect of welding current (I),

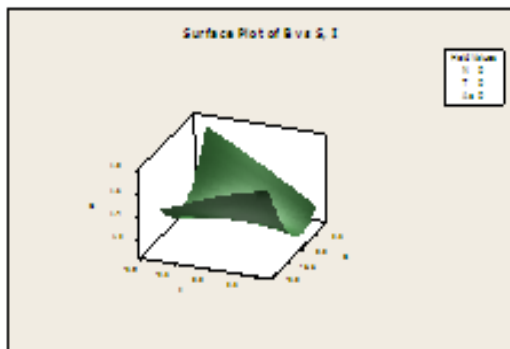


Fig 10. Surface plot for interaction

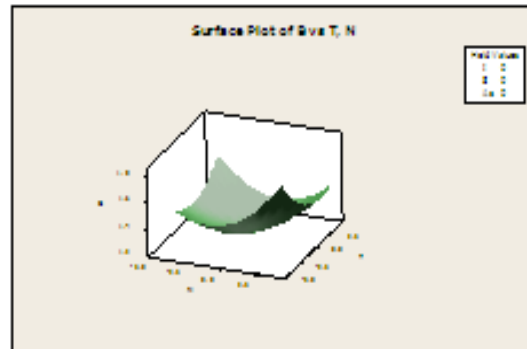


Fig. 11. Surface plot for the interaction effects

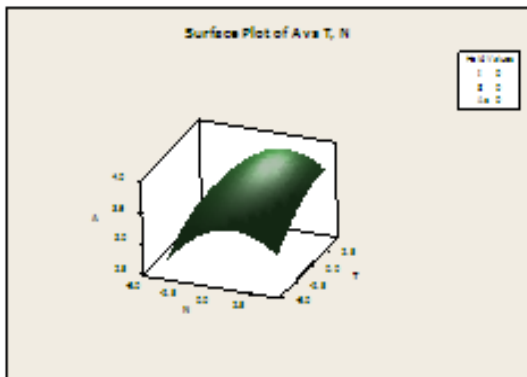


Fig.12. Surface plot for interaction effect on Welding gun angle (T), contact tip to Work distance (N) on coefficient of internal shape

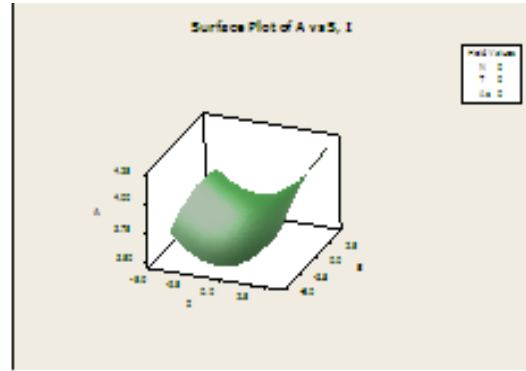


Fig. 13. Surface plot for the interaction effects welding current (I), welding speed(S) on coefficient of internal shape (A).

VI. OPTIMIZATION OF PROCESS PARAMETER USING RESPONSE SURFACE METHODOLOGY

Optimization procedure in RSM is initiated by picking several starting point, from which, searching for optimal factors continued. Two types of solutions are obtained for the search. First is local solution for each starting point there is a local solution. These solutions are best combinations for each factor settings found for the particular starting point. Next is global solution, there is only one global solution which is the best of all local solutions. Global solution is the best combination of factor settings for achieving desired responses. The optimum operating conditions for achieving desirable weld bead geometry are obtained using the statistical software, MINTAB 15.

6.1 Results of optimization

6.1.1 Single objective optimization

- (1) Objective: Minimization of depth of penetration. Optimum process parameters are I=225amp, S=182mm/min, N=26mm, T=110degree, Ac=10and Predicted response, P=1.6mm.
- (2). Objective: Maximizing the reinforcement. Optimum process parameters I=300amo, S=182mm/min, N=26mm, T=110degree, Ac=-10Predicted response, R=7.2875mm.
- (3). Objective: Maximizing the Bead width. Optimum process parameters I=300amp, S=150mm/min, N=26mm, T=70 degree, Ac=-10Predicted response W=15mm.
- (4). Objective: Maximizing the Coefficient of external shape. Optimum process parameters I=280amp, S=148mm/min, N=24mm, T=68degree, Ac=-8Predicted response, $(\phi_e) = 1.3$.
- (5) Objective: Minimizing coefficient of internal shape .Optimum process parameters. I=300amp, S=150mm/min, N=26mm, T=70degree, Ac=-10Predicted response, $(\phi_a) = 3.9$.
- (6) Objective: Minimizing percent of dilution. Optimum process parameters are I=300amp, S=150mm, N=26mm, T=70deg, Ac=-10 Predicted response, D%=11.2.

The typical (sample) optimization plots for single objective optimization are shown in Fig 14 and Fig 15.

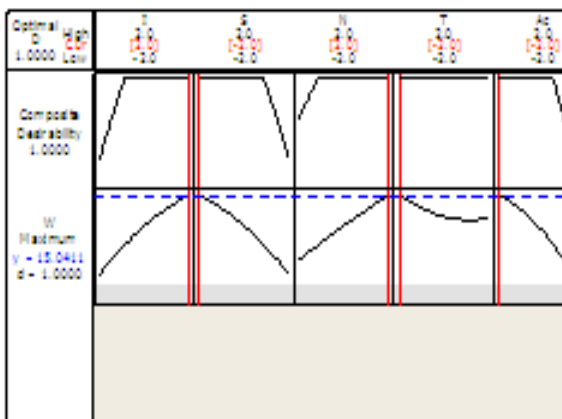


Fig 14.Optimization plot for Bead width

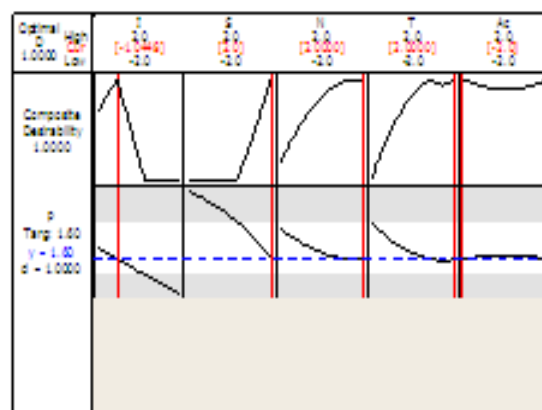


Fig 15 Optimization plot for penetration

6.2 Multi –objective optimization.

As for cladding is concerned the desirable weld bead geometry is one which has maximum depth of penetration minimum bead width, minimum reinforcement and minimum percentage of dilution .This can be achieved by adopting multi objective optimization procedure. To identify the combination of input that jointly optimizes the responses such as penetration, reinforcement, and bead width, dilution, coefficient of external and internal shape were optimized using RSM.

The optimization procedure was carried out using MINITAB 15 with multiple objectives as maximizing penetration and coefficient of external shape, minimizing reinforcement, dilution, bead width and coefficient of internal shape. The optimum parameter setting so obtained for achieving the objectives are I=300amps.S=166mm/min, N=12mm, T=75 degree, Ac=-5. And the optimization plot is depicted in fig 16.

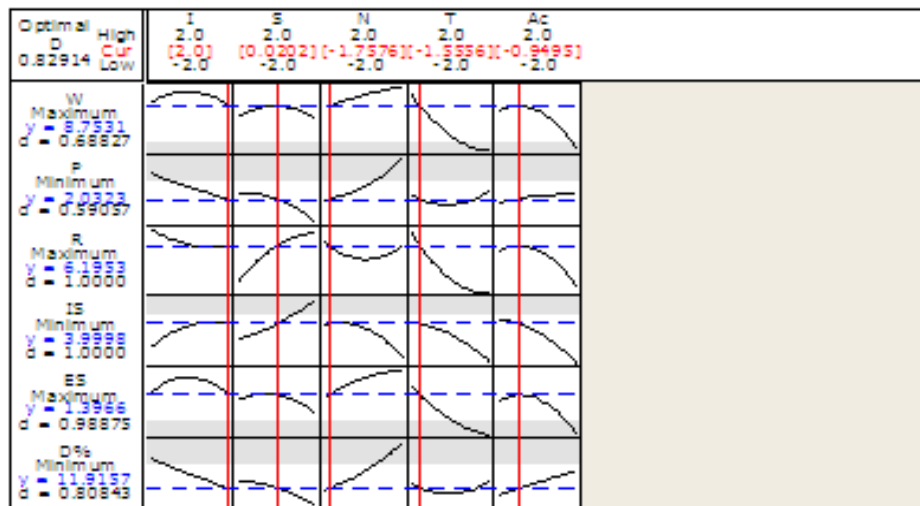


Fig. 12. Optimization plot for combined optimization of weld bead geometry

VII. CONCLUSIONS

1. Regression models were developed using RSM to predict weld bead geometry for 317L stainless steel wire on to IS 2062 structural steel plates.
2. Confirmation experiments showed that developed models are reasonably accurate.
3. It was found that welding current plays an important role in influencing bead geometry.
4. Multi objective optimization by RSM using MINITAB 15 was efficiently carried out.

VIII. ACKNOWLEDGEMENT

The authors sincerely acknowledge the help and facilities extended to them by the department of mechanical engineering SVS college of Engineering, Coimbatore, India.

REFERENCE

- [1]. Kannan,T.;Murugan,N.(2006).Effect of flux cored arc welding process parameters on duplex stainless steel clad quality, Journal of Material Processing Technology vol.176 pp 230-239.
- [2]. Kannan,T.; Murugan,N.(2006).Prediction of ferrite number of duplex stainless steel clad metals using RSM, Welding Journal. pp. 91 - 99.
- [3]. Gunaraj,V.; Murugan, N. (2005).Prediction and control of weld bead geometry and shape relationships in submerged arc welding of pipes, Journal of Material Processing Technology. Vol. 168, pp. 478 – 487.
- [4]. Kim, I.S.; Son, K.J.; Yang, Y. S.; Yarangada, P, K, D.V. (2003).Sensitivity analysis for process parameters in GMA welding process using factorial design method, International Journal of Machine tools and Manufacture. Vol.43, pp. 763 - 769.
- [5]. Cochran, W.G.; Coxz, G.M. (1987).Experimental Design. pp.370, New York, John Wiley & Sons.
- [6]. Serdar Karaoglu.; Abdullah Secgin. (2008).Sensitivity analysis of submerged arc welding process parameters,Journal of Material Processing Technology. Vol-202, pp 500-507.
- [7]. Gunaraj, V.; Murugan, N.(1999) .Prediction and comparison of the area of the heat effected zone for the bead on plate and bead on joint in SAW of pipes,Journal of Material processing Technology. Vol. 95, pp. 246 - 261.
- [8]. Montgomery,D.C.:(2003).Design and analysis of Experiments,John Wiley & Sons (ASIA) Pvt. Ltd.
- [9]. Kannan,T.; Yoganath.(2010).Effect of process parameters on clad bead geometry and shape relationships of stainless steel cladding deposited by GMAW,Int. Journal of Manufacturing Technology.Vol-47, pp 1083-1095.
- [10]. Palani.P.K;Murugan.N(2007).Optimization of weld bead geometry for stainless steel claddings deposited by FCAW, Journal of material processing Technology Vol-190,pp 291-299.
- [11]. Giridharan, P.K.; Murugan,N.; (2009). Optimization of pulsed GTA welding process parameters for the welding of AISI 304 L stainless steel, International Journal of Advanced Manufacturing Technology 40: pp.478 - 489.

Facial Verification Technology for Use In Atm Transactions

Aru, Okereke Eze, Ihekweaba Gozie

Department of Computer Engineering Michael Okpara University of Agriculture, Umudike, Umuahia, Abia State, Nigeria Opara, F.K.

Department of Electrical/Electronics Engineering Federal University of Technology, Owerri, Imo State, Nigeria

Abstract: There is an urgent need for improving security in banking region. With the birth of the Automatic Teller Machines, banking became a lot easier though with its own troubles of insecurity. Due to tremendous increase in the number of criminals and their activities, the ATM has become insecure. ATM systems today use no more than an access card and PIN for identity verification. The recent progress in biometric identification techniques, including finger printing, retina scanning, and facial recognition has made a great efforts to rescue the unsafe situation at the ATM. This research looked into the development of a system that integrates facial recognition technology into the identity verification process used in ATMs. An ATM model that is more reliable in providing security by using facial recognition software is proposed. The development of such a system would serve to protect consumers and financial institutions alike from intruders and identity thieves. This paper proposes an automatic teller machine security model that would combine a physical access card, a PIN, and electronic facial recognition that will go as far as withholding the fraudster's card. If this technology becomes widely used, faces would be protected as well as PINs. However, it obvious that man's biometric features cannot be replicated, this proposal will go a long way to solve the problem of Account safety making it possible for the actual account owner alone have access to his accounts. The combined biometric features approach is to serve the purpose both the identification and authentication that card and PIN do.

Keywords: ATM, Security, Face, Verification, Fraud, PIN, etc

I. INTRODUCTION

To use an ATM with facial recognition system, all you need is walk to the atm. its digital camera is on 24hours a day, and its computer will automatically initiate a face recognition procedure, whenever the computer detects a human face in camera obtains a picture of your face, the computer compares the image of your face to the images of registered customers in its database. If your face (as seen by the ATMs camera) matches the picture of the in the data base you are automatically recognized by the machine.

The machine will then play a recording will be heard through a loudspeaker, the recording will say "your face is recognized".

ATM is one such machine which made money transactions easy for customers to bank. The other side of this improvement is the enhancement of the culprit's probability to get his 'unauthentic' share. Traditionally, security is handled by requiring the combination of a physical access card and a PIN or other password in order to access a customer's account. This model invites fraudulent attempts through stolen cards, badly-chosen or automatically assigned PINs, cards with little or no encryption schemes, employees with access to non-encrypted customer account information and other points of failure. Our paper proposes an automatic teller machine security model that would combine a physical access card, a PIN, and electronic facial recognition. By forcing the ATM to match a live image of a customer's face with an image stored in a bank database that is associated with the account number, the damage to be caused by stolen cards and PINs is effectively neutralized. Only when the PIN matches the account and the live image and stored image match would a user be considered fully verified. The main issues faced in developing such a model are keeping the time elapsed in the verification process to a negligible amount, allowing for an appropriate level of variation in a customer's face when compared to the database image, and that credit cards which can be used at ATMs to withdraw funds are generally issued by institutions that do not have in-person contact with the customer, and hence no opportunity to acquire a photo. Because the system would only attempt to match two (and later, a few) discrete images,

searching through a large database of possible matching candidates would be unnecessary. The process would effectively become an exercise in pattern matching, which would not require a great deal of time. With appropriate lighting and robust learning software, slight variations could be accounted for in most cases. Further, a positive visual match would cause the live image to be stored in the database so that future transactions would have a broader base from which to compare if the original account image fails to provide a match – thereby decreasing false negatives.

When a match is made with the PIN but not the images, the bank could limit transactions in a manner agreed upon by the customer when the account was opened, and could store the image of the user for later examination by bank officials. In regards to bank employees gaining access to customer PINs for use in fraudulent transactions, this system would likewise reduce that threat to exposure to the low limit imposed by the bank and agreed to by the customer on visually unverifiable transactions.

In the case of credit card use at ATMs, such a verification system would not currently be feasible without creating an overhaul for the entire credit card issuing industry, but it is possible that positive results (read: significant fraud reduction) achieved by this system might motivate such an overhaul.

The last consideration is that consumers may be wary of the privacy concerns raised by maintaining images of customers in a bank database, encrypted or otherwise, due to possible hacking attempts or employee misuse. However, one could argue that having the image compromised by a third party would have far less dire consequences than the account information itself. Furthermore, since nearly all ATMs videotape customers engaging in transactions, it is no broad leap to realize that banks already build an archive of their customer images, even if they are not necessarily grouped with account information

II. COMBATING AUTOMATED TELLER MACHINE FRAUDS THROUGH FACIAL RECOGNITION ATM TECHNOLOGY

ATMs have brought so much relief to the financial world. Various problems were solved with the advent of these machines ranging from keeping the banking hall free of traffic with its attendant issues. Gone are the days of maintaining long queues in the banking hall which made the work of bankers more difficult thus leading to all forms of errors. Even to customers, having to leave the comfort of their homes for financial transactions before bankers close for the day's business is a major problem solved by Automated Teller Machines. However, as man begins to realize the gains of technology brought about by this machine to supplement human tellers, little did one know that the joy shall be short lived by the various sharp practices leading to financial losses.

As banks are losing, so are the customers. News Media are filled with various forms of complaints on how users are losing money to fraudsters. Some have vowed never to come near usage of various cards – debit, credit or prepaid– local or international. The problem may even go as deep as engaging in legal battle between banks and their customers. The need to find a lasting solution is the main focus of this paper.

2.1 Present Controls

Considering the volume of transactions being processed by several branches of a commercial bank, proper control in form identification and authentication should be in place. Several control measures have been put in place to ensure interests of all concerned parties such as issuers, acquirers, third party processors, switching companies and cardholders are protected. Some of the controls in place include:

About ATM

- Well lit up to discourage shady deeds at night
- Fortified with camera for footage
- Keypad protector against key logger and shoulder surfing
- Dual control of physical access to the machine
- Default password disabled to avoid unauthorized access
- Lines of demarcation between a current user and the next person on the queue to prevent shoulder surfing.
- Timely reconciliation of cash loading with ATM Till account
- Surveillance through physical monitoring and CCTV cameras

B. About Cards

- Strong algorithms are used in generating PANs
- Storage of card details is done on protected systems
- Card details (such as PAN, expiry date) are jealously guarded.
- While communicating, PAN is masked

- Strong Encryption is used when transferring files especially, between TPP and Issuer
- Magnetic stripe type is outlawed in some countries to avoid card cloning.
- Some restrictions are placed on cards in terms of allowable transactions and withdrawal limits

C. About PIN

- Where PIN mailers are used, they are not dispatched at the same time with the cards and usually through a different medium.
- PIN selectable options are used to prevent insider compromise
- PINs are masked during usage against shoulder surfing.

III. SECURING CUSTOMERS THROUGH FACIAL RECOGNITION AUTHENTICATION

ATM usage usually, works on two-factor authentication requiring something you have and something you know or you are. To use an ATM presently, demands having a card that has to be authenticated by PIN as a second factor authentication. To aid memory, some users write their PINs in diaries or store them on some other unprotected devices.

The moment the card is accessible, PIN is guessed or obtained through other means such as social engineering, shoulder surfing or outright collection under duress. Recently, Biometric ATMs are introduced to be used along with card. This will definitely impact on the amount frauds if fully implemented. Further development has produced biometric authentication in Japan where customer's face is used as a means of authentication. Phil (2012), examined the "You are the cash card" roll out in Japan where authentication is just by your face, PIN and the card.

3.1 Secure Atm By Facial Recognition Technology (Image Processing)

To use an ATM with facial recognition system, all you need is walk to the atm. its digital camera is on 24hours a day, and its computer will automatically initiate a face recognition procedure, whenever the computer detects a human face in camera obtains a picture of your face, the computer compares the image of your face to the images of registered customers in its database .If your face (as seen by the ATMs camera) matches the picture of the in the data base you are automatically recognized by the machine.

An Image may be defined as a two dimensional function $f(x,y)$ where x and y are spatial(plane) coordinates x , y is called intensity or gray level of the image at that point. When x , y and the amplitude values of f are all finite, discrete quantities, we call the image a digital image.

Interest in digital image areas: improvement of pictorial information for human interpretation: and representation for autonomous machine perception.

The entire process of Image Processing and starting from the receiving of visual information to the giving out of description of the scene, may be divided into three major stages which are also considered as major sub areas, and are given below

Discretization and representation: Converting visual information into a discrete form

3.2 Methodology

The first and most important step of this project will be to locate a powerful open-source facial recognition program that uses local feature analysis and that is targeted at facial verification. This program should be compilable on multiple systems, including Linux and Windows variants, and should be customizable to the extent of allowing for variations in processing power of the machines onto which it would be deployed. We will then need to familiarize ourselves with the internal workings of the program so that we can learn its strengths and limitations. Simple testing of this program will also need to occur so that we could evaluate its effectiveness. Several sample images will be taken of several individuals to be used as test cases – one each for "account" images, and several each for "live" images, each of which would vary pose, lighting conditions, and expressions.

Once a final program is chosen, we will develop a simple ATM black box program. This program will serve as the theoretical ATM with which the facial recognition software will interact. It will take in a name and password, and then look in a folder for an image that is associated with that name. It will then take in an image from a separate folder of "live" images and use the facial recognition program to generate a match level between the two. Finally it will use the match level to decide whether or not to allow "access", at which point it will terminate. All of this will be necessary, of course, because we will not have access to an actual ATM or its software.

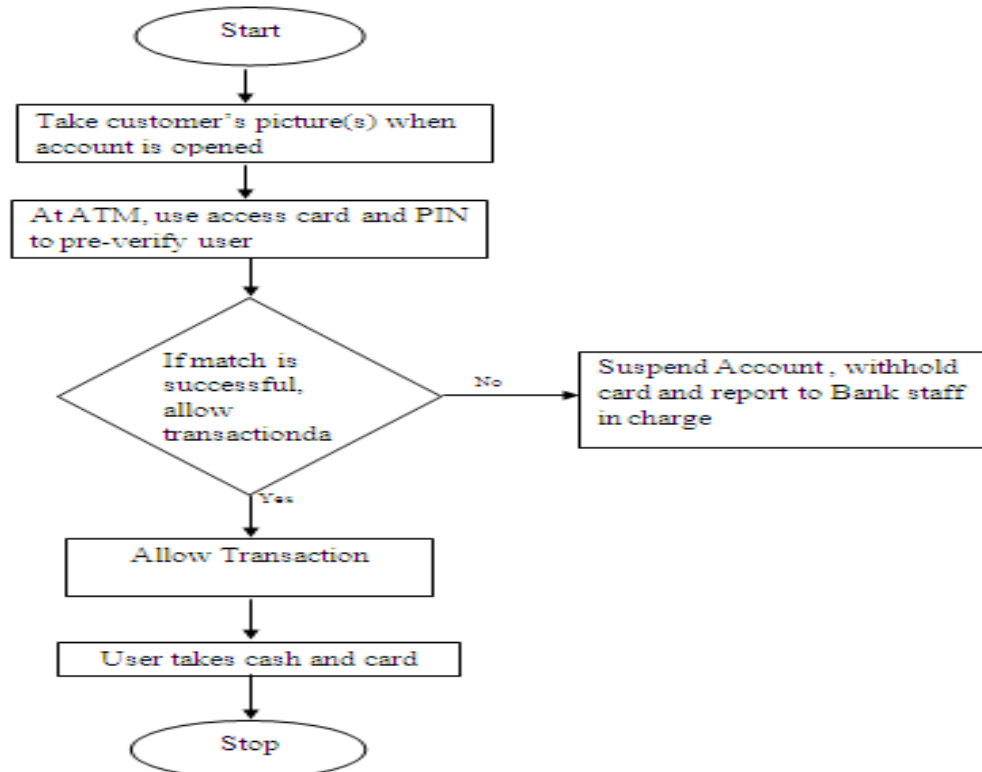
Both pieces of software will be compiled and run on a Windows XP and a Linux system. Once they are both functioning properly, they will be tweaked as much as possible to increase performance (decreasing the time spent matching) and to decrease memory footprint.

Following that, the black boxes will be broken into two components – a server and a client – to be used in a two-machine network. The client code will act as a user interface, passing all input data to the server code, which will handle the calls to the facial recognition software, further reducing the memory footprint and processor load required on the client end. In this sense, the thin client architecture of many ATMs will be emulated.

We will then investigate the process of using the black box program to control a USB camera attached to the computer to avoid the use of the folder of “live” images.

Lastly, it may be possible to add some sort of DES encryption to the client end to encrypt the input data and decrypt the output data from the server – knowing that this will increase the processor load, but better allowing us to gauge the time it takes to process.

3.2.1 Flow Chart of The Operation



3.3 FACE RECOGNITION SOFTWARE:

Face recognition technology: Ideal for access control, financial transactions and ATM machines.

3.3.1 The face key recognition technology performs the following tasks:

- Locates a moving object within the camera view
- Determines if the moving object is face
- Compares live faces with samples from database
- Face recognition technology can work with both low resolution USB
- Cameras and low or high resolution CCTV cameras

3.3.2 Face capturing technology: Captured and stored with time and date.

Face finding technology captures all the faces in a camera's view. Then it stores each image in a separate folder for quick reviews—or for use with another face key technology. Each face is saved with a time and date stamp. In addition to faces, facial profiles and images of human bodies can be captured and stored.

Search and match advisory technology:

Search and match advisory technology is available to assist in the identification of facial images extracted from the video stream or from a watch list database. This function operates by comparing a subject's photo to a database of faces and selecting the faces from the database which look the most like the subject's face....your face is your key.

3.4 Atm Fraud Types To Be Prevented By Atm Facial Recognition Technology

- Unauthorised financial operations using lost or stolen cards and pin codes which many inexperienced card owners write down on a card or store the PIN code together with the card.
- Fraud based on Trust- The card or its duplicate can be used by a fraudster without the permission of the card owner.
- Installation of additional devices that allow the reading of a cards magnetic stripe and save on video numerical combinations typed on cash machine keyboard.

3.5 ATM Security - Importance of ATM Security

Importance of ATM security

Having a solid security to ATMs is very vital for banks to maintain their quality service and reputation. Most leading and established banks do consider this fact as a top priority when you have a reliable security to your ATMs there are many positive outcomes. Mainly you will win the customers' trust and loyalty, reduction of financial losses due to technical and non-technical robberies, and added security will improve the rate of transactions and eventually the banks can profit through it.

3.6 Advantages Of Facial Recognition Technology

Eradicate Fraud costs for the bank

- * Deliver a practical and workable solution that addresses the requirements of the regulatory authorities.
- * Limit the financial risks given that they were forced to take responsibility for financial loss [rather than being allowed to pass this on to the account-holder]
- * Provide a framework that still allowed for high withdrawal limits to cater for the demands of a cash-focused customer base
- * Take societal responsibility to reduce rising levels of crime that were associated with cash-card transactions
- * Increase customer satisfaction

For the account-holder, the potential advantages are:

- * Different charges for transactions given that the transaction takes place in a more secure manner
- * Higher withdrawal and transaction limits
- * Peace of mind given the higher level of security applied to the account

IV. CONCLUSION

We thus develop an ATM model that is more reliable in providing security by using facial recognition software. By keeping the time elapsed in the verification process to a negligible amount we even try to maintain the efficiency of this ATM system to a greater degree.

Biometrics as means of identifying and authenticating account owners at the Automated Teller Machines gives the needed and much anticipated solution to the problem of illegal transactions. In this paper, we have tried to proffer a solution to the much dreaded issue of fraudulent transactions through Automated Teller Machine by biometrics that can be made possible only when the account holder is physically present. Thus, it eliminates cases of illegal transactions at the ATM points without the knowledge of the authentic owner. Using a biometric feature for identification is strong and it is further fortified when another is used at authentication level.

REFERENCES

- [1]. Adeoti, J. (2011). Automated Teller Machine (ATM) frauds in Nigeria: the way out.
- [2]. Adini (2010). Nigerian banks look to biometric ATM machines to reduce fraud.
- [3]. <http://nairavilla.com/topic/743>. accessed October 12,2012.
- [4]. Bhargav-Spantzel A., Squicciarini A., Bertino E. Kong X & Zhang W.(2010). Biometrics-Based Identifiers for Digital Identity Management.
- [5]. Consultative Group for International Agricultural Research, CGIAR (2009). Network user identification and authentication good practice guide.
- [7]. Das, S. & Debbarma, J.(2011). Designing a biometric strategy (fingerprint) measure for enhancing ATM security in India e-Banking system. International Journal of Information and Communication Technology Research vol 1 no 5 p 197-203.
- [8]. Devinaga, R. (2010). ATM risk management and controls. European journal of economic, finance and administrative sciences. ISSN 1450-2275 issue 21.
- [9]. George Webster (2010). Biometric ATM gives cash via facial recognition scan. [Http://edition.cnn.com](http://edition.cnn.com). accessed October 10, 2012.
- [10]. Heather Crawford (2011). Applying Usable Security Principles to Authentication.
- [11]. Jacobs, B. & Poll, E. (2010) Biometrics and Smart Cards in Identity Management.
- [12]. Mohammed, L. (2010). Use of biometrics to tackle ATM fraud.
- [13]. Researchers at MIT, Baback Moghaddam and Alex Pentland, and one a commercial product from Identix called FaceIt

Aru, Okereke Eze

is a lecturer in the Department of Computer Engineering, Michael Okpara University of Agriculture, Umuahia, Abia State, Nigeria. His research Interests include Computer Hardware design and maintenance, Security system design, , expert systems, Design of Microcontroller and Microprocessor based system, digital systems design using microcontrollers and other computer related subjects.

Dr. Ihekweaba, Gozie

is the Head, Department of Computer Engineering, Michael Okpara University of Agriculture, Umuahia, Abia State, Nigeria. Her research interests include Computer Hardware design and maintenance, Security system design, expert systems etc.

Dr. Opara, F.K.

is the Head, Department of Electrical/Electronics Engineering, Federal University of Technology, Owerri, Imo State, Nigeria. His research interests include Computer Hardware design and maintenance, Electronic and Communication Systems, Electronic Security system designs etc.

Preventing ADDOS Attack by Using Secure TRNG Based Port Hopping

T. Siva¹, E. S. Phalguna Krishna², K. Pavan Kumar³

1,2,3 Department of CSE, Sree Vidyanikethan Engineering college, Tirupathi, A.P, INDIA.

Abstract: Now a day's each and every where we are using client-server communication for different information service systems. Normally client server communication can be differentiating by using IP Address and Protocol Port number from one machine to another machine. In network environment we are already having DOS/DDOS Attacks Another Subset of this attack scenario is DOS/DDOS attack is Application Denial of Service(ADOS)attack ,In this the adversary attacks open Ports/Ideal ports present at server side for this the adversary Know need huge machines ,zombie systems and no need sending packets of data with high bandwidth. To control this type of A-DOS attacks the existing enterprise security devices are not suitable like firewalls, anti-viruses and IDS/IPS Systems why because the adversary not using high bandwidth, spam messages, zombie`s or botnet`s for their attack scenarios.

To safeguard this type of DOS/DDOS or Application denial of service attacks we are having some port hopping mechanisms i.e Port hopping by using Pseudo Random Number Generation (PRNG)based port hopping ,Acknowledgement based port hopping and proactive Reinitialization based on this existing once and their disadvantages like in PRNG attackers can predict the random number generation by using pre-calculated list or based on mathematical functions .we introduce new port hopping technique i.e True Random Number Generation based port hopping

Keywords: DOS/DDOS attacks, Application Denial of Service attacks (ADOS), Zombie Systems, PRNG, True Random Number Generation.

I. INTRODUCTION

The Internet is becoming increasingly pervasive everyday with the emergence of new wireless technologies and devices that provide anytime anywhere access to the Internet. Today, hosts connected to the Internet include mainly servers and client computers, PDA etc. In the future, other devices such as embedded appliances, cars and anything that runs on electricity will be connected, especially with the emergence of IPv6. These hosts will benefit enormously from the Internet connectivity. However, when they are connected to the Internet, they will become potential attack targets. Presently, conventional enterprise security mechanisms, such as firewall and intrusion detection/prevention systems (IDS/IPS) are used to provide managed security services in an enterprise or ISP framework. As we have more types of devices and applications connected, the current security measures will not be appropriate for the new paradigms.

Consequently, new and simple security methodologies are needed to address the new security concerns of new types of devices or appliances, which typically run very simple applications. One of the main threats of Internet security is DoS (Denial of Service) and DDoS (Distributed DoS) attacks . Such attacks have paralyzed high profile web sites. Although there has been less publicity since then, research and measurements [2] have shown that the attacks are still raging on day to day. As such devices typically have lower networking bandwidth and computing resources, they are more vulnerable to such attacks as compared to servers protected by layers of firewalls and IDS/IPS. Many techniques have been proposed and studied to address the problem of DoS(or)DDoS attacks. However, the drawback of most approaches is they are complex and that significant changes to the Internet routers are generally required.

II. GENERAL CLIENT SERVER COMMUNICATION

The client-server characteristic describes the relationship of cooperating programs in an application. The server provides a function or service to one or many clients, initiate requests for such services. The model assigns any one roles to the computers in a network: Client or server. A server is a computer system that shares its resources; a client is a computer or computer program that initiates communication with a server in order to make use of a resource. Data, CPUs, printers, and data storage devices are some examples of resources. Clients and servers exchange information in a request-response messaging pattern. The client sends a request message, and the server returns a response message. This sharing of computer system resources is called time-sharing, because it allows multiple applications and services to use the computer's resources at the same time. All client-server protocols operate in the application layer.

III. IP ADDRESS AND PORT NUMBERS IN OSI REFERENCE MODEL

In computer network programming, the **application layer** is an abstraction layer reserved for communications protocols and methods designed for process-to-process communications through an Internet Protocol (IP) computer network. Application layer protocols use the underlying transport layer protocols to establish host-to-host connections.

In the OSI model, the definition of its application layer is narrower in scope. The OSI model states the application layer as being the user interface. The OSI application layer is responsible for displaying data/Information and images to the user in a human understanding format and to interface with the presentation layer below it. The transport layer is responsible for giving services to the application layer it receives services from the network layer.

1.1 Process-to-Process Communication

The responsibility of a transport-layer protocol is to provide **process-to-process communication**. A process is an application-layer entity that uses services of the transport layer. The network layer is responsible for communication at the computer system level (host-to-host communication). A network layer protocol can deliver the message only to the destination computer system. However, this is an incomplete delivery. The message still needs to be handed to the correct process. This is where a transport layer protocol come into picture. A transport layer protocol is responsible for delivery of the message to the appropriate process [3]. Figure 1 shows the domains of a network layer and a transport layer.

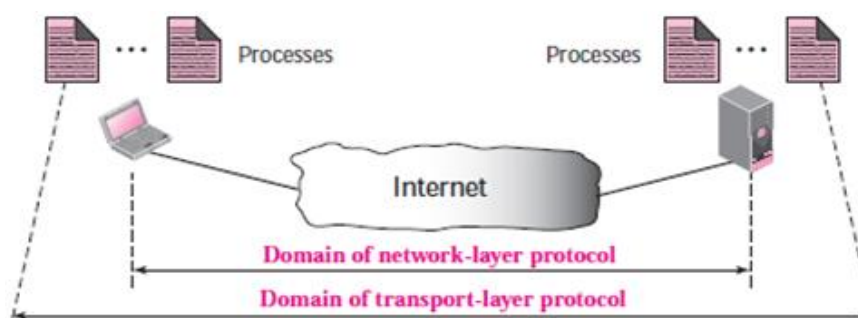


Figure 1. Network layer vs Transport layer

Although there are a few ways to achieve process-to-process communication, the most common thing is through the client-server paradigm. A process on the local host, called a client, needs services from a process usually on the remote host system, called a server. Both processes (client and server) have the same name. For communication, we must define the

- Local host
- Local process
- Remote host
- Remote process

The local host and the remote host are stated using IP addresses. To define the processes, we need second identifiers called port numbers. The port numbers are integers between 0 and 65,535. The client program defines itself with a port number, called the ephemeral port number [3]. The word ephemeral means short lived and is used because the life of a client is normally short time. An ephemeral port number is recommended to be greater than 1,023 for some client/server programs to work correctly. The server process must also define itself with a port number. This port number, however, cannot be chosen randomly. If the computer at the server site runs a server process and assigns a random number as the port number, the process at the client side that wants to access that server and use its services will not know the port number. TCP/IP has decided to use universal

port numbers for servers known as well-known port numbers[3]. There are some exceptions to this type of rule, for example, there are clients that are assigned well-known port numbers. Every client process knows the well-known port number of the corresponding server process. For example, while the daytime client process, can use an ephemeral (temporary) port number 52,000 to identify itself instead of original port number, the daytime server process must use the well-known (permanent) port number 13. Figure 2 shows concept of port numbers in transport layer.

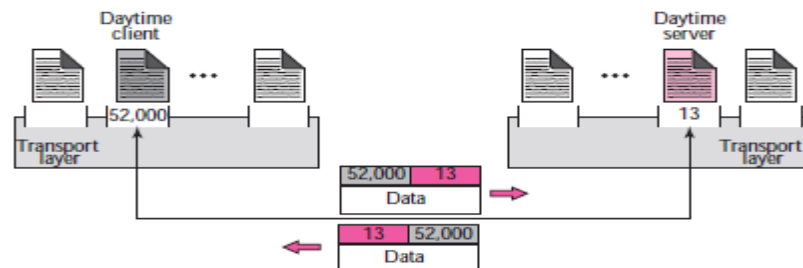


Figure 2. Port numbers used at transport layer

It should be clear by now that the IP addresses and port numbers play different roles in selecting the final destination of data. The destination IP address defines the host among the different hosts in the world. After the host has been selected, the port number defines one of the processes on this particular host

1.2 ICANN Ranges

ICANN has divided the port numbers into three ranges: well-known, registered, and dynamic (or private).

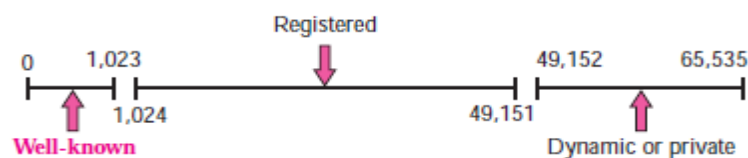


Fig 4. ICANN ranges

Well-known ports.

The ports ranging from 0 to 1,023 are assigned and controlled by ICANN. These are the well-known ports.

Registered ports.

The ports ranging from 1,024 to 49,151 are not assigned or controlled by ICANN. They can only be registered with ICANN to prevent duplication of port numbers.

Dynamic ports.

The ports ranging from 49,152 to 65,535 are neither controlled nor registered. They can be used as temporary or private port numbers. The original recommendation was that the ephemeral port numbers for clients be chosen from this range.

IV. APPLICATION DENIAL OF SERVICE ATTACKS

Application DoS attacks exploit flaws in the application layer design and implementation to prevent authorized access to the victim's services[4]. They represent a set of attacks on different applications, as they are aimed specifically at disrupting operation rather than diverting the application access controls. Attacks based on exploiting these flaws can offer the attacker a number of advantages over traditional DoS attacks:

- Application DOS attacks are efficient: The attacker may not need as much resource machines at their disposal to successfully complete the attack. Application level attacks target bottlenecks and resources limitations within the application not use large amount of bandwidth and do not require many compromised "zombie" systems.
- The attacks will not be detectable or preventable by existing enterprise security monitoring solutions: Since the attacks do not consume more amounts of bandwidth and it maybe indistinguishable from normal traffic.
- Application DOS attacks are harder to trace: Application level attacks normally use HTTP or HTTPS as their transport communication. Many of these proxy servers do not keep logs of connection attempts and could therefore successfully hide the true origin of the attacking host. Proxy servers can therefore be used to obfuscate the true origin of the attacker.

Distributed denial of service (DDoS) attacks size and frequency grown dramatically as attackers take advantage of botnets and other high-speed Internet access technologies to overwhelm their victim's network infrastructure.

Arbor Networks' sixth annual report[5] on ADDOS attacks: A small serve on this Application DDOS attacks is Worldwide Infrastructure Security Report has shown that not only are DDoS attacks getting larger and more frequent, but they are also becoming more sophisticated as they pinpoint specific applications with smaller, more targeted and stealthy attacks. This means that Internet Service Providers (ISPs) with complex services must now be prepared to protect themselves from different types of DDoS attacks:

- 1) Volumetric DDoS Attacks: Network infrastructure and servers block with high-bandwidth-consuming flood attacks. Trace backing and detection is easy with enterprise security devices.
- 2) Application-Layer DDoS Attacks: This attempt to target specific well-known applications such as Hypertext Transfer Protocol (HTTP), Voice over Internet Protocol (VoIP) or domain name system (DNS).Trace backing and Detection is not possible.

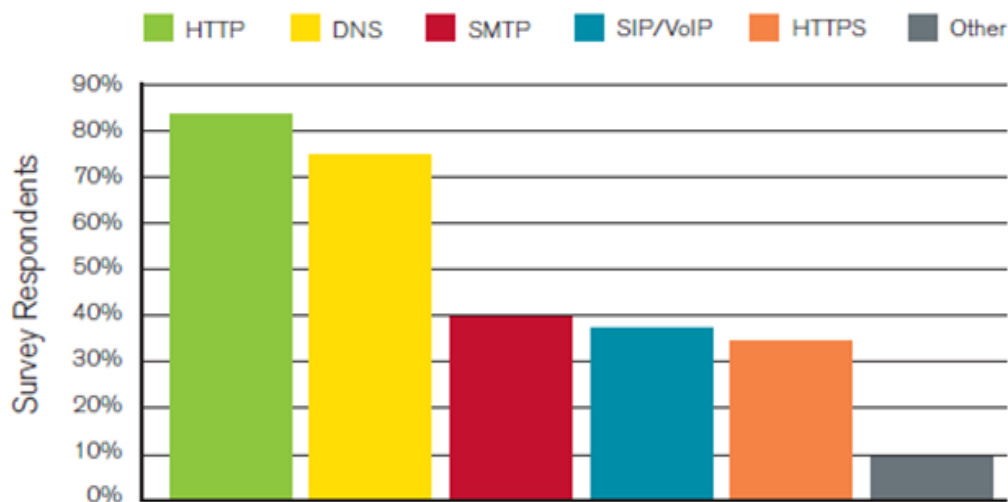


Fig 5. **Layer 7 DDoS Attacks:** Application-layer attacks are on the rise, according to Arbor's sixth annual Report. In other words, ISPs and enterprises must now be prepared to protect themselves from two very different types of DDoS attacks:

Volumetric DDoS Attacks

These attacks try to overwhelm the network infrastructure (e.g., switches, routers, etc.) with bandwidth-consuming such as Internet Control Message Protocol (ICMP) or User Datagram Protocol (UDP) floods. Alternatively, they can attempt to overwhelm servers, load-balancers and firewalls by using Transmission Control Protocol (TCP) state exhaustion attacks such as TCP SYN floods and idle session attacks e.t.c.

Application-Layer DDoS Attacks

These attacks generally consume low bandwidth and when compared to volumetric attacks. However, they can have a similar impact to service as they target specific characteristics of well-known applications such as HTTP, DNS, VoIP or Simple Mail Transfer Protocol (SMTP) e.t.c.

V. EXISTING PORT HOPPING TECHNIQUES

This port hopping technique is compatible with the UDP and TCP protocols and can be implemented using the socket communications for the UDP protocol, and for setting up TCP communications [2]. Secure Overlay Service (SOS) that proactively mitigates DoS attacks. It is geared towards supporting services or similar types of communications. The architecture is constructed using a combinations of secure overlay tunneling[2], routing via consistent hashing and filtering mechanisms. Again, the drawback of this scheme is the necessity to make changes to the Internet infrastructure routers. Netbouncer for DoS/DDoS mitigation which proposed to test the legitimacy of arrival incoming packets. This approach is an end point based solution to DoS/DDoS protection, in that changes are made to the servers or clients, but not to the Internet routers. The tests are carried out by the end hosts, and can be conducted at the network layer (IP), transport layer (TCP) application layer. For example, at the IP layer, the end host can test if the IP address in an arrival incoming packet is associated with a live host. Such test can be carried out using ICMP echo messages. The key issue of this approach is to find a simple and effective test.

1.3 Random Number Generation Port Hopping Mechanism

To controlling Application Denial of service attacks we are having some port hopping and reinitialization mechanisms.

PRNGs are algorithms that use mathematical formulae or simply precalculated list of tables to produce sequences of numbers that appear randomly. A good example of a PRNG is the linear congruential method. A good deal of research has gone into pseudo-random number theory, and modern algorithms for generating pseudo-random numbers are so good that the numbers look exactly like they were really random. Change the server's port numbers dynamically[2] as a function of time. In this, time is divided into discrete slots S_i , where $i = \{0, 1, 2, \dots\}$, each of duration τ . In conventional TCP/UDP services, the port number used is unchanged for a specific communication interval. In this scheme, different port numbers are used in different time slots for the same communication service. Let P_i represents the port number used by the server in time slot S_i . P_i is determined by equation (1), where k is a shared cryptographic key between the server and the client communication and f is a pseudo-random number generator. $P_i = f(i, k)$ (1)

When a client needs to communicate with the server, it will identify the server's current port number P_i using the shared secret key k and the time slot number i . When the server receives packets of data that carry "invalid" port numbers, they can be easily detected and filtered off. There is no need for the server to examine the contents of the packets in order to identify if a packet is malicious. As a result, the computational resources needed to detect and filter off the malicious data packets is reduced. In this l as the overlapping time slot factor. This parameter is used to address two issues: the time synchronization error between the client side and the server side, and the transmission delay between them. This mechanism reserves a part of the previous and next time slot to allow for packet exchange taking place near the boundaries of significant time slots. Let t_i be the start of time slot i and P_i be the associated port number. Then P_i is defined to be valid from time $(t_i - \frac{1}{2}\tau)$ to $(t_{i+1} + \frac{1}{2}\tau)$.

For example, When $l = 0$, a port number is valid only within a specific time port does not increase the chance of a security breach, as a single application is listening on all open ports. Give a generic analysis of the communication success rate over a port-based rationing channel in different attack situations. In this differentiate between directed attacks, where the adversary knows the port used and blind attacks, in which the adversary does not know the port. Not surprisingly, Directed attacks are extremely harmful: that it will have to resort to blind attacks. Our basic idea is to change the filtering criteria in a manner that cannot be predicted by the adversary. This port-hopping approach minimizes the technique of a frequency-hopping spread spectrum in radio communication channel In earlier work, Presented Drum [4], a gossip based multicast protocol resistant to DoS attacks. Drum does not use pseudorandom port hopping, and it heavily relies on well-known ports that can be easily attacked. Therefore, Drum is far less resistant to DoS attacks than the protocol present here. Describe a protocol that allows for DoS-resistant from A, and these acks allow the parties to hop through ports together. However, although the ack-based protocol works well as long as the adversary fails to attack the correct port, once the adversary identifies the port used, it can perform directed attack that renders the protocol useless. By attacking the found data port or simultaneously attacking the found data and ack ports, the attacker can effectively drop the success rate to 0, no port hopping will occur. To solve this matter, there is a time-based proactive reinitialization of the ports used for the ack-based protocol communication, independent of any messages passed in the system.

1.4 Ack-Based Port Hopping

We present an ack-based port-hopping[6] protocol, which uses two port-based rationing communication channels, from B to A and vice versa. For simplicity, we assume that $R_{AB} = 2R_{BA} = 2R$. B always keeps two open ports for data reception from A, and A keeps one port open for acks from B. The protocol hops ports upon a successful round-trip on the most recent port used, using a pseudorandom function PRF*. In order to avoid hopping upon adversary messages, all protocol messages carry authentication information, using a second pseudorandom function PRF on $\{0,1\}^*$. If Acknowledgement lost then attacker can attack blind attacks

1.5 Adding Proactive Reinitializations

Introduce a proactive reinitialization[6] mechanism that allows choosing new seeds for the ack-based protocol depending on time and not on the messages passed in the system. We denote by $t_A(t)|t_B(t)$ the local clocks of A and B, respectively, where t is the real time. In this we get that $0 \leq |t_A(t) - t| \leq \Phi$, $0 \leq |t_B(t) - t| \leq \Phi$ here also assume that $t_A, t_B \geq 0$. If A reinitializes the ack-based protocol then sends a message to B at time $t_A(t_0)$, this message can reach B at anywhere in the real-time interval $(t_0, t_0 + \Delta]$. Therefore, the port used by A at $t_A(t_0)$ must be opened by B at least throughout this interval session. To handle the extreme case where A sends a message at the moment of reinitialization, B must use the appropriate suitable port starting at time $t_B(t_0) - \Phi$. We define δ as

the number of time units between reinitializations of the protocol and assume for simplicity and effectiveness of resource consumption that $\delta > 4\Phi + \Delta$. Every δ time units, A sends a new seed value to the ack-based protocol, and B anticipates it by creating a new instance of the protocol, which waits on the new expected ports. Once communication is established using the new protocol instance or once it is clear that the old instance is not going to be used anymore, the old instance is terminated.

1.6 PRNG Port hopping Disadvantages

- PRNGs generate random numbers based on mathematical formulae or precalculated list, so attacker can easily predict or know the random numbers.
- Deterministic: Given sequence of numbers may be reproduced later date if know the starting point in the sequence.
- PRNGs are periodic: Means that the sequence will eventually repeat at any point itself .

VI. NEW TRNG PORT HOPPING

TRNGs extract randomness from physical phenomena and introduce it into a computer system. We can imagine this as a die connected to a computer system. The physical phenomenon can be very simple, like the little variations in somebody's mouse movements or in the amount of time between keystrokes. In practice, however, we have to be careful about which source you chosen. For example, it can be tricky to use keystrokes in this one, because keystrokes are often buffered by the computer operating system, meaning that several keystrokes are collected before they are sent to the programming waiting for them. To a program waiting for the keystrokes, it will seem as though the keys were pressed almost simultaneously, and there may not be a lot of randomness there after all.

However, there are many other ways to get true randomness into computer system. A really good physical phenomenon to use is a radioactive source. The points in time at which a radioactive source decays are completely unpredictable by the persons, and they can quite easily be detected and fed into a computer system, avoiding any buffering mechanisms in the operating systems. Another suitable physical phenomenon is atmospheric noise, which is quite easy to pick up with a normal radio changes. Another one is background noise from an office or laboratory, but you will have to watch out for different patterns. The fan from computer might contribute to the background noise, and since the fan is a rotating device, chances are the noise it produces won't be as random as atmospheric noise. In this way we can implement different TRNG sources and generate different random numbers for port hopping.

Table 1. Comparison of PRNGs and TRNGs

Characteristic	PRNG	TRNG
Periodicity	Periodic	Aperiodic
Determinism	Deterministic	Nondeterministic
Efficiency	Excellent	Poor

The above table represent the difference between the Pseudo Random Number Generation and True Random Number Generation based on some characteristics.

VII. CONCLUSION

In this one we are given general client server communication by using IP Address and protocol port number. How adversaries can pose DOS/DDOS and Application Denial of Service (ADOS) attacks in client server environment. Given control measures of DOS/DDOS Attacks (like Firewalls ,Anti-viruses and IDS/IPS) and mitigating ADOS by Pseudo Random Number Generation (PRNG) port hopping based on disadvantages like prediction of next port number by using PRF and pre calculated lists. Introduce secure Random number generation i.e True Random Number Generation (TRNG) based port hopping.

REFERENCES

- [1]. Zhang Fu, Marina Papatriantafidou, and Philippas Tsigas "Mitigating Distributed Denial of Service Attacks in Multiparty Applications in the Presence of Clock Drifts" Ieee Transactions On Dependable And Secure Computing, Vol.9, No.3, May/June 2012.
- [2]. H. Lee and V. Thing, "Port Hopping for Resilient Networks," Proc. IEEE 60th Vehicular Technology Conf. (VTC2004-Fall), vol. 5, pp. 3291-3295, 2004.
- [3]. A Text book of "TCP/IP Protocol Suite", Fourth Edition by Behrouz A. Forouzan
- [4]. Stephen de Vries "A Corsaire White Paper: Application Denial of Service (DoS) Attacks" 1 April 2004.
- [5]. Arbor Application Brief: "The Growing Threat of Application-Layer DDoS Attacks".2011.
- [6]. G. Badishi, A. Herzberg, and I. Keidar, "Keeping Denial-of-Service Attackers in the Dark," IEEE Trans. Dependable and Secure Computing, vol. 4, no. 3, pp. 191-204, July-Sept. 2007.
- [7]. <http://www.random.org/randomness>.

A modified model for parabolic trough solar receiver

M-C. EL JAI¹, F-Z. CHALQI¹

¹(Lab. IMAGES. University of Perpignan. France)

Abstract: The aim of this paper is to give an original mathematical model that describes the heat exchange between the main components of a thermal solar collector in an Integrated Solar Combined Cycle (ISCC) plant. The obtained model is used to perform easier simulations of the studied system and gives the temperature evolutions of the heat transfer fluid and of the metal tube receiver. The model could also be used to optimize the solar collector design according to desired objectives.

Keywords: Distributed parameter systems, heat transfer fluid, modelling, solar parabolic trough collector.

I. INTRODUCTION

The fight against the problem of climate change caused by pollution of air and water is increasing. It becomes overwhelmingly urgent. This is mainly due to the continued exploitation of fossil fuels resources. It is therefore essential to find a solution allowing production of CO₂-free energy to meet our daily and industrial needs. The solar energy is one of the renewable energies. It is free and especially clean, and can perfectly help to solve this problem. The exploitation of this energy would be useful and more advantageous in solar plants by concentrating the sunlight. This energy can be stored as heat energy for 12 hours by using as heat transfer fluid the molten salt, the stone or the phase change materials.

The process of concentrating solar energy can be achieved by a system based on concentration of lenses, or reflective mirrors such that the sunrays converge onto a target of a smaller size and located at the focal plan of this surface.

Generally, there are two main methods used to perform the concentration of solar energy (see Fig. 1):

- Line-focusing systems: linear concentration.
- Point-focusing systems: concentration point.

In the first class, there are two types of solar plant: solar power tower (Big Solar Furnace in Odeillo, France, 1MW), and solar power of parabolic Dish-Stirling (Dish Stirling prototype plants of 10 kW each in Almeria, Spain).

In the second class, we find two types of solar plant: solar plant of parabolic trough (Nevada Solar One Power Plant, 64MW and Ain Beni-Mathar solar plant northeast Morocco, 472 MW), and solar plant of Fresnel linear collectors (PE1 solar plant in Murcia, Spain, 1.4 MW).



Fig. 1: Different methods for solar concentration

The thermodynamic solar power plants (known concentration in Fig. 2) use a lot of mirrors that make direct the solar rays to a heat transfer fluid to be heated at high temperatures. For this reason, the reflecting mirrors have to follow the sun's movement to collect and concentrate a maximum rate of solar radiation throughout the solar cycle used. The heat produced by the heat transfer fluid will be used to generate electricity using steam turbines or gas.

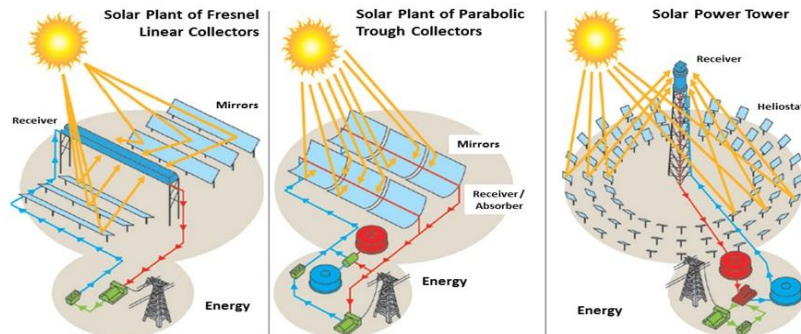


Fig. 2: Different types of solar concentration plants [1]

The technology of thermodynamic solar has current applications as power generation, solar power booster, and generation of steam for industrial processes.

In this paper, we are interested in solar plant of parabolic trough and specifically in solar plant which operating with the Integrated Solar Combined Cycle (ISCC). Here we concentrate on the case of cylindro-parabolic plants as that developed in Ain Beni-Mathar, located northeast of Morocco. The studied plant uses an integrated solar system combined with a system running a natural gas to produce electricity continuously even in the absence of the sun.

This solar plant consists of a solar field, a solar heat exchanger, two gas turbines, a steam turbine and an air condenser. The solar plant principle can be described as follows (Fig. 3). The extracted gases from the turbines are injected in two boilers. The solar energy collected by the trough parabolic mirrors, allows increasing the flow of vapor produced in the recovery boilers. An amount of water from the condenser enters the boiler. When it has been heated to the evaporation point, a part of the water will be led to the solar heat exchanger where it will be heated to the boiling point, evaporated and overheated to return then to the steam generator. It will be re-overheated before being introducing into the steam turbine of three levels (high, medium and low pressure) [2].

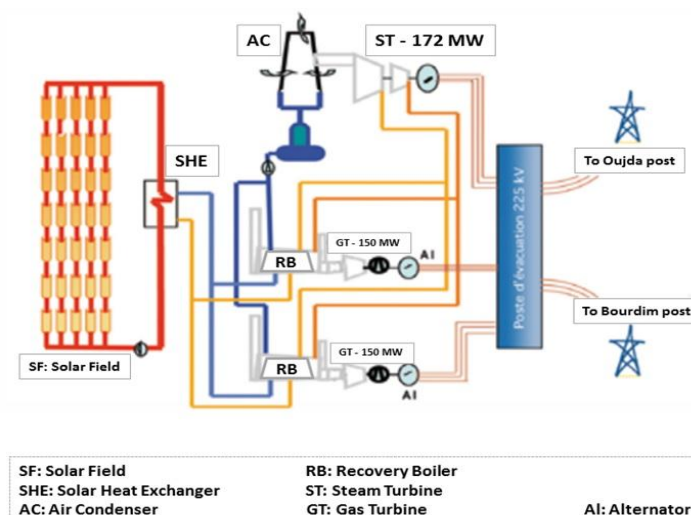


Fig. 3: Principle of Ain Beni-Mathar solar thermal plant [2].

However, the annual efficiency of these solar plants is affected by the instantaneous variations of the weather. The movement of the sun, the clouds, and the wind speed defines these variations. They are observed essentially at the parabolic trough of solar field. Therefore it is necessary to model the operating of these solar collectors for improving the efficiency of the solar field and to contribute to a better performance of the entire solar plant.

The paper is organized as follows. The next section describes the physical interactions of the solar plant components. Based on the energy balance, a general model is established. The various parameters depend strongly on the temperature of the main elements of the collector. However this model which looks simple is very complex for numerical implementation. The next section is devoted to a different writing of the model which leads to a look-like logistic model. The new version can be easily implemented and used for design or control problems. It is illustrated by simulation results.

II. THE PHYSICAL SYSTEM

2.1 DESCRIPTION OF THE SOLAR FIELD

The solar plant is an Integrated Combined Cycle Thermo-Solar Power plant, located in northeast of Morocco. It consists of 256 parabolic trough solar collectors. These collectors are classified in 64 parallel loops; each loop is 618 meters long, see Fig. 4. The receiver tubes are located at the focal axis of the parabolic trough solar collectors. They contain a heat transfer fluid which temperature can reach 393 °C.

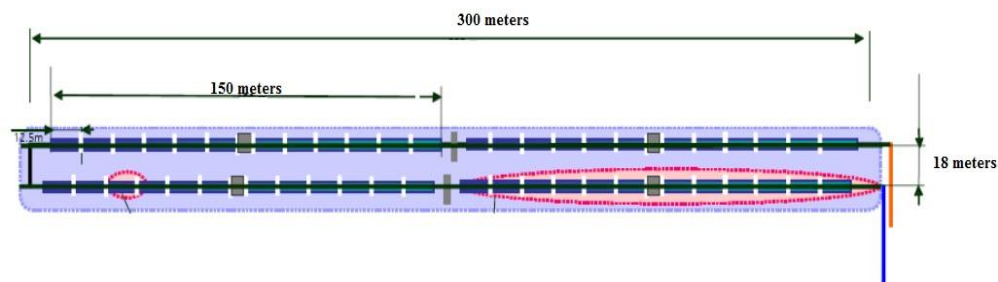


Fig. 4: The receiver loop [2]

The collector used in this solar thermal plant consists of parabolic reflectors (a series of mirrors), a metallic structure, a solar tracking system, and receiver tube. This type of parabolic trough solar collectors may have a concentration ratio of about 80%.

The mirror is made of borosilicate glass, whose transmittance is approximately 98%. This glass is covered with a layer of silver in its lower part, with a special coating and protection. The best reflector can reflect 97% of incident radiation.

The role of the solar tracking mechanism is adapted to maintain the incident solar radiation perpendicular to the reflector. The radiation is reflected to the focal line of the parabola where a receiver tube contains the heat transfer fluid.

The tube receiver or heat collection element (HCE) is of Schott PTR 70 type [3]. It is composed of two concentric tubes. The stainless-steel absorber tube, surrounded by a partially evacuated glass envelope to minimize heat losses, see Fig. 5. The receiver tube contains a heat transfer fluid which is a synthetic oil (Therminol VP-1, [4]).



Fig. 5: The solar receiver tube [3]

2.2 FIRST MODELLING APPROACH

Modelling parabolic trough solar collectors has been explored by many authors [5, 6, 7, 8, 9, 10]. The modelling principle is based on energy balance between the essential elements of the heat collection element (HCE) which are the receiver tube, and the heat transfer fluid. The Fig. 6 shows a transversal section of the different thermal exchanges [5, 6, 8] between the receiver tube, and the heat transfer fluid, and their environment.

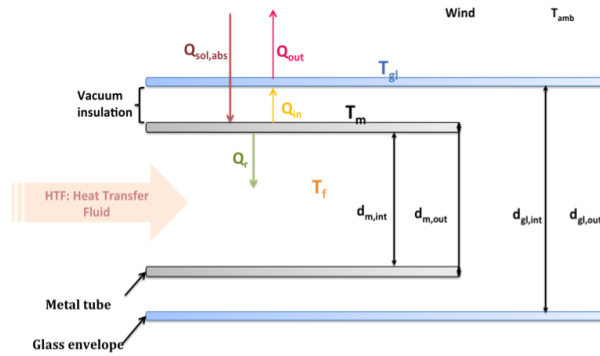


Fig. 6: Scheme of the different thermal exchanges of the HCE

The main purpose of this modelling is to predict the equilibrium temperature of the fluid at the output of the solar field generated by the flow rate at the entrance of the receiver tube. The following hypotheses are considered:

1. The properties of the fluid depend on the temperature.
2. In each section of the tube, the fluid flow is assumed to be uniformly distributed and equal to a mean
3. The solar radiation and the fluid flow vary on time and are the same for the whole receiver tube
4. The fluid is assumed to be incompressible.

The state variables we consider are the temperature of the fluid T_f , the absorber tube T_m and the glass envelope T_{gl} . The energy balance for the heat collection element leads to three partial differential equations of three temperatures. The first equation describes the fluid temperature T_f . It depends of time t and on space x . The second and third equations describe the absorber tube temperature T_m and the glass envelope temperature T_{gl} .

The obtained system of equations is then given by:

$$\left\{ \begin{aligned} \rho_f C_f A_f \frac{\partial T_f(x,t)}{\partial t} + \rho_f C_f \frac{\dot{V}_f}{N_{col}} \frac{\partial T_f(x,t)}{\partial x} &= Q_r(x,t) \\ \rho_m C_m A_m \frac{\partial T_m(x,t)}{\partial t} &= Q_{sol,abs}(x,t) - Q_{in}(x,t) - Q_r(x,t) \\ \rho_{gl} C_{gl} A_{gl} \frac{\partial T_{gl}(x,t)}{\partial t} &= Q_{in}(x,t) - Q_{out}(x,t) \end{aligned} \right. \quad (1)$$

In this system of equations, the amounts of energy were considered and defined from thermodynamics. These energies are often heat exchange between the different components of the HCE, either by convection or conduction, or radiation, taking into account the impact of the environment [5, 6, 7, 8, 10]. The heat transfer fluid, flowing inside the metal tube, receives by convection an amount of heat that depends mainly to the characteristics of fluid such as the density, the specific heat, the kinematic viscosity, the thermal conductivity [2] etc. These characteristics are related to the fluid temperature. The heat received is given by:

$$Q_r = h_{m,f} A_{surf,m,in} (T_m - T_f) \quad (2)$$

The amount of the absorbed solar energy, $Q_{sol,abs}$, by the parabolic trough solar collector depends on the weather and the cleanliness of the collectors and is defined by:

$$Q_{sol,abs} = I_s F(\cos\theta) D_{eff} \eta_{opt} \gamma \quad (3)$$

The two concentric tubes (metal and glass) of the receiver tube, are exchanging the heat by conduction and by radiation [5, 6, 7, 8]. This heat energy depends on the different characteristics of the stainless steel and the glass, and is defined by:

$$Q_{in} = Q_{in,rad} + Q_{in,cond} \quad (4)$$

where

$$Q_{in,rad} = \frac{\sigma A_{surf,m,out} (T_m^4 - T_{gl}^4)}{\frac{1}{\epsilon_m} + \frac{1 - \epsilon_{gl}}{\epsilon_{gl}} \frac{d_{m,out}}{d_{gl,in}}} \tag{5}$$

$$Q_{in,cond} = \frac{2 \pi k_{eff,air} (T_m - T_{gl})}{\ln(\frac{d_{gl,in}}{d_{m,out}})} \tag{6}$$

An amount of thermal energy is exchanged, by convection and radiation [5, 6, 7, 8], between the glass envelope and the environment. This thermal energy is defined by the characteristics of the glass and those defining the ambient air, as follows:

$$Q_{out} = Q_{out,rad} + Q_{out,conv} \tag{7}$$

where

$$Q_{out,rad} = \sigma \epsilon_{gl} A_{surf,gl,out} (T_{gl}^4 - T_{amb}^4) \tag{8}$$

$$Q_{out,conv} = h_{gl,amb} A_{surf,gl,out} (T_{gl} - T_{amb}) \tag{9}$$

After replacing in equations (1) and dividing by ρCA for each, we obtain a system of partial differential equations (PDE) which can be rewritten in the following simple form

$$\left\{ \begin{aligned} \frac{\partial T_f(x,t)}{\partial t} + \alpha_0 \frac{\partial T_f(x,t)}{\partial x} &= a_1 T_f + a_2 T_m \\ \frac{\partial T_m(x,t)}{\partial t} &= b_1 T_f + b_2 T_m + b_3 T_{gl} + b_4 T_m^4 + b_5 T_{gl}^4 + b_6 \\ \frac{\partial T_{gl}(x,t)}{\partial t} &= c_1 T_m + c_2 T_{gl} + c_3 T_m^4 + c_4 T_{gl}^4 + c_5 \end{aligned} \right. \tag{10}$$

where the coefficients a_i , b_i and c_i are given in the annex. The model of the solar trough collector allows the knowledge of the fluid temperature evolution only at the output of the receiver tube. Furthermore it could help to choose the parameters of the plant in such a way that the temperature can be maintained at a desired equilibrium value, despite instantaneous variations of the weather. This could be regulated by a convenient flow rate at the entrance of the receiver tube. However numerical simulation of the complete obtained model above (10), leads to various difficulties, due to the complexity of the model coefficients which all depend nonlinearly on the temperature.

So it becomes necessary to modify the obtained model for easier simulations. The first assumption is to assume that a perfect vacuum exists between the two concentric metal and glass tubes. In this case we can neglect the glass behavior and thus we obtain a system coupling fluid and metal temperatures dynamics. This assumption allows to study the heat exchange between the fluid and the metal tube. The first exchange describes the amount Q_g of energy defined in equation (2), while the second exchange is defined by $Q_{abs,sol} - Q_g - Q_{m,amb}$. The amount of energy $Q_{m,amb}$ describes the heat exchange between the metal tube and its environment. This thermal energy is given by :

$$Q_{m,amb} = h_{m,amb} A_{surf,m,out} (T_m - T_{amb})$$

Finally the model can be described by a model reformulated as follows

$$\left\{ \begin{aligned} \rho_f C_f A_f \frac{\partial T_f(x,t)}{\partial t} + \rho_f C_f \frac{\dot{V}_f}{N_{col}} \frac{\partial T_f(x,t)}{\partial x} &= h_{m,f} A_{surf,m,in} (T_m - T_f) \\ \rho_m C_m A_m \frac{\partial T_m(x,t)}{\partial t} &= I_s F(\cos\theta) D_{eff} \eta_{opt} \gamma - h_{m,amb} A_{surf,m,out} (T_m - T_{amb}) \\ &\quad - h_{m,f} A_{surf,m,in} (T_m - T_f) \end{aligned} \right. \tag{11}$$

which can be simplified to the following form

$$\left\{ \begin{aligned} \frac{\partial T_f(x,t)}{\partial t} + a_0 \frac{\partial T_f(x,t)}{\partial x} &= a_1 T_f + a_2 T_m \\ \frac{\partial T_m(x,t)}{\partial t} &= b_1 T_f + \beta_1 T_m + \beta_2 \end{aligned} \right. \quad (12)$$

Where, the coefficients β_i are different from the b_i 's and are given in the annex. One can notice that the various coefficients depend on the temperature of the fluid or the metal tube

III. MODIFIED MODEL

Firstly the model (12) can be easily studied from mathematical point of view. For that purpose we rewrite it in a matrix form, by considering the vector z defined by $z = \begin{pmatrix} T_f \\ T_m \end{pmatrix}$. Thus the above system can be easily represented in the following vector form

$$\dot{z} = A_1 z + B_1 \quad (13)$$

Where A_1 is a matrix of order $(2 * 2)$ and B_1 is a matrix of order $(2 * 1)$, defined by

$$A_1 = \begin{pmatrix} -a_0 \frac{\partial}{\partial x} + a_1 & a_2 \\ b_1 & \beta_1 \end{pmatrix} \text{ and } B_1 = \begin{pmatrix} 0 \\ \beta_2 \end{pmatrix} \quad (14)$$

This formulation shows that the considered system is well posed from mathematical point of view and, under the condition that the coefficients are bounded, the system admits a unique solution. In what follows we consider the model (12) and we explore some coefficients which affect dramatically the resolution. In spite of the simplicity of the model (12), it is not consistent with the nature of the system. Furthermore its numerical implementation leads to surprising numerical results. It is difficult to find in the literature models which can lead to realistic simulations. Most of the models describe very complex physics but lead to non possible simulations. A model can be considered as a fine model if it is simple and can be implemented easily for simulations. That is why we consider a modified model which could be used by solar plant modelers without complex physical considerations.

3.1 MODELLING APPROACH

The main difficulties in the above model are due to the temperatures sensitivity with respect to the model coefficients. However we have noticed that some of the coefficients depend nonlinearly of the temperature. Various simulations show that the solution evolves dramatically for small variations of certain coefficients. A numerical study of the coefficients leads to a second assumption which consists to neglect the coefficients which value are lower than 10^{-10} . On an other hand the coefficients α_1 and β_1 are slightly linear with respect to the fluid temperature T_f as shown in Fig. 7.

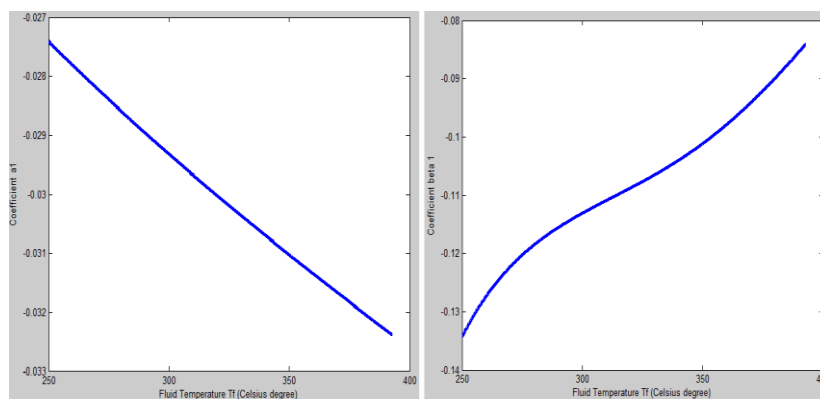


Fig. 7: Evolution of the coefficients α_1 and β_1

This suggests to consider a linear description for these coefficients and to reformulate the system under the form

$$\left\{ \begin{aligned} \frac{\partial T_f(x,t)}{\partial t} + a_0 \frac{\partial T_f(x,t)}{\partial x} &= (\alpha_{a_1} T_f + \beta_{a_1}) T_f + a_2 T_m \\ \frac{\partial T_m(x,t)}{\partial t} &= b_1 T_f + (\alpha_{\beta_1} T_f + \beta_{\beta_1}) T_m + \beta_2 \end{aligned} \right. \quad (15)$$

In the first equation of (15) the term $(\alpha_{a_1} T_f + \beta_{a_1})$ can be rewritten in the form

$$\alpha_{a_1} T_f + \beta_{a_1} = -\alpha_{a_1} [K - T_f]$$

where $\beta_{a_1} = \alpha_{a_1} K$. Thus the first equation can be stated by

$$\frac{\partial T_f(x,t)}{\partial t} + a_0 \frac{\partial T_f(x,t)}{\partial x} = -\alpha_{a_1} [K - T_f] T_f + a_2 T_m \quad (16)$$

This formulation can be seen as equations of an equilibrium model where the temperature will be stabilized around a certain value. One can consider other approaches for the coefficients modelization but they do not lead to any improvement of the model.

3.2 SIMULATIONS

The obtained model consists in a system of two nonlinear partial differential equations.

$$\left\{ \begin{aligned} \frac{\partial T_f(x,t)}{\partial t} + a_0 \frac{\partial T_f(x,t)}{\partial x} &= -\alpha_{a_1} [K - T_f] T_f + a_2 T_m \\ \frac{\partial T_m(x,t)}{\partial t} &= b_1 T_f + \alpha_{\beta_1} T_f T_m + \beta_{\beta_1} T_m + \beta_2 \end{aligned} \right. \quad (17)$$

It evolves in time t and depends on one-dimensional space x . Formally it derives from the system (12) and therefore it is well posed from mathematical point of view.

In this section we give a numerical approach for the resolution of (17). The discretization principle for solving boundary-value problems consist of replacing each of the derivatives in the differential equation by an approximate difference quotient approximation. The difference quotient is generally chosen so that a certain approximation order error is maintained. Other methods for solving (finite elements) these equations could be considered.

The model (17) is explicitly nonlinear. In this system, we know the mean values for all the remaining coefficients. The range of variation of the temperature can lead to an explicit approximation of the coefficients. Thus we find the following mean values for the considered coefficients:

$\alpha_{a_1} = -3.46610^{-5}$	$\beta_{a_1} = -0.0188$
$\alpha_{\beta_1} = 3.2210^{-4}$	$\beta_{\beta_1} = -0.2141$

For the discretization let L be the length of a loop of the HCE and Δx a step size. Denote N_x the number of space paths of length Δx (see Fig. 8), then $\Delta x = L/N_x$. In the considered plant we have $L = 61.8$ meters. For the time horizon, we consider the time step denoted Δt and N_t the number of time steps. If we denote t_{period} the time length between the sunrise and the sunset (with a maximum solar flux), then $\Delta t = t_{\text{period}}/N_t$.

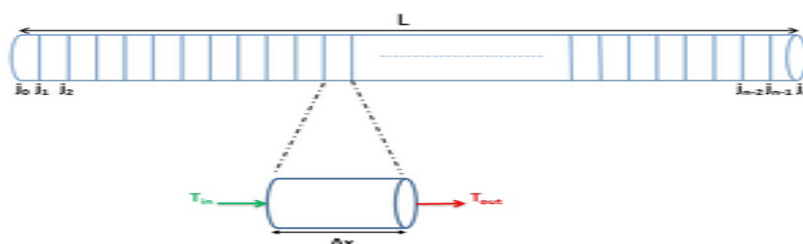


Fig. 8: Discretization of the heat collection element

The resolution of the reformulated model requires initial and boundary conditions. We assume that $T_f(0, x) = T_{f,0}$ the initial known temperature of the fluid. We also denote $T_{in}(0, x) = T_{in,0}$, the initial temperature of the metal tube, assumed to be known. In practical applications we consider $T_{in,0} = T_{f,0}$.

3.2.1 TIME EVOLUTION TEMPERATURES

The model previously modified is given in (17) where T_f is the fluid temperature and T_{in} is the metal tube temperature. For the time evolution of the fluid temperature at any point of the receiver tube, it is not necessary to consider the space evolution. So we consider firstly that the partial derivative in space vanishes, thus the first equation of (17) becomes

$$\frac{\partial T_f(x, t)}{\partial t} = -\alpha_{a1} [K - T_f] T_f + \alpha_2 T_m \tag{18}$$

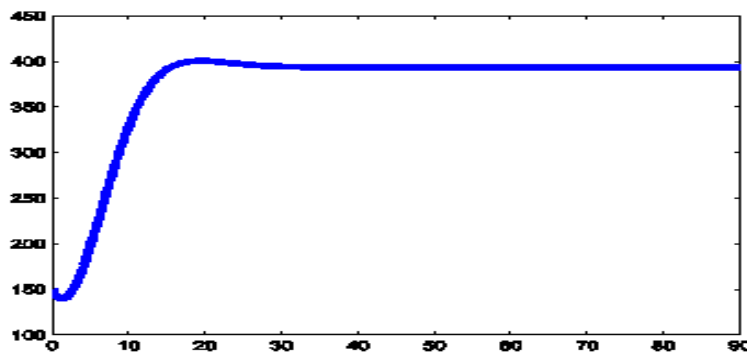


Fig. 9: Evolution of the fluid temperature T_f .

In this case we neglect the space variable and denote

$$T_f^n \cong T_f(n\Delta t)$$

and we apply a modified Euler method (more accurate) with the initial conditions $T_{f,0}$ and $T_{in,0}$. Then we obtain the evolution graphs given in Fig. 9 for the fluid temperature and in Fig. 10 for the metal tube temperature.

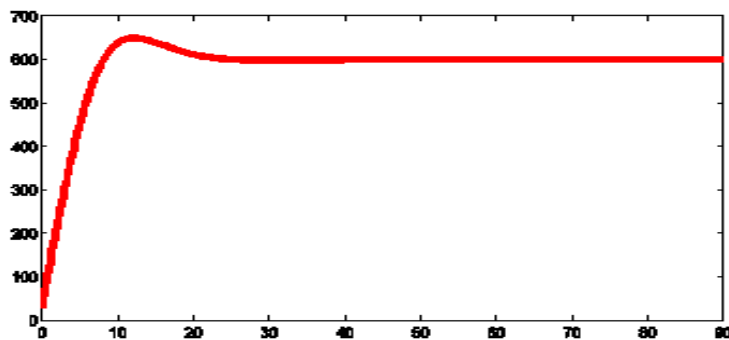


Fig. 10: Time evolution of the metal tube temperature T_{in} .

We notice that the metal tube temperature is always higher than that of the fluid. For the fluid and the receiver tube the figures show that the temperature evolves until an equilibrium level which maintains the fluid temperature at about 400° Celsius. These results are consistent with the measurements obtained by the output, under ideal conditions.

Remark 3.1

In the applications depending on the considered plant one can introduce a weighting term ξ to adapt the evolution of the fluid temperature (which may depend on physical parameters and day insulation). For that purpose we can rewrite the term $\alpha_{a1} T_f + \beta_{a1} [K - T_f]$ considering

$$\alpha_{a_1} T_f + \beta_{a_1} = -\alpha_{a_1} [K - \xi T_f]$$

The figure (11) shows the influence of the coefficient ξ on the time evolution of the fluid temperature.

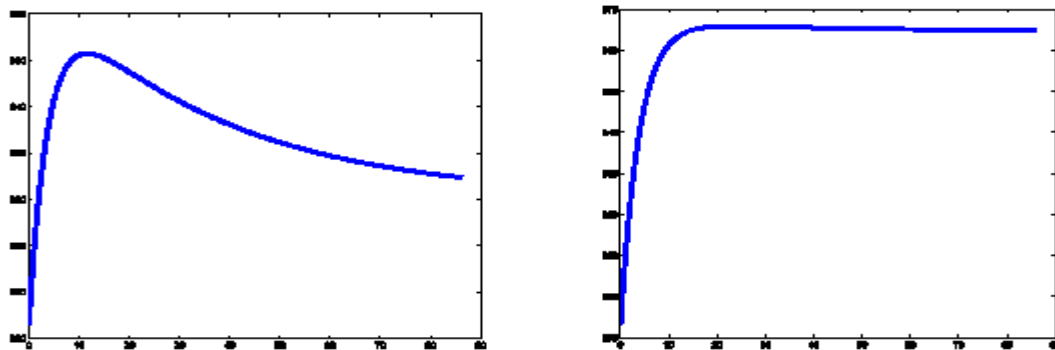


Fig. 11: Evolution of the fluid temperature T_f in time in the cases where the weighting term $\xi = 0.19$, and $\xi = 0.16$

The Fig. 11 shows that at the beginning of the time interval, and for a weighting term equal to 0.19, the fluid temperature T_f increases with time to a maximum value ranging from 352°C to 362°C. Then the fluid temperature T_f decreases to a value of about 324°C. However when the weighting term ξ is equal to 0.16, the fluid temperature T_f increases with time to reach a maximum value of about 365.9°C and remains maintained at this value. The weighting term ξ can be used in the discretized equation for an adaptation of the evolution to any situation.

3.2.2 TIME AND SPACE EVOLUTION OF THE TEMPERATURES

Introduce now the mesh points of coordinates $\{j\Delta x, n\Delta t\}$, for $n = 1, 2, \dots, N_t$ and $j = 1, 2, \dots, N_x$ and let T_i^n be an approximated value of the temperature $T(j\Delta x, n\Delta t)$ (T_f for the fluid and T_m for the metal tube) denoted

$$T_j^n \cong T(j\Delta x, n\Delta t)$$

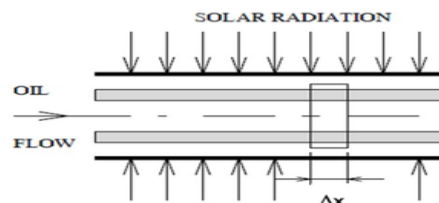


Fig. 12: Element of the distributed parameter model

With these notations we illustrate the efficiency of the given model considering the following finite difference first order approximations of the derivatives

$$\frac{\partial T(j\Delta x, n\Delta t)}{\partial t} = (T_j^{n+1} - T_j^n) / \Delta t \quad \text{and} \quad \frac{\partial T(j\Delta x, n\Delta t)}{\partial x} = (T_j^n - T_{j-1}^n) / \Delta x \quad (19)$$

The resolution of the reformulated model requires initial and boundary conditions. The initial conditions have been stated in previous section. Additionally we consider boundary condition at the entrance of the receiver tube given by $T_f(t, 0) = T_{f_0}$ and $T_m(\tau, 0) = T_{m_0}$ assumed to be known.

In this case, we have to discretize the principal model in equation (17). Denote $\tau = \Delta t, \Delta x$ and apply the finite difference discretization in time and space given in (19) (see [11]), we obtain

$$\begin{cases} T_{f,j}^{n+1} = [1 - ra_0 - \Delta t \alpha_{a_1} (K - T_{f,j}^n)] T_{f,j}^n + ra_0 T_{f,j-1}^n + \Delta t a_2 T_{m,j}^n \\ T_{m,j}^{n+1} = \Delta t \alpha_{\beta_1} T_{f,j}^n T_{m,j}^n + \Delta t b_1 T_{f,j}^n + [1 + \Delta t \beta_{\beta_1}] T_{m,j}^n + \Delta t \beta_2 \end{cases} \quad (20)$$

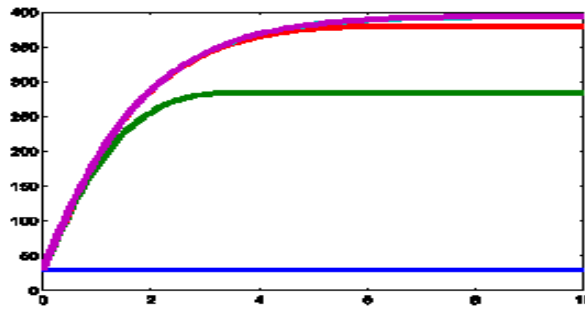


Fig. 13: Global (time-space) temperature evolution of the fluid

For the illustrative simulation, we have considered a time step equal to 0.005 second and a space step equal to 0.1 meter.

The Fig. 13 presents the obtained results for the fluid temperature T_f throughout the receiver tube at different times, and Fig. 14 that of the metal tube T_{ill} .

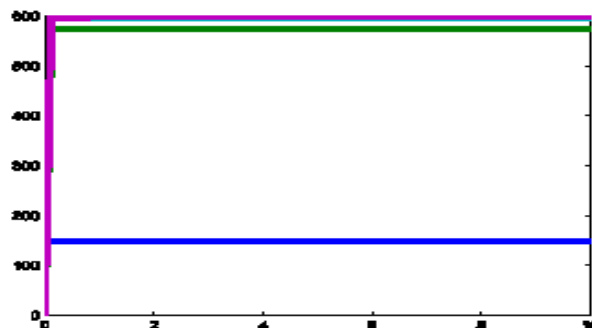


Fig. 14: Global (time-space) temperature evolution of the metal tube.

The Fig. 13 and 14 show that the temperatures increase from initial temperature at the entrance of the tube to reach a maximal value of about 400°C for the fluid and 600°C for the metal tube. The metal tube temperature reaches its equilibrium value very quickly all along the tube, because all the tube is in the focal line of the solar receiver and is directly exposed to the sunlight.

The nomenclature and the annex given after would help to achieve the illustrative simulations.

Remark 3.2

The modified model introduced in the previous section has reduced the model to a system of two differential equations (17). We can notice that the receiver tube is all located in the focal line of the parabolic trough. Consequently we can consider that the whole receiver tube is excited by the same amount of energy and thus its temperature is equal to a mean value T^* .

This is obviously illustrated by the Fig. 14. Additionally the users could be interested only by the fluid temperature evolution and not that of the metal tube. This suggests that the fluid receives the same amount of energy all along the tube which can be considered as a passive control on the fluid. Therefore we can simplify the model by neglecting the receiver tube equation and considering that the fluid is excited by its contact with the metal tube, by a certain amount to be identified. This allows to consider the following simplified partial differential equation which state is the fluid temperature T_f

$$\frac{\partial T_f(x,t)}{\partial t} + a_0 \frac{\partial T_f(x,t)}{\partial x} = -\alpha_{a_1} [K - T_f] T_f + a_2 \tilde{T} \tag{21}$$

where T^* is assumed to be known. The system is augmented by initial and boundary conditions.

We can assume that the mean value T^* is equal to that given by measurements of the metal tube temperature. In this case the various coefficients of the model do not fit with the physical values of the previous model. Thus the model can be improved using an identification of the other coefficients $\alpha_{a_1}, \alpha_{a_2}, \alpha_{a_3}, \alpha_{a_4}$. The following figures show that the results are very significant and that the model can be drastically reduced.

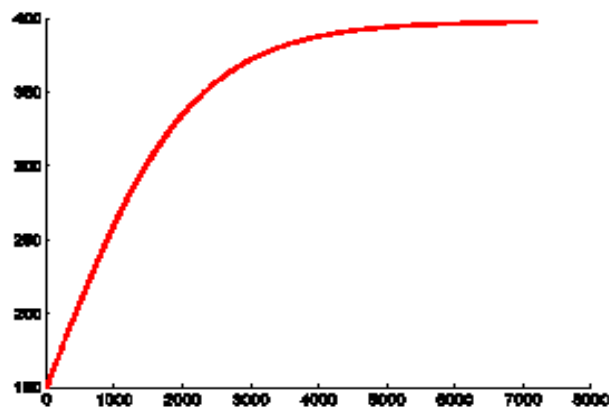


Fig. 15: Fluid temperature evolution (at a fixed point of the tube) without considering the space impact.

The numerical simulations have been achieved considering the following values: $\alpha_0 = 0.04$, $\alpha_1 = 2 \cdot 10^{-6}$, $K = 310$ and $\alpha_2 = 0.07$.

The Fig. 15 shows that the result is quite similar to that of the complex model considered in the first section.

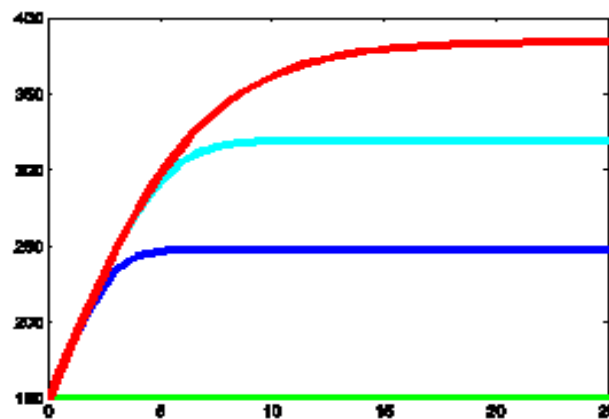


Fig. 16: Fluid temperature evolution, at different times, all along the receiver tube

The Fig. 15 and 16 show that the temperature level at the end of the tube is about 375°. This temperature level can be adjusted and regulated at any convenient desired level, depending of the real conditions of the trough solar receiver.

IV. CONCLUSION

In this paper we give an original modified model of the heat collector element within an Integrated Combined Cycle Thermo-Solar Power Plant. The given approach is more accurate and easier to implement. This model has necessitated the study of heat exchange between the three components of the heat collection element. The reformulation of the model was based by considering a perfect vacuum between the two concentric tubes (metal tube inside the glass envelope) of the heat collection element (HCE). The model established consists in two first order partial differential equations depending on time and one dimension space variable, and may be reduced to one partial differential equation. The different simulation results show that both the fluid temperature T_f and the metal tube temperature T_m evolve until reaching a certain equilibrium value. The obtained results are consistent with the plant values. The proposed model can be improved by considering an identification of some of the coefficients. This identification depends on the considered solar plant and will be explored in a future work.

V. ACKNOWLEDGEMENTS

We would like to thank

- 1) Professor A. EL JAI (University of Perpignan, France) for his advice throughout this work; as well for modelling aspects as for numerical approach of the studied problem.
- 2) Lorenzo Castro Gómez-Valadés, Process Engineer (ISCC Ain Beni Mathar Morocco), for his kind help and the data of the ISCC plant.

REFERENCES

- [1]. S. Andrieux, Le solaire thermodynamique à concentration, 2012, 1-4.
- [2]. F-Z. CHALQI, Bilan thermique de la central thermo-solaire d'Ain Béni-Mathar (ABM), Université de Perpignan Via Domitia, Août 2012.
- [3]. Schott Solar Csp Gmbh, Schott PTR 70 Receivers, Mainz (Germany), 2009.
- [4]. Solutia, Therminol VP-1, Louvain-la-Neuve (France), 2002.
- [5]. Thorsten A. Stuetzle, Automatic Control of the 30 MWe SEGS VI Parabolic Trough Plant, University of Wisconsin-Madison, Madison, 2002.
- [6]. R. Forristall, Heat transfer analysis and modeling of a parabolic trough solar receiver implemented in engineering equation solver, Technical report, National Renewable Energy laboratory, 2003.
- [7]. N. Hamani, A. Moumimi, N. Moumimi, A. Saadi and Z. Mokhtari, Simulation de la température de sortie de l'eau dans un capteur solaire cylindro-parabolique dans le site de Biskra, Revue des Energies renouvelables, Vol. 10. N°2, 2007, 215-224.
- [8]. F. Burkholder and C. Kulscher, Heat loss testing of Schott's 2008 PTR70 parabolic trough receiver, Technical report (NREL/TP-550-45633. May 2009).
- [9]. B. Kelly and D. Kearney, Parabolic Trough Solar System Piping Model, Final Report, National Renewable Energy laboratory, 2006.
- [10]. Ming Qu, D. H. Archer and S. V. Masson, A linear Parabolic trough Solar Collector Performance Model, Renewable Energy Resources and a Greener Future Vol.VIII-3-3, Proceedings of the Sixth International Conference for Enhanced Building Operations, Shenzhen, China, November 6 - 9, 2006.
- [11]. A. El Jai, Eléments d'analyse numérique (PUP, 2nd edition, 2010).

ANNEX

ρ_f : HTF density

ρ_{in} : Metal (Stainless steel) density

ρ_{gl} : Glass density

C_f : HTF specific heat

C_{in} : Metal (Stainless steel) specific heat

C_{gl} : Glass specific heat

$d_{in,mt}$: Inside diameter of the metal tube

$d_{out,mt}$: Outside diameter of the metal tube

$d_{in,gl}$: Inside diameter of the glass

$d_{out,gl}$: Outside diameter of the glass

A_f : Noted also $A_{in,mt}$. Cross-sectional area inside the metal tube

A_{in} : Cross-sectional area of the metal tube

A_{gl} : Cross-sectional area of the glass

$A_{surf,gl,mt}$: Inner surface area per length of the metal tube

$A_{surf,mt,gl}$: Outer surface area per length of the metal tube

$A_{surf,gl,gl}$: Outer surface area per length of the glass envelope

I_s : Solar Direct irradiance

$F(\cos \theta)$: Incidence modifier function

θ : Angle of incidence, degree

D_{eff} : Effective width of the collector

η_{dirt} : Optical efficiency: Factor depending of dirt on the mirrors

$k_{eff,air}$: Effective thermal air conductivity

T_{amb} : Ambient temperature

\dot{V}_f : Overall HTF volume flow rate

N_{col} : Total number of collectors

ϵ_{in} : Metal (Stainless steel) emissivity

ϵ_{gl} : Glass emissivity

σ : Stefan-Boltzmann constant

$h_{in,f}$: Convection heat transfer coefficient between the metal tube and the HTF

$h_{gl,amb}$: Convection heat transfer coefficient between the glass and the ambient

$h_{in,amb}$: Convection heat transfer coefficient between the metal tube and the ambient.